



The University of
Nottingham

UNITED KINGDOM · CHINA · MALAYSIA

Optically Amplified Free-space Optical Communication Systems

Aladeloba Abisayo, MSc

Department of Electrical and Electronic Engineering

Faculty of Engineering

Thesis submitted to the University of Nottingham

for the degree of Doctor of Philosophy, July 2013

Abstract

This thesis investigates terrestrial atmospheric FSO communication systems operating under the influence of turbulence-induced scintillation, beam spreading, optical interchannel crosstalk, amplified spontaneous emission noise and pointing errors. On-off keying-non-return-to-zero (OOK-NRZ) and digital pulse position (DPPM) are the modulation schemes used for the calculations.

The possibility of using sophisticated performance evaluation techniques such as moment generating function (MGF)-based Chernoff bound (CB), modified Chernoff bound (MCB) and saddlepoint approximation (SPA) for terrestrial DPPM and OOK-NRZ-based FSO communication systems employing optical amplification are investigated and compared with the conventional Gaussian approximation (GA) method. Relative to the other techniques, the MCB can be considered a safe estimation method for practical systems since it provides an upper bound upon the BER.

The turbulent optically preamplified DPPM FSO receiver employing integration over a time slot and comparing the results to choose the largest slot, is seen to give better advantage (about 7 - 9 dB) compared to an equivalent employing OOK-NRZ signalling. The atmospheric turbulence-induced spreading of the beam, ASE noise, and pointing error are seen to combine in a problematic way resulting in high BERs, depending on the size of the receiver and the beam's jitter standard deviation.

Using FSO communication for the distribution links of a passive optical network-like wavelength division multiplexing access network is investigated in the presence of atmospheric turbulence, ASE noise and interchannel crosstalk. The results show that, for clear atmosphere, FSO distribution link length up to 2000 m can be reliably used (depending on turbulence strength) to achieve human eye safety and high capacity access networks. Also, error floors occur due to turbulence accentuated crosstalk effect for the cases of (i) signal turbulent, but crosstalk not and (ii) crosstalk turbulent, but signal not.

Acknowledgements

First and foremost, I would like to thank my academic supervisors Dr Andrew J. Phillips and Dr Malcolm S. Woolfson for their support throughout my PhD research. I have benefited vastly from their technical expertise, insights and high standards in research and teaching.

I would like to express my deepest gratitude to Department of Electrical and Electronics Engineering, University of Nottingham, UK, under the Tower Innovation Scholarship, Dr Babalakin and Mr Oniagba for their generosity in funding me through my PhD research.

I also would like to say a big thank you to all my colleagues, and the postdoctoral researchers in the Photonic and Radio Frequency Engineering Group (PRFEG) at the University of Nottingham, UK, for their support and for making my time in Nottingham an enjoyable one.

Most importantly, I would like to thank my family – my parents, Mr Robert Aladeloba and Mrs Grace Aladeloba, my siblings, Abidemi, Akinyinka, Akintomi, and my extended family members for their wonderful support throughout my study. This dissertation is dedicated to them as a token of my gratitude.

Contents

Abstract	ii
Acknowledgements.....	iii
Contents	iv
List of Acronyms	viii
List of Figures	xi
List of Tables	xvi
CHAPTER 1 Introduction.....	1
1.1 Historical perspective.....	1
1.2 Background.....	2
1.3 Organisation of thesis	5
1.4 New contributions to knowledge	6
1.5 References.....	10
CHAPTER 2 Basic components of FSO communication systems	13
2.1 Overview.....	13
2.2 Transmitter system.....	13
2.2.1 Semiconductor lasers	14
2.2.2 Laser safety and standards	15
2.2.3 Light emitting diodes	17
2.2.4 FSO modulation formats.....	19
2.2.4.1 On-off keying	19
2.2.4.2 Digital pulse position modulation	20
2.3 Optical amplifier	21
2.3.1 Principle of optical amplification.....	24
2.3.2 Erbium-doped fibre amplifier	27
2.3.3 Semiconductor optical amplifier.....	28
2.3.4 Comparison between EDFA and SOA	29
2.4 Receiver system	30
2.4.1 Direct detection – positive-intrinsic-negative photodiode.....	32
2.4.2 Direct detection – Avalanche photodiode.....	32
2.5 Summary	33
2.6 References.....	33
CHAPTER 3 Factors affecting FSO communication systems	37
3.1 Overview.....	37
3.2 Physical obstacles	37
3.3 Atmospheric attenuation	37

3.3.1	Scattering	38
3.3.2	Absorption.....	39
3.4	Atmospheric scintillation	40
3.4.1	Probability density function models	44
3.5	Beam spreading.....	53
3.6	Pointing loss.....	54
3.7	Summary	55
3.8	References.....	55
CHAPTER 4	Optical receiver performance	59
4.1	Overview.....	59
4.2	Receiver circuitry noise	59
4.2.1	Thermal noise.....	59
4.2.2	Shot noise.....	60
4.3	Linear crosstalk.....	61
4.3.1	Interchannel crosstalk	62
4.3.2	Intrachannel crosstalk	62
4.4	Performance evaluation methods	63
4.4.1	Gaussian approximation.....	64
4.4.2	Methods using the moment generating function (MGF)	66
4.5	Summary	70
4.6	References.....	70
CHAPTER 5	Analysis of FSO communication systems impaired by atmospheric turbulence and ASE noise	73
5.1	Introduction.....	73
5.2	Receiver system	74
5.3	Atmospheric channel models.....	75
5.4	Moment generating function for optical signal.....	79
5.5	Bit error rate analysis	80
5.6	Results and discussion	83
5.7	Summary	94
5.8	References.....	94
CHAPTER 6	DPPM with aperture-averaging for turbulent optically preamplified FSO communication systems	98
6.1	Introduction.....	98
6.2	Digital pulse position modulation	100
6.3	Optically preamplified receiver	100
6.4	Atmospheric turbulence models	101

6.5	Theoretical analysis	103
6.6	Results and discussion	107
6.7	Summary	119
6.8	References.....	120
CHAPTER 7 Inclusion of pointing error and geometric spreading in the optically preamplified receiver model for turbulent FSO communication systems		
7.1	Introduction.....	123
7.2	Theoretical model	124
7.2.1	Receiver model	125
7.2.2	Atmospheric channel model with pointing error	126
7.2.3	Optically preamplified receiver model	129
7.2.4	BER for OOK-NRZ	130
7.2.5	BER for DPPM	130
7.2.6	Average BER	132
7.3	Results and discussion	132
7.4	Summary	146
7.5	References.....	146
CHAPTER 8 WDM FSO network impaired by ASE noise and turbulence- accentuated interchannel crosstalk.....		
8.1	Introduction.....	150
8.2	System design and description.....	152
8.2.1	Upstream transmission.....	153
8.2.2	Downstream transmission.....	155
8.2.3	Optical amplifier placement.....	156
8.3	Turbulence modelling	156
8.4	General BER analysis	158
8.5	Turbulence accentuated crosstalk	161
8.5.1	Example results	161
8.6	BER Evaluation for Hybrid WDM-PON-FSO System	166
8.6.1	Upstream transmission:.....	166
8.6.2	Downstream transmission:.....	167
8.7	Results and Discussion	169
8.7.1	Downstream transmission:.....	170
8.7.2	Upstream transmission:.....	174
8.8	Summary	181
8.9	References.....	181
CHAPTER 9 Conclusion and future works		
		185

9.1 Summary	185
9.2 Conclusions.....	188
9.3 Future work.....	191
9.4 References.....	192

List of Acronyms

American National Standards Institute.....	ANSI
Amplified spontaneous emission.....	ASE
Aperture averaging.....	AA
Arrayed waveguide grating.....	AWG
Avalanche photodiode.....	APD
Binary symmetric channel.....	BSC
Bit error rate.....	BER
Chernoff bound.....	CB
De-multiplexer.....	demux
Dense wavelength division multiplexing.....	DWDM
Differential phase-shift keying.....	DPSK
Differential quadrature phase-shift keying.....	DQPSK
Digital pulse position modulation.....	DPPM
Distributed Bragg reflector.....	DBR
Distributed feedback.....	DFB
Erbium-doped fibre amplifier.....	EDFA
Fabry Perot amplifier.....	FPA
Field-of-view.....	FOV
Forward error correction.....	FEC
Free-space optical.....	FSO
Gamma-gamma.....	GG
Gaussian approximation.....	GA
Geometric spreading.....	GS
International Electrotechnical Commission.....	IEC
K distribution.....	KD
Light amplification by stimulated emission of radiation.....	LASER
Light emitting diode.....	LED

Lognormal.....	LN
Maximum permissible exposure.....	MPE
Moderate turbulence.....	MT
Modified Chernoff bound.....	MCB
Moment generating function.....	MGF
Multiplexer.....	mux
Negative exponential.....	NE
No turbulence.....	NT
Noise figure.....	NF
Non-return-to-zero.....	NRZ
On-off keying.....	OOK
Optical amplifier.....	OA
Optical bandpass filter.....	OBPF
Optical line terminator.....	OLT
Optical network unit.....	ONU
Optical signal-to-noise ratio.....	OSNR
Optically pre-amplifier.....	OPA
Passive optical network.....	PON
Pointing and tracking.....	PAT
Pointing error.....	PE
Positive-intrinsic-negative.....	P-I-N
Power spectral density.....	PSD
Probability density function.....	pdf
Radio frequency.....	RF
Receiver collecting lens.....	RCL
Return-to-zero.....	RZ
Saddlepoint approximation.....	SPA
Semiconductor laser amplifier.....	SLA
Semiconductor optical amplifier.....	SOA

Signal with interferer, no turbulence.....	S,XT
Signal with no turbulence, interferer with turbulence.....	S,turbXT
Signal with turbulence, interferer with no turbulence.....	turbS,XT
Signal with turbulence, no interferer.....	turbS
Strong turbulence.....	ST
Time division multiple access.....	TDMA
Time division multiplexing.....	TDM
Travelling-wave amplifier.....	TWA
Variable optical attenuator.....	VOA
Vertical cavity surface emitting laser.....	VCSEL
Wavelength division multiplexing.....	WDM
Weak turbulence.....	WT

List of Figures

Figure 2.1	Response/absorption of the human eye at various wavelengths (redrawn from [4])	16
Figure 2.2	Schematic representation of a forward-biased LED, including the recombination and emission process	18
Figure 2.3	Illustration of DPPM frame for $M = 4$ ($n = 2^4 = 16$ slots)	21
Figure 2.4	Important processes in gain medium. Stimulated photon has same frequency, phase, polarisation and direction as incident photon	24
Figure 2.5	A simple erbium-doped fibre amplifier (redrawn from [1])	28
Figure 2.6	Schematic diagram of a typical semiconductor optical amplifier [1]	29
Figure 2.7	Block diagram of a typical FSO receiver	30
Figure 3.1	Atmospheric absorption transmittance over a sea level 1820 m horizontal path [3]	40
Figure 3.2	Scintillation index for plane wave as a function of square root of Rytov variance, $D_{RX} = 1$ mm	43
Figure 3.3	Lognormal pdf as a function of normalised irradiance, for a range of $\sigma_{\ln I}^2$	47
Figure 3.4	K distribution pdf as a function of normalised irradiance, for a range of α & σ_R^2	48
Figure 3.5	Values of α and β for different Rytov variances (and $d=0$)	51
Figure 3.6	Gamma-gamma pdf as a function of normalised irradiance, for a range of α & σ_R^2	51
Figure 3.7	Negative exponential pdf as a function of normalised irradiance, for various $\langle I \rangle$	52
Figure 3.8	Laser beam spreading in the far field [42]	54
Figure 4.1	A simplified front end receiver circuit	60
Figure 4.2	Chernoff bound	68
Figure 5.1	Optically preamplified FSO receiver	75
Figure 5.2	BER vs. normalised average received irradiance at receiver collecting lens (RCL) input [dB] using $G = 8.8$ dB and $D_{RX} = 4$ mm for (a) no turbulence, and weak turbulence using LN and GG distributions, (b) no turbulence, weak, moderate, strong, and saturated turbulences using GG distribution, (c) strong turbulence using GG and KD, and (d) saturated turbulence using NE distribution	86
Figure 5.3	BER vs. normalised average received irradiance at receiver collecting lens (RCL) input [dB] using $G = 30.6$ dB and $D_{RX} = 4$ mm for (a) no turbulence, and weak turbulence using LN and GG distributions, (b) no turbulence, weak, moderate, strong, and saturated	89

	turbulences using GG distribution, (c) strong turbulence using GG and KD, and (d) saturated turbulence using NE distribution	
Figure 5.4	BER vs. normalised average received irradiance at receiver collecting lens (RCL) input [dB] for no turbulence, and weak turbulence using LN and GG distributions $G = 30.6$ dB, $D_{RX} = 4$ mm and (a) $r = \infty$, $B_0 = 76$ GHz, (b) $r = \infty$, $B_0 = 20$ GHz	91
Figure 5.5	Atmospheric turbulence induced power penalty vs. Rytov variance for OOK-NRZ FSO modelled using GG distribution with (a) low-gain optical preamplifier ($G = 8.8$ dB) and (b) high-gain optical preamplifier ($G = 30.6$ dB). Note that these are theoretical values and in practice BER of 10^{-12} will not be obtainable under high Rytov variance conditions	93
Figure 6.1	Illustration of DPPM frames for $M = 4$ ($n = 2^4 = 16$ slots)	100
Figure 6.2	Optically preamplified FSO receiver	101
Figure 6.3	AA factor vs. RCL diameter for $l=1500$ m	109
Figure 6.4	BER vs. average power at receiver collecting lens (RCL) input (dBm) using $M = 5$, $l=1500$ m, $D_{RX} = 1$ mm, 20 mm and 50 mm for NT and WT with AA (a) $G = 8.8$ dB and (b) $G = 30.6$ dB	111
Figure 6.5	BER vs. average power at receiver collecting lens (RCL) input (dBm) using $M = 5$, $l=1500$ m, $D_{RX} = 1$ mm, 20 mm and 50 mm for NT and MT with AA (a) $G = 8.8$ dB and (b) $G = 30.6$ dB	113
Figure 6.6	BER vs. average power at receiver collecting lens (RCL) input (dBm) using $M = 5$, $l=1500$ m, $D_{RX} = 1$ mm, 20 mm and 50 mm for NT and ST with AA (a) $G = 8.8$ dB and (b) $G = 30.6$ dB	114
Figure 6.7	BER vs. average power at receiver collecting lens (RCL) input (dBm) using $M = 5$, $l=1500$ m and 2000 m, $G = 30.6$ dB, $D_{RX} = 1$ mm for NT and WT, MT and ST, all with AA	115
Figure 6.8	Receiver sensitivity (dBm) vs. DPPM coding level M at BER of 10^{-9} using $G = 30.6$ dB, $l=1500$ m, $D_{RX} = 1$ mm, 20 mm and 50 mm for NT and (a) WT, (b) MT and (c) ST, all with AA	117
Figure 6.9	BER vs. average power at receiver collecting lens (RCL) input (dBm) for DPPM and OOK using MCB, while $M = 5$, $l=1500$ m, $G = 30.6$ dB, and $D_{RX} = 20$ mm for NT and (a) WT (b) MT (c) ST, all with AA	119
Figure 7.1	The direct detection optically preamplified FSO receiver. Decision circuit is thresholded for OOK-NRZ and a comparison over slots in frame for DPPM	126
Figure 7.2	MCB BER as a function of average transmitted optical power (dBm) for normalized PE standard deviation	137

	$\sigma_{PE}/r_{RX} = 0.1, 3 \text{ \& } 5, M = 5, G = 30\text{dB}$ for NT with GS, WT only (with GS, no PE) and combined WT, PE and GS (a) $D_{RX} = 25 \text{ mm}$ ($w_z/r_{RX} = 30$) (b) $D_{RX} = 50 \text{ mm}$ ($w_z/r_{RX} = 15$)	
Figure 7.3	MCB BER as a function of average transmitted optical power (dBm) for normalized PE standard deviation $\sigma_{PE}/r_{RX} = 0.1, 3 \text{ \& } 5, M = 5, G = 30\text{dB}$ for NT with GS, MT only (with GS, no PE) and combined MT, PE and GS (a) $D_{RX} = 25 \text{ mm}$ ($w_z/r_{RX} = 30$) (b) $D_{RX} = 50 \text{ mm}$ ($w_z/r_{RX} = 15$)	138
Figure 7.4	MCB BER as a function of average transmitted optical power (dBm) for normalized PE standard deviation $\sigma_{PE}/r_{RX} = 0.1, 3 \text{ \& } 5, M = 5, G = 30\text{dB}$ for NT with GS, ST only (with GS, no PE) and combined ST, PE and GS (a) $D_{RX} = 25 \text{ mm}$ ($w_z/r_{RX} = 30$) (b) $D_{RX} = 50 \text{ mm}$ ($w_z/r_{RX} = 15$)	139
Figure 7.5	Required optical power (dBm) at MCB BER of 10^{-9} as a function of the DPPM coding level ($M = 1-5$) for NT with GS, WT only with GS, and combined WT, PE and GS using $\sigma_{PE}/r_{RX} = 3 \text{ \& } 5$, and $D_{RX} = 50 \text{ mm}$ ($w_z/r_{RX} = 15$). Also shown are the corresponding powers for OOK-NRZ	140
Figure 7.6	Required optical power (dBm) at MCB BER of 10^{-9} as a function of the DPPM coding level ($M = 1-5$) for NT with GS, MT only with GS, and combined MT, PE and GS using $\sigma_{PE}/r_{RX} = 3 \text{ \& } 5$, and $D_{RX} = 50 \text{ mm}$ ($w_z/r_{RX} = 15$). Also shown are the corresponding powers for OOK-NRZ	141
Figure 7.7	Required optical power (dBm) at MCB BER of 10^{-9} as a function of the DPPM coding level ($M = 1-5$) for NT with GS, ST only with GS, and combined ST, PE and GS using $\sigma_{PE}/r_{RX} = 3 \text{ \& } 5$, and $D_{RX} = 50 \text{ mm}$ ($w_z/r_{RX} = 15$). Also shown are the corresponding powers for OOK-NRZ	141
Figure 7.8	DPPM and OOK BER as a function of average transmitted optical power (dBm) for normalized PE standard deviation $\sigma_{PE}/r_{RX} = 3, M = 5, G = 30 \text{ dB}$, $D_{RX} = 25 \text{ mm}$ ($w_z/r_{RX} = 30$) for NT with GS, WT only (with GS, no PE) and combined WT, PE and GS, using SPA and MCB	142
Figure 7.9	DPPM and OOK BER as a function of average transmitted optical power (dBm) for normalized PE standard deviation $\sigma_{PE}/r_{RX} = 3, M = 5, G = 30 \text{ dB}$, $D_{RX} = 25 \text{ mm}$ ($w_z/r_{RX} = 30$) for NT with GS, MT only (with GS, no PE) and combined MT, PE and GS, using	143

	SPA and MCB	
Figure 7.10	DPPM and OOK BER as a function of average transmitted optical power (dBm) for normalized PE standard deviation $\sigma_{PE}/r_{RX} = 3$, $M = 5$, $G = 30$ dB, $D_{RX} = 25$ mm ($w_z/r_{RX} = 30$) for NT with GS, ST only (with GS, no PE) and combined ST, PE and GS, using SPA and MCB	143
Figure 7.11	Power penalty (dB) (relative to NT with GS) as a function of normalized PE standard deviation σ_{PE}/r_{RX} using $M = 5$ (DPPM only), $G = 30$ dB for WT, MT and ST (all with GS) (a) $D_{RX} = 25$ mm ($w_z/r_{RX} = 30$) (b) $D_{RX} = 50$ mm ($w_z/r_{RX} = 15$)	145
Figure 8.1	Schematic representation of a WDM network using FSO link for the final distribution stage, with optical amplifier located at remote node (case A) or at OLT demux input (case B). ONUs will be distributed at different angles around the remote node	153
Figure 8.2	Probability density functions in the presence of one interchannel crosstalk of similar type to the signal. Data pattern here is 1010, crosstalk pattern is 0110	158
Figure 8.3	BER versus average received signal optical power (dBm) for WT and ST (no amplifier) (a) $C_{XT} = 30$ dB (b) $C_{XT} = 15$ dB	163
Figure 8.4	BER versus average received signal optical power (dBm) for WT and ST ($G=30$ dB) (a) $C_{XT} = 30$ dB (b) $C_{XT} = 15$ dB	164
Figure 8.5	Downstream required transmitted optical power (dBm) at target BERs of 10^{-12} and 10^{-6} as a function of the FSO link length (m) for no interferer and single interferer cases (a) $L_{demux,XT} = 30$ dB and (b) $L_{demux,XT} = 15$ dB. OA was at the remote node (Case A)	172
Figure 8.6	Downstream required transmitted optical power (dBm) at target BERs of 10^{-12} and 10^{-6} as a function of the transmitter divergence angle (rad) with $l_{fso} = 1000$ m for no interferer and single interferer cases (a) $L_{demux,XT} = 30$ dB and (b) $L_{demux,XT} = 15$ dB. OA was at the remote node (Case A)	174
Figure 8.7	Upstream required transmitted optical power (dBm) at target BERs of 10^{-12} and 10^{-6} as a function of the FSO link length (m) with equal signal and interferer FSO link lengths, $L_{demux,XT} = 30$ dB for no interferer and single cases	175
Figure 8.8	Upstream required transmitted optical power (dBm) at target BERs of 10^{-12} and 10^{-6} as a function of the transmitter divergence angle (rad) for no interferer and	176

single interferer cases with $l_{fso} = 1000$ m and $L_{demux,XT} = 30$ dB

Figure 8.9 Upstream required transmitted optical power (dBm) at target BERs of 10^{-12} and 10^{-6} as a function of the FSO link lengths for signal and interferer (m) for the single interferer case with $L_{demux,XT} = 15$ dB 178

Figure 8.10 Upstream required transmitted optical power (dBm) (under the assumption of a power control algorithm that ensures the average power at the RCL or OLT for each signal is fixed) at target BERs of 10^{-12} and 10^{-6} as a function of the FSO link lengths for signal and interferer (m) for the single interferer case with $L_{demux,XT} = 15$ dB 180

List of Tables

Table 2.1	Laser safety classifications for a point-source emitter (based on IEC60825-1, Amendment 2) adapted from [46]	16
Table 2.2	MPE (in mW/cm^2) for FSO wavelengths of 850 nm and 1550 nm [6]	17
Table 2.3	Typical LED materials, their wavelengths and bandgap energy [4]	18
Table 2.4	Comparison of surface and edge emitting LEDs [7]	19
Table 2.5	Band gap energies and cutoff wavelengths for different semiconductor materials [1]	32
Table 3.1	Typical atmosphere particles, their radius range and concentration [4]	38
Table 3.2	Classification of pointing error [18]	55
Table 5.1	Commonly used atmospheric turbulence model	78
Table 5.2	Typical parameters for characterising weak -to-saturated turbulence regimes [19, 36]	78
Table 5.3	Parameter values used for the numerical results	84
Table 6.1	Parameters used in calculations	107
Table 7.1	Parameter values for calculation	133
Table 8.1	List of key parameters used in the calculation for both transmissions	169

CHAPTER 1 Introduction

1.1 Historical perspective

The transmission of light through the air has a long history. Some examples include the use of polished metal plates as sunlight reflectors by ancient Romans and Greeks for long haul signalling, the use of fire beacons and smoke fire by Chinese and American Indians also for signalling, and the use of a sunlight powered device by the U.S. military to send telegraph information between mountain tops in the early 1800's [1]. Another example of early through-the-air optical communications is the development of the optical telegraph, by Lesuerre during the Franco-Prussian War (1870-1871). The optical telegraph was used to send coded signals over long distances with the aid of sunlight (during the day) or oil lamps (during the night), and telescope. The commonly referred to first demonstration of through-the-air optical transmission is the experimental work of Alexander Graham Bell in 1880 known as the Photophone [2, 3]. In this experiment, he transmitted spoken word, with the aid of solar radiation, over a length of about 200 m by using primitive devices such as a flexible reflective membrane, a parabolic reflector, and a photoconductive selenium cell as receiver.

Following this, enhanced optical communication has been fuelled by the invention of electronic devices such as transistors, vacuum tubes and integrated circuits, light emitting diodes and notably Light Amplification by Stimulated Emission of Radiation in the 1960's by Theodore Maiman at the Hughes Research Laboratories, California [3-5]. After the advent of the laser, initial developments in optical communications were performed mainly in military and space laboratories. Some of the laboratory demonstrations carried-out in the 1960s and 1970s include long distance laser communications in Hughes research laboratories using helium-neon (He-Ne) laser excited by a high frequency radio transmitter, a high-pass filter and a photomultiplier detector [3]. Laser was first used for TV transmission by the North American Aviation research group [3].

The initial enthusiasm for applying laser for through-the-air communications purposes was soon dispelled due to the following reasons: the adverse conditions that characterise the atmospheric channel, the need for more research and development of better optical components, the need for line of sight and the development of effective pointing and tracking mechanisms, and ultimately though, due to the development of the optical fibre.

1.2 Background

The global increase in demand for broadband communications has led to the development of new and enabling technologies to support the conventional methods such as the coaxial cable, copper, microwave and radio frequency (RF) systems. Free-space optical (FSO) communications has benefited from the developments in optoelectronics and can be a key technology for achieving cost-effective high-speed optical links.

FSO communications, also referred to as optical wireless or through-the-air optical communications, typically entails transmitting information-bearing near-infrared light through the air between two or more transceivers. The majority of FSO communication systems use windows of 780-850 nm and 1520-1600 nm [6-9], although the 1550 nm wavelength is arguably the most attractive for reasons including the low absorption characteristic of air in this wavelength, and the availability of more transmittable optical power compared to the 800 nm wavelength under the eye safety standards [9, 10].

FSO communications can be classified into various forms based on the optical link length such as applications for chip-level and board-level optical interconnects (with a range of micrometres), for indoor communications (with range of a few metres), for terrestrial communications such as between tall buildings, between end-users and fibre optic backbone, and as a backup link for optical fibre (with range of a few kilometres), for satellite communications e.g. bi-directional links between high altitude platforms, and between ground station and satellite (with range of up to thousands of kilometres) [4, 6, 7, 9].

FSO communications offer several advantages over the existing RF and microwave systems, such as greater information capacity (up to 300 THz, for a wavelength of 1 μm , compared to the 300 GHz of the microwaves and 300 GHz of the radio waves) [6, 9, 11], the compactness of the transmitter and receiver design as well as the low power consumption (due to the short optical wavelength), the nonexistence of spectrum licensing for frequencies above 300 GHz, and the improved security due to the narrow FSO laser beam [4, 6, 7, 9]. The relatively low overall cost and ease of deployment are the advantages FSO systems offer over the optical fibre systems which have additional costs from optical fibre cable, right of way and trenching [7, 11, 12].

The primary factors limiting the performance of FSO communication systems are linked to the short wavelengths of the optical system and they include atmospheric attenuation in form of scattering and absorption, and optical scintillation. There is an inverse relationship between the attenuation and scintillation effects, for example it is practically impossible to have a strong turbulence effect in severe fog conditions [9, 13]. Attenuation is caused by gas molecules such as water vapour, CO_2 , CH_4 , and particulates such as fog, haze, clouds and smoke suspended in the atmosphere resulting in reduction of the received optical power whilst scintillation introduces random fluctuations in both amplitude and phase of the optical signal at the detector [4, 6, 7, 9, 14-19]. The turbulence-induced scintillation period for FSO communication systems are usually in the order of milliseconds [10, 12, 17, 18].

In addition to the atmospheric effects, FSO communication systems can also be affected by pointing errors due to weak earthquakes, strong winds, and thermal expansion and cooling, resulting in misalignment of the transceivers, and, consequentially, degradation of the FSO communication system performance [15, 20-23]. Laser safety is an important requirement for design of FSO communication systems as potential exposure to high power laser beams can cause damage to the eyes or skin if the transmitter is operated above safety standards. According to the American National Standards Institute (ANSI), the maximum permissible exposure (MPE) at

wavelength of 1550 nm should be about 100 mW/cm^2 for a 10 s eye exposure [9, 15].

Optical amplifiers have become integral components for optical communication systems as a means of extending the system link length and reducing the required optical power in an optically preamplified receiver case. The price to be paid for the amplification process is the generation of additional noise types namely the signal-spontaneous beat noise and spontaneous-spontaneous beat noise during the process of converting the optical signal into photocurrent. The amplified spontaneous emission (ASE) accompanying the amplified optical signal can be classified as Gaussian, although it manifests as non-Gaussian beat noises in the electrical domain. The traditional evaluation method for describing the signal and noise behaviour in an optically preamplified FSO and fibre systems is the Gaussian approximation (GA). The GA is deficient as it is based only on the mean and variance and as such, to improve accuracy, it should be replaced with a more comprehensive method for describing the signal and noise behaviour at the receiver, such as the moment generating function (MGF)-based techniques, namely the Chernoff bound (CB), modified Chernoff bound (MCB), and saddlepoint approximation (SPA) [24-26].

Several atmospheric models have been reported in the literature [4, 6, 7, 9, 17, 24, 27] for characterising weak-, medium-, and strong turbulence conditions. The commonly reported model is the lognormal distribution, which is only used to characterise weak turbulence conditions since the multiple scattering which occurs in strong turbulence regimes is not accounted for by the lognormal approximation [6]. Moreover, the lognormal probability density function (pdf), when compared with experimental results, is proven to underestimate the behaviour of the optical signal at its peak and extreme tails, and since the bit error rate (BER) calculations depend on the accuracy of the pdf tails, the results obtained using this model should be treated with caution. The gamma-gamma model has gained much popularity, as it can be applied for characterising weak-to-strong turbulence conditions, and its pdf is close to experimental results [6, 27]. Other commonly used models are the K distribution, which is used for the strong

turbulence only and the negative exponential distribution, which is used for saturated turbulence regimes [6, 9, 24-29].

The on-off keying (OOK) modulation scheme is the most popular for commercial FSO and fibre systems due to the simplicity of the transceiver hardware [4, 9-11]. However, the draw-back for standard OOK-based FSO systems is the requirement of adaptive thresholds for optimum performance over an unstable atmospheric channel. Another modulation scheme which is well established in deep space FSO systems [30, 31], and applicable for terrestrial FSO systems, is the digital pulse position modulation (DPPM) scheme. In comparison to the OOK scheme, the DPPM is advantageous in terms of power efficiency, but at the expense of a more complex system (arising from the symbol and slot synchronization), and additional bandwidth requirements. Also, DPPM reception can be implemented without a decision threshold.

A passive optical network (PON)-like wavelength division multiplexing (WDM) access network, using FSO communications as a distribution link, is proposed in this thesis. The implications of using OOK-NRZ signalling over a turbulent FSO communications-based WDM network, with the placement of an optical amplifier at the head end and the inclusion of interchannel crosstalk, is theoretically investigated for upstream and downstream transmissions. In the upstream, the atmospheric turbulence and crosstalk combine in a problematic way, resulting in increased power requirements to achieve the target BERs.

This thesis provides a comprehensive treatment and analysis of the performance of terrestrial FSO communication systems corrupted by various impairments such as atmospheric turbulence, ASE noise, pointing error and optical crosstalk, in form of BERs, required optical powers and power penalties, using OOK non-return-to-zero (NRZ) and DPPM schemes.

1.3 Organisation of thesis

This thesis consists of eight further chapters, besides this introduction chapter. The next chapter presents a general overview of the fundamental characteristics and performance of the optical sources, modulation formats

(with main focus on OOK-NRZ and DPPM schemes), optical amplifiers (and associated noises), and photodetectors which are applicable in FSO communication systems. This chapter also reviews the laser safety standards with particular reference to eye safety. In chapter 3, the factors that can affect the smooth performance of FSO communication systems are reviewed. The pdfs used in this thesis for modelling the turbulence effects on optical signals traversing the atmospheric channel are discussed in some detail. The receiver impairments, such as optical amplifier noises, electrical noises, and optical crosstalk, are discussed in chapter 4. The performance evaluation methods used in the thesis, namely the GA, CB, MCB and SPA methods, are discussed. In chapter 5, numerical results and analysis, using the different pdfs models and evaluation methods discussed in earlier chapters, for an OOK-NRZ based-FSO communication system experiencing atmospheric turbulence and ASE noise are provided. The performance of a DPPM-based FSO communication system using a GG pdf, and similar improved evaluation methods, were investigated in chapter 6. The numerical results are presented to reveal the system performance dependence on atmospheric turbulence, ASE noise, optical link length, and aperture diameter. A combined performance analysis of chapter 5 and 6 impairments, using OOK-NRZ and DPPM modulation formats, with the inclusion of pointing error and beam divergence effects, is presented in chapter 7. A wavelength division multiplexing (WDM)-based network impaired by interchannel crosstalk and ASE noise, and using FSO communications in the distribution link, is proposed in chapter 8. Chapter 9 concludes the whole thesis and describes the future work that could be performed in the subject.

1.4 New contributions to knowledge

This thesis studies the use of optical amplifiers in a preamplifier configuration to increase the average power efficiency at the FSO system receiver and to reduce the impact of the thermal noise effect that is associated with electrical amplification. Unfortunately, the operating mode of the optical amplifier generates an additional noise type known as the

ASE noise, which is Gaussian in the optical domain. At the PIN photodiode, the ASE noise beats with the optical signal and itself to form the signal-spontaneous and spontaneous-spontaneous beat noises, respectively. In FSO communication systems literature [10, 32, 33], these beat noises have been generally treated as Gaussian due to the simplicity of the GA method, even though they are not really Gaussian. Moreover, GA calculations are based on the first order statistics (i.e. the mean and variance) of the sampled received data. Just as there was for fibre communications there is a need for a more robust statistical analysis of the total signal and noise behaviour for an optically preamplified FSO system such as the application of MGF-based CB and MCB. This motivated the writing of a paper entitled: '*Improved BER Evaluation for Optically preamplified Free-space Optical Communication Systems in Turbulent Atmosphere*'. This paper has been published in *IET Optoelectronics* [24] and it forms the basis of chapter 5. The presence of turbulence created additional complexity, relative to the optical fibre case, in applying the MCB, CB and SPA. The implication of this is that the tightest bound is obtained by finding the optimum value for the s parameter (in the MGF formulation) which would be recalculated for each irradiance fluctuation. The overall BER is obtained by averaging the product of BER and turbulence pdf over the fluctuating mean irradiance for the bit stream at a particular time. The results, for no turbulence and the whole range of turbulence conditions considered, show that the GA, MCB and SPA methods give approximately the same BER values for a low gain optical amplifier ($G = 8.8$ dB), while the CB differs in having high BER values. In the high gain optical amplifier case ($G = 30.6$ dB), the SPA gives the lowest BER, followed by the GA, while the MCB and CB have higher but similar BERs. Although the GA is seen to fall below the bounds in the high gain case, on varying the system parameters, for example using an infinite extinction ratio and optical bandpass filter bandwidths of 76 GHz and 20 GHz, the results show that the GA exceeds the bounds at high powers (and thus is demonstrably less accurate). The MCB is easier to calculate than the SPA, whilst the GA has the simplest formulation of the four methods, as it uses two moments. The results in this thesis suggests that the MCB method should be considered for practical optically-amplified

FSO receiver modelling, since it has the advantage of being a tighter (compared to the CB) upper bound on the BER. Finally, the GG pdf represents a sensible approach for modelling the whole range of turbulence conditions.

The DPPM format represents an interesting way of enhancing the receiver sensitivity of a FSO communication system, and it has been studied for terrestrial FSO communication [9, 34, 35]. Furthermore, the use of aperture averaging for reducing the effect of atmospherically induced scintillation has been proposed in literature, and has also been investigated in this thesis. The use of fuller statistical methods such as the CB and MCB mentioned earlier (and comparison with the traditional GA) for optically preamplified FSO receiver systems, the potential improvement in receiver sensitivity offered by the DPPM format, and the reduction in BER that can be achieved through aperture averaging have motivated the writing of the second paper entitled: '*Performance Evaluation of Optically Preamplified DPPM Turbulent Free-space Optical Communication Systems*'. This paper has been published in *IET Optoelectronics* [36] and it forms the basis of chapter 6. The MCB is developed for the first time for any type of optically preamplified DPPM-based system. The predicted results at a binary data rate of 2.5 Gbps and wavelength of 1.55 μm suggest that the optically preamplified DPPM-based FSO system offers a sensitivity benefit of about 7-9 dB at a BER of 10^{-9} (depending on the turbulence level) compared with an equivalent OOK-NRZ- FSO system. The sensitivity curve indicate that optically preamplified DPPM-based FSO system offers sensitivity at BER of 10^{-9} (about 21.5 photons/bit using MCB) better than the fundamental limit of an optically preamplified OOK-NRZ system (~38 photons/bit) in the non-turbulent atmospheric condition. The aperture-averaging method is seen to give significant reduction in BER especially in the strong turbulence condition. This can be linked to the levelling effect which occurs when the receiver collecting lens diameter falls between the spatial coherence radius and the scattering disk. Finally, the DPPM-based MCB method is seen to give the best BER estimation, as it is exceeded by

the GA in the high optical amplified gain case, while the CB gives looser bounds in low optical amplifier gain.

One of the main problems for FSO communication systems are the issues of pointing and tracking errors which arise due to mechanical vibrations or natural phenomena (e.g. strong winds, thermal expansion and weak earthquakes). This problem has been studied together with the atmospheric scintillation effects for clean air atmosphere in the literature [21, 23, 37]. The combined pointing error and turbulence effect has been investigated for optically preamplified DPPM and OOK-NRZ-FSO systems, assuming a clean atmosphere situation. A third paper entitled: ‘*DPPM FSO Communication Systems Impaired by Turbulence, Pointing Error and ASE Noise*’ was presented at the International Conference of Transparent Optical Networks (ICTON) 2012 [38], and it forms the basis of chapter 7. The results show how the inclusion of pointing error and beam spreading loss increases the power penalty of the optically preamplified FSO system. The results also indicate that increasing the RCL diameter at a particular beam width further increases the system power penalty due to combined turbulence, beam spreading and pointing error. The DPPM-based FSO system offers sensitivities significantly greater than an equivalent OOK-NRZ-based system in all turbulence conditions. Although the SPA gives a slightly lower BER compared to the MCB, the MCB still represents a more optimistic result, since it has the advantage of being an upper bound on the BER.

A comprehensive system design and performance evaluation for a WDM optical access network (a PON variant), using FSO communication for the distribution network, has been proposed. The aim of this design is to provide a high-speed optical access network in terrains where installation of optical fibre for conventional PON might be considered impractical or too expensive. The analysis includes the interchannel crosstalk effect (which is natural in WDM networks), the ASE noise, air-fibre coupling loss, beam spreading loss and the atmospheric turbulence effect. These impairments combine in a problematic way, which, to the best of the author’s knowledge, have not been addressed previously. In the upstream

transmission, there is a turbulence-accentuation of the crosstalk which results in higher required transmit power, bit error rate floors and less achievable FSO transmission distance compared to the downstream transmission. A fourth paper entitled: ‘*WDM Free-Space Optical Network with Turbulence-accentuated Interchannel Crosstalk*’ has been submitted to *Journal of Optical Communications and Networking*, and it is still under review. It forms the basis of chapter 8.

1.5 References

- [1] O. Bouchet, H. Sizun, C. Boisrobert, F. DeFornel, and P. Favennec, *Free-space optics: propagation and communications*, Wiley-ISTE Limited, London, 2006.
- [2] A. G. Bell, "Upon the production and reproduction of sound by light," *Journal of the Society of Telegraph Engineers*, vol. 9, pp. 404-426, 1880.
- [3] F. E. Goodwin, "A review of operational laser communication systems," *Proceedings of the IEEE*, vol. 58, pp. 1746-1752, 1970.
- [4] D. O. Caplan, "Laser communication transmitter and receiver design," *Journal of Optical Fibre Communication Report*, vol. 4, pp. 225-362, 2007.
- [5] J. M. Senior, *Optical fibre communications: principles and practice*, Third Edition, Pearson Education Limited, Essex, England, 2009.
- [6] L. C. Andrews and R. L. Phillips, *Laser beam propagation through random media*, Second Edition, SPIE Press, Bellingham, Washington, 2005.
- [7] S. Karp, R. M. Gagliardi, S. E. Moran, and L. B. Stotts, *Optical channels: fibers, clouds, water and the atmosphere*, New York: Plenum Press, 1988.
- [8] D. Killinger, "Free space optics for laser communication through the air," *Optics and Photonics News*, vol. 13, pp. 36-42, Oct. 2002.
- [9] A. K. Majumdar, "Free-space laser communication performance in the atmospheric channel," *Journal of Optical and Fiber Communications Research*, vol. 2, pp. 345-396, 2005.
- [10] M. Razavi and J. H. Shapiro, "Wireless optical communications via diversity reception and optical preamplification," *IEEE Transactions on Wireless Communications*, vol. 4, no. 3, pp. 975-983, May 2005.
- [11] H. A. Willebrand and B. S. Ghuman, *Free-space optics: enabling optical connectivity in today's networks*, Sams Publishing, Indianapolis, Indiana 46240 USA, 2002.
- [12] T. H. Carbonneau and D. R. Wisely, "Opportunities and challenges for optical wireless; the competitive advantage of free space telecommunications links in today's crowded marketplace," *Proc.*

- SPIE Wireless Technologies and Systems: Millimeter-Wave and Optical*, vol. 3232, pp. 119-128, Jan. 1998.
- [13] D. Bushuev and S. Arnon, "Analysis of the performance of a wireless optical multi-input to multi-output communication system," *J. Opt. Soc. Amer. A, Opt. Image Sci.*, vol. 23, no. 7, pp. 1722-1730, 2006.
- [14] L. C. Andrews, R. L. Phillips, C. Y. Hopen, and M. A. Al-Habash, "Theory of optical scintillation," *J. Opt. Soc. Am. A*, vol. 16, no. 6, pp. 1417-1429, 1999.
- [15] S. Bloom, E. Korevaar, J. Schuster, and H. A. Willebrand, "Understanding the performance of free-space optics," *Journal of Optical Networking*, vol. 2, pp. 178-200, June 2003.
- [16] W. Popoola, Z. Ghassemlooy, M. S. Awan, and E. Leitgeb, "Atmospheric channel effects on terrestrial free space optical communication links," *ECAI International Conference - 3rd Edition, Pitesti, Romania*, pp. 17-23, 3-5 July 2009.
- [17] X. Zhu and J. M. Kahn, "Free-space optical communication through atmospheric turbulence channels," *IEEE Transactions on Communications*, vol. 50, no. 8, pp. 1293-1300, Aug. 2002.
- [18] D. Heatly, D. R. Wisely, I. Neild, and P. Cochrane, "Optical wireless: The story so far," *IEEE communications magazine*, vol. 32, no. 12, pp. 72-82, Dec. 1998.
- [19] K. A. Winick, "Atmospheric turbulence-induced signal fades on optical heterodyne communication links," *Applied Optics*, vol. 25, no. 11, pp. 1817-1825, June 1986.
- [20] S. Arnon, "Optimization of urban optical wireless communication systems," *IEEE Transactions on Wireless Communications*, vol. 2, no. 4, pp. 626-629, 2003.
- [21] A. A. Farid and S. Hranilovic, "Outage capacity optimization for free-space optical links with pointing errors," *Journal of Lightwave Technology*, vol. 25, no. 7, pp. 1702-1710, 2007.
- [22] W. Gappmair, S. Hranilovic, and E. Leitgeb, "Performance of PPM on terrestrial FSO links with turbulence and pointing errors," *IEEE Communications Letters*, vol. 14, no. 5, pp. 468-470, 2010.
- [23] H. G. Sandalidis, T. A. Tsiftsis, G. K. Karagiannidis, and M. Uysal, "BER performance of FSO links over strong atmospheric turbulence channels with pointing errors," *IEEE Communications Letters*, vol. 12, no. 1, pp. 44-46, 2008.
- [24] A. O. Aladeloba, A. J. Phillips, and M. S. Woolfson, "Improved bit error rate evaluation for optically pre-amplified free-space optical communication systems in turbulent atmosphere," *IET Optoelectronics*, vol. 6, no. 1, pp. 26-33, Feb. 2012.
- [25] J. O'Reilly and J. R. F. Da Rocha, "Improved error probability evaluation methods for direct detection optical communication systems," *IEEE Transactions on Information Theory*, vol. 33, no. 6, pp. 839-848, Nov. 1987.
- [26] L. F. B. Ribeiro, J. R. F. Da Rocha, and J. L. Pinto, "Performance evaluation of EDFA preamplified receivers taking into account intersymbol interference," *Journal of Lightwave Technology*, vol. 13, no. 2, pp. 225-232, Feb. 1995

- [27] M. A. Al-Habash, L. C. Andrews, and R. L. Phillips, "Mathematical model for the irradiance probability density function of a laser beam propagating through turbulent media," *Opt. Eng.*, vol. 40, no. 8, pp. 1554-1562, Aug. 2001.
- [28] L. C. Andrews and R. L. Phillips, "Mathematical genesis of the I-K distribution for random optical fields," *J. Opt. Soc. Am. A*, vol. 3, no. 11, pp. 1912-1919, 1986.
- [29] Z. Ghassemlooy, W. O. Popoola, and E. Leitgeb, "Free-space optical communication using subcarrier modulation in gamma-gamma atmospheric turbulence," *9th International Conference on Transparent Optical Networks, Rome, Italy*, vol. 13, pp. 156-160, July 2007.
- [30] J. R. Lesh, J. Katz, H. H. Tan, and D. Zwillinger, "2.5 bit/detected photon demonstration program, analysis and phase I results," *TDA Progress Rep., Jet propulsion Laboratory, Pasadena, CA*, pp. 115-132, Oct.1981.
- [31] A. Biswas, V. Vilnrotter, W. Farr, D. Fort, and E. Sigman, "Pulse position modulated ground receiver design for optical communications from deep space," *Proc. SPIE, San Jose, CA*, vol. 4635, pp. 224-235, Jan. 2002.
- [32] N. A. Olsson, "Lightwave systems with optical amplifiers," *Journal of Lightwave Technology*, vol. 7, no. 7, pp. 1071-1082, July 1989.
- [33] Y. Yamamoto, "Noise and error rate performance of semiconductor laser amplifiers in PCM-IM optical transmission systems," *IEEE Journal of Quantum Electronics*, vol. 16, no. 10, pp. 1073-1081, Oct. 1980.
- [34] K. Kaisaleh, "Performance analysis of free-space on-off-keying optical communication systems impaired by turbulence," *Proc. SPIE*, vol. 4635, pp. 150-161, 2002.
- [35] S. S. Muhammad, W. Gappmair, and E. Leitgeb, "PPM channel capacity evaluation for terrestrial FSO links," *Proceedings of the 2006 International Workshop on Satellite and Space Communications*, pp. 222-226, 14-15 Sept. 2006.
- [36] A. O. Aladeloba, A. J. Phillips, and M. S. Wolfson, "Performance evaluation of optically preamplified digital pulse position modulation turbulent free-space optical communication systems," *IET Optoelectronics*, vol. 6, no. 1, pp. 66-74, Feb. 2012.
- [37] D. K. Borah and D. G. Voelz, "Pointing error effects on free-space optical communication links in the presence of atmospheric turbulence," *Journal of Lightwave Technology*, vol. 27, no. 18, pp. 3965-3973, Sept. 2009.
- [38] A. O. Aladeloba, A. J. Phillips, and M. S. Wolfson, "DPPM FSO communication systems impaired by turbulence, pointing error and ASE noise," *14th International Conference on Transparent Optical Networks (ICTON), Coventry, UK*, pp. 1-4, 2-5 July 2012.

CHAPTER 2 Basic components of FSO communication systems

2.1 Overview

This chapter presents the different types of transmitter and receiver designs that are particularly used for FSO communication systems. The fundamental characteristics and mode of operation of the optical sources, modulators, optical amplifiers and detectors are also reviewed. The amplifier noises that accompany an optically amplified signal are also discussed as their introduction, during conversion of the signal to current at the photodetector, have severe effects on the system signal-to-noise ratio. While there are many modulation possibilities for FSO communications, the on-off keying and digital pulse position modulation formats are the main focus of this thesis and they are introduced in this chapter.

2.2 Transmitter system

The essential components of a transmitter system are the optical source, the modulator, the driver circuit and the transmitter optics. The main function of the transmitter is to provide optical signal into the communication channel (i.e. the atmosphere) at sufficient power level, and with sufficient signal quality that would enable it to traverse the channel and have data recovered at the receiver. Lasers are the most important light sources for outdoor FSO communications, whilst the light emitting diodes (LEDs) are used where low data rates and short haul communications are required, such as indoor FSO systems. Modulation of the light beam can be achieved by direct modulation, which involves changing the optical source current in sympathy with the data, and the external modulation, which involves using an external modulator e.g. Mach-Zehnder interferometer after the light source to adjust the light properties in sympathy with the data. The external modulation approach is obviously more expensive than the direct modulation, but it gives better extinction ratio and minimizes chirp.

The consequences of chirp include increased dispersion penalties, limited extinction ratio (~10 dB), and degradation of receiver sensitivity [8]. Due to these limitations, except for dispersion penalties, direct modulation is generally not a preferable approach for FSO communications.

2.2.1 Semiconductor lasers

The term *laser* was originally an acronym for “light amplification by stimulated emission of radiation” but has now passed into general use. It is an optical gain medium placed within a resonant optical cavity which causes it to oscillate via positive feedback. Semiconductor lasers use semiconductors as the gain medium, they have compact sizes which make them very easy to fabricate, they have high conversion efficiency and are capable of providing optical output powers between 0 and 20 dBm [1, 2]. Furthermore, semiconductor lasers emit a coherent, near-monochromatic (if single longitudinal mode), and highly directional light beam. These features make semiconductors very popular as a light source for optical communication systems.

Examples of semiconductor lasers include Fabry-Perot lasers, Vertical cavity surface emitting lasers (VCSELs), distributed Bragg reflectors (DBR), and distributed feedback (DFB) lasers. Fabry-Perot lasers are the simplest type of semiconductor laser. The gain medium is between two highly reflective facets which are planar and parallel to each other. Fabry-Perot lasers usually emit several longitudinal modes and are therefore not popular sources for high performance FSO communications. Fabry-Perot lasers operate with wavelength within 1300-1500 nm, have long life span, low eye safety criteria, typical output power of about 28 mW, and are used typically for short distance communication applications [3].

The DFB lasers have both the feedback region and gain region combined, while the DBR lasers have Bragg reflectors at either end of the gain medium. Both the DFB and DBR lasers can be designed to ensure that only one wavelength oscillates. DFB lasers are more popular in current high speed (up to 40 Gbps [3]) and long distance optical communication systems, despite being more complex to fabricate and thus relatively more expensive

than Fabry-Perot lasers. Semiconductor (InGaAs/InP) DFB and DBR lasers have an operating wavelength of 1550 nm and excellent life span [3]. They are compatible with erbium-doped amplifiers (EDFAs) and can achieve output signal power between 1-2 W when amplified [3].

Vertical cavity surface-emitting lasers also have the single longitudinal mode due to their sufficiently small cavity length. VCSELs are relatively cheap to manufacture due to their small size which also makes them easily integrated into multiwavelength arrays. They have reasonable good output powers of several milliwatts, and are capable of operating at speeds of up to 10 Gbit/s. Commercial VCSELs operating at wavelengths of 850 nm already exist, while 1300 nm VCSELs are now commercially available [1-3]. The main disadvantages of VCSELs are that they are not capable of operating at room temperature, and they require very high mirror reflectivities for the laser oscillation to occur [1, 2].

2.2.2 Laser safety and standards

One of the key things to be considered in designing a FSO communication system is the laser safety standards. High power laser beams are capable of damaging the skin, and eye (which is dependent on the wavelength, as shown in Fig. 2.1, and has light focussing ability). Several countries have regulatory bodies that develop standards for lasers sold within their domain. Examples of laser safety standards organisations include the American National Standards Institute (ANSI), the International Electrotechnical Commission (IEC), and the European Committee for Electrotechnical Standardization (CENELEC) [3-5]. Each of these organisations have developed ways of classifying lasers, the specific criteria vary slightly from one body to the other, but the IEC classifications will be considered in this section.

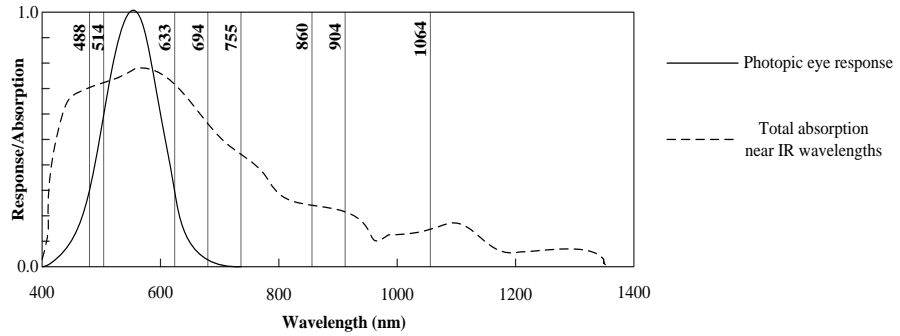


Figure 2.1 Response/absorption of the human eye at various wavelengths (redrawn from [4])

Table 2.1 shows the IEC (IEC60825-1, Amendment 2) laser classifications for 850 nm and 1500 nm wavelengths and their permissible emission levels [46]. It can be seen from Table 2.1 that the Class 1 band is well-suited for indoor FSO communication systems since the lasers require no warning labels and can be used without any special safety precautions. However in the outdoor FSO communication systems, where good power budget is required, the Class 3B band can be used but with certain precautions taken, such as locating the transmitter system at rooftops or high walls where the laser beam cannot be easily seen by the human eye. Devices in Class 4 band emit very high powers that are dangerous to the eyes and skin, and they have high fire risk.

Table 2.1 Laser safety classifications for a point-source emitter (based on IEC60825-1, Amendment 2) adapted from [46]

	850 nm	1550 nm
Class 1	Up to 0.78 mW*	Up to 10 mW
Class 1M	Up to 0.78 mW**	Up to 10 mW
Class 2	Band reserved for visible light wavelengths (400-700 nm)	
Class 3R	0.22-2.2 mW	10-50 mW
Class 3B	2.2-50 mW	50-500 mW
Class 4	>500 mW	>500 mW

* For sources with angular subtense < 0.21 mrad.

** For sources with angular subtense < 1.5 mrad.

2.2.2.1 Maximum permissible exposure (MPE)

Asides from laser classifications, standard organisations have also proposed what is known as maximum permissible exposure which simply refers to the highest amount of irradiance (measured in W/cm^2), for a given wavelength and exposure time, that can be considered safe with a low probability of causing damage to the human eye or the skin. The MPE is usually about 10 % of the dose that has a 50 % chance of creating damage under worst-case conditions. Table 2.2 shows the MPE in mW/cm^2 and exposure time in seconds for common FSO communication system wavelengths of 850 nm and 1550 nm [6], the values for the skin are much lower, since the skin is usually less sensitive to laser radiation. It can be seen from Table 2.2 that the 1550 nm wavelength entries have higher MPEs than the 850 nm wavelength one. This can be attributed to the fact that almost all the radiation at 1550 nm can be absorbed by the cornea, whereas about 50 % can reach the retina for 850 nm wavelength emissions [6]. Additionally, the 1550 nm wavelength suffers reduced attenuation due to atmospheric absorption and scattering, and it is a well-suited wavelength for optical amplifiers, EDFAs.

Table 2.2 MPE (in mW/cm^2) for FSO wavelengths of 850 nm and 1550 nm [6]

Exposure Time (s)	1	2	4	10	100	1000	10000
MPE (mW/cm²) at 850 nm	3.6	3.0	2.5	2.0	1.1	0.65	0.36
MPE (mW/cm²) at 1550 nm	560	330	190	100	100	100	100

2.2.3 Light emitting diodes

A light-emitting diode (LED) is fundamentally a semiconductor PN junction, as shown in Fig. 2.2. The light is generated by radiative recombination of minority carriers injected across a forward-biased PN

junction through the spontaneous emission process. Also, unwanted non-radiative recombination competes with radiative recombination, resulting in reduction of the LED efficiency. Because only the spontaneous emission occurs within the entire bandwidth of the gain medium, the output light generated by a LED would be incoherent, would have a wide spectrum and emit into a wide solid angle.

The wavelength (or energy) of the emission spectrum is determined by the bandgap of the material as shown in Table 2.3 [4]. Other characteristics of LEDs include their low cost and low output powers (typically of the order of -20dBm [1]) when compared to the laser, their low data rate (up to a few hundreds of Mbps), their long life span of about 11 years [4] and their suitability (only) for short distance optical communications because they emit an incoherent beam with wide spectrum and solid angle.

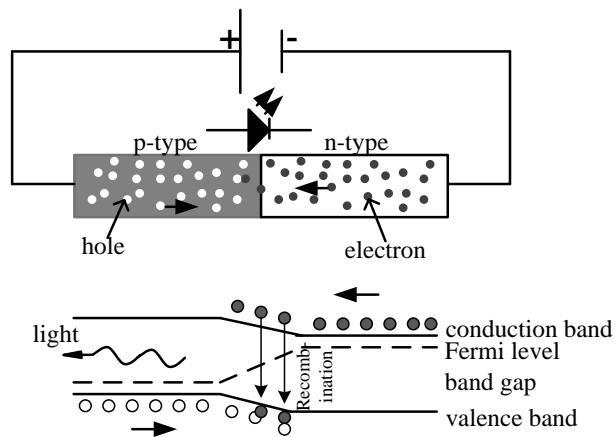


Figure 2.2 Schematic representation of a forward-biased LED, including the recombination and emission process

Table 2.3 Typical LED materials, their wavelengths and bandgap energy [4]

Material	Wavelength (μm)	Bandgap energy (eV)
GaInP	0.64-0.68	1.82-1.94
GaAs	0.65-0.87	0.9-1.4
AlGaAs	0.8-0.9	1.4-1.55
InGaAs	1.0-1.3	0.95-1.24
InGaAsP	0.9-1.7	0.73-1.35

The LED structures can be classified based on the light emission method into surface-emitting and edge-emitting LEDs, which, by their names, simply describes how the light is taken from the LED. Table 2.4 shows the comparison between the surface-emitting and edge-emitting LEDs [7]. It can be deduced from the table that the edge-emitting LED has better performance in terms of coupled power and maximum modulation frequency, which makes it capable of achieving longer optical link lengths and higher data rates than the surface-emitting LED.

Table 2.4 Comparison of surface and edge emitting LEDs [7]

LED type	Maximum modulation frequency (MHz)	Output power (mW)	Fibre coupled power (mW)
Surface emitting	60	< 4	< 0.2
Edge emitting	200	< 7	< 1.0

2.2.4 FSO modulation formats

A range of modulation schemes, with varying strengths and weaknesses, have been proposed for FSO communication systems. Examples of FSO modulation schemes are on-off keying (OOK), digital pulse position modulation (DPPM), differential phase-shift keying (DPSK), differential quadrature phase-shift keying (DQPSK) and variants of subcarrier intensity modulation [8-14]. In designing high-performance FSO systems, the chosen modulation scheme should be able to meet the following standards: minimum required optical power to achieve a target BER considering the limitations on transmittable optical power, simple transceiver design, and low bandwidth usage (although there is abundant bandwidth in optical frequencies, optoelectronic devices have constraints on bandwidth). The emphasis of this thesis would be on the OOK and DPPM techniques.

2.2.4.1 On-off keying

Most commercial FSO communication systems use OOK as a modulation format mainly because the transmitter and receiver hardware are

relatively simple [3, 4, 8, 10, 15, 16] and well developed (given the history of optical fibre communications). In the OOK format, data are transmitted in digital format as light ON (representing 1) and light OFF (representing 0). The OOK modulation scheme can be applied as non-return-to-zero (NRZ) or return-to-zero (RZ) signalling schemes, with the latter been characterized by the duty cycle. In the NRZ-OOK, the pulse duration is equal to the bit duration $T_b = 1/R_b$ (where R_b is the data rate), whilst in the RZ-OOK the pulse duration (xT_b) is a fraction x , of the bit duration such that several variations of the RZ-OOK exist. At the receiver, the “1” or “0” logical decision is determined by the received frame energy being above or below a predetermined threshold. Unlike in OOK-based optical fibre systems, where the decision threshold is normally steady (except in some burst mode systems), the OOK-based FSO system’s threshold is ideally dependent on the received signal power and the turbulence-induced scintillation noise (a fixed threshold would be very suboptimal but is sometimes used). Therefore, to achieve near optimal performance in the OOK-based FSO systems, the threshold level of the decision circuit at the receiver would be varied in sympathy with the fluctuating average incident optical signal. The Kalman filter based method of [47] is one way of practically achieving near optimal threshold for each instantaneous irradiance level.

2.2.4.2 Digital pulse position modulation

Digital pulse position modulation is a strong contender as the modulation scheme for FSO communication systems because of its superior power efficiency compared to the OOK-NRZ based system. In comparison to optical fibre systems, DPPM can be conveniently applied in FSO systems due to the non-dispersive nature of the channel. Some of the shortcomings of the DPPM scheme include increased bandwidth requirement and more complex design when compared to OOK-NRZ (e.g. the demodulator is controlled by slot and frame synchronisation circuits). Most of the earlier works on DPPM for FSO communications were done for a deep space application [17-19], whilst other works were performed for optical fibre

systems [20-23]. Moreover, some research has been performed on slot and frame synchronisation for optical fibre DPPM systems [24-26]. Phillips *et al.* [27] investigated the receiver sensitivity performance of an intersatellite system employing DPPM and an optical preamplifier. Furthermore a number of authors [10, 11, 28, 29] have studied this modulation method for terrestrial FSO communications. Kiasaleh [28] studied the DPPM scheme and avalanche photodiode for theoretical analysis (facilitated by a Gaussian approximation (GA)) of a FSO communication system.

In DPPM, M bits at the raw data rate are assigned to a frame which is then divided into $n = 2^M$ equal sized time slots, where M is referred to as the coding level. The length of a DPPM slot is then written as $t_s = MT_b/n$. Each frame consists of a single pulse occupying one DPPM slot and the pulse position in the frame corresponds to the value of the M bit word. Figure 2.3 illustrates the OOK-NRZ and equivalent 16-DPPM signal.

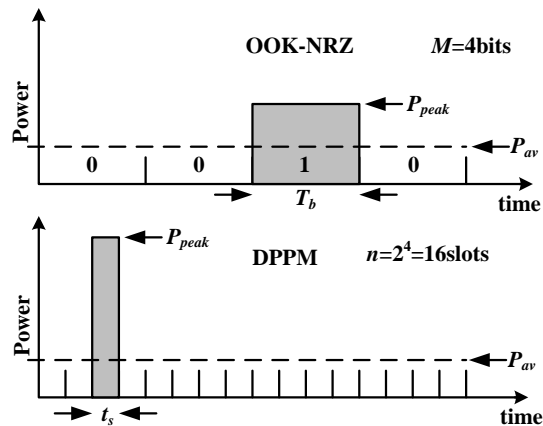


Figure 2.3 Illustration of DPPM frame for $M = 4$ ($n = 2^4 = 16$ slots)

2.3 Optical amplifier

Over the last 10 - 20 years, optical amplifiers have become essential components in optical communication systems and have successfully replaced electrical repeaters as a means of compensating for optical signal loss. An advantage offered by optical amplifiers over repeaters include the fairly large gain bandwidth offered by the optical amplifier which makes it practical for wavelength division multiplexing (WDM) whereby a single

amplifier can amplify multiple signals on different wavelengths simultaneously, while without the optical amplifier separate repeaters would be needed for each wavelength. Additionally, optical amplifiers are easily adaptable for many bit rates and signal modulation formats without a need to replace the amplifier, while the repeaters are designed to work at a particular bit rate (or at around only one wavelength) and modulation format [1, 30].

The early research into optical amplifiers led to the development of the semiconductor optical amplifier (SOA), which was initially referred to as the semiconductor laser amplifier (SLA) [31-33]. SOAs were initially fabricated from a semiconductor laser by replacing the end mirrors with antireflective coatings (so reflections needed for laser operation were eliminated (in the case of travelling-wave amplifier (TWA)) or reduced (in the case of Fabry Perot amplifier (FPA))). While the SOA technology was only able to achieve a few dB improvement in power levels compared to the electrical repeaters, continuous research in the laboratory led to the development of the EDFA which is capable of providing a large amount (typically 30-40 dB [1, 8, 14, 34]) of optical gain over a wide spectral range (approximately 30-60 nm). Perhaps the most notable work that underpinned the later commercial deployment of the EDFA in the mid 1990's was Poole's successful doping of silica fibre with a number of rare-earth doped ions [35]. This enabled the development of low noise EDFA for use in the 1550 nm transmission window. The optical amplification process however comes at the expense of introduction of optical noise, known as amplified spontaneous emission (ASE) noise, into the amplified signal. The ASE noise degrades the optical signal-to-noise ratio (OSNR).

Some work has been performed for optically preamplified non-turbulent (fibre) systems [40, 48, 49]. Yamamoto [48] derived expressions for the mean and variance of incident photons in an optically preamplified case using Poisson distribution (for coherent signals) and Bose-Einstein distribution (for incoherent signals). The noise variance comprises of the ASE beat noises, shot noise and thermal noise, and these noise were used in Gaussian approximation BER calculations. Ribeiro [49] derived a more accurate method of modelling the signal and noise analysis in an optically

preamplified case, using moment generating function approaches. The signal mean and variances obtained was similar to that of Yamamoto. The BER results obtained by Ribeiro [49] using the MCB method gave the most optimistic result compared to the CB, SPA and GA methods. Olsson [40] investigated the performance of optically preamplified, coherent and direct detection in-line receiver systems. The photocurrent equivalent of the noise variances were also derived by [40] for quantum efficiency of unity.

Similarly FSO communication systems can benefit from using an optical amplifier in various ways. The optical preamplifier configuration can be used to boost optical signal strength which has been degraded due to various atmospheric phenomena, to overcome the eye-limit restrictions on transmitted laser power, to suppress the limiting effect of the receiver thermal noise generated in the electronic amplifier, as well as to effectively improve receiver sensitivity. The performance of optically preamplified receivers in FSO communication systems has been investigated using different methods by these authors [14, 36-39]. Razavi [14] investigated an optically preamplified FSO system employing diversity techniques. The performance calculation followed a semi classical photon counting approach with the BER and power penalty results been based on the Gaussian approximation. The adaptive optics technique was reported to give the best results compared to other techniques used, such as the aperture averaging and linear combining. The binary PPM scheme was reported to give better performance than the OOK scheme. Abtahi [38], the use of saturated optical amplifier for suppressing turbulence-induced scintillation noise was investigated in the laboratory, with the scintillation effect having been stimulated in a temperature-regulated turbulence box. Several receiver configurations were considered whilst comparing the advantages of SOA and EDFA. The EDFA-based receiver was reported to give the best BERs, even though the saturated SOA is been favoured for commercial use simply because it is cheaper and more compact compared to the EDFA-based receiver. Although analysing the actual behaviour of the signal and noise statistics at the receiver has proved difficult, the work performed in this thesis and published in [36, 37] provides a more comprehensive evaluation of the system.

2.3.1 Principle of optical amplification

In all optical amplifiers (and lasers), there are three physical processes that must be considered namely photon absorption, spontaneous emission, and stimulated emission, with the latter contributing essential amplification. Fig. 2.4 shows the important processes in the gain medium of an atomic system with two energy levels.

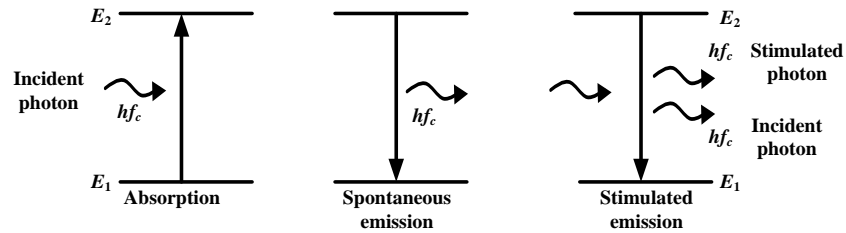


Figure 2.4 Important processes in a gain medium. The stimulated photon has same frequency, phase, polarisation and direction as the incident photon

In the thermal equilibrium state the density of electrons or ions in the upper energy level, E_2 which is of most interest is typically negligible compared to the lower energy level E_1 , such that an input photon in the gain medium would much more likely to be absorbed rather than to stimulate an emission. In order to reverse this process such that the stimulated emission is more likely than absorption, additional energy is pumped into the gain medium to increase the proportion of electrons or ions in E_2 . This additional energy can be applied by optical (e.g. EDFA pump lasers) or electrical (e.g. SOA drive current) means.

When the number of electrons or ions in E_2 , that is N_2 , is artificially increased more than the number of electrons or ions in E_1 , that is N_1 , then we have a *population inversion*. The population inversion or spontaneous emission parameter n_{sp} is given as [1]

$$n_{sp} = \frac{N_2}{N_2 - N_1} \quad (2.1)$$

The best inversion occurs when $n_{sp} \rightarrow 1$, that is when $N_2 \gg N_1$, but typical optical amplifiers have values around 2-5 [1, 40]. When population

inversion occurs and an incident photon of energy $E_2 - E_1$ interacts with the inverted gain medium, electrons easily decay from E_2 to E_1 , resulting in the generation of a stimulated photon which has identical properties (frequency, phase, direction, and polarisation) as the incident photon. This process is known as *stimulated emission*. Aside from stimulated emission, spontaneous emission is also capable of happening simultaneously during population inversion as electrons or ions decay from E_2 to E_1 . The spontaneous emitted photon is characterised by random frequency, phase, direction and polarisation. Hence the stimulated emission is coherent, while the spontaneous emission is incoherent. Furthermore, the presence of the spontaneously emitted photons in the gain medium leads to them also being amplified (the medium has no ability to distinguish between signal and noise photons). The amplified spontaneous emission will now appear as noise at the output of the amplifier. The power spectral density (PSD) in a single polarisation for ASE noise is given as

$$N_0 = n_{sp}(G-1)hf_c \quad (2.2)$$

where G is the amplifier gain, h is Planck's constant and hf_c is the energy of a single photon.

The amount of signal degradation caused by the ASE produced by an optical amplifier is quantified by the amplifier noise figure (NF) which has typical values of about 4-7 dB [1, 2, 30], and is given as

$$NF = \frac{SNR_i}{SNR_o} \quad (2.3)$$

where SNR_i is the electrical signal-to-noise ratio at the amplifier input, and SNR_o is the electrical signal-to-noise ratio at the amplifier output (where the electrical detection is idealized to include only shot noise and signal-spontaneous beat noise).

The n_{sp} is related to the NF of an optical amplifier by [8]

$$\begin{aligned} n_{sp} &= \frac{NF}{2} \left(\frac{G}{G-1} \right) \\ &\approx \frac{NF}{2} \quad \text{for } G \gg 1 \end{aligned} \quad (2.4)$$

2.4.1.1 Amplifier Noise

An optical amplifier does not only provide optical gain as it also introduces ASE noise (degrading the amplitude and phase quality) of the amplified signal [30]. This leads to the degradation of the SNR of the amplified signal. The ASE noise is typically regarded as Gaussian in the optical domain (strictly for linear optical amplifiers) [40, 48, 49] and is generally considered to have a white (flat) PSD in the region of any particular signal wavelength. The photodetection process can be described as square law detection whereby the signal beats with ASE noise upon detection, causing signal-spontaneous beat noise, and the ASE beats with itself, causing spontaneous-spontaneous beat noise. The ASE beat noises, unlike the ASE noise, are not really Gaussian but instead they relate to chi-square statistics (purely spontaneous-spontaneous noise) and non-central chi-square (due to the presence of the signal). The obtained photocurrent is given as

$$\overline{i(t)} = R \overline{(E_{\text{sig}}(t) + E_{\text{ASE}}(t))^2} = R \overline{[E_{\text{sig}}(t)]^2 + 2E_{\text{sig}}(t)E_{\text{ASE}}(t) + [E_{\text{ASE}}(t)]^2} \quad (2.5)$$

where $E_{\text{sig}}(t)$ and $E_{\text{ASE}}(t)$ are the signal and ASE optical fields in units $\text{W}^{1/2}$ (so it can be directly related to signal and noise power), R is the photodiode responsivity (2.9), and the bar above the equation means time averaging over optical frequencies. The variances of the signal-spontaneous ($\sigma_{\text{sig-ASE}}^2$) and spontaneous-spontaneous ($\sigma_{\text{ASE-ASE}}^2$) noise currents at the receiver are given, respectively, as [40]

$$\sigma_{\text{sig-ASE}}^2 = 4R^2 G P N_0 B_e \quad (2.6)$$

$$\sigma_{\text{ASE-ASE}}^2 = 2m_t R^2 N_0^2 B_0 B_e \left(1 - \frac{B_e}{2B_0}\right) \quad (2.7)$$

where m_t is the number of polarisation states of ASE noise, B_0 is the optical bandpass filter (OBPF) bandwidth and B_e is the noise equivalent bandwidth.

2.3.2 Erbium-doped fibre amplifier

EDFAs are the most commonly used rare earth doped fibre amplifier because of the superior properties of the erbium ion (Er^{3+}) such as its wide gain bandwidth [41] and the limited decay metastable lifetime [30]. Other rare earth doped fibre amplifiers include the neodymium (Nd^{3+}) and praseodymium (Pr^{3+}) doped fibre amplifiers which both operate around 1300 nm. In optical communication systems, EDFAs are the most attractive for several reasons such as the simplicity of the device, the reliability of the pump lasers, polarisation independent since it's an all fibre device, low NF (about 3 dB [42]), the high optical gains achievable (typically 30 – 40 dB, though about 50 dB have been demonstrated [43]), and the immunity to signal distortion and crosstalk (due to the long spontaneous lifetime [41]) during dense wavelength division multiplexing (DWDM). EDFAs operate mainly in the C-band (1530 – 1565 nm), although they have also been developed to operate in the 1565 – 1610 nm range of the L-band [1, 30]. The C- and L- band EDFAs operate using similar principles.

EDFAs are made by doping the silica fibre core with Er^{3+} . Fig. 2.5 shows the schematic diagram of a simple EDFA. Most commercial EDFAs would contain at least some of multiple gain stages (erbium-doped fibre which can be ~20 m long, depending on level of doping), pump lasers (which can be co- or counter- propagating, or both (bi-directional), or multiple), wavelength multiplexer for combining the input signal and pump signal, an isolator to reduce back propagating ASE saturating the medium, variable optical attenuators (VOAs), an input and output power monitoring feeding one or more control loops, and a gain flattening filter to offset the natural spectral shape of the Er^{3+} gain. The principle of operation of the EDFA is such that the Er^{3+} is excited into higher energy levels by absorbing light supplied by the pump laser, from which there is decay to the upper energy level of the desired transition. The amplification is achieved as a result of the stimulated emission of photons by the optical signal. The pump lasers operate at wavelengths of 980 nm, 1480 nm, and also 800 nm is possible. The 980 nm is the most popular due to the better population inversion attainable, while the 800 nm suffers from excited state absorption.

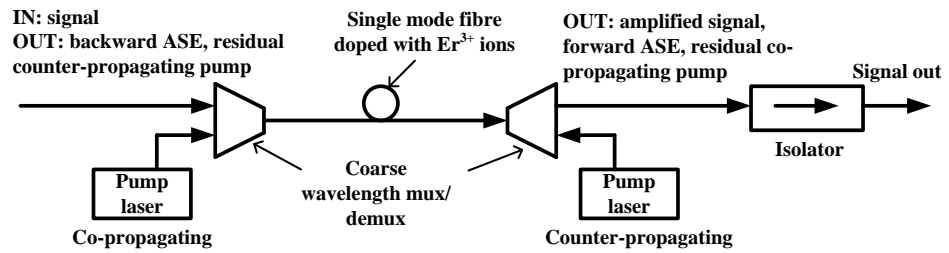


Figure 2.5 A simple erbium-doped fibre amplifier (redrawn from [1])

2.3.3 Semiconductor optical amplifier

SOAs are generally based on the same principles as semiconductor lasers, just that they are more purposely designed for signal amplification by introducing antireflective coatings and/or angle cleaving of the chip facet, to eliminate the cavity reflections that exist in lasers [1, 2]. There are in principle two major types of SOAs based on the level of residual reflectivity, the travelling-wave amplifiers, and the resonant or Fabry-Perot amplifiers. In an FPA, some facet reflectivities (lower than that of the laser) are deliberately retained, which results in multiple reflections in the active region. This gives rise to resonant cavity and gain spectra with a series of peaks. At these peaks of the spectrum, the gains are much higher. In contrast, the TWA eliminates the facet reflectivity by applying antireflective coatings at both facets. The TWA provides single pass amplification, has higher bandwidth (about 5 THz [41]), and has noise figure of a few dBs.

Figure 2.6 shows the schematic of typical SOA. Depending on the wavelength of operation, the common materials used for SOAs are InGaAsP/InP or GaAs/GaAlAs. The SOA consists of two energy levels separated by an energy difference called the *bandgap*. The higher energy level for a p-type semiconductor material is the conduction band, while the lower energy level is the valence band. In order to achieve population inversion, electrons are pumped into the conduction band, from the valence band by forward-biasing of the SOA. When population inversion is reached, the presence of an optical signal in the active region will cause more stimulated emissions than absorption as electrons transit from the

conduction band to the valence band, hereby resulting in optical signal amplification.

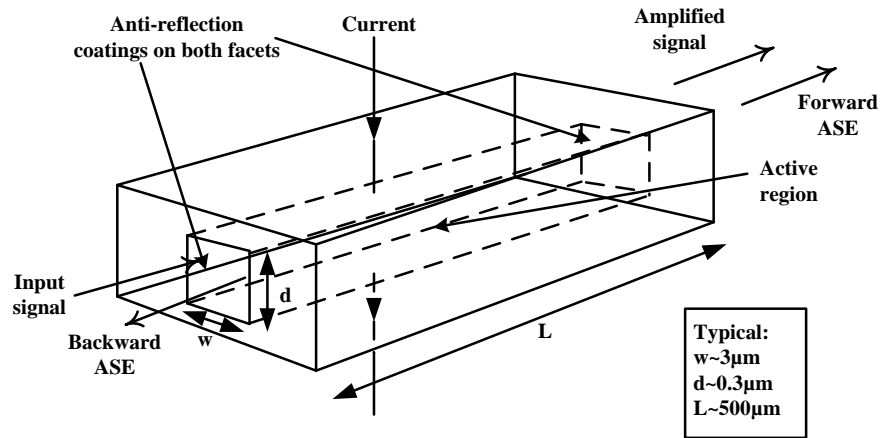


Figure 2.6 Schematic diagram of a typical semiconductor optical amplifier

[1]

2.3.4 Comparison between EDFA and SOA

EDFAs are widely preferred to SOAs in optical communication systems mainly for the following reasons. EDFAs can have high gains of about 30-40 dB, with gains as high as 50 dB also having been reported [43, 44], while the SOA can achieve gains of about 20 dB, they have potentially better noise figures (which can approach theoretical limits of 3 dB) than the SOAs (the high reflectivity values (typically greater than 10^{-4}) present in most SOAs creates ripples (or noise) in the gain spectrum while the EDFAs are natural TWAs that don't need antireflective coatings and hence have no gain ripple issues), they have lower insertion loss than the SOAs since it is an all-fibre device, and they have cylindrical geometry which makes them almost polarisation insensitive, while SOAs require careful design.

In EDFAs, the spontaneous emission lifetime is within range of 5 - 10 ms [45] which is large enough compared to the bit period of interest for the electron transition (from higher energy level to lower energy level) to respond to the optical signal fluctuations, hence the amplified signal is not distorted. In contrast, the SOA spontaneous emission lifetime is usually within the range of 100 - 200 ps [45], which implies that the electron

transition easily responds to the fluctuations of the optical signal at Gbps rates, hence major impairments due to crosstalk can occur.

SOA advantages over the EDFA include the possibility of engineering SOAs for different wavelength regions (unlike the EDFAs which are restricted mainly to the C-band), the much smaller size, weight and power of the SOAs than the EDFAs. EDFAs contains a couple of high power pump lasers, fibre, control electronics and other optical components, which make them easily integrated with planar waveguide optics, although erbium-doped waveguide amplifier (EDWA) are being developed to rival the SOA in terms of compatibility. However, an EDFA made from cheap pumps lasers, and other cheap optical components, can be used to reduce cost whilst still achieving a similar performance.

2.4 Receiver system

The primary functions of the optical receiver are to photodetect and demodulate the optical signal with an acceptable BER. The quality of the electrical signal generated at the receiver output is dependent on the received optical power and any impairment in the form of noise, distortion and crosstalk. The block diagram of a direct detection optical receiver is shown in Fig. 2.7.

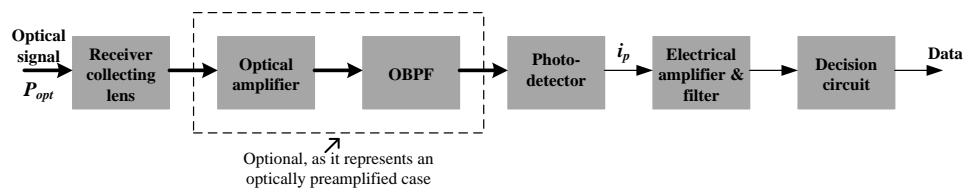


Figure 2.7 Block diagram of a typical FSO receiver

The received optical signal is focussed on the photodetector by the receiver collecting lens (RCL). In an optically preamplified configuration which is often used in this thesis, an optical amplifier can be placed before the photodetector to provide added gain to the input signal. In the preamplifier case, an optical bandpass filter (OBPF) will be required to limit the ASE noise generated during optical signal amplification. The optical

signal can be fed into the optical amplifier (e.g. an EDFA) by using a collimator (as per [38]) and a short-length optical fibre.

The photodetector converts the optical signal impinging on its surface into usable photocurrent. The mode of operation of the semiconductor photodetector is based on internal photoelectric effect which basically involves photon energy absorption by the valence band electron, raising it into the conduction band (if the photon energy is greater than bandgap) and thus creating a hole in the valence band. The electron-hole pair created will give rise to photocurrent when a bias is applied. The key parameters used for characterising the photodetector are the quantum efficiency and the responsivity.

The quantum efficiency, η , is the average number of photoelectrons (electron-hole pairs) generated per incident photon. It is formally defined as

$$\eta = \frac{\text{Detected field power}}{\text{Incident field power}} = 1 - \exp(-\alpha_a l_a) \quad (2.8)$$

where α_a is the absorption coefficient which depends on wavelength λ , and is zero for $\lambda > \lambda_{\text{cutoff}}$, $\lambda_{\text{cutoff}} = 1.24/E_g$ is the cut-off wavelength for a specific detector material (in μm) and l_a is the length of the absorbing region.

Responsivity, R (in A/W), gives the photocurrent generated per unit incident optical power. It is given as

$$R = \frac{i_p}{P_{opt}} = \frac{\eta q}{hf_c} \quad (2.9)$$

Amplification of the generated electrical signal to a usable level can be achieved by using a front-end amplifier, whilst an electrical filter with noise equivalent bandwidth B_e is used to reduce the electrical domain noise. The electrical amplifier and filter is followed by the decision circuit which estimates the output data. The modulation technique used at the transmitter will determine the design of the decision circuit.

2.4.1 Direct detection – positive-intrinsic-negative photodiode

A positive-intrinsic-negative (P-I-N) photodiode is formed by depositing an intrinsic semiconductor material used for light absorption between a p -type and a n -type semiconductor. The p -type and n -type materials can be made of InP, which is transparent in the 1300 and 1550 nm wavelength bands, as shown in Table 2.5 [1]. The intrinsic region is typically made of InGaAs or InGaAsP and the width of the intrinsic region is thicker than that of the p -type and n -type semiconductors so as to ensure most of the light absorption takes place in this region. This is illustrated in Fig. 2.13. Furthermore, since the intrinsic material is completely different from the p -type and n -type material, then such a P-I-N photodiode structure is termed heterostructure or double heterojunction [1, 2].

Table 2.5 Band gap energies and cutoff wavelengths for different semiconductor materials [1]

Material	E_g (eV)	λ_{cutoff} (μm)
Si	1.17	1.06
Ge	0.775	1.6
GaAs	1.424	0.87
InP	1.35	0.92
$\text{In}_{0.55}\text{Ga}_{0.45}\text{As}$	0.75	1.65
$\text{In}_{1-0.45y}\text{Ga}_{0.45y}\text{As}_y\text{P}_{1-y}$	0.75-1.35	1.65-0.92

2.4.2 Direct detection – Avalanche photodiode

In the Avalanche photodiode (APD) there is an internal multiplication process, resulting from photoelectrons producing secondary electron-hole pairs. The total number of secondary electron-hole pairs generated by a primary photoelectron is a random number. Its mean value is called the multiplication factor M of the APD. This gain process potentially improves the receiver sensitivity as it increases the signal before it combines with receiver thermal noise. In designing an APD, the gain has to be chosen to give optimum signal-to-noise ratio.

In comparison to the P-I-N photodiode, the APD advantage comes from the receiver thermal noise being typically larger than the shot noise, so

increment in signal level is not met with corresponding rise in overall noise level. APDs are limited in benefit when used in conjunction with optical amplification because of the signal dependent shot noise.

2.5 Summary

This chapter has described the basic FSO communications components which consist of the optical transmitter, the receiver structure, the optical amplifiers, and the way in which the intercepted field is being converted between electrical and optical forms. The optical amplifier noises are introduced in this chapter with more detail to follow in chapter three. The main modulation formats used in this thesis, namely the OOK-NRZ and DPPM schemes, are discussed in details. Finally, the existing international laser safety standards and procedures were reviewed.

2.6 References

- [1] R. Ramaswami and K. N. Sivarajan, *Optical networks- a practical perspective*, Second Edition, Academic Press, London, 2002.
- [2] G. P. Agrawal, *Fibre - optic communication systems*, Third Edition, New York: John Wiley & Sons, Inc, 2003.
- [3] S. Bloom, E. Korevaar, J. Schuster, and H. A. Willebrand, "Understanding the performance of free-space optics," *Journal of Optical Networking*, vol. 2, no. 6, pp. 178-200, June 2003.
- [4] H. A. Willebrand and B. S. Ghuman, *Free-space optics: enabling optical connectivity in today's networks*, Sams Publishing, Indianapolis, Indiana 46240 USA, 2002.
- [5] D. J. Heatley, D. R. Wisely, I. Neild, and P. Cochrane, "Optical wireless: the story so far," *IEEE Communications Magazine*, vol. 36, pp. 72-82, Dec. 1998.
- [6] O. Bouchet, H. Sizun, C. Boisrobert, F. DeFornel, and P. Favennec, *Free-space optics: propagation and communications*, Wiley-ISTE Limited, London, 2006.
- [7] M. J. Sibley, *Optical communications*, Second Edition, Macmillian Press Limited, London, 1995.
- [8] D. O. Caplan, "Laser communication transmitter and receiver design," *Journal of Optical Fibre Communication Report*, vol. 4, pp. 225-362, 2007.
- [9] S. Karp, R. M. Gagliardi, S. E. Moran, and L. B. Stotts, *Optical channels: fibers, clouds, water and the atmosphere*, New York: Plenum Press, 1988.

- [10] A. K. Majumdar, "Free-space laser communication performance in the atmospheric channel," *Journal of Optical and Fiber Communications Research*, vol. 2, pp. 345-396, 2005.
- [11] S. S. Muhammad, W. Gappmair, and E. Leitgeb, "PPM channel capacity evaluation for terrestrial FSO links," *Proceedings of the International Workshop on Satellite and Space Communications*, pp. 222-226, Sept.2006.
- [12] W. O. Popoola, *Subcarrier intensity modulated free-space optical communication systems*, Thesis report, p. 73, Sept. 2009.
- [13] W. O. Popoola and Z. Ghassemlooy, "BPSK subcarrier intensity modulated free-space optical communications in atmospheric turbulence," *Journal of Lightwave Technology*, vol. 27, no. 8, pp. 967-973, Apr. 2009.
- [14] M. Razavi and J. H. Shapiro, "Wireless optical communications via diversity reception and optical preamplification," *IEEE Transactions on Wireless Communications*, vol. 4, no. 3, pp. 975-983, May 2005.
- [15] X. Zhu and J. M. Kahn, "Free-space optical communication through atmospheric turbulence channels," *IEEE Transactions on Communications*, vol. 50, no. 8, pp. 1293-1300, Aug. 2002.
- [16] J. T. Li and M. Uysal, "Optical wireless communications: system model. capacity and coding," *Vehicular Technology Conference*, vol. 1, pp. 168-172, Oct. 2003.
- [17] S. Karp and R. Gagliardi, "The design of a pulse-position modulated optical communication system," *IEEE Transactions on Communication Technology*, vol. 17, no. 6, pp. 670-676, Dec. 1969.
- [18] J. R. Lesh, J. Katz, H. H. Tan, and D. Zwillinger, "2.5 bit/detected photon demonstration program, analysis and phase I results," *TDA Progress Rep., Jet propulsion Laboratory, Pasadena, CA*, pp. 115-132, Oct. 1981.
- [19] A. Biswas, V. Vilnrotter, W. Farr, D. Fort, and E. Sigman, "Pulse position modulated ground receiver design for optical communications from deep space," *Proc. SPIE, San Jose, CA*, vol. 4635, pp. 224-235, Jan. 2002.
- [20] I. Garrett, "Pulse-position modulation for transmission over optical fibres with direct or heterodyne detection," *IEEE Transaction on Communications*, vol. 31, no. 4, pp. 518-527, Apr. 1983.
- [21] R. A. Cryan, I. G. Unwin, M. J. Sibley, and N. M. Calvert, "Optical fibre digital pulse-position modulation assuming a Gaussian received pulse shape," *IEE Proceedings - Optoelectronics*, vol. 137, no. 2, pp. 89-96, Apr. 1990.
- [22] R. A. Cryan and R. T. Unwin, "Optical and suboptimal detection of optical fibre digital PPM," *IEE Proceedings - Optoelectronics*, vol. 140, no. 6, pp. 367-375, Dec. 1993.
- [23] J. J. O. Pires and J. R. F. Da Rocha, "Pulse position modulation over optical fibres with avalanche photodiode receiver," *IEE Proceedings - Optoelectronics*, vol. 133, no. 5, pp. 309-313, Oct. 1986.
- [24] J. M. H. Elmirghani, R. A. Cryan, and F. M. Clayton, "Spectral characterisation and frame synchronisation of optical fibre digital fibre PPM," *Electronics Letters*, vol. 28, no. 16, pp. 1482-1483, July 1992.

- [25] X. M. Sun and F. M. Davidson, "Word timing recovery in direct detection optical PPM communication systems with Avalanche photodiodes using a phase lock loop," *IEEE Trans. Commun.*, vol. 38, no. 5, pp. 666-673, May 1990.
- [26] G. Ling and R. Gagliardi, "Slot synchronisation in optical PPM communications," *IEEE Trans. Commun.*, vol. 34, no. 12, pp. 1202-1208, Dec. 1986.
- [27] A. J. Phillips, R. A. Cryan, and J. M. Senior, "An optically preamplified intersatellite PPM receiver employing maximum likelihood detection," *IEEE Photonic Technology Letter*, vol. 8, no. 5, pp. 691-693, May 1996.
- [28] K. Kiasaleh, "Performance of APD-based, PPM free-space optical communication systems in atmospheric turbulence," *IEEE Transactions on Communications*, vol. 53, no. 9, pp. 1455-1461, Sept. 2005.
- [29] S. S. Muhammad, T. Javornik, E. Leitgeb, and O. Koudelka, "Reed Solomon coded PPM for terrestrial FSO links," *International Conference on Electrical Engineering*, pp. 1-5, Apr. 2007.
- [30] M. J. Yadlowsky, E. M. Deliso, and V. L. Da Silva, "Optical fibers and amplifiers for WDM systems," *Proceedings of the IEEE*, vol. 85, no. 11, pp. 1765-1779, Nov. 1997.
- [31] P. Diamant and M. C. Teich, "Evolution of the statistical properties of photons passed through a traveling-wave laser amplifier," *IEEE Journal of Quantum Electronics*, vol. 28, no. 5, pp. 1325-1334, May 1992.
- [32] M. J. O'Mahony, "Semiconductor laser optical amplifiers for use in future fiber systems," *Journal of Lightwave Technology*, vol. 6, no. 4, pp. 531-544, Apr. 1988.
- [33] Y. Yamamoto, "Characteristics of AlGaAs Fabry-Perot cavity type laser amplifiers," *IEEE Journal of Quantum Electronics*, vol. 16, no. 10, pp. 1047-1052, Oct. 1980.
- [34] P. Ghiggino, "Discussion on the use of optical amplifiers in IM-DD receivers," *GEC Journal of Research*, vol. 12, no. 3, pp. 163-173, 1995.
- [35] S. B. Poole, D. N. Payne, and M. E. Fermann, "Fabrication of low-loss optical fibres containing rare-earth ions," *Electronics Letters*, vol. 21, no. 17, pp. 737-738, Aug. 1985.
- [36] A. O. Aladeloba, A. J. Phillips, and M. S. Woolfson, "Performance evaluation of optically preamplified digital pulse position modulation turbulent free-space optical communications systems," *IET Optoelectronics*, vol. 6, no. 1, pp. 66-74, Feb. 2012.
- [37] A. O. Aladeloba, A. J. Phillips, and M. S. Woolfson, "Improved bit error rate evaluation for optically pre-amplified free-space optical communication systems in turbulent atmosphere," *IET Optoelectronics*, vol. 6, no. 1, pp. 26-33, Feb. 2012.
- [38] M. Abtahi, P. Lemieux, W. Mathlouthi, and L. A. Rusch, "Suppression of turbulence-induced scintillation in free-space optical communication systems using saturated optical amplifiers," *Journal of Lightwave Technology*, vol. 24, no. 12, pp. 4966-4973, Dec. 2006.

- [39] Q. L. Cao, M. Brandt-Pearce, and S. G. Wilson, "Free space optical MIMO system using PPM modulation and a single optical amplifier," *Second International Conference in Communications and Networking in China*, pp. 1113-1117, Aug. 2007.
- [40] N. A. Olsson, "Lightwave systems with optical amplifiers," *Journal of Lightwave Technology*, vol. 7, no. 7, pp. 1071-1082, July 1989.
- [41] A. Yariv and P. Yeh, *Photonics - Optical electronics in modern communications*, Sixth Edition, Oxford University Press, Inc., New York, 2007.
- [42] R. I. Laming and D. N. Payne, "Noise characteristics of erbium-doped fiber amplifier pumped at 980 nm," *IEEE Photonics Technology Letters*, vol. 2, no. 6, pp. 418-421, June 1990.
- [43] R. I. Laming, M. N. Zervas, and D. N. Payne, "Erbium-doped fiber amplifier with 54 dB gain and 3.1 dB noise figures," *IEEE Photonics Technology Letters*, vol. 4, no. 12, pp. 1345-1347, Dec. 1992.
- [44] W. J. Miniscalco, B. A. Thompson, E. Eichen, and T. Wei, "Very high gain Er³⁺ fiber amplifier pumped at 980 nm," *Conference on Optical Fiber Communication, San Francisco, California*, vol. 1, p. 192, Jan. 1990.
- [45] I. T. Monroy and E. Tangdionga, *Crosstalk in WDM communication networks*, Kluwer Academic Publishers, Norwell, Massachusetts, USA, 2002.
- [46] I. E. C. (IEC), "Safety of Laser Products—Part 1: Equipment Classification, Requirements, and User's Guide, IEC 60825-1 (IEC, 2001), <http://www.iec.ch>. New classification standard adopted as of 1 March 2001," Amendment 2 (2001).
- [47] C. Chen, H. Yang, H. Jiang, J. Fan, C. Han, and Ding, Y., "Mitigation of Turbulence-Induced Scintillation Noise in Free-Space Optical Communication Links Using Kalman Filter", *IEEE Congress on Image and Signal Processing*, Hainan, China, vol. 5, pp. 470-473, May 2008.
- [48] Y. Yamamoto, "Noise and error rate performance of semiconductor laser amplifiers in PCM-IM optical transmission systems," *IEEE Journal of Quantum Electronics*, vol. 16, no. 10, pp. 1073-1081, Oct. 1980.
- [49] L. F. B. Ribeiro, J. R. F. Da Rocha, and J. L. Pinto, "Performance evaluation of EDFA preamplified receivers taking into account intersymbol interference," *Journal of Lightwave Technology*, vol. 13, no. 2, pp. 225-232, Feb. 1995

CHAPTER 3 Factors affecting FSO communication systems

3.1 Overview

This chapter describes the physical factors and atmospheric effects, such as attenuation due to scattering and absorption, importantly, and also turbulence-induced scintillation, which limit the overall performance of FSO communication systems. The commonly used probability density functions (pdf) for modelling of optical scintillation under weak-, moderate-, and strong turbulence regimes, are also presented.

3.2 Physical obstacles

The presence of physical obstructions e.g. birds, trees and tall buildings along the line-of-sight of a FSO channel are evidently capable of severely affecting the quality of optical signal (probably loss of signal) received at the detector. Most of this can be avoided by proper planning and site measurements [1], though clearly birds remain problematic.

3.3 Atmospheric attenuation

Atmospheric particles exist in various concentration, chemical composition, shape and size (with radius range of 0.01 - 10 μm [1-4]). They are the main contributors of attenuation via scattering in the atmosphere, and they can be classified into two types, namely aerosols and hydrometers, depending on their sizes. Aerosols are very small particles with radii equal to or less than 1 μm . Examples of aerosols include smog, smoke, fog, clouds, dust, and soil particles. Unlike aerosols, hydrometers are denser due to their water content and have radii larger than 1 μm . Examples are mist, raindrops, snow, hail and many types of clouds. Table 3.1 shows typical atmospheric particles, their radius range and concentration [4]. Generally, atmospheric molecules and particles absorb some of the optical signal energy, converting it to heat energy (absorption) or change the direction of

propagation of the signal (scattering), thereby reducing the amount of optical signal arriving at the receiver. The transmittance of optical signal propagating through the atmosphere is described by the Beer-Lambert law as [1, 3, 5, 6]

$$\tau(\lambda, l) = \frac{P_R}{P_T} = \exp(-\beta(\lambda)l) \quad (3.1)$$

where $\tau(\lambda, l)$ is the atmosphere's transmittance at wavelength λ and optical link length l , the total attenuation coefficient $\beta(\lambda)$ is the sum of the attenuation coefficients due to absorption, being $\beta_{abs}(\lambda)$ and scattering $\beta_{sca}(\lambda)$ (in m^{-1}). The product of $\beta(\lambda)$ and l is called the optical depth [7], P_T is the transmitted optical power, and P_R is the received optical power.

Table 3.1 Typical atmospheric particles, their radius range and concentration [4]

Type	Radius [μm]	Concentration [cm^{-3}]
Air molecules	10^{-4}	10^{19}
Aiken nucleus	10^{-3} - 10^{-2}	10^4 - 10^2
Aerosol	10^{-2} -1	10^3 -10
Fog	1-10	100-10
Cloud	1-10	300-10
Raindrops	10^2 - 10^4	10^{-2} - 10^{-5}

3.3.1 Scattering

Scattering simply involves the redirection of optical signal from the intended propagation path by molecules and particles suspended in the atmosphere, resulting in no energy loss. The scattering effect can be classified into Rayleigh scattering and Mie scattering, dependent on relationship between the size of the attenuator, r_a , and the optical signal wavelength, λ , while the geometric optics is not a scattering method but rather it is a way of analysing a particular type of scattering. The size parameter, $x_0 = 2\pi r_a / \lambda$ [1-4], is commonly used to describe the scattering

type such that when $x_0 \ll 1$, there is Rayleigh scattering, when $x_0 \approx 1$, there is Mie scattering, and when $x_0 \gg 1$, the scattering can be described by geometric optics.

Rayleigh's scattering coefficient, (in m^{-1}), is given as [3]

$$\beta_{\text{Rayleigh}}(\lambda) = \frac{fq^4\lambda_0^4}{6\pi\epsilon_0^2m^2c^4}\frac{1}{\lambda^4} \quad (3.2)$$

where f is the oscillator strength, q is the electronic charge, λ_0 is the wavelength corresponding to the natural frequency, $\omega_0 = 2\pi c/\lambda_0$, ϵ_0 is the dielectric constant, c is the speed of light in vacuum, and m is the mass of the oscillating entity. From (3.2), it can be seen that the Rayleigh scattering coefficient is inversely related to the optical wavelength such that at longer wavelengths the scattering effect is minimal. A typical example of Rayleigh scattering is the blue sky.

Mie scattering is caused by particles which have radii equal to the typical FSO wavelength window (0.8-1.6 μm), for example fog and cloud. The Mie scattering coefficient, (in km^{-1}), can be written as [5]

$$\beta_{\text{Mie}}(\lambda) = \frac{3.91}{V} \left(\frac{\lambda \times 10^9}{550} \right)^{-\delta(V)} \quad (3.3)$$

where V is the visibility defined as the distance travelled by a parallel luminous beam through the atmosphere until the intensity drops to 0.02 times its initial value [3, 7]. It is measured in km using a transmissiometer.

3.3.2 Absorption

Interactions between gas molecules and photons occur as the optical signal traverses the atmosphere, resulting in conversion of part of the optical energy into heat energy, a decrease in the amount of received optical signal, and extinguishing of the photon into the molecules kinetic energy. This process is referred to as absorption. Moreover, the absorption effect is dependent on the size and concentration of the gas molecules, and the optical signal wavelength. Figure 3.1 shows the range for wavelengths of minimal absorption (the transmission window) for typical absorbing attenuators such as H_2O , CO_2 and O_3 . Since attenuation due to absorption is

wavelength-dependent, most commercial FSO system designs can be chosen such that the wavelength falls within the atmospheric transmission window.

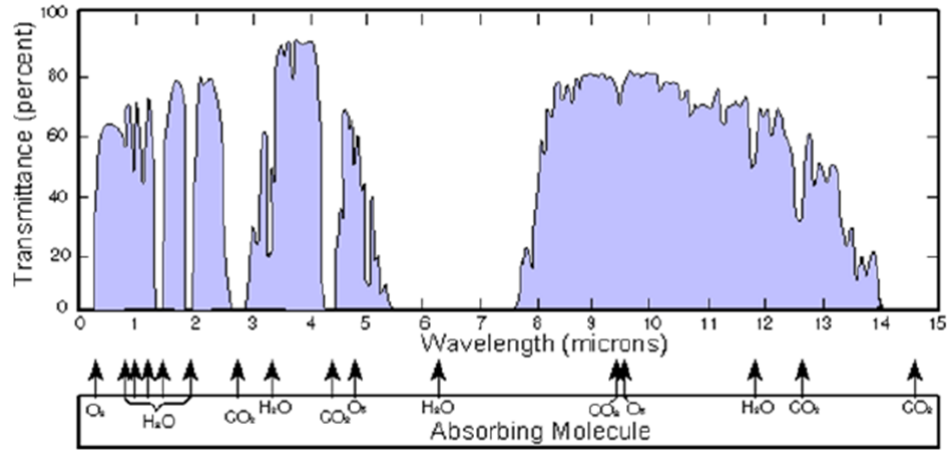


Figure 3.1: Atmospheric absorption transmittance over a sea level 1820 m horizontal path [3]

3.4 Atmospheric scintillation

Inhomogeneous heating of air particles, mainly by the sun, and wind blowing over the earth's surface, creates temperature differences along the atmospheric channel. These varying temperature gradients in turn generate random irregularities in the atmosphere's refractive index, known as optical turbulence [1, 2, 7-13]. The relationship between the index of refraction of the atmosphere n , optical wavelength λ (in μm), temperature T (in kelvin) and pressure P (in millibar) is given approximately as [2]:

$$n = 1 + 77.6 \times 10^{-6} \frac{P}{T} \left(1 + \frac{7.52 \times 10^{-3}}{\lambda^2} \right) \quad (3.4)$$

Whilst a simplified equation for the rate of change in index of refraction with temperature is given by [2]

$$-dn/dT = 7.8 \times 10^{-5} P/T^2 \quad (3.5)$$

Optical turbulence divides the air pocket into turbulence eddies based on the index of refraction. Based on Kolmogorov theory [14], turbulence eddies are classified, based on their sizes, into inner scale l_0 (with size of a

few millimetres) and outer scale L_0 (with size of a few metres). The outer scales of turbulence have focussing effects on the optical signal and are characterised by turbulence eddies larger than the Fresnel zone $\sqrt{l/k}$ or the scattering disk, whichever is larger. The inner scales of turbulence have diffractive effects on the optical signal, and are characterised by turbulence eddies smaller than the Fresnel zone, or the spatial coherence radius ρ_0 , whichever is smaller [7, 13, 15, 16]. For a valid optical link length, the correlation width of irradiance fluctuations (which can be defined as the distance beyond which there is no further correlation of the optical beam due to turbulence effects) $d_0 \approx \sqrt{\lambda l}$ [15] can be classified as a medium scale size (i.e. $l_0 < d_0 < L_0$) which does not contribute to irradiance fluctuation. Moreover, Tatarskii predicted that in weak turbulence conditions, d_0 is of the order of the first Fresnel zone, whereas in strong turbulence conditions, d_0 is defined by the spatial coherence radius of the optical signal [14, 17].

The presence of optical turbulence is responsible for the fluctuation of the optical signal at the detector, known as scintillation [1, 7, 12, 13], exacerbating the spreading of the optical beam (the fundamental contribution to beam spreading comes from diffraction), and loss of spatial and temporal coherence of the laser beam [2, 7, 13, 18]. The scintillation coherence time is usually in order of 1 to 10 ms, which is considerably longer than typical FSO bit periods [6, 19] implying that irradiance fluctuation can be considered constant over a large number of transmitted bits. Furthermore, the scintillation noise is the main impairment in clear atmosphere conditions, and it causes an increase in bit error rate. The magnitude of scintillation is described by the scintillation index σ_I^2 , which is given as

$$\sigma_I^2 = \frac{\langle I^2 \rangle - \langle I \rangle^2}{\langle I \rangle^2} = \frac{\langle I^2 \rangle}{\langle I \rangle^2} - 1 \quad (3.6)$$

where I is the instantaneous irradiance of the optical signal and $\langle I \rangle$ denotes the average irradiance of the optical signal. Equation (3.6) can be written as

a function of the mean, $\mu_{\ln I}$, and variance, $\sigma_{\ln I}^2$, respectively, of the natural logarithm of I is given as

$$\sigma_I^2 = \frac{(\exp(\sigma_{\ln I}^2) - 1) \exp(2\mu_{\ln I} + \sigma_{\ln I}^2)}{\exp(2\mu_{\ln I} + \sigma_{\ln I}^2)} = \exp(\sigma_{\ln I}^2) - 1 \quad (3.7)$$

Aperture averaging

If the receiver collecting lens (RCL) diameter is increased beyond the eddy size causing the irradiance fluctuations, then uncorrelated irradiance fluctuations over the aperture size will be averaged together such that the scintillation noise becomes minimal. This effect is known as aperture averaging [2, 7, 12, 20-22], and it is a well-known method for reducing the deleterious effects of scintillation in FSO communication systems. The decrease in irradiance fluctuation is typically measured using the aperture averaging factor $A = \sigma_I^2(D_{RX}) / \sigma_I^2(0)$, where $\sigma_I^2(D_{RX})$ is the scintillation index for RCL diameter D_{RX} ($D_{RX} = 0$ for a point receiver). The aperture averaging factor A is given by [7, 12]

$$A = \frac{16}{\pi D_{RX}^2} \int_0^{D_{RX}} b_I(\rho, l) \left(\cos^{-1} \left(\frac{\rho}{D_{RX}} \right) - \frac{\rho}{D_{RX}} \sqrt{1 - \frac{\rho^2}{D_{RX}^2}} \right) \rho d\rho, \quad (3.8)$$

where ρ is the separation distance between two points and $b_I(\rho, l)$ is the normalised covariance function.

In very weak turbulence, $\sigma_I^2 \approx \sigma_{\ln I}^2$ and the scintillation index aperture-averaged plane wave for negligible inner scale can be given as [7, 12]

$$\sigma_I^2 = \exp \left[\frac{0.49 \sigma_R^2}{(1 + 0.65d^2 + 1.11\sigma_R^{12/5})^{7/6}} + \frac{0.51 \sigma_R^2 (1 + 0.69\sigma_R^{12/5})^{-5/6}}{1 + 0.90d^2 + 0.62d^2 \sigma_R^{12/5}} \right] - 1 \quad (3.9)$$

where $\sigma_R^2 = 1.23 C_n^2 k^{7/6} l^{11/6}$ is the Rytov variance for plane wave, C_n^2 is the refractive index structure constant with typical range from around $10^{-17} \text{ m}^{-2/3}$ to around $10^{-13} \text{ m}^{-2/3}$ [2, 7, 12], $k = 2\pi/\lambda$ is the optical wave number and $d = \sqrt{k D_{RX}^2 / 4l}$ is the normalised RCL radius [7, 12, 20]. Note that for horizontal path communication link which is generally assumed in this work C_n^2 is constant.

Figure 3.2 shows the scintillation index for a whole range of turbulence strengths and $D_{RX}=1$ mm. It can be seen in Fig. 3.2 that scintillation index, σ_I^2 , increases with square root of the Rytov variance, σ_R , for very weak turbulence conditions, and further increases beyond σ_R of unity until it reaches a maximum value of about 1.2, known as the focusing regime [7]. However, as turbulence strength increases further (beyond the focusing regime) there is a loss of spatial coherence, the focusing effect is weakened and the scintillation index gradually decreases towards unity.

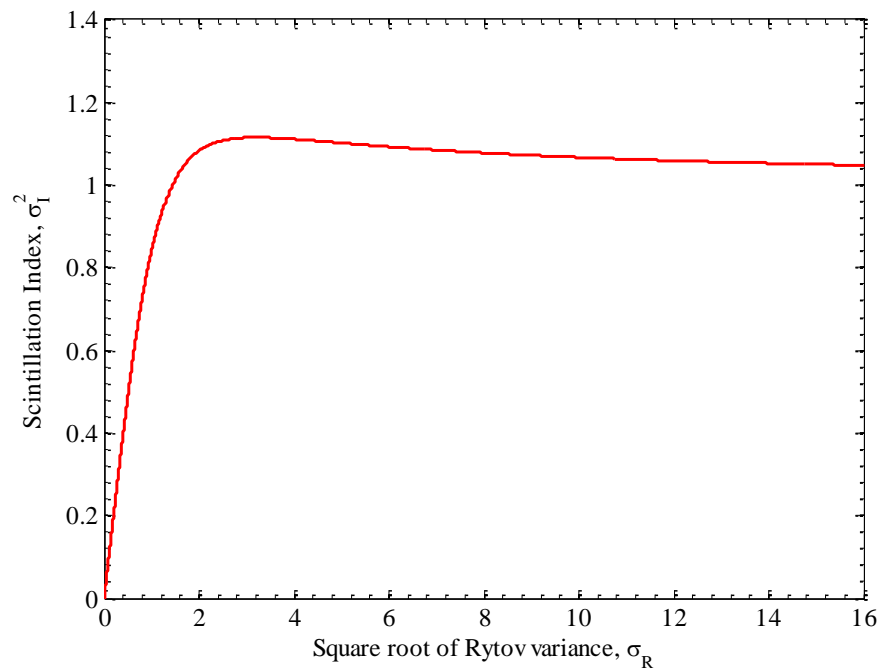


Figure 3.2 Scintillation index, σ_I^2 , for a plane wave as a function of σ_R , the square root of Rytov variance, for $D_{RX} = 1$ mm

The coupling of optical signal from air into an optical fibre results in the decrease in the amount of received average power known as coupling loss and it is dependent on the strength of turbulence [23]. The air-fibre coupling loss, the short single mode fibre is positioned in the focal plane of the RCL, can be calculated numerically by using [23]

$$L_c = 1 - \left\{ 8a^2 \int_0^1 \int_0^1 \exp \left[- \left(a^2 + \frac{A_{RX}}{A_C} \right) (x_1^2 + x_2^2) \right] \times I_0 \left(2 \frac{A_{RX}}{A_C} x_1 x_2 \right) x_1 x_2 dx_1 dx_2 \right\} \quad (3.10)$$

where $a = D_{RX} \pi W_m / 2\lambda f$ is the ratio of the RCL radius to the radius of the backpropagated fibre mode, W_m is the fibre mode field radius at the fibre end face, f is the focal length of the receiver lens, $A_{RX} = \pi D_{RX}^2 / 4$ is the area of the RCL, $A_C = \pi \rho_0^2$ is the spatial coherence area of the incident plane wave, $\rho_0 = (1.46 C_n^2 k^2 l_{fso})^{-3/5}$ is the spatial coherence radius, and $I_0(\cdot)$ is the modified Bessel function of the first kind and zero order.

3.4.1 Probability density function models

Several mathematical models based on probability density function (pdf) of irradiance fluctuations have been proposed in the literature for predicting the reliability of optical signals traversing the atmospheric channel [7, 11, 24-27]. The lognormal distribution is commonly used to model the weak turbulence conditions, although it is not regarded as completely accurate, as its pdf underestimates the pdf tail as obtained from measured data [7, 27, 28]. Consequentially, the lognormal pdf would generally give optimistic bit error rates. The pioneering experimental work of Gracheva and Gurvich [29] over long FSO link lengths reveals the lognormal pdf as being inappropriate for strong turbulence fluctuations.

To address the strong turbulence conditions, a number of models were developed, such as the K-distribution and the lognormally-modulated exponential distribution [7, 24, 27, 30]. Both models agree with measured data, although the latter is less popular as a closed-form solution for its integral is unknown implying quite cumbersome numerical calculations. Moreover, the I-K distribution, the lognormally modulated Rician distribution (also known as the Beckmann's distribution [31]) and recently the gamma-gamma distribution can be used to model the whole range of turbulence conditions [7, 24, 28, 31]. Both the lognormally modulated Rician distribution and gamma-gamma distribution give similar results as

experimental data in weak, moderate and strong turbulence conditions. However the gamma-gamma distribution is commonly used due to the direct relationship between the pdf parameters and atmospheric parameters such as the σ_R^2 and C_n^2 , and the existence of a closed-form expression for the pdf [7, 12, 24]. Beyond the limits of the strong turbulence, that is, the saturation regime, the number of discrete scattering regions is sufficiently large, and the irradiance fluctuations are best described using the negative exponential distribution [7].

3.4.1.1 Lognormal distribution

The lognormal distribution follows the first-order Rytov approximation and it is only valid for predicting weak turbulence irradiance fluctuations (with $\sigma_I^2 < 0.75$ [2, 7]), as the multiple scattering of the turbulence eddies that occur during stronger turbulence levels and/or longer optical link lengths are not accounted for by the Rytov parameter [7, 12, 22, 32]. Based on the central limit theorem, an optical signal propagating through the atmosphere consisting of numerous regions which are characterised by uncorrelated index of refractions, would have normally distributed log-amplitude with pdf given as [7, 15, 32]

$$p_X(X) = \frac{1}{(2\pi\sigma_X^2)^{1/2}} \exp\left\{-\frac{(X - \langle X \rangle)^2}{2\sigma_X^2}\right\} \quad (3.11)$$

where X represent the log-amplitude fluctuation, $\langle X \rangle$ is the ensemble average of log-amplitude X , and σ_X^2 is the variance of the log-amplitude fluctuation (also known as the Rytov parameter).

The irradiance I is related to the log-amplitude X by

$$I = I_0 \exp(2X - 2\langle X \rangle) \quad (3.12)$$

Whilst I_0 is the irradiance in absence of turbulence, and the average irradiance $\langle I \rangle$ is given as [15]

$$\langle I \rangle = E[I_0 \exp(2X - 2\langle X \rangle)] = I_0 \exp(2\sigma_X^2) \quad (3.13)$$

On using the transformation of variable, $p_{LN}(I) = p_X(X) \left| \frac{dX}{dI} \right|$, the lognormal pdf as a function of I can be written as [15]

$$p_{LN}(I) = \frac{1}{2I} \frac{1}{(2\pi\sigma_X^2)^{1/2}} \exp\left\{-\frac{[\ln(I) - \ln(I_0)]^2}{8\sigma_X^2}\right\} \quad (3.14)$$

Given that the variance of the natural logarithm of I , $\sigma_{\ln I}^2 = \exp(4\sigma_X^2) - 1 \approx 4\sigma_X^2$ (in weak turbulence) [32] and substituting (3.13) into (3.14), the pdf can be written as lognormal [12, 22, 32, 33]

$$p_{LN}(I) = \frac{1}{I(2\pi\sigma_{\ln I}^2)^{1/2}} \exp\left\{-\frac{\left[\ln\left(\frac{I}{\langle I \rangle}\right) + \frac{\sigma_{\ln I}^2}{2}\right]^2}{2\sigma_{\ln I}^2}\right\}, \quad I > 0 \quad (3.15)$$

Figure 3.3 shows the lognormal distribution pdf as a function of the normalised irradiance, I for $\sigma_{\ln I}^2$ of 0.01, 0.05, 0.1 and 0.5. It can be seen that, as $\sigma_{\ln I}^2$ increases, the pdf becomes more skewed to the left and it spreads more with longer right-hand tails. The spreading of the pdf at high turbulence strength implies that more optical power would be required to sustain the FSO link as the turbulence strength increases. Overall the lognormal distribution is a popular model for predicting turbulence behaviour in weak turbulence conditions due to its simplicity, however, the lognormal pdf tails, which have direct consequences on communication performance analysis, do not coincide with measured data for either a plane wave or a spherical wave.

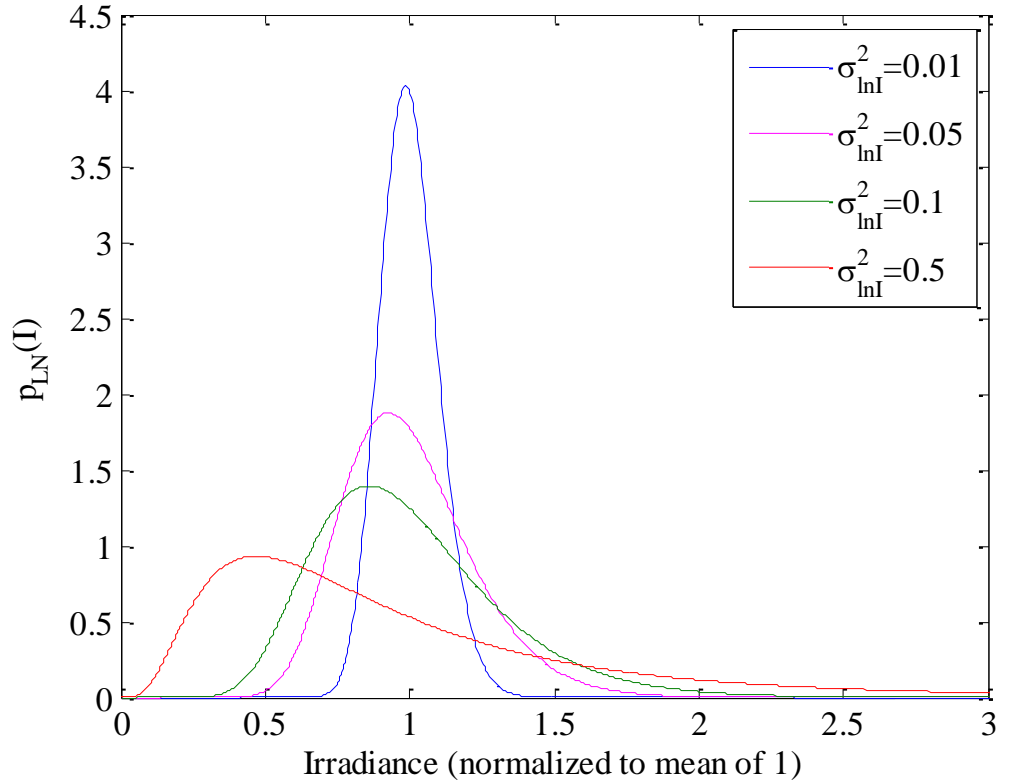


Figure 3.3 Lognormal pdf as a function of normalised irradiance, for a range of $\sigma_{\ln I}^2$

3.4.1.2 K distribution

The K distribution is a widely accepted model for characterising the strong turbulence regime, although it was originally proposed to model non-Rayleigh sea echo [7, 24, 30, 34]. The K distribution is popular because of the closeness of the pdf to measured data for strong turbulence and its direct relationship to atmospheric parameters [30, 34]. The unconditional pdf as a function of the normalised irradiance is given by

$$p_{KD}(I) = \int_0^{\infty} p_1(I|b)p_2(b)db, \quad I > 0 \quad (3.16)$$

where $p_1(I|b)$ is the negative exponential distribution conditioned on mean irradiance b (3.17) and $p_2(b)$ is the gamma distribution (3.18).

$$p_1(I|b) = \frac{1}{b} \exp(-I/b), \quad I > 0 \quad (3.17)$$

$$p_2(b) = \frac{\alpha(\alpha b)^{\alpha-1}}{\Gamma(\alpha)} \exp(-\alpha b), \quad b > 0 \quad (3.18)$$

In (3.18), $\Gamma(\alpha)$ is the gamma function and α is the channel parameter related to the effective number of discrete scatterers (given in (3.23)). On substituting (3.17) and (3.18) into (3.16), the K distribution pdf can be written as [7, 24, 30, 35, 36]

$$P_{KD}(I) = \frac{2\alpha}{\Gamma(\alpha)} (\alpha I)^{(\alpha-1)/2} K_{\alpha-1}(2\sqrt{\alpha I}), \quad I > 0 \quad (3.19)$$

where $K_n(\cdot)$ is the modified Bessel function of the 2nd kind of order n . The K distribution scintillation index $\sigma_I^2 = 1 + 2/\alpha$, always exceeds unity but as $\alpha \rightarrow \infty$, the scintillation index gradually approaches unity, the gamma distribution approaches a delta function and the K distribution becomes a negative exponential. Figure 3.4 shows the K distribution pdf as a function of the normalised irradiance, I for σ_R^2 of 2.02, 20.2, and 202.2, and corresponding α values of 3.99, 7.40, and 18.81, respectively, using a point receiver. It can be seen from Fig. 3.4 that, as the turbulence strength increases, the pdf peak decreases, and the right-hand tail spreads out more covering larger powers.

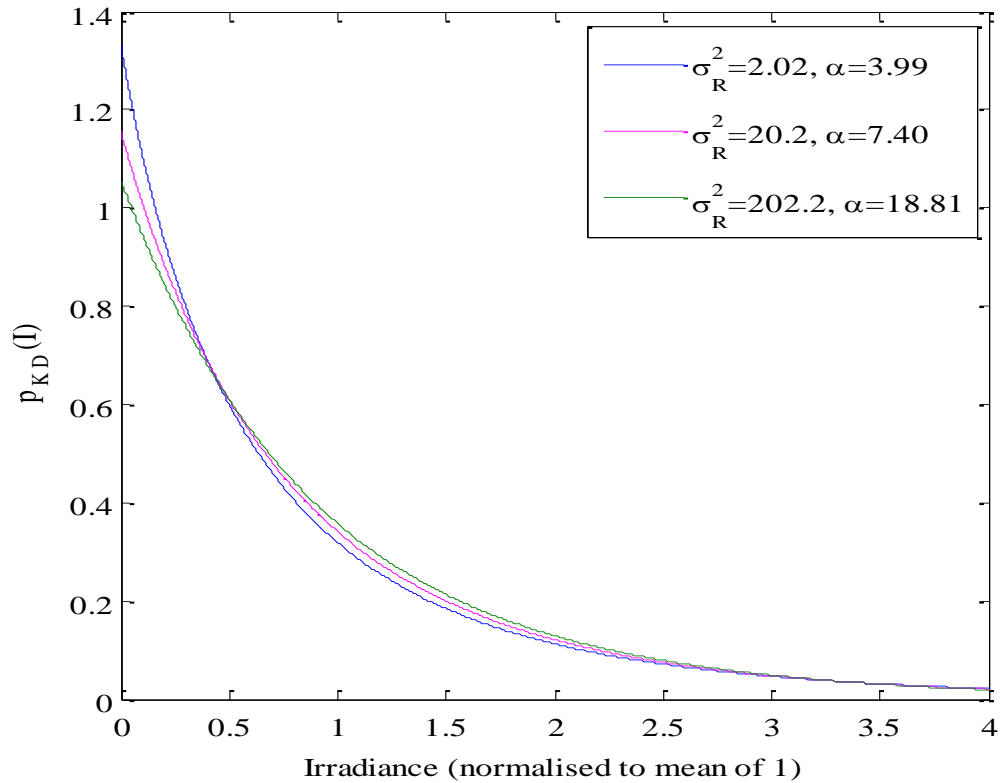


Figure 3.4 K distribution pdf as a function of normalised irradiance, for a range of α & σ_R^2

3.4.1.3 Gamma-gamma distribution

Recently, Andrews and Phillips developed a universal pdf model of irradiance fluctuations [7], although the pdf was highlighted in related but in different context by Nakagami [37], Lewinski [38], and of Teich and Diamant [39]. The gamma-gamma distribution takes into consideration the modulation of the inner scale size over the optical link length by the outer scale size of the atmosphere, making it suitable for modelling weak-to-strong turbulence conditions. The total normalised irradiance is thus given as $I = I_x I_y$, where I_x and I_y are outer scale and inner scale irradiance fluctuations, respectively, which each have gamma distributions,

$$p_x(I_x) = \frac{\alpha(\alpha I_x)^{\alpha-1}}{\Gamma(\alpha)} \exp(-\alpha I_x), \quad \alpha > 0, I_x > 0, \quad (3.20)$$

$$p_y(I_y) = \frac{\beta(\beta I_y)^{\beta-1}}{\Gamma(\beta)} \exp(-\beta I_y), \quad \beta > 0, I_y > 0, \quad (3.21)$$

The unconditional gamma-gamma pdf is given as

$$\begin{aligned} p_{GG}(I) &= \int_0^{\infty} p_y(I|I_x) p_x(I_x) dI_x \\ &= \frac{2(\alpha\beta)^{(\alpha+\beta)/2}}{\Gamma(\alpha)\Gamma(\beta)} I^{-\frac{(\alpha+\beta)}{2}} K_{\alpha-\beta}(2\sqrt{\alpha\beta}I), \quad I > 0, \end{aligned} \quad (3.22)$$

where $p_y(I|I_x)$ is the conditional gamma pdf derivable from (3.21) by replacing $I_y = I/I_x$, α is the effective number of large-scale eddies of the scattering process and β is the effective number of small-scale eddies of the scattering process.

When aperture averaging effect is taken into consideration, for a plane wave assumption, α and β are given as [7, 12, 24]

$$\alpha = \left\{ \exp \left[\frac{0.49\sigma_R^2}{(1 + 0.65d^2 + 1.11\sigma_R^{12/5})^{7/6}} \right] - 1 \right\}^{-1}, \quad (3.23)$$

$$\beta = \left\{ \exp \left[\frac{0.51\sigma_R^2(1 + 0.69\sigma_R^{12/5})^{-5/6}}{1 + 0.90d^2 + 0.62d^2\sigma_R^{12/5}} \right] - 1 \right\}^{-1}, \quad (3.24)$$

Considering a point receiver ($d = 0$), α and β parameters are plotted as a function of the Rytov variance in Fig. 3.5. It can be seen from Fig. 3.5 that at $\alpha \gg 1$ and $\beta \gg 1$, the Rytov variance is less than unity implying a weak turbulence condition. As the Rytov variance approaches unity, α and β values decrease substantially until deep in the moderate-to-strong turbulence regime where α gradually increases again until it becomes unbounded in the saturation and β continues to decrease until it gets to unity in the saturation regime. Under the saturation region condition, the gamma-gamma distribution approaches the K and ultimately the negative exponential distribution. Specifically, the gamma-gamma distribution reduces to the K distribution (3.19) when $\beta=1$. Figure 3.6 shows the gamma-gamma pdf as a function of the normalised irradiance using $\sigma_R^2 = 0.5$ (weak turbulence), 1 (moderate turbulence), and 3.5 (strong turbulence), each having corresponding α and β values of [5.98, 4.39], [4.39, 2.56], and [4.22, 1.36], respectively. It can be seen from Fig. 3.6 that the weak turbulence case give a narrow pdf whereas turbulence strength increases; the pdf is skewed towards the left-hand side and spreads out over a large power range.

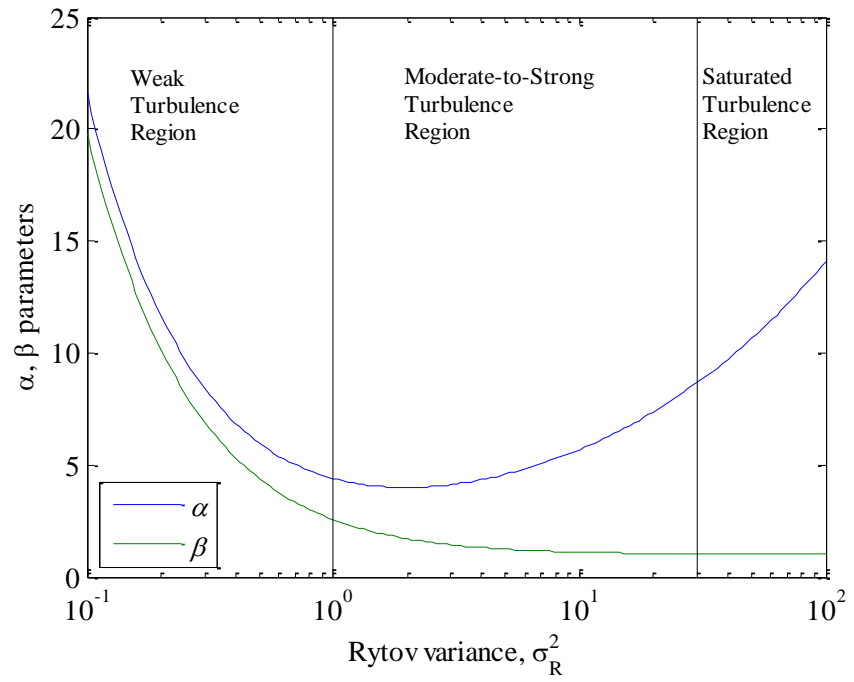


Figure 3.5 Values of α and β for different Rytov variances (and $d = 0$)

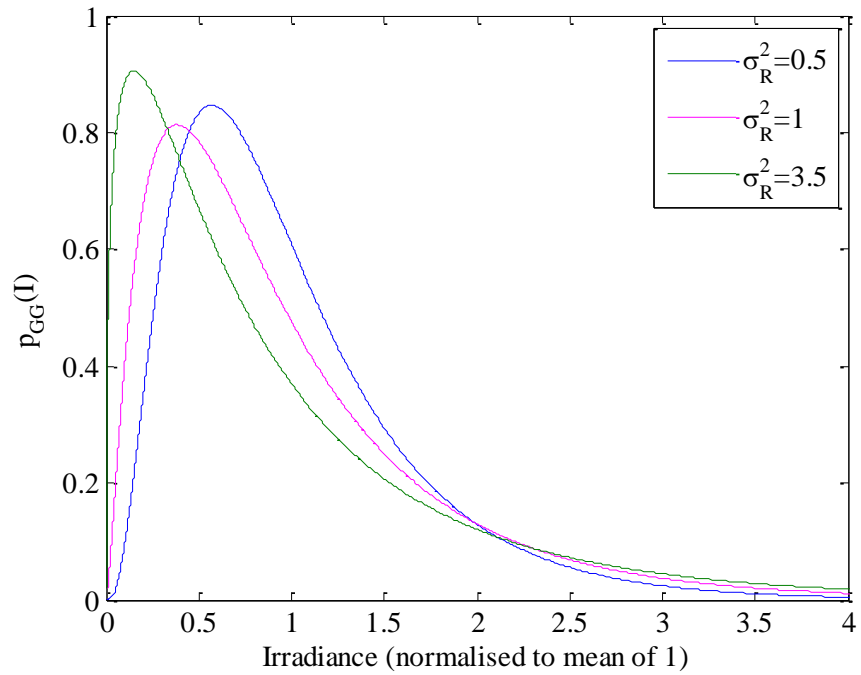


Figure 3.6 Gamma-gamma pdf as a function of normalised irradiance, for a range of α & σ_R^2

3.4.1.4 Negative exponential distribution

In very strong irradiance fluctuations i.e. far into the saturated turbulence regime, where the number of independent scatterings become sufficiently large and the optical link length spans several kilometres, the value of the scintillation index tends to unity (as shown in Fig. 3.2). The optical field traversing this medium is experimentally verified to follow the negative exponential statistics for irradiance with pdf given as [2, 7]

$$p_{NE}(I) = \frac{1}{\langle I \rangle} \exp(-I/\langle I \rangle), \quad \langle I \rangle > 0, \quad (3.25)$$

Whilst Fig. 3.7 shows the negative exponential as a function of irradiance for $\langle I \rangle = 0.5, 1, 2$.

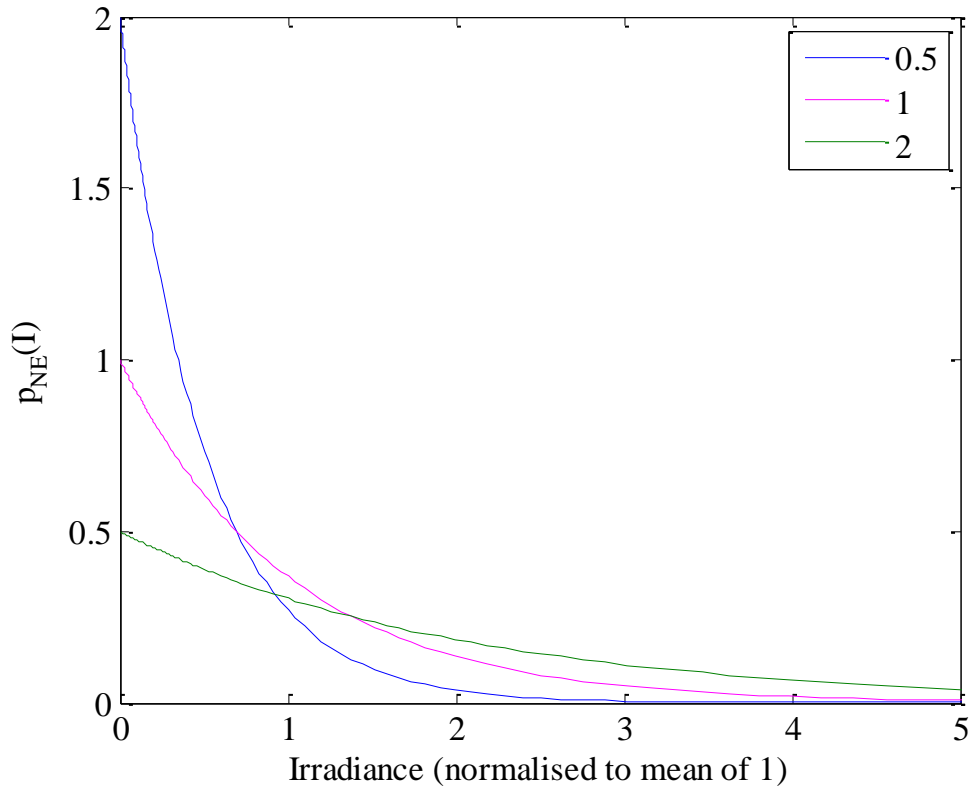


Figure 3.7 Negative exponential pdf as a function of normalised irradiance, for various $\langle I \rangle$

3.5 Beam spreading

A laser beam emanating from a transmitter of diameter D_{TX} is characterized by its planar angular cross-section $\theta = \lambda/D_{TX}$, where λ is the optical wavelength [2]. The schematic representation of the beam spreading in the far field region and with total angular spread $\Theta = 2\theta$ is shown in Fig. 3.8. On traversing the atmosphere in the absence of turbulence, the optical beam experiences angular spread due to diffraction and arrives at the receiver with a beam width given as [40]

$$w_d = w_0 \left[1 + \left(\frac{l}{l_R} \right)^2 \right]^{1/2} \quad (3.26)$$

where $w_0 \cong \lambda/\pi\theta$ is the waist size, l is the optical link length, and $l_R = \pi w_0^2/\lambda$ is the Rayleigh range (the distance at which the diffraction-limited beam width spreads by a factor of $\sqrt{2}$).

However, optical turbulent eddies present in the atmospheric channel introduce random deflections of the optical beam, thereby inducing further beam spreading than what is typically experienced due to diffraction alone. The total beam width due to diffraction and turbulence can be written as [41]

$$w_{total} = w_d \left[1 + 1.33\sigma_R^2 \left(\frac{2l}{kw_d^2} \right)^{5/6} \right]^{1/2} \quad (3.27)$$

Beam spreading loss occurs due to the spreading of the transmitted beam to a size greater than the receiver aperture. In order to minimize this loss, the receiver aperture can be increased or the transmitter divergence can be reduced (which may require pointing and tracking). Beam spreading loss (in dB) can be given approximately as

$$L_{bs} = 20 \log_{10} \left\{ \frac{D_{RX}}{w_0 + w} \right\}, \quad (3.28)$$

where w is either the diffraction-limited beam width (3.26) or the beam width due to diffraction and turbulence (3.27).

Table 3.2 Classification of pointing error [18]

Classes	Duration	Causes
Low-frequency	Minutes to Months	Daily temperature variations
Moderate-frequency	> 1 sec	Wind-induced vibrations
High-frequency	0.1-1 sec	Large machinery vibration (e.g. large fans) Human Activities (e.g. walking, shutting doors)

3.7 Summary

This chapter has examined the common problems facing FSO communications in atmospheric channel such as turbulence-induced scintillation, air-fibre coupling loss and beam spreading, atmospheric attenuation due to scattering and absorption, and pointing error due to building sway. The mathematical models for predicting irradiance fluctuations due to atmospheric turbulence namely the lognormal, gamma-gamma, K and negative exponential distributions were discussed in some detail. The lognormal is valid only for weak turbulence regions, the K distribution is useful only for modelling strong turbulence regions, the negative exponential is valid for modelling saturated regions whilst the gamma-gamma is valid for the whole turbulence regions. Both the K and gamma-gamma pdfs have similar values as measured data. These models would be used in subsequent chapters to characterise optical signal reception and in deriving the expressions for average BERs.

3.8 References

- [1] J. C. Ricklin, S. M. Hammel, F. D. Eaton, and S. L. Lachinova, "Atmospheric channel effects on free-space laser communication," *J. Opt. Fiber Commun.*, vol. 3, no. 2, pp. 111-158, 2006.
- [2] S. Karp, R. M. Gagliardi, S. E. Moran, and L. B. Stotts, *Optical channels: fibers, clouds, water and the atmosphere*, New York: Plenum Press, 1988.

- [3] H. A. Willebrand and B. S. Ghuman, *Free-space optics: enabling optical connectivity in today's networks*, Sams Publishing, Indianapolis, Indiana 46240 USA, 2002.
- [4] M. E. Thomas, "Optical propagation in linear media: atmospheric gases and particles, solid-state components, and water," *Oxford University Press, New York*, 2006.
- [5] A. Prokes, "Atmospheric effects on availability of free space optics systems," *Optical Engineering*, vol. 48, no. 6, pp. 1-10, June 2009.
- [6] D. Killinger, "Free space optics for laser communication through the air," *Optics and Photonics News*, vol. 13, no. 10, pp. 36-42, Oct. 2002.
- [7] L. C. Andrews and R. L. Phillips, *Laser beam propagation through random media*, Second Edition, SPIE Press, Bellingham, Washington, 2005.
- [8] M. Abtahi, P. Lemieux, W. Mathlouthi, and L. A. Rusch, "Suppression of turbulence-induced scintillation in free-space optical communication systems using saturated optical amplifiers," *Journal of Lightwave Technology*, vol. 24, no. 12, pp. 4966-4973, Dec. 2006.
- [9] T. H. Carbonneau and D. R. Wisely, "Opportunities and challenges for optical wireless; the competitive advantage of free space telecommunications links in today's crowded marketplace," *Proc. SPIE Wireless Technologies and Systems: Millimeter-Wave and Optical*, vol. 3232, pp. 119-128, Jan. 1998.
- [10] M. Razavi and J. H. Shapiro, "Wireless optical communications via diversity reception and optical preamplification," *IEEE Transactions on Wireless Communications*, vol. 4, no. 3, pp. 975-983, May 2005.
- [11] X. Zhu and J. M. Kahn, "Free-space optical communication through atmospheric turbulence channels," *IEEE Transactions on Communications*, vol. 50, no.8, pp. 1293-1300, Aug. 2002.
- [12] A. K. Majumdar, "Free-space laser communication performance in the atmospheric channel," *Journal of Optical and Fiber Communications Research*, vol. 2, no. 4, pp. 345-396, 2005.
- [13] L. C. Andrews, R. L. Phillips, C. Y. Hopen, and M. A. Al-Habash, "Theory of optical scintillation," *J. Opt. Soc. Am. A*, vol. 16, no. 6, pp. 1417-1429, June 1999.
- [14] V. I. Tatarskii, "Wave propagation in a turbulent medium, translated from Russian by R. A. Silverman," *McGraw-Hill, New York*, 1961.
- [15] X. M. Zhu and J. M. Kahn, "Communication techniques and coding for atmospheric turbulence channels," *Journal of Optical and Fiber Communications Reports*, vol. 4, no. 6, pp. 363-405, 2007.
- [16] F. S. Vetelino, C. Young, L. Andrews, and J. Rekolons, "Aperture averaging effects on the probability density of irradiance fluctuations in moderate-to-strong turbulence," *Applied Optics*, vol. 46, no. 11, pp. 2099-2108, Apr. 2007.
- [17] V. I. Tatarskii, "The effects of the turbulent atmosphere on wave propagation," *U.S. Department of Commerce*, 1971.
- [18] S. Bloom, E. Korevaar, J. Schuster, and H. A. Willebrand, "Understanding the performance of free-space optics," *Journal of Optical Networking*, vol. 2, no. 6, pp. 178-200, June 2003.

- [19] X. Zhu , J. M. Kahn, and J. Wang, "Mitigation of turbulence-induced scintillation noise in free-space optical links using temporal-domain detection techniques," *IEEE Photonic Technology Letter*, vol. 15, no. 4, pp. 623-625, Apr. 2003.
- [20] M. A. Khalighi, N. Schwartz, N. Aitamer, and S. Bourennane, "Fading reduction by aperture averaging and spatial diversity in optical wireless systems," *Journal of Optical Communications and Networking, IEEE/OSA*, vol. 1, no. 6, pp. 580-593, Nov. 2009.
- [21] F. S. Vetelino, C. Young, and L. C. Andrews, "Fade statistics and aperture averaging for Gaussian beam waves in moderate-to-strong turbulence," *Applied Optics*, vol. 46, no. 18, pp. 3780-3789, June 2007.
- [22] F. S. Vetelino, C. Young, L. Andrews, and J. Reolons, "Aperture averaging effects on the probability density of irradiance fluctuations in moderate-to-strong turbulence," *Applied Optics*, vol. 46, no. 11, pp. 2099-2108, Apr. 2009.
- [23] Y. Dikmelik and F. M. Davidson, "Fiber-coupling efficiency for free-space optical communication through atmospheric turbulence," *Applied Optics*, vol. 44, no. 23, Aug. 2005.
- [24] M. A. Al-Habash, L. C. Andrews, and R. L. Phillips, "Mathematical model for the irradiance probability density function of a laser beam propagating through turbulent media," *Opt. Eng.*, vol. 40, no. 8, pp. 1554-1562, Aug. 2001.
- [25] L. C. Andrews and R. L. Phillips, "Mathematical genesis of the I-K distribution for random optical fields," *J. Opt. Soc. Am. A*, vol. 3, no. 11, pp. 1912-1919, Nov. 1986.
- [26] J. H. Churnside and S. F. Clifford, "Log-normal Rician probability-density function of optical scintillations in the turbulent atmosphere," *J. Opt. Soc. Am. A*, vol. 4, no. 10, pp. 1923-1930, Oct. 1987.
- [27] J. C. Churnside and R. G. Frehlich, "Experimental evaluation of log-normally modulated Rician and IK models of optical scintillation in the atmosphere," *J. Opt. Soc. Am. A*, vol. 6, no. 11, pp. 1760-1766, Nov. 1989.
- [28] R. J. Hill, R. G. Frehlich, and W. D. Otto, "The probability distribution of irradiance scintillation," *NOAA technical memorandum ERL ETL*, vol. 274, 1997.
- [29] M. E. Gracheva and A. S. Gurvich, "Strong fluctuations in the intensity of light propagated through the atmosphere close to the earth," *Izvestiya VUZ. Radiofizika*, vol. 8, pp. 717-724, 1965.
- [30] G. Parry and P. N. Pusey, "K distributions in atmospheric propagation of laser light," *J. Opt. Soc. Am. A*, vol. 69, no. 5, pp. 796-798, May 1979.
- [31] R. J. Hill and R. G. Frehlich, "Probability distribution of irradiance for the onset of strong scintillation," *J. Opt. Soc. Am. A*, vol. 14, no. 7, pp. 1530-1540, July 1997.
- [32] J. C. Ricklin, S. Bucaille, and F. M. Davidson, "Performance loss factors for optical communication through clear air turbulence," *Proceedings of the SPIE*, vol. 5160, pp. 1-12, 2004.

- [33] L. C. Andrews, R. L. Phillips, and P. T. Yu, "Optical scintillations and fade statistics for a satellite-communication system," *Applied Optics*, vol. 34, no. 33, pp. 7742-7751, Nov. 1995.
- [34] E. Jakeman and P. N. Pusey, "Significance of K distributions in scattering experiments," *Phys. Rev. Lett.*, vol. 40, no. 9, pp. 546-550, Feb. 1978.
- [35] T. A. Tsiftsis, H. G. Sandalidis, G. K. Karagiannidis, and M. Uysal, "Optical wireless links with spatial diversity over strong atmosphere turbulence channels," *IEEE Trans. on Wireless Communications*, vol. 8, no. 2, pp. 951-957, Feb. 2009.
- [36] M. Uysal and J. Li, "BER performance of coded free-space optical links over strong turbulence channels," in *Proc. IEEE Vehicular Technology Conference (VTC Spring)*, Milan, Italy, vol. 1, pp. 168-172, May 2004.
- [37] M. Nakagami, "The m-distribution - a general formula of intensity distribution of rapid fading," in *Statistical Methods in Radio Wave Propagation*, W.C. Hoffman, Ed., Pergamon, New York, pp. 3-36, 1960.
- [38] D. J. Lewinski, "Nonstationary probabilistic target and cluster scattering models," *IEEE Transactions on Antenna Propagation*, vol. 31, no. 3, pp. 490-498, 1983.
- [39] M. C. Teich and P. Diament, "Multiple stochastic representations for K distributions and their Poisson transform," *J.Opt. Soc. Am. A*, vol. 6, no. 1, pp. 80-91, 1989.
- [40] A. A. Farid and S. Hranilovic, "Outage capacity optimization for free-space optical links with pointing errors," *Journal of Lightwave Technology*, vol. 25, pp. 1702-1710, July 2007.
- [41] N. S. Kopeika and A. Zilberman, "Vertical profiles of aerosol and optical turbulence strength and their effects on atmospheric propagation," *Proc. of SPIE*, San Jose, CA, USA, vol. 3927, no. 232, pp. 460-467, Jan. 2000.
- [42] S. B. Alexander, *Optical communication receiver design*, SPIE Optical Engineering Press, Bellingham, Washington, vol. TT22, 1997.
- [43] S. Arnon, "Optimization of urban optical wireless communication systems," *IEEE Transactions on Wireless Communications*, vol. 2, no. 4, pp. 626-629, July 2003.
- [44] H. G. Sandalidis, T. A. Tsiftsis, G. K. Karagiannidis, and M. Uysal, "BER performance of FSO links over strong atmospheric turbulence channels with pointing errors," *IEEE Communications Letters*, vol. 12, no. 1, pp. 44-46, Jan. 2008.
- [45] P. J. Winzer, A. Kalmar, and W. R. Leeb, "Role of amplified spontaneous emission in optical free space communication links with optical amplification - impact on isolation and data transmission; utilization for pointing, acquisition, and tracking," *SPIE Proceedings Series*, vol. 3615, pp. 134-141, 1999.

CHAPTER 4 Optical receiver performance

4.1 Overview

This chapter describes the system impairments that can occur in FSO communication systems, namely the receiver noise and the optical crosstalk. This chapter also describes a number of evaluation methods used to analyse the performance of an optically preamplified receiver. Some of the BER evaluation methods highlighted in this project include the Gaussian approximation, and the moment generating function-based Chernoff bound, modified Chernoff bound, and saddlepoint approximation.

4.2 Receiver circuitry noise

The received photocurrent is usually accompanied by additional noise currents, namely the thermal noise current, shot noise current and ASE beat noise currents (in an optically amplified case). The receiver noises typically arise in two forms namely intrinsic noise and coupled noise sources [1]. The intrinsic noise sources arise from fundamental physical effects in the optoelectronic and electronic devices. Examples of intrinsic noises are the receiver thermal and electronic shot noises. The coupled noise sources arise as a result of the interactions between the receiver and the surrounding environment. Examples of coupled noises are background noise, scintillation noise, ASE beat noise and optical crosstalk noise.

4.2.1 Thermal noise

Thermal noise (also called Johnson noise) arises due to thermally induced random fluctuations in the electrons at the resistor. The amount of electron motion is a direct function of the absolute temperature of the resistance. Figure 4.1 shows a simplified version of the receiver circuit. (However, the high impedance and trans-impedance front ends are popular options). The thermal noise current in a load resistor R_L is a zero-mean

Gaussian random process, depending on temperature T and its variance is given as [1, 2]

$$\sigma_{th}^2 = (4k_B T / R_L) B_e \quad (4.1)$$

where $k_B = 1.38 \times 10^{-23}$ J/K is Boltzmann constant, $I_t = \sqrt{4k_B T / R_L}$ is the thermal noise spectral density with typical values in order of a few pA/ $\sqrt{\text{Hz}}$ and B_e the noise equivalent bandwidth of the receiver.

The electrical amplifier also contributes noise, characterised by the noise figure F_n (with typical values of 3-5 dB [2]). When the front-end amplifier noise contribution is included, the thermal noise contribution of the receiver has variance [1, 2]

$$\sigma_{th}^2 = (4k_B T / R_L) F_n B_e \quad (4.2)$$

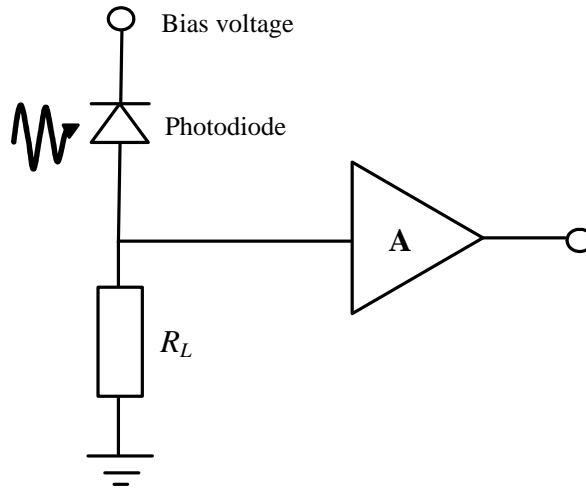


Figure 4.1 A simplified front end receiver circuit

4.2.2 Shot noise

Shot noise arises due to inherent randomness of the arrival of photons at the receiver. The shot noise current has variance

$$\sigma_{sh}^2 = 2q i_n B_e \quad (4.3)$$

where q is the electronic charge, 1.602×10^{-19} C, and i_n is the average photocurrent induced by the received optical signal.

In the case of an APD, the photocurrent is given by $i_n = G_m RP$, and the shot noise current at the APD output has variance [2, 3]

$$\sigma_{sh}^2 = 2qG_m^2 F_A(G_m) RPB_e \quad (4.4)$$

where $F_A(G_m)$ is called the excess noise factor of the APD ($F_A = 1$ for a PIN photodiode) and is an increasing function of the multiplicative (Avalanche) gain G_m . It is given by [2]

$$F_A(G_m) = k_A G_m + (1 - k_A)(2 - 1/G_m) \quad (4.5)$$

where k_A is the ionization coefficient ratio (with value in range 0-1) and is a property of the semiconductor material used to make up the APD.

4.3 Linear crosstalk

There are two types of linear crosstalk that can occur in a WDM system, namely interchannel crosstalk and intrachannel crosstalk. Assuming an optical signal with power, P_{sig} , angular frequency, ω_{sig} , and phase, ϕ_{sig} , and assuming the signal is accompanied by a single crosstalk signal with power, P_{XT} , angular frequency, ω_{XT} , and phase, ϕ_{XT} , with both being incident on a PIN photodiode followed by electrical low pass filtering of bandwidth B_e , then the optical signal and crosstalk electric fields (with unit $W^{1/2}$) can be written, respectively, as

$$E_{sig}(t) = \sqrt{2P_{sig}(t)} \cos(\omega_{sig}t + \phi_{sig}) \quad (4.6)$$

$$E_{XT}(t) = \sqrt{2P_{XT}(t)} \cos(\omega_{XT}t + \phi_{XT}) \quad (4.7)$$

The resulting photocurrent comes from square law detection, and assuming there is full beating due to the signal and crosstalk being in the same polarisation. It is given by

$$i(t) = R \overline{[E_{sig}(t) + E_{XT}(t)]^2} = R \overline{[E_{sig}(t)]^2 + 2E_{sig}(t)E_{XT}(t) + [E_{XT}(t)]^2} \quad (4.8)$$

On substituting (4.6) and (4.7) into (4.8), the output photocurrent will be obtained as

$$i(t) = R(P_{sig}(t) + P_{XT}(t) + 2\sqrt{P_{sig}(t)P_{XT}(t)} \cos((\omega_{sig} - \omega_{XT})t + \phi_{sig} - \phi_{XT})) \quad (4.9)$$

4.3.1 Interchannel crosstalk

The interchannel crosstalk occurs when the crosstalk signal and the desired signal have sufficiently different wavelengths on the ITU-T frequency channel. Here the frequency of the beat term (50 GHz or 100 GHz [4]) is greater than the receiver's electrical filter bandwidth and so it does not pass to the decision device. The resultant photocurrent at the decision device, around the decision time, can be written as [5]

$$i_d(t) = R(P_{sig}(t) + P_{XT}(t)) \quad (4.10)$$

4.3.2 Intrachannel crosstalk

The intrachannel crosstalk typically occurs when the crosstalk signal and the desired signal have the same (at least nominal) frequency on the ITU-T frequency grid. More specifically it is when the frequency beat term is within the receiver's electrical bandwidth. Intrachannel crosstalk effects are generally more severe than the interchannel crosstalk effects. It is commonly referred to as co-channel crosstalk and can be further divided into two forms, namely co-channel homodyne crosstalk (itself subdivisible depending on phase correlation), and co-channel heterodyne crosstalk.

4.3.2.1 Co-channel homodyne

Co-channel homodyne crosstalk occurs when the interferer and the desired signal come from the same source, so both signals have the same wavelength and frequency, although they travel to the receiver by a different path. It can be classified into phase correlated, and phase uncorrelated. The photocurrent at the decision device, at around the decision time, can be written as

$$i_d(t) = R\left(P_{sig}(t) + P_{XT}(t) + 2\sqrt{P_{sig}(t)P_{XT}(t)}\cos(\phi_{sig} - \phi_{XT})\right) \quad (4.11)$$

Phase correlated

If the propagation delay between the signal and interferer is less than the laser source coherence length, then the phase delays are correlated. This is

also referred to as the multipath fading effect. Here, there will be a slow change in the argument of cosine meaning that the cosine value will potentially sit at, or around, the worst case (for a ONE) of -1, for a relatively long time.

Phase uncorrelated

If the propagation delay between the signal and interferer is greater than the laser source coherence length, then the phase delays are uncorrelated and the cosine term varies more rapidly. This is also referred to as the interferometric fading effect.

4.3.2.2 Co-channel heterodyne

Co-channel heterodyne crosstalk occurs when the signal and interferer have the same nominal wavelengths but originate from different sources (thus having different frequencies). The photocurrent at the decision device, at around the decision time, is given by:

$$i_d(t) = R(P_{sig}(t) + P_{XT}(t) + 2\sqrt{P_{sig}(t)P_{XT}(t)}\cos((\omega_{sig} - \omega_{XT})t + \phi_{sig} - \phi_{XT})) \quad (4.12)$$

4.4 Performance evaluation methods

The performance of a digital optical communication system is usually quantified by its bit error rate (BER). Bit errors can occur in FSO communication systems due to impairments such as optical attenuation, turbulence-induced scintillation and beam spreading, pointing error due to building sway, receiver and ASE beat noises, and optical crosstalk. In designing a FSO communication system, it is very important to perform an evaluation of the acceptable BER (in the absence of forward error correction) i.e. 10^{-9} for laboratory experiments [6-8], 10^{-6} for intersatellite link [9] and 10^{-12} for commercial telecommunications applications [2].

A number of computational methods have been developed over the years for calculating the BER of a direct detection optical system. Some of the common methods used in the project include the Gaussian approximation (GA), Chernoff bound (CB), modified Chernoff bound (MCB), and

saddlepoint approximation (SPA) [10-13]. The performance of these methods depends on their accuracy, speed of computation, and complexity of formulation, although the most important criterion will be the computational accuracy of the method.

4.4.1 Gaussian approximation

The GA is a widely used method for performance evaluation, mainly because of its simplicity and the extremely short computational time. This method takes into consideration the first two moments, i.e. mean and variance, and then assumes a Gaussian shape, in order to characterise the pdf tail. In the presence of additional impairments, apart from the Gaussian receiver thermal noise in the electrical domain, the GA will not give a complete statistical description of the signal and noise behaviour.

In an optically preamplified receiver configuration, the mean and variances were developed by Olsson [14], and are given as:

$$i = RGP \quad (4.13)$$

$$\sigma_{th}^2 = I_t^2 B_e \quad (4.14)$$

$$\sigma_{sh}^2 = 2qR(GP + N_0 B_0) B_e \quad (4.15)$$

$$\sigma_{sig-ASE}^2 = 4R^2 G P N_0 B_e \quad (4.16)$$

$$\sigma_{ASE-ASE}^2 = 2R^2 N_0^2 (2B_0 - B_e) B_e \quad (4.17)$$

Assuming that the binary symbols are *a priori* equally probable, the BER under the Gaussian approximation can be written as

$$\begin{aligned} BER &= P(1|0)P(0) + P(0|1)P(1) \\ &= \frac{1}{2} \int_{i_D}^{\infty} f_{X_0}(x_0) dx_0 + \frac{1}{2} \int_{-\infty}^{i_D} f_{X_1}(x_1) dx_1 \end{aligned} \quad (4.18)$$

where i_D is the decision threshold, and $f_X(x)$ is the pdf of the Gaussian distribution with continuous random variable X , given by

$$f_X(x) = \frac{1}{\sqrt{2\pi}\sigma_X} \exp\left(-\frac{(x - i_X)^2}{2\sigma_X^2}\right) \quad (4.19)$$

On substituting (4.19) into (4.18), the BER can be written as

$$BER_{GA} = \frac{1}{2} \left(\frac{1}{2} \operatorname{erfc} \left(\frac{i_D - i_0}{\sqrt{2\sigma_0^2}} \right) \right) + \frac{1}{2} \left(\frac{1}{2} \operatorname{erfc} \left(\frac{i_1 - i_D}{\sqrt{2\sigma_1^2}} \right) \right) \quad (4.20)$$

where i_0 and i_1 represent the random variables for the total signal and noise current for transmitted 0 and 1.

If $P(0|1)$ and $P(1|0)$ are equated, then the channel is said to be a binary symmetric channel (BSC). When this is done, it effectively sets:

$$\frac{i_D - i_0}{\sigma_0 \sqrt{2}} = \frac{i_1 - i_D}{\sigma_1 \sqrt{2}} \quad (4.21)$$

and simple algebra shows that there is an ‘optimal’ decision threshold, given by:

$$i_{D_{opt}} = \frac{\sigma_1 i_0 + \sigma_0 i_1}{\sigma_1 + \sigma_0} \quad (4.22)$$

To minimize the BER, an optimum threshold can be obtained by differentiating BER_{GA} (4.20) with respect to i_D and setting the result to zero.

$$\frac{dBER_{GA}}{di_D} = 0 \quad (4.23)$$

The solution of (4.23) gives the optimal decision threshold $i_{D_{opt}}$, which can be written as

$$i_{D_{opt}} = \frac{1}{\sigma_0^2 - \sigma_1^2} \left(i_1 \sigma_0^2 - i_0 \sigma_1^2 - \sigma_0 \sigma_1 \sqrt{(i_0 - i_1)^2 - 2(\sigma_0^2 - \sigma_1^2) \ln \left(\frac{\sigma_1}{\sigma_0} \right)} \right) \quad (4.24)$$

When $\sigma_1 \approx \sigma_0$ such that the $\ln()$ term can be neglected, $i_{D_{opt}}$ in (4.22) is recovered. However, frequently, when signal dependent noise (APD shot or, when OSNR poor, signal spontaneous beat noise) dominates then $\sigma_1 \gg \sigma_0$, and the mathematical optimum deviates from the BSC threshold.

On substituting (4.22) into (4.20), the GA BER can be written as

$$BER_{GA} = \frac{1}{2} \operatorname{erfc} \left(\frac{Q}{\sqrt{2}} \right) \quad (4.25)$$

where $Q = \frac{i_1 - i_0}{\sigma_1 + \sigma_0}$

4.4.2 Methods using the moment generating function (MGF)

The evaluation methods based on the MGF are capable of giving improved computational accuracy compared to the GA, as it provides the required characterisation of the signal and noise processes. Essentially, the MGF is the Laplace transform of the PDF of a variable X . For continuous random variable, it is given by

$$M_X(s) = E(e^{sx}) = \int_{-\infty}^{\infty} p_X(x) e^{sx} dx \quad (4.26)$$

and for a discrete random variable, it is given by

$$M_X(s) = E(e^{sx}) = \sum_{r=0}^{\infty} p_r e^{sr} \quad (4.27)$$

where p_r is the probability of $X = r$, i.e. $P(X = r)$.

Personick [15] developed the first MGF-based analysis for the optically preamplified receiver. The MGF is given as [15]:

$$\begin{aligned} M_C(s) &= \int_0^{\infty} \left[\sum_0^{\infty} p(c|\Lambda) e^{sc} \right] p(\Lambda) d\Lambda \\ &= \int_{-\infty}^{\infty} e^{\Lambda(e^s - 1)} p(\Lambda) d\Lambda \\ &= \left[1 - \frac{\eta N_0}{hf_c} (e^s - 1) \right]^{-L} \exp \left\{ \frac{\frac{\eta}{hf_c} \sum \left| \frac{1}{\sqrt{T}} \int_T n(t) e^{-i(2\pi kt/T)} dt \right|^2 (e^s - 1)}{1 - \frac{\eta N_0}{hf_c} (e^s - 1)} \right\} \end{aligned} \quad (4.28)$$

$$\Lambda = \frac{\eta}{hf_c} \int_{-T_b/2}^{T_b/2} |\varepsilon_r(t)|^2 dt \quad (4.29)$$

$$\varepsilon_r(t) = m(t) e^{i\omega t} + n(t) \quad (4.30)$$

where C is the total number of primary photoelectron counts, $\varepsilon_r(t)$ is the exponential Fourier series of the input optical field, Λ is the average number of received primary counts in a baud interval given $\varepsilon_r(t)$, $m(t)$ is the

complex envelope of signal, $n(t)$ is the optical field of noise, ω is the optical carrier frequency, and $L = B_e T_b$.

Other authors such as Fyath and O'Reilly [16] and Ribeiro *et al.* [13] developed various versions of MGF. In [12], MGF-based bounds and GA, for comparison purpose, were used for APD receivers analysis. In [13], Ribeiro *et al.* developed a MGF including time varying effects and the mean and variance obtained coincides with those proposed by Yamamoto for use in a GA [17].

The MGF, for random variable Y describing signal and ASE noise, as derived by Ribeiro is written as [13]

$$M_Y(s) = \frac{\exp\left\{\int_{-\infty}^{\infty} \left[\frac{R'G(e^{sqh_r(t-\tau)} - 1)h_p(\tau)}{1 - R'N_0(e^{sqh_r(t-\tau)} - 1)} \right] d\tau \right\}}{\exp\left\{\int_{-\infty}^{\infty} B_0 \ln[1 - R'N_0(e^{sqh_r(t-\tau)} - 1)] d\tau \right\}} \quad (4.31)$$

where $h_p(\tau)$ is the optical power pulse at the amplifier input, τ is the fluorescence lifetime, $h_r(t)$ is the receiver impulse response, G is the amplifier gain, B_0 is the optical bandpass filter (OBPF), N_0 is the ASE noise power spectral density (in W/Hz), and $R' = \eta/hf_c$.

On introducing the receiver thermal noise MGF, which is statistically independent from the MGF of the optical signal plus ASE noise, the combined MGF can be written as

$$M_Z(s) = M_{th}(s)M_Y(s) \quad (4.32)$$

where $M_{th}(s) = \exp(s^2 \sigma_{th}^2 / 2)$.

4.4.2.1 Chernoff bound

The MGF can be used in a CB on the BER. This provides a fairly tight upper bound on the BER, which is often more helpful than a GA (as it is not known when the GA is being pessimistic or optimistic). The BER, assuming transmitted 1's and 0's are equal probable, can be given by:

$$BER = \frac{1}{2} [P(1|0) + P(0|1)] \quad (4.33)$$

The general expression for the CB is derived using an exponential bounding function, $e^{s(x-i_D)} \geq U(x-i_D)$, $s > 0$, when considering the positive tail as shown in Fig. 4.2, such that [10]:

$$\begin{aligned} P(X > i_D) &= E\{U(X - i_D)\} \\ &\leq E\{\exp[s(X - i_D)]\} = E\{\exp(sX) \exp(-si_D)\} \\ &= \exp(-si_D) E\{\exp(sX)\} \\ &= \exp(-si_D) M_X(s) \quad s > 0 \end{aligned} \quad (4.34)$$

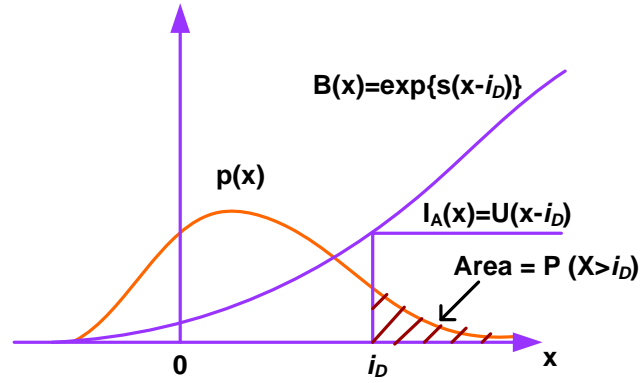


Figure 4.2 Chernoff bound

On applying the CB to each of the conditional probabilities in (4.33), $P(1|0)$ and $P(0|1)$ can be re-written, respectively, as

$$P(1|0) = P(i_0 > i_D) \leq \exp(-s_0 i_D) M_{i_0}(s_0) \quad s_0 > 0 \quad (4.35)$$

$$P(0|1) = P(i_1 < i_D) \leq \exp(-s_1 i_D) M_{i_1}(s_1) \quad s_1 < 0 \quad (4.36)$$

where i_0 and i_1 represent the random variables for the total signal and noise current for transmitted 0 and 1.

The CB upon BER can be conveniently written as in (4.37), by assuming a single variable $s = s_0 = -s_1$, with only slight loss of tightness, [10, 13]

$$BER_{CB} \leq \frac{1}{2} [\exp(si_D) M_{i_1}(-s) + \exp(-si_D) M_{i_0}(s)] \quad (4.37)$$

4.4.2.2 Modified Chernoff bound

The MCB uses similar principles as the CB, but it has the potential of providing tighter bounds upon the BER. The MCB was originally developed by Prabhu [18] for investigating electrical communication systems corrupted by additive interference and independent zero-mean Gaussian noise. Subsequently, the MCB has been extended for analysing optical communication receivers, for example in [19, 20].

The MCB upon the BER for an equal probable symbol 1 and 0 is given by [10, 11, 13]

$$BER_{MCB} \leq \frac{1}{2s\sqrt{2\pi\sigma_{th}^2}} \left(M_{i_1}(-s)\exp(s i_D) + M_{i_0}(s)\exp(-s i_D) \right) \quad s > 0 \quad (4.38)$$

Equation (4.38) is performed for a one-dimensional optimization on the variable ($s = s_0 = -s_1$), leading to slight loss of tightness, but an improved computational speed. The MCB is generally considered to be a safe estimation method for FSO communications BER evaluation [11, 21].

4.4.2.3 Saddlepoint approximation

The SPA was first developed by Helstrom [22, 23]. The SPA has similar formulation as the MCB except that it includes second derivatives of the MGF which makes it more complex. The SPA is believed to be lower BERs compared to the MCB, while the MCB has compact formulation and is computationally quicker [11, 13]. The BER using SPA for an equal probable symbol 1 and 0 is given by [10, 11, 13]

$$BER_{SPA} = \frac{1}{2s\sqrt{2\pi}} \left(\frac{M_{i_0}(s)\exp(-s i_D)}{\sqrt{\psi_0''(s)}} + \frac{M_{i_1}(-s)\exp(s i_D)}{\sqrt{\psi_1''(s)}} \right) \quad s > 0 \quad (4.39)$$

$$\psi_0(s) = \ln \left(\frac{M_{i_0}(s)\exp(-s i_D)}{s} \right) \quad (4.40)$$

$$\psi_1(s) = \ln \left(\frac{M_{i_1}(-s)\exp(s i_D)}{s} \right) \quad (4.41)$$

4.5 Summary

This chapter presents a general description of system impairments in amplified FSO communications such as receiver noises (Gaussian thermal noise and shot noise), ASE beat noises (signal-spontaneous and spontaneous-spontaneous) and optical crosstalk (interchannel and intrachannel). Computational methods based on GA, CB, MCB and SPA, which are used to analyse the detection performance disturbed by ASE beat noises are presented. The GA has the simplest and the fastest computational method followed by the MCB and SPA. However, the MGF methods give more accurate statistical characterization of the signal and noise behaviour in an amplified FSO receiver compared to the GA (which uses minimum statistics). Finally, the MCB is believed to give more optimistic predictions since it is very much tighter bound than CB. In comparison to SPA, MCB is faster and has the advantage of being upper bound on BERs. The evaluation methods would be investigated for optically amplified FSO systems in subsequent chapters.

4.6 References

- [1] S. B. Alexander, *Optical communication receiver design*, SPIE Optical Engineering Press, Bellingham, Washington, vol. TT22, 1997.
- [2] R. Ramaswami and K. N. Sivarajan, *Optical networks- a practical perspective*, Second Edition, Academic Press, London, 2002.
- [3] A. K. Majumdar, "Free-space laser communication performance in the atmospheric channel," *Journal of Optical and Fiber Communications Research*, vol. 2, no. 4, pp. 345-396, 2005.
- [4] C. H. Lee, W. V. Sorin, and B. Y. Kim, "Fiber to the home using a PON infrastructure," *Journal of Lightwave Technology*, vol. 24, no. 12, pp. 4568-4583, Dec. 2006.
- [5] A. J. Phillips, "Power penalty for burst mode reception in the presence of interchannel crosstalk," *IET Optoelectronics*, vol. 1, no. 3, pp. 127-134, 2007.
- [6] S. Bloom, E. Korevaar, J. Schuster, and H. A. Willebrand, "Understanding the performance of free-space optics," *Journal of Optical Networking*, vol. 2, no. 6, pp. 178-200, June 2003.
- [7] D. O. Caplan, "Laser communication transmitter and receiver design," *Journal of Optical Fibre Communication Report*, vol. 4, pp. 225-362, 2007.

- [8] S. Karp, R. M. Gagliardi, S. E. Moran, and L. B. Stotts, *Optical channels: fibers, clouds, water and the atmosphere*, New York: Plenum Press, 1988.
- [9] A. J. Phillips, R. A. Cryan, and J. M. Senior, "An optically preamplified intersatellite PPM receiver employing maximum likelihood detection," *IEEE Photonic Technology Letter*, vol. 8, no. 5, pp. 691-693, May 1996.
- [10] K. W. Cattermole and J. J. O'Reilly, *Mathematical topics in telecommunications volume 2: problems of randomness in communication engineering*, Pentech Press Limited, Plymouth, 1984.
- [11] I. T. Monroy and E. Tangdiongga, *Crosstalk in WDM communication networks*, Kluwer Academic Publishers, Norwell, Massachusetts, USA, 2002.
- [12] J. O'Reilly and J. R. F. Da Rocha, "Improved error probability evaluation methods for direct detection optical communication systems," *IEEE Transactions on Information Theory*, vol. 33, no.6, pp. 839-848, Nov. 1987.
- [13] L. F. B. Ribeiro, J. R. F. Da Rocha, and J. L. Pinto, "Performance evaluation of EDFA preamplified receivers taking into account intersymbol interference," *Journal of Lightwave Technology*, vol. 13, no. 2, pp. 225-232, Feb. 1995
- [14] N. A. Olsson, "Lightwave systems with optical amplifiers," *Journal of Lightwave Technology*, vol. 7, no. 7, pp. 1071-1082, July 1989.
- [15] S. D. Personick, "Applications for quantum amplifiers in simple digital optical communication systems," *Bell System Technical Journal*, vol. 52, pp. 117-133, 1973.
- [16] R. S. Fyath and J. J. O'Reilly, "Comprehensive moment generating function characterisation of optically preamplified receivers," *IEE Proceedings - Optoelectronics*, vol. 137, no. 6, pp. 391-396, Dec. 1990.
- [17] Y. Yamamoto, "Noise and error rate performance of semiconductor laser amplifiers in PCM-IM optical transmission systems," *IEEE Journal of Quantum Electronics*, vol. 16, no. 10, pp. 1073-1081, Oct. 1980.
- [18] V. K. Prabhu, "Modified Chernoff bounds for PAM systems with noise and interference," *IEEE Trans. on Inform. Theory*, vol. 28, no. 1, pp. 95-100, Jan. 1982.
- [19] J. R. F. Da Rocha and J. J. O'Reilly, "Modified chernoff bound for binary optical communication," *Electronics Letters*, vol. 18, no. 16, pp. 708-710, Aug. 1982.
- [20] J. J. O'Reilly, J. R. F. Da Rocha, and K. Schumacher, "Optical fiber direct detection receivers optimally tolerant to jitter," *IEEE Trans. Commun.*, vol. 34, no. 11, pp. 1141-1147, Nov. 1986.
- [21] A. O. Aladeloba, A. J. Phillips, and M. S. Woolfson, "Improved bit error rate evaluation for optically pre-amplified free-space optical communication systems in turbulent atmosphere," *IET Optoelectronics*, vol. 6, no. 1, pp. 26-33, Feb. 2012.

- [22] C. W. Helstrom, "Performance analysis of optical receivers by saddlepoint approximation," *IEEE Trans. Commun.*, vol. 27, no. 1, pp. 186-191, Jan. 1979.
- [23] C. W. Helstrom, "Computing the performance of optical receivers with Avalanche diode detectors," *IEEE Trans. Commun.*, vol. 36, no. 1, pp. 61-66, Jan. 1988.

CHAPTER 5 Analysis of FSO communication systems impaired by atmospheric turbulence and ASE noise

5.1 Introduction

The application of optical preamplification to overcome the impact of receiver thermal noise is one way of improving the receiver sensitivity of FSO communication systems. Aside from the optical gain, the optical preamplifier also generates amplified spontaneous emission (ASE) noise which in turn generates additional beat noises (spontaneous-spontaneous and signal-spontaneous) in the electrical domain at the receiver. The overall electrical domain noise is non-Gaussian, although it has often been approximated as Gaussian in probability density functions (pdfs) used for describing binary signals dominated by ASE noise [1, 2]. The inadequacy of this approach (despite a fortuitous near cancelling of erroneous Gaussian tails that gives the approach some credibility [3]) led to more advanced techniques being developed in fibre system performance calculations [4, 5]. However when FSO reception in the presence of ASE and turbulence has been considered so far, it has typically been with the Gaussian approximation (GA) assumed for the conditional error probability for a given irradiance [6, 7]. A noncentral chi square pdf approach has also recently been used [8].

The moment generating function (MGF) represents a convenient statistical way of describing the signal plus ASE noise in a system employing an optically preamplified receiver while the Chernoff bound (CB), the modified Chernoff bound (MCB), and the saddlepoint approximation (SPA) are techniques that use this description to obtain upper bounds upon (or approximation of) the bit error rate (BER) [5, 9-11]. Like the pdf, the MGF can provide a detailed statistical characterisation of the signal plus noise processes encountered in direct detection optical receivers [10, 11]. This chapter presents a MGF based approach for modelling the performance of an on-off keying (OOK), non-return-to-zero (NRZ),

intensity modulated turbulent FSO system with an optically preamplified receiver. Unlike in OOK-NRZ-based optical fibre systems where the decision threshold is steady, the OOK-NRZ-based FSO system threshold is dependent on the instantaneous irradiance. The decision circuit at the receiver thus uses an adaptive threshold because of the near optimal performance that is achievable. This, however, implies that the threshold level varies in sympathy with the fluctuating average incident optical signal, though it should be noted that turbulence fluctuations are much slower (~ 1 kHz [7, 12, 13]) than the bit rates to be used. The lognormal (LN), gamma-gamma (GG), K (KD) and negative exponential (NE) distributions are employed in this analysis, and the results obtained are compared with the customary GA approach. The work in this chapter led to publication [14].

5.2 Receiver system

Figure 5.1 shows the schematic diagram of an optically preamplified FSO receiver. A laser source with operating wavelength λ of $1.55 \mu\text{m}$ is assumed in this thesis. The optical beam spreads out as it approaches the receiver with beam pattern characterised by its planar angular cross section $\theta = \lambda/D_{TX}$ [15, 16] (assuming a diffraction-limited optical system), where D_{TX} is the transmitter aperture diameter. Non-return-to-zero (NRZ) OOK modulation is assumed. At the receiver, the receiver collecting lens (RCL) is assumed to be perfectly aligned with the transmitter lens in a pointing, acquisition, and tracking (PAT) scheme. It collects the incident laser beam which is coupled to a fibre using a collimator (following [17]) and then optically amplified. The process of optical preamplification produces ASE noise whose field is statistically described as Gaussian. An optical bandpass filter (OBPF) is placed after the preamplifier to reduce significantly the ASE noise in the incident optical signal. Another OBPF (not shown) can be placed before the preamplifier to reduce the ambient light. The use of an additional OBPF before the optical amplifier is neglected in the current paper because the ambient light (that accompanies the optical signal) even after optical amplification is typically small compared to the ASE, and can

be filtered by the OBPF after the optical amplifier, which must be retained to control ASE-ASE beat noise. A P-I-N photodiode with quantum efficiency η is placed after the optical amplifier to convert the information-bearing light into an electrical signal. An avalanche photodiode could also be used which is advantageous compared to a P-I-N photodiode with no optical preamplifier, but of only limited value with the optical preamplifier. This electrical signal is then electrically preamplified and filtered before being passed to the decision device where the threshold is applied. The process of photodetection can be described as a square law detection in which the signal beats with ASE noise, causing signal-spontaneous beat noise, and also the ASE beats with itself, causing spontaneous-spontaneous beat noise. Typically these beat noises, and particularly the signal-spontaneous beat noise, mean that the receiver is no longer dominated by receiver thermal noise. As stated earlier the threshold is assumed to adapt to the instantaneous irradiance at the receiver. Consequently an optimal threshold for each instantaneous irradiance level is assumed. This can be realistically approached e.g. in the Kalman filter based method of [18].

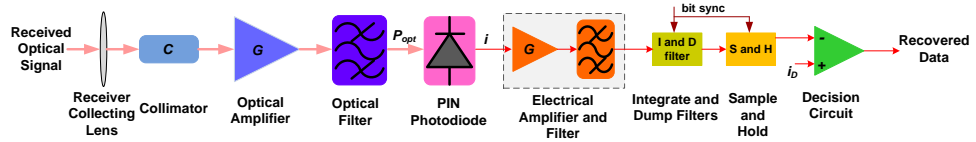


Figure 5.1: Optically preamplified FSO receiver

5.3 Atmospheric channel models

In clear air conditions, optical beam propagation through the atmosphere is particularly affected by turbulence-induced scintillation which significantly reduces the performance of the link [16, 19, 20]. The major consequence of scintillation is fluctuations in the irradiance at the receiver, which results in high BERs [19, 21-24]. Several mathematical models have been proposed to characterise different turbulence regimes using pdfs for the randomly varying irradiance [7, 16, 19, 20, 25]. The modified Rician, LN distribution, and more recently the GG distribution, are the commonly reported models for characterising the weak turbulence regime, although the

modified Rician pdf which does not agree with experimental measurements is less popular [19, 25]. In the strong turbulence regimes, several models such as the K, GG and NE distributions have been proposed, with the latter best suited for saturated regimes [16, 19]. However, it should be noted that the GG distribution gives a better fit to weak irradiance fluctuation measured data when compared to the LN distribution [19, 25-27], whilst both the K and GG distributions show excellent fits with strong turbulence measured data [19, 28]. Table 5.1 shows the pdfs of all atmospheric turbulence models considered in this paper. I is the instantaneous irradiance and is greater than zero for all pdfs, and $\langle I \rangle$ is the average received irradiance. The α and β parameters will be defined below. The Rytov variance, σ_R^2 , is a parameter commonly used to classify weak ($\sigma_R^2 < 1$), moderate ($\sigma_R^2 \sim 1$), strong ($\sigma_R^2 > 1$), and saturated ($\sigma_R^2 \rightarrow \infty$) turbulent optical links. It is given by [16, 19, 25, 28-30]

$$\sigma_R^2 = 1.23C_n^2 k^{7/6} l^{11/6} \quad (5.1)$$

where C_n^2 is the refractive-index structure constant (whose value is typically within range $10^{-17} \text{m}^{-2/3} \leq C_n^2 \leq 10^{-13} \text{m}^{-2/3}$ [16, 19, 25, 28, 29]) and it is taken to be constant for horizontal path communication link and modelled as a function of altitude for uplinks and downlinks [19, 25, 30]. Here $k = 2\pi/\lambda$ and l represent the optical wave number and length of the optical link, respectively. Typical values of σ_I^2 , α and β used for modelling weak, moderate, strong and saturated turbulence regimes are shown in Table 5.2. σ_I^2 , used for LN distribution, is the variance of the natural logarithm irradiance (normalised to its mean).

In the LN distribution model, whilst mathematically simple, the pdf peak and tail values do not correspond with experimental data [19, 25]. This implies that accuracy of statistical analysis such as detection and fade probabilities arrived at using this model will be significantly affected. Another shortcoming of the LN distribution is that the Rytov variance on

which it depends will not be able to account of multiple scattering caused by turbulence eddies as the optical link length increases [19, 25].

The GG distribution was developed for atmospheric turbulence modelling by Andrews and Phillips [19], although the pdf was highlighted in related works of Nakagami [31], Lewinski [32] and of Teich and Diamant [33]. This model takes into consideration both the large-scale and small-scale effects on optical beam traversing a turbulent atmospheric channel. This implies that the GG distribution model is valid for both weak and strong turbulence regimes. The GG pdf thus depends on the effective number of large-scale eddies of the scattering process α , and the effective number of small-scale eddies of the scattering process β . In weak turbulence conditions, α and $\beta \gg 1$. In strong turbulence conditions, α and β decrease substantially, such that in the saturation regime, $\beta \rightarrow 1$ as GG approaches NE [19], although α will increase again as the saturation deepens. Note that the GG distribution reduces to the K distribution when β is unity, whilst the K distribution tends to the negative exponential distribution as $\alpha \rightarrow \infty$.

The KD is a widely accepted model for characterising the strong turbulence regime, although it was originally proposed to model non-Rayleigh sea echo [19, 28]. The KD scintillation index $S.I. = 1 + 2/\alpha$, always exceeds unity and has strong agreement with experimental data in similar conditions. In very strong irradiance fluctuations i.e. the saturation turbulence regime, where the number of independent scatterings becomes large and the optical link length spans several kilometres, the value of the scintillation index tends to unity (from above). The optical field traversing this medium is experimentally verified to follow the negative exponential statistics for irradiance [16, 28].

Table 5.1: Commonly used atmospheric turbulence models

Distribution Type	Probability Density Function	Notes
Lognormal [19, 25, 34]	$p_{LN}(I, \langle I \rangle) = \frac{1}{I\sigma_I\sqrt{2\pi}} \exp\left(-\frac{\left[\ln\left(\frac{I}{\langle I \rangle} + \frac{1}{2}\sigma_I^2\right)\right]^2}{2\sigma_I^2}\right)$	For plane wave propagation: $\sigma_I^2 = \exp\left[\frac{0.49\sigma_R^2}{(1+1.11\sigma_R^{12/5})^{7/6}} + \frac{0.51\sigma_R^2}{(1+0.69\sigma_R^{12/5})^{5/6}}\right] - 1$
Gamma-Gamma [19, 25, 27, 28, 31-33, 35]	$p_{GG}(I, \langle I \rangle) = \frac{1}{\langle I \rangle} \frac{2(\alpha\beta)^{\alpha+\beta/2}}{\Gamma(\alpha)\Gamma(\beta)} \left(\frac{I}{\langle I \rangle}\right)^{\frac{(\alpha+\beta)}{2}-1} K_{\alpha-\beta}\left(2\sqrt{\alpha\beta}\left(\frac{I}{\langle I \rangle}\right)\right)$	For plane wave propagation: $\alpha = \left\{ \exp\left[\frac{0.49\sigma_R^2}{(1+1.11\sigma_R^{12/5})^{7/6}}\right] - 1 \right\}^{-1}$
K [19, 27, 33]	$p_{KD}(I, \langle I \rangle) = \frac{2\alpha}{\Gamma(\alpha)} \left(\alpha \frac{I}{\langle I \rangle}\right)^{(\alpha-1)/2} K_{\alpha-1}\left(2\sqrt{\alpha}\left(\frac{I}{\langle I \rangle}\right)\right)$	$\beta = \left\{ \exp\left[\frac{0.51\sigma_R^2}{(1+0.69\sigma_R^{12/5})^{5/6}}\right] - 1 \right\}^{-1}$
Negative Exponential [16, 19]	$p_{NE}(I, \langle I \rangle) = \frac{1}{\langle I \rangle} \exp\left(-\frac{I}{\langle I \rangle}\right)$	

Table 5.2: Typical Parameters for Characterising Weak -to- Saturated Turbulence Regimes [19, 36]

Parameter	Turbulence Regimes			
	Weak ($\sigma_1^2 < 1$)	Moderate ($\sigma_1^2 \approx 1$)	Strong ($\sigma_1^2 > 1$)	Saturated ($\sigma_1^2 \rightarrow \infty$)
σ_1^2	0.2	1.6	3.5	25
α	11.651	4.027	4.226	8.048
β	10.122	1.911	1.362	1.032

5.4 Moment generating function for optical signal

For a given irradiance I , the optical power at the optical amplifier input during an OOK-NRZ bit of data $j \in \{0,1\}$ is expressed mathematically as

$$P_j(I) = a_j IA \quad (5.2)$$

where $a_1 = \frac{2r}{r+1}$, $a_0 = \frac{2}{r+1}$, A is the area of the receiver aperture and r is the extinction ratio (typically 10). Clearly I is the mean irradiance for the bit stream at a particular time.

The moment generating function (MGF) (conditional on I) can then be obtained from, for example [5, 10, 11], under the assumption of an integrating response over bit period T (which has a noise equivalent bandwidth $B_e = \frac{1}{2T}$):

$$M_{Y_j}(s|I) = \frac{\exp\left[\frac{R'GsqsP_j(I)}{1 - \frac{R'N_0sq}{T}}\right]}{\left[1 - \frac{R'N_0sq}{T}\right]^L} \quad (5.3)$$

where q is the electron charge, s is the standard parameter in the transform domain for the MGF, $L = B_0 m_t T$ is the product of spatial and temporal modes, B_0 is the optical bandpass filter (OBPF) bandwidth in Hz, $m_t = 2$ is number of polarisation modes, $N_0 = n_{sp}(G-1)hf$ is the ASE power spectral density (PSD) in W/Hz (in single polarisation), n_{sp} is the spontaneous emission factor, $R' = \eta/hf$, G is the optical amplifier gain, h is the Planck's constant and f is the optical frequency in Hz.

On introducing the Gaussian receiver thermal noise, a new overall conditional MGF for the signal at the decision device is obtained [5, 10, 11]

$$M_{Z_j}(s|I) = M_{th}(s)M_{Y_j}(s|I) \quad (5.4)$$

where $M_{th}(s) = \exp\left(\frac{\sigma_{th}^2 s^2}{2}\right)$ is the thermal noise MGF and σ_{th}^2 is the thermal noise variance at the decision circuit. The conditioning of the MGF on I will be removed in the BER calculation in the next section.

5.5 Bit error rate analysis

In this section, the application of MGF methods, specifically the CB, MCB and SPA for the BER evaluation is presented for weak-to-strong turbulence regimes, using the LN, GG, KD and NE atmospheric turbulence models.

The BER for a given irradiance I is:

$$BER(I) = \frac{1}{2} [P(1|0, I) + P(0|1, I)] \quad (5.5)$$

where $P(1|0, I)$ represents the probability of receiving a 1 given that 0 was transmitted and $P(0|1, I)$ represents the probability of receiving a 0 given that 1 was transmitted.

On applying the CB separately to each conditional probability, equations (5.6) and (5.7) are obtained

$$P(1|0, I) = P(i_0(I) > i_D(I)) \leq \exp(-s_0 i_D(I)) M_{z_0}(s_0 | I) \quad s_0 > 0 \quad (5.6)$$

$$P(0|1, I) = P(i_1(I) < i_D(I)) \leq \exp(s_1 i_D(I)) M_{z_1}(-s_1 | I) \quad s_1 > 0 \quad (5.7)$$

where $i_D(I)$ is the decision threshold.

The CB therefore gives the upper bound on the BER (conditioned on I) as

$$BER_{CB}(I) = \frac{1}{2} [\exp(-s i_D(I)) M_{z_0}(s | I) + \exp(s i_D(I)) M_{z_1}(-s | I)] \quad s = s_0 = s_1 > 0 \quad (5.8)$$

where $M_{z_0}(s|I)$ and $M_{z_1}(s|I)$ are given by (5.4). The setting of $s_0 = s_1 = s$ is a computational convenience that incurs a very small accuracy penalty (as s_0 and s_1 can of course be optimised separately) [5, 10, 11].

The MCB involves a similar approach to the CB except that it typically provides a tighter upper bound on the BER in non-turbulent systems [5, 10, 11, 37]. The MCB BER (conditioned on I) is thus given by [5, 10, 11]

$$BER_{MCB}(I) = \frac{1}{2} \left[\frac{\exp(-si_D(I))M_{z_0}(s|I)}{s\sigma_{th}\sqrt{2\pi}} + \frac{\exp(si_D(I))M_{z_1}(-s|I)}{s\sigma_{th}\sqrt{2\pi}} \right] \quad s > 0 \quad (5.9)$$

The expression for the BER (conditioned on I) using SPA is given by [5, 10, 11]

$$BER_{SPA}(I) = \frac{1}{2s\sqrt{2\pi}} \left(\frac{\exp(-si_D(I))M_{z_0}(s|I)}{\sqrt{\psi_0''(s|I)}} + \frac{\exp(si_D(I))M_{z_1}(-s|I)}{\sqrt{\psi_1''(s|I)}} \right) \quad s > 0 \quad (5.10)$$

$$\psi_0(s|I) = \ln \left(\frac{M_{z_0}(s|I)\exp(-si_D(I))}{s} \right) \quad (5.11)$$

$$\psi_1(s|I) = \ln \left(\frac{M_{z_1}(-s|I)\exp(si_D(I))}{s} \right) \quad (5.12)$$

The optimum threshold for the CB is obtained by differentiating $BER_{CB}(I)$ with respect to i_D and setting the result to zero. The resultant optimum decision threshold for a particular I is given by [5]

$$i_{Dopt_{CB}}(I) = \frac{\ln(M_{Y_0}(s|I)/M_{Y_1}(-s|I))}{2s} \quad (5.13)$$

The same value of $i_{Dopt_{CB}}(I)$ is obtained for the MCB and SPA.

On substituting equation (5.13) into (5.8), (5.9) and (5.10), the bounds upon the BER with optimal threshold can be written as [5]

$$BER_{CB}(I) = M_{th}(s) \sqrt{M_{Y_1}(-s|I)M_{Y_0}(s|I)}, \quad s > 0 \quad (5.14)$$

$$BER_{MCB}(I) = \frac{M_{th}(s)}{s\sigma_{th}\sqrt{2\pi}} \sqrt{M_{Y_1}(-s|I)M_{Y_0}(s|I)}, \quad s > 0 \quad (5.15)$$

$$BER_{SPA}(I) = \frac{M_{th}(s)}{2s\sqrt{2\pi}} \sqrt{M_{Y_1}(-s|I)M_{Y_0}(s|I)} \left[\frac{1}{\sqrt{\psi_0''(-s)}} + \frac{1}{\sqrt{\psi_1''(s)}} \right], \quad s > 0 \quad (5.16)$$

For the GA, in which at sampling instant, the noise experienced by a 0 or 1 is zero mean Gaussian with variance σ_{d0}^2 or σ_{d1}^2 and the mean signal level is $i_0(I)$ or $i_1(I)$, the BER is given by [1, 2, 5, 7]

$$BER_{GA}(I) = \frac{1}{2} \operatorname{erfc} \left(\frac{Q(I)}{\sqrt{2}} \right) \quad (5.17)$$

$$Q(I) = \frac{i_1(I) - i_0(I)}{\sigma_{d1}(I) + \sigma_{d0}(I)}. \quad (5.18)$$

where $\sigma_{dj}^2(I) = \sigma_{s-sp,j}^2(I) + \sigma_{sp-sp}^2 + \sigma_{th}^2$ represents the total noise variance for $j \in \{0,1\}$ noise components. $\sigma_{s-sp,j}^2(I) = 4R'^2 q^2 GP_j(I) N_0 B_e$ is the signal-spontaneous emission beat noise variance and $\sigma_{sp-sp}^2 = 2m_t q^2 R'^2 N_0^2 B_0 B_e$ is the spontaneous-spontaneous emission beat noise variance. As shot noise is not included in the MGF (though it can be adapted to do so) it is also neglected here.

In the case of the CB (5.14), MCB (5.15) and SPA (5.16) the tightest bound is obtained by finding the optimum value for s for each irradiance I . For adaptive threshold OOK, facilitated by the slow fading of the irradiance, where it is assumed that the appropriate optimum threshold can be realised, the overall BER is given as:

$$BER_{X,Y}(\langle I \rangle) = \int_0^\infty BER_X(I) p_Y(I, \langle I \rangle) dI \quad (5.19)$$

where $BER_X(I)$ represents the BERs shown in (5.14), (5.15) and (5.16) ($X = \text{CB, MCB, SPA, GA}$ with CB, MCB and SPA understood to refer to the optimum s (which varies with I)) while $p_Y(I, \langle I \rangle)$ represents the atmospheric turbulence models shown in Table 5.1 ($Y = \text{LN, GG, KD}$ or NE).

5.6 Results and discussion

In Table 5.3, the system parameter values used in this section are listed. For simplicity, coupling losses are neglected. To obtain the results for more realistic coupling between air and optical amplifier input it is simply necessary to shift the curves by the appropriate number of dB. The typical coupling loss value is about 8-10 dB [6], although the optical amplification process helps to compensate for these losses. The receiver thermal noise is 7×10^{-7} A, chosen to give receiver sensitivity (with no turbulence or ASE) of -23 dBm at a BER of 10^{-12} . The choice of RCL diameter of 4 mm approximately gives a point receiver (so aperture averaging is neglected) because it is less than the spatial coherence width $\rho_0 = (1.46C_n^2 k^2 l)^{-3/5}$ [19] at the receiver for typical link lengths and C_n^2 values. For example the calculated minimum (for $C_n^2 = 10^{-13} \text{ m}^{-2/3}$) and maximum (for $C_n^2 = 10^{-17} \text{ m}^{-2/3}$) values for ρ_0 at a typical optical link length, $l = 1000$ m are 0.0094 m and 2.36 m, respectively. The α and β values used in this analysis (where required) were adopted from [19, 36] (see Table 5.2) as they have the closest fit to measured turbulence data (Rytov variance σ_R^2).

Table 5.3: Parameter values used for the numerical results

Parameter	Description	Value
R_b	Bit rate	2.5 Gb/s [7]
λ	Optical wavelength	1550 nm [7]
B_0	Optical-filter bandwidth	76 GHz
G	Optical amplifier gains	30.6 dB and 8.8 dB [5, 7]
n_{sp}	Spontaneous emission parameter	1.5 (equivalent to noise figure of 4.77 dB)
η	Quantum efficiency	1 [7]
r	Extinction ratio	10 dB
D_{RX}	Receiver collecting lens diameter	4 mm [17]

Figure 5.2 (overleaf and page 86) shows the BER curves for CB, MCB, SPA and GA at low gain optical amplifier ($G = 8.8$ dB), using the parameters in Table 5.2 to model weak, moderate, strong and saturated turbulence regimes. The CB is clearly seen to exceed the MCB, SPA and GA which give relatively similar BERs for all employed atmospheric turbulence models. The BER curves obtained for LN distribution differs from the GG distribution by about 3 dB at target BER of 10^{-12} , as shown in Figure 5.2 (a). The discrepancy is well known in non-amplified systems [19, 25]. The discrepancy is clearly lower at worse BERs so the LN approach (which is easier to calculate) can be more appropriate when forward error correction (FEC) is available. The NE distribution is mainly used for characterising the fully saturated turbulence condition, whereas the GG and K distributions are more appropriate for characterising the strong to saturated turbulence regime as $\alpha \rightarrow \infty$ (and as $\beta \rightarrow 1$ for GG distribution only). Therefore, in Figure 5.2(d), the NE distribution results are given, and these would almost coincide with the saturation regime results for the GG and K distributions using the appropriate parameters from Table 5.2, and which are thus not shown. Figure 5.2(c) shows the discrepancy between the

K and the GG distributions for the strong turbulence regime, where it can be seen that the KD curves are almost the same as the fully saturated NE in Figure 5.2(d). The GG by contrast differs by virtue of using a value of β that is not unity.

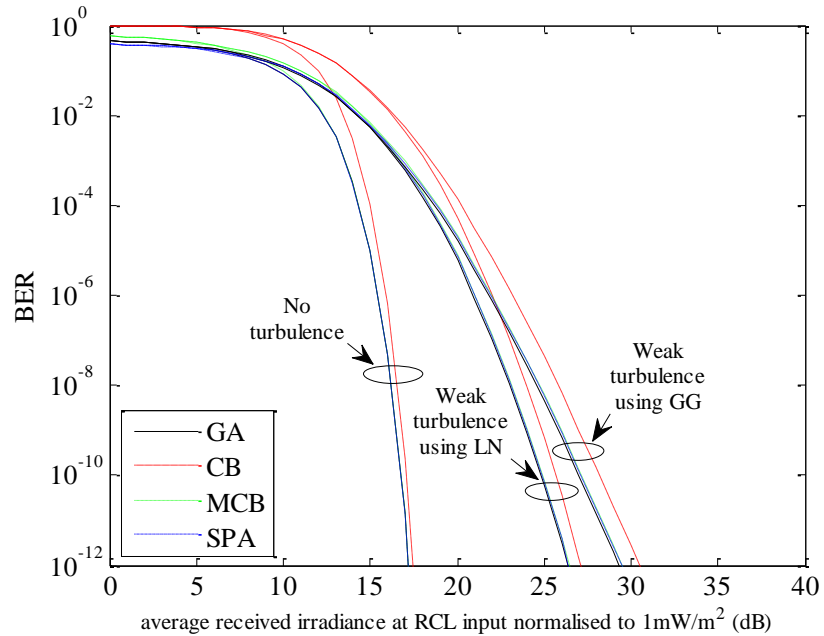


Figure 5.2 (a) no turbulence, and weak turbulence using LN and GG distributions,

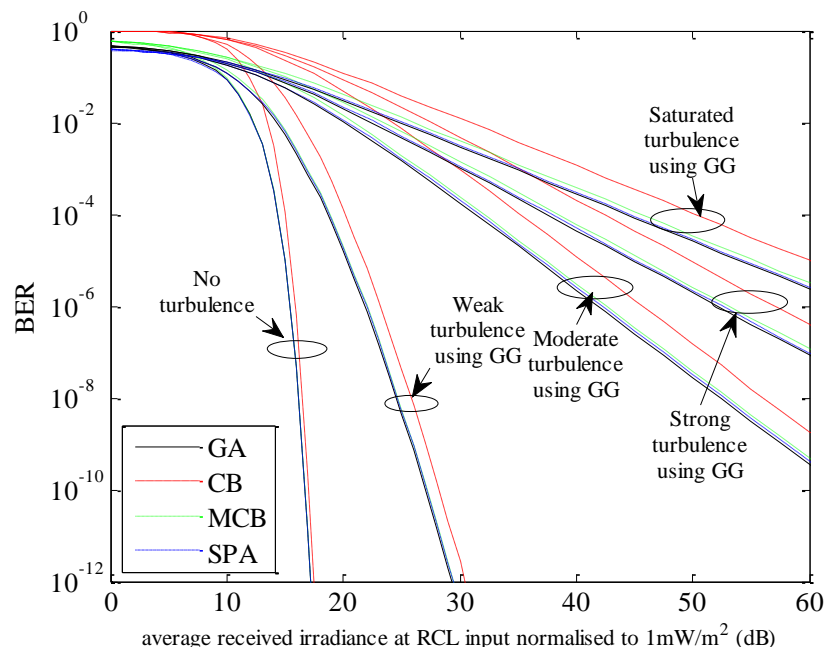


Figure 5.2 (b) no turbulence, weak, moderate, strong, and saturated turbulences using GG distribution,

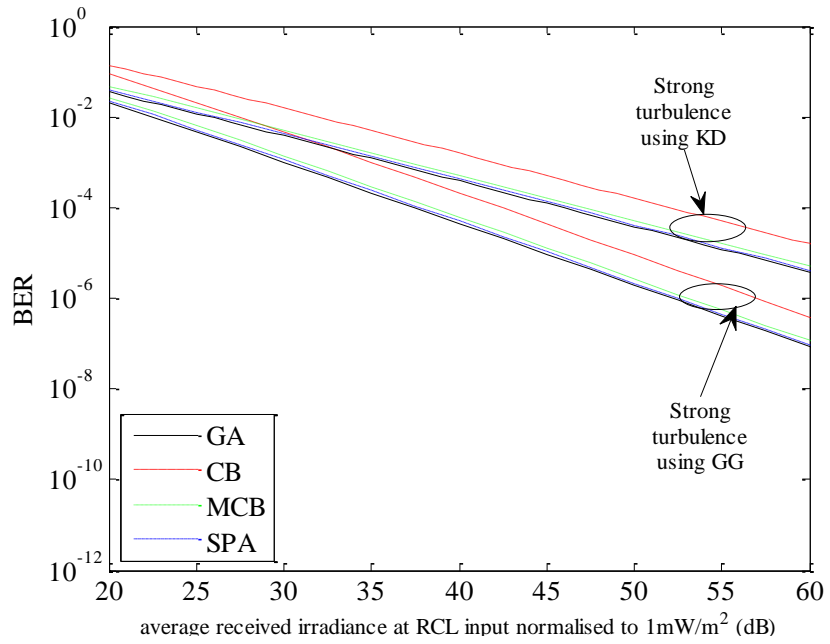


Figure 5.2 (c) strong turbulence using GG and KD,

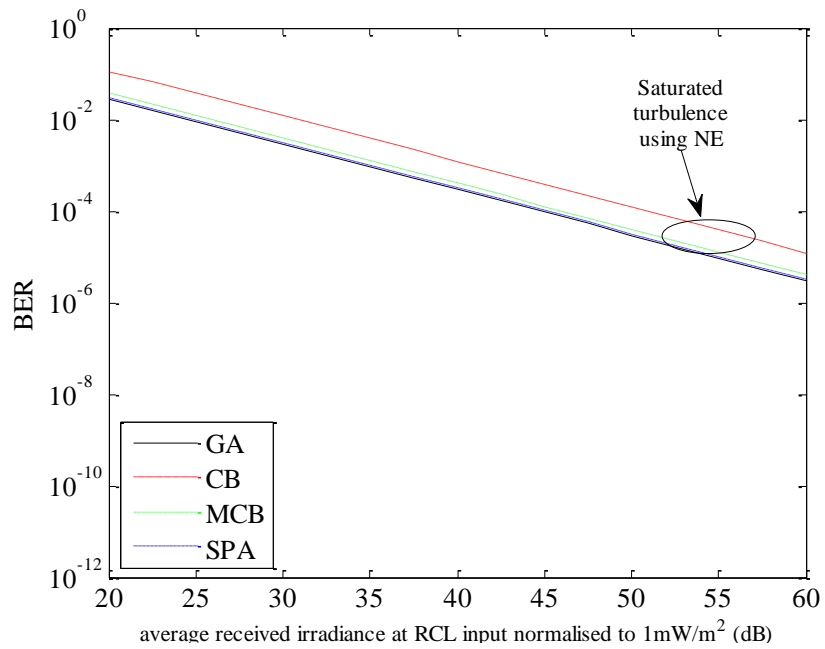


Figure 5.2 (d) saturated turbulence using NE distribution

Figure 5.2: BER vs. normalised average received irradiance at receiver collecting lens (RCL) input [dB] using $G = 8.8$ dB and $D_{RX} = 4$ mm

Figure 5.3 (below and pages 88, 89) shows the BER curves for the high gain ($G = 30.6$ dB) case using the same parameters as before to characterise the atmospheric turbulence regimes. Here the CB and MCB BER curves are almost matching, whilst the GA and SPA differs from both CB and MCB, even more as the turbulence strength increases. The similarity of the CB and MCB is due to the dominance of the signal dependent noise. Consideration of both Figures 5.2 and 5.3 indicates that the MCB with GG distribution is probably the most sensible approach for modelling optically preamplified FSO receiver in all atmospheric turbulence regimes. This is because the MCB gives a tighter bound than the CB especially when the contribution of the thermal noise is relatively high and because the GG distribution is reasonable over a whole range of turbulence conditions. Moreover, the difference between the SPA and MCB in the high gain case is small (~ 1 dB at BER of 10^{-9} for WT condition) and the bound can be considered to be a safe assessment method for the BER. It is also noteworthy that all strong and saturated theoretical BER curves continue almost linearly for higher powers than shown but these would of course ultimately overload the receiver.

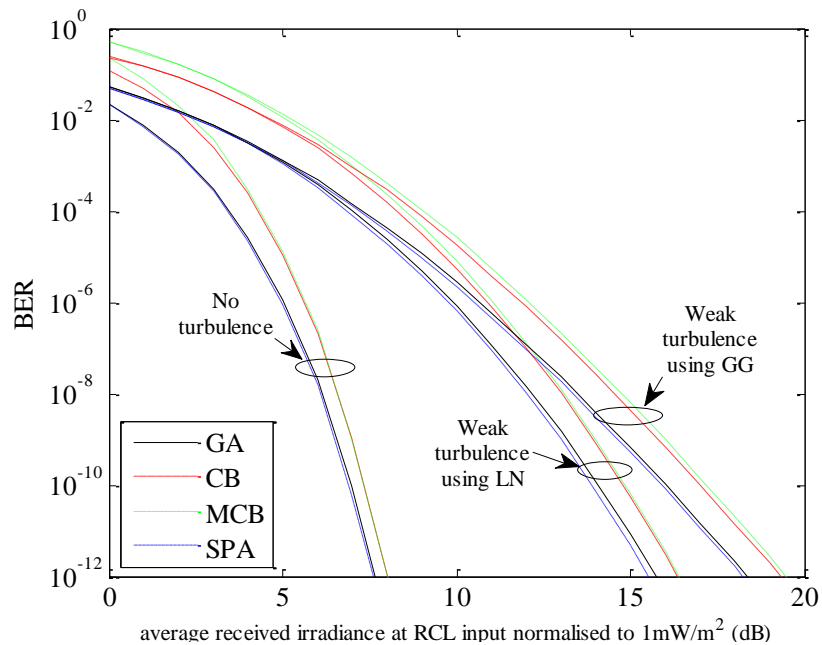


Figure 5.3 (a) no turbulence, and weak turbulence using LN and GG distributions,

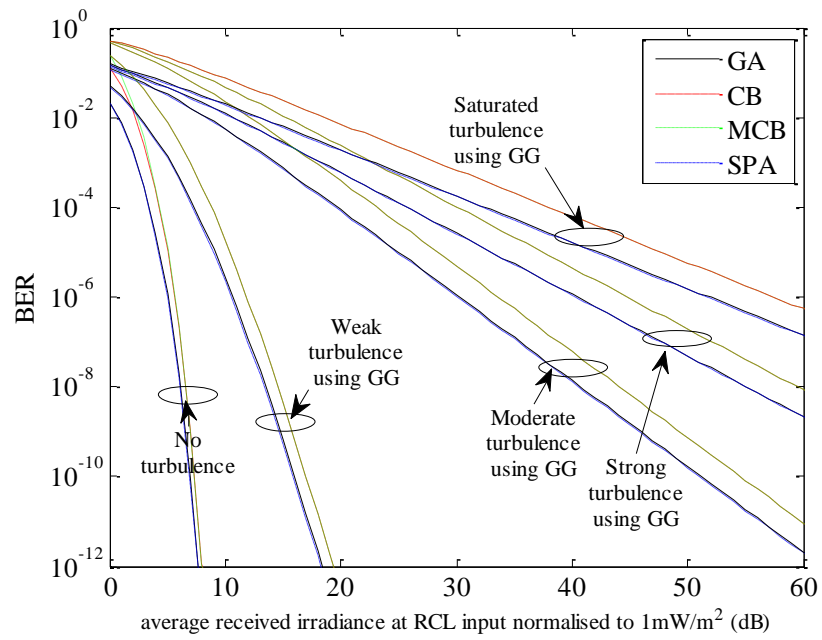


Figure 5.3 (b) no turbulence, weak, moderate, strong, and saturated turbulences using GG distribution,

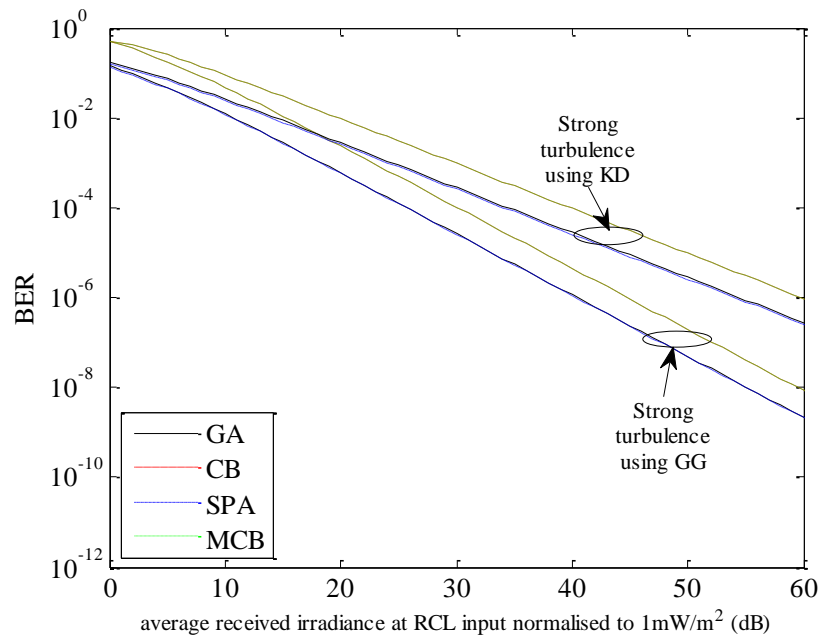


Figure 5.3 (c) strong turbulence using GG and KD,

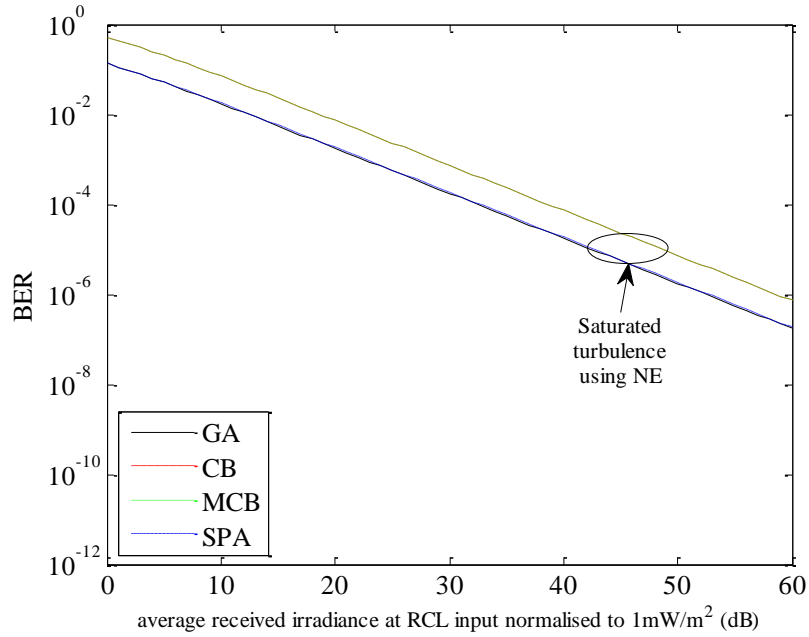
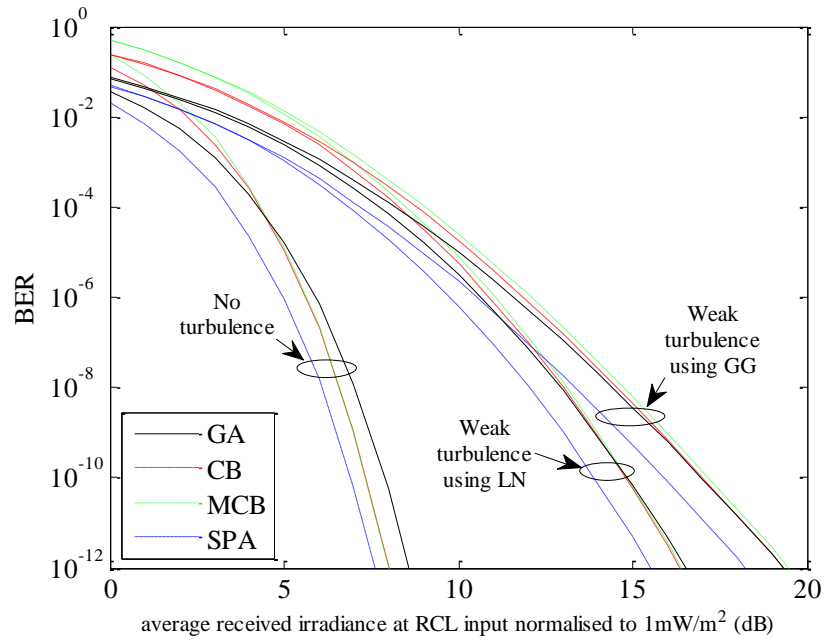


Figure 5.3 (d) saturated turbulence using NE distribution

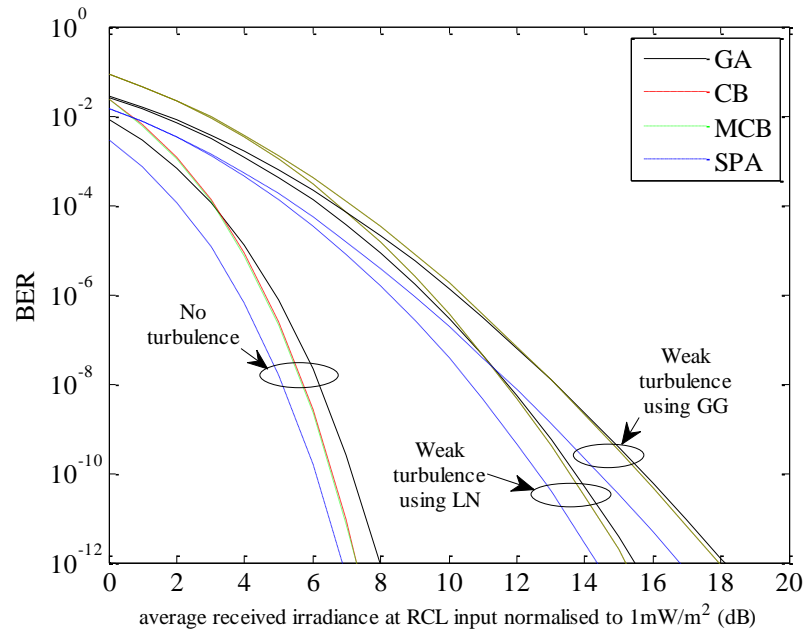
Figure 5.3: BER vs. normalised average received irradiance at receiver collecting lens (RCL) input [dB] using $G = 30.6$ dB and $D_{RX} = 4$ mm

Although the GA falls below the bounds in these calculations, the uncertainty regarding whether it is above or below the real BER is well reported in related MGF analyses [5, 9], arising ultimately because of its moment deficiency. This can also be illustrated by specific cases, using some different parameters than previously as shown in Figure 5.4 (page 91) which gives the BER curves for the high gain ($G = 30.6$ dB) case using (a) $r = \infty$, $B_0 = 76$ GHz, (b) $r = \infty$, $B_0 = 20$ GHz. It can be seen from Figure 5.4 that the GA can exceed the MCB (which is almost matching the CB) for the no turbulence regime for both cases, while as the turbulence increases to the weak regime, the GA can still slightly exceed the MCB, SPA (and CB) for both the LN and GG cases in Figure 5.4b, while in Figure 5.4a this is only true for the LN case. Generally, in the high gain cases severe turbulence conditions will move the GA-MCB (and CB) crossover points to better BER (below the range plotted). It should be further noted that the choice of

different receiver filters, other than the integrating response used here, with the possibility of intersymbol interference, and also the use of RZ modulation (of various pulse shapes), will also both impact on the relative merit of the GA and the CB/MCB, as for example investigated in [5] for the non-turbulent case.



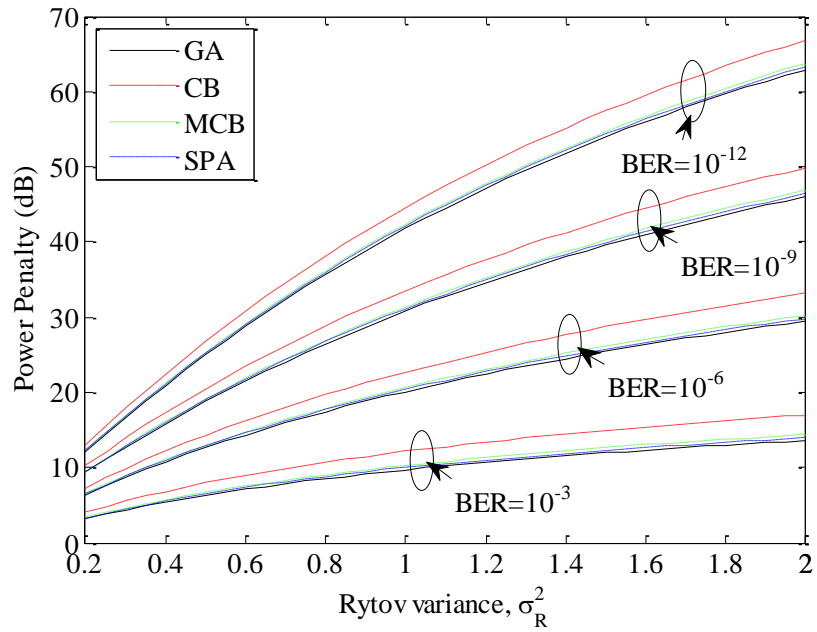
(a)



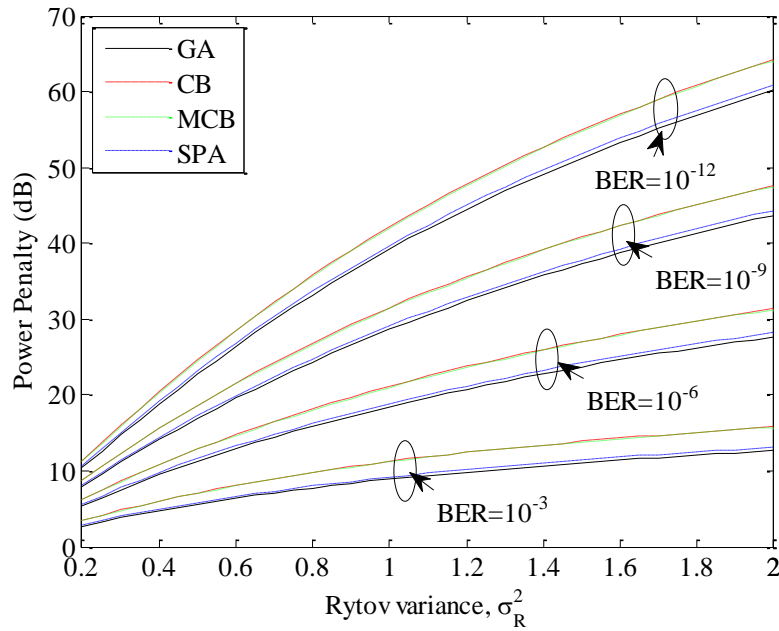
(b)

Figure 5.4: BER vs. normalised average received irradiance at receiver collecting lens (RCL) input [dB] for no turbulence, and weak turbulence using LN and GG distributions $G = 30.6$ dB, $D_{RX} = 4$ mm and (a) $r = \infty$, $B_0 = 76$ GHz, (b) $r = \infty$, $B_0 = 20$ GHz

Returning to the original parameters of Table 5.3, power penalty plots are shown in Figure 5.5 (on page 93) for the following BER levels: 10^{-3} , 10^{-6} , 10^{-9} and 10^{-12} . In this work, the power penalty refers to the additional power needed in the presence of impairments (turbulence and ASE noise) to return the FSO system to the BER achievable without the impairments. As might be expected, the penalty increases as the turbulence strength (described by the Rytov variance) increases and as the BER decreases. Beyond $\sigma_1^2 = 0.2$, the penalty increases very sharply until very high fading conditions where the change in penalty gradually falls, for instance, at high gain $G = 30.6$ dB and BER of 10^{-6} using MCB, when the Rytov variance rises from $\sigma_1^2 = 0.1$ to $\sigma_1^2 = 0.2$, the penalty only rises from 3.5 dB to 5 dB. But when it increases to $\sigma_1^2 = 1.6$, the power penalty rises to 27 dB. It should be noted that the power penalties shown in Figure 5.5 are theoretical values. In practice, for example, a BER of 10^{-12} will not be obtainable under high Rytov variance conditions.



(a)



(b)

Figure 5.5: Atmospheric turbulence induced power penalty vs. Rytov variance for OOK-NRZ FSO modelled using a GG distribution with (a) low-gain optical preamplifier ($G = 8.8$ dB) and (b) high-gain optical preamplifier ($G = 30.6$ dB). Note that these are theoretical values and in practice BER of 10^{-12} will not be obtainable under high Rytov variance conditions.

5.7 Summary

BER modelling for an optically preamplified OOK FSO system operating over atmospheric turbulence has been investigated using MGF-based techniques such as the CB, MCB and SPA, for the first time. The results obtained were compared with the GA approach for both high and low gains using the main candidate atmospheric turbulence models to characterise the weak, moderate, strong and saturated turbulence regimes. Overall it can be seen that the SPA is closer to the real BER values, although the MCB differs from the SPA by a few dBs, and it has the advantage of being a bound. Furthermore, the MCB gives the tightest bound upon the BER compared to the CB, particularly at lower gains, and that it also can be exceeded by the GA at higher gains, hence it is a logical method to use. The GG distribution is further seen to be the most flexible model for characterising atmospheric turbulence across a whole range of conditions.

5.8 References

- [1] N. A. Olsson, "Lightwave systems with optical amplifiers," *Journal of Lightwave Technology*, vol. 7, no.7, pp. 1071-1082, July 1989.
- [2] Y. Yamamoto, "Noise and error rate performance of semiconductor laser amplifiers in PCM-IM optical transmission systems," *IEEE Journal of Quantum Electronics*, vol. 16, no. 10, pp. 1073-1081, Oct. 1980.
- [3] M. P. Dlubek, A. J. Phillips, and E. C. Larkins, "Optical signal quality metric based on statistical moments and Laguerre expansion," *Optical and Quantum Electronics*, vol. 40, no. 8, pp. 561-575, July 2008.
- [4] B. Chan and J. Conradi, "On the non-Gaussian noise in erbium-doped fiber amplifiers," *Journal of Lightwave Technology*, vol. 15, no. 4, pp. 680-687, Apr. 1997.
- [5] L. F. B. Ribeiro, J. R. F. Da Rocha, and J. L. Pinto, "Performance evaluation of EDFA preamplified receivers taking into account intersymbol interference," *Journal of Lightwave Technology*, vol. 13, no. 2, pp. 225-232, Feb. 1995
- [6] Q. L. Cao, M. Brandt-Pearce, and S. G. Wilson, "Free space optical MIMO system using PPM modulation and a single optical amplifier," *Second International Conference in Communications and Networking*, Shanghai, China, vol. 1, pp. 1113-1117, Aug. 2007.
- [7] M. Razavi and J. H. Shapiro, "Wireless optical communications via diversity reception and optical preamplification," *IEEE Transactions on Wireless Communications*, vol. 4, no. 3, pp. 975-983, May 2005.

- [8] T. G. Ulmer, S. R. Henion, and F. G. Walther, "Power penalty from amplified spontaneous emission in spatial diversity links for fade mitigation," *IEEE Photonics Technology Letters*, vol. 21, no. 3, pp. 170-172, Feb. 2009.
- [9] J. O'Reilly and J. R. F. Da Rocha, "Improved error probability evaluation methods for direct detection optical communication systems," *IEEE Transactions on Information Theory*, vol. 33, no. 6, pp. 839-848, Nov. 1987.
- [10] K. W. Cattermole and J. J. O'Reilly, *Mathematical topics in telecommunications volume 2: problems of randomness in communication engineering*, Pentech Press Limited, Plymouth, 1984.
- [11] I. T. Monroy and E. Tangdiongga, *Crosstalk in WDM communication networks*, Kluwer Academic Publishers, Norwell, Massachusetts, USA, 2002.
- [12] X. Zhu, J. M. Kahn, and J. Wang, "Mitigation of turbulence-induced scintillation noise in free-space optical links using temporal-domain detection techniques," *IEEE Photonic Technology Letter*, vol. 15, no. 4, pp. 623-625, Apr. 2003.
- [13] X. M. Zhu and J. M. Kahn, "Communication techniques and coding for atmospheric turbulence channels," *Journal of Optical and Fiber Communications Reports*, vol. 4, no. 6, pp. 363-405, 2007.
- [14] A. O. Aladeloba, A. J. Phillips, and M. S. Woolfson, "Improved bit error rate evaluation for optically pre-amplified free-space optical communication systems in turbulent atmosphere," *IET Optoelectronics*, vol. 6, no. 1, pp. 26-33, Feb. 2012.
- [15] D. O. Caplan, "Laser communication transmitter and receiver design," *Journal of Optical Fibre Communication Report*, vol. 4, no. 4-5, pp. 225-362, 2007.
- [16] S. Karp, R. M. Gagliardi, S. E. Moran, and L. B. Stotts, *Optical channels: fibers, clouds, water and the atmosphere*, New York: Plenum Press, 1988.
- [17] M. Abtahi, P. Lemieux, W. Mathlouthi, and L. A. Rusch, "Suppression of turbulence-induced scintillation in free-space optical communication systems using saturated optical amplifiers," *Journal of Lightwave Technology*, vol. 24, no. 12, pp. 4966-4973, Dec. 2006.
- [18] C. Chen, H. Yang, H. Jiang, J. Fan, C. Han, and Y. Ding, "Mitigation of Turbulence-Induced Scintillation Noise in Free-Space Optical Communication Links Using Kalman Filter," *IEEE Congress on Image and Signal Processing*, Hainan, China, vol. 5, pp. 470-473, May 2008.
- [19] L. C. Andrews and R. L. Phillips, *Laser beam propagation through random media*, Second Edition, SPIE Press, Bellingham, Washington, 2005.
- [20] X. Zhu and J. M. Kahn, "Free-space optical communication through atmospheric turbulence channels," *IEEE Transactions on Communications*, vol. 50, no. 8, pp. 1293-1300, Aug. 2002.

- [21] S. Bloom, E. Korevaar, J. Schuster, and H. A. Willebrand, "Understanding the performance of free-space optics," *Journal of Optical Networking*, vol. 2, no. 6, pp. 178-200, June 2003.
- [22] O. Bouchet, H. Sizun, C. Boisrobert, F. DeFornel, and P. Favennec, *Free-space optics: propagation and communications*, Wiley-ISTE Limited, London, 2006.
- [23] T. H. Carbonneau and D. R. Wisely, "Opportunities and challenges for optical wireless; the competitive advantage of free space telecommunications links in today's crowded marketplace," *Proc. SPIE Wireless Technologies and Systems: Millimeter-Wave and Optical*, vol. 3232, pp. 119-128, Jan. 1998.
- [24] H. A. Willebrand and B. S. Ghuman, *Free-space optics: enabling optical connectivity in today's networks*, Sams Publishing, Indianapolis, Indiana 46240 USA, 2002.
- [25] A. K. Majumdar, "Free-space laser communication performance in the atmospheric channel," *Journal of Optical and Fiber Communications Research*, vol. 2, no. 4, pp. 345-396, 2005.
- [26] J. Akella, M. Yuksel, and S. Kalyanaraman, "Multi-channel communication in free-space optical networks for the last-mile," *Proc. of 15th IEEE Workshop on Local & Metropolitan Area Networks*, Princeton NJ, pp. 43-48, June 2007.
- [27] Z. Ghassemlooy, W. O. Popoola, and E. Leitgeb, "Free-space optical communication using subcarrier modulation in gamma-gamma atmospheric turbulence," *9th International Conference on Transparent Optical Networks*, Rome, Italy, vol. 13, pp. 156-160, July 2007.
- [28] M. A. Al-Habash, L. C. Andrews, and R. L. Phillips, "Mathematical model for the irradiance probability density function of a laser beam propagating through turbulent media," *Opt. Eng.*, vol. 40, no. 8, pp. 1554-1562, Aug. 2001.
- [29] H. E. Nistazakis, T. A. Tsiftsis, and G. S. Tombras, "Performance analysis of free-space optical communication systems over atmospheric turbulence channels," *IET Communications*, vol. 3, no. 8, pp. 1402-1409, 2009.
- [30] L. C. Andrews, R. L. Phillips, C. Y. Hopen, and M. A. Al-Habash, "Theory of optical scintillation," *J. Opt. Soc. Am. A*, vol. 16, no. 6, pp. 1417-1429, June 1999.
- [31] M. Nakagami, "The m-distribution - a general formula of intensity distribution of rapid fading," in *Statistical Methods in Radio Wave Propagation*, W.C. Hoffman, Ed., Pergamon, New York, pp. 3-36, 1960.
- [32] D. J. Lewinski, "Nonstationary probabilistic target and cluster scattering models," *IEEE Transactions on Antenna Propagation*, vol. 31, no. 3, pp. 490-498, 1983.
- [33] M. C. Teich and P. Diament, "Multiply stochastic representations for K distributions and their Poisson transforms," *J. Opt. Soc. Am. A* vol. 6, no. 1, pp. 80-91, 1989.
- [34] K. Kaisaleh, "Performance analysis of free-space on-off-keying optical communication systems impaired by turbulence," *Proc. SPIE*

- in Free-Space Laser Communication Technologies XIV*, San Jose, CA, vol. 4635, pp. 150-161, Jan. 2002.
- [35] L. C. Andrews and R. L. Phillips, "Free space optical communication link and atmospheric effects: single aperture and arrays," *Proc. SPIE*, vol. 5338, pp. 265-275, Jan. 2004.
- [36] W. O. Popoola and Z. Ghassemlooy, "BPSK subcarrier intensity modulated free-space optical communications in atmospheric turbulence," *Journal of Lightwave Technology*, vol. 27, no. 8, pp. 967-973, Apr. 2009.
- [37] J. O'Reilly and J. R. F. Da Rocha, "Improved error probability evaluation methods for direct detection optical communication systems," *IEEE Transactions on Information Theory*, vol. 33, no. 6, pp. 839-848, Nov. 1987

CHAPTER 6 DPPM with aperture-averaging for turbulent optically preamplified FSO communication systems

6.1 Introduction

Digital pulse position modulation (DPPM) is interesting as a transmission format for optical communication systems mainly due to the improved receiver sensitivity that is attainable; although at the cost of bandwidth [1-4] (only a problem if used in dense wavelength division multiplexing). Initially, most of the work on DPPM was performed for deep space optical communication [5, 6] and, later optical-fibre systems [1, 7]. Furthermore a number of authors [2, 3, 8] have studied this modulation method for terrestrial FSO communication. Kiasaleh [8] studied the DPPM scheme and avalanche photodiode for theoretical analysis (facilitated by a Gaussian approximation (GA)) of an FSO communication system.

An optical preamplifier configuration is used to increase power at the photodetector and thus effectively improve the receiver sensitivity. This benefit however comes with the drawback of having to manage the signal-to-noise ratio degradation due to the amplified spontaneous emission (ASE) noise arising from optical amplification, which in turn generates signal-spontaneous and spontaneous-spontaneous beat noises. These are in addition to the usual electrical domain noises. Phillips *et al.* [4] studied DPPM for an intersatellite link using an optical preamplifier at the receiver, and an integrate-and-compare detection scheme. That study forms part of the basis for this analysis.

Yamamoto [9] derived expressions for the mean and variance of an optically preamplified signal, in order to facilitate a GA. However this is not a full description of the signal plus ASE noise, which is not really Gaussian distributed but instead is related to chi-square (ASE only) and non-central chi-square (signal plus ASE) distributions. Personick [10] and, later, Ribeiro *et al.* [11] derived alternative formulations based on a moment generating function (MGF), which gives a full statistical description of a system

employing an optically preamplified direct detection receiver. Bit error rate (BER) (in [9-11] for on-off keying (OOK) systems) is then evaluated using MGF based techniques such as Chernoff bound (CB) and modified Chernoff bound (MCB). In this paper, the performance of optically preamplified DPPM FSO communications in a turbulent channel is investigated for the first time using such MGF based techniques and also a GA. The gamma-gamma (GG) atmospheric turbulence model is used to characterise the weak turbulence (WT), moderate turbulence (MT) and strong turbulence (ST) regimes. The GG distribution model is well known to be a good approximation to experimental data [12-15]. Other probability density functions (pdfs) for atmospheric turbulence can of course be used with the same BER evaluation method.

Several diversity techniques have been proposed in the literature for mitigating turbulence-induced scintillation in FSO communication systems. Some of the common methods include time diversity [14, 16], spatial diversity [13, 14, 16, 17], using multiple transmitters and/or receivers [2, 13, 14, 16], and aperture averaging (AA) [2, 13-18]. Due to the simplicity and effectiveness of the aperture averaging technique, its impact in the WT, MT and ST regimes will be investigated in this chapter. BER analysis based on CB and GA for optically preamplified DPPM has previously been used in intersatellite [4] and optical fibre [7] systems but not for FSO communications impaired by turbulence. To the best of the author's knowledge, BER analysis based on MCB has not previously been used for any optically preamplified DPPM system. This chapter provides an analysis of optically preamplified DPPM in the presence of atmospheric turbulence using the MCB, CB, and GA BER evaluation methods. Finally, using the MCB, a comparison with an equivalent on-off keying non-return-to-zero (NRZ) based FSO system is effected to confirm the advantage of the DPPM receiver sensitivity. The work in this chapter led to a publication [19].

6.2 Digital pulse position modulation

Basically, DPPM entails dividing a frame of M bits, with duration T_b , into $n = 2^M$ equal-sized slots with duration $t_s = MT_b/n$. Figure 6.1 shows example time waveforms of an OOK-NRZ and equivalent 16-DPPM signal ($M = 4$). An input word is then represented by placing an optical pulse in one of the DPPM time slots in the frame. In this analysis, the incident DPPM signal is detected by integrating over each DPPM slot and comparing the results throughout the frame to obtain the largest result [4, 20]. No threshold is therefore necessary. Since the information is represented by the position of a pulse, a timing reference has to be recovered before demodulation is possible. The achievement of timing synchronisation has been investigated for FSO systems [21, 22] but in this thesis it is assumed perfect. Further, the DPPM receiver is controlled by slot synchronization and frame synchronization circuits, as shown in Figure 6.2.

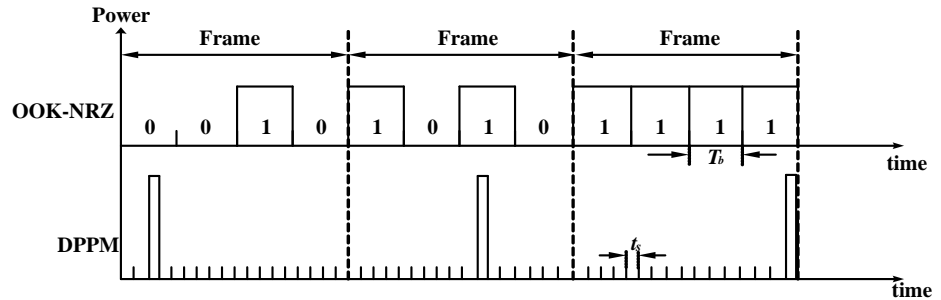


Figure 6.1: Illustration of DPPM frames for $M = 4$ ($n = 2^4 = 16$ slots)

6.3 Optically preamplified receiver

The performance of a standard P-I-N photodiode direct detection receiver configuration for an FSO communication system can be improved significantly by using an optical preamplifier after the receiver collecting lens (RCL), as shown in Figure 6.2. An optical amplifier of gain G and noise figure NF is placed before the photodiode. The incoming optical signal is coupled by means of a collimator into a short fibre through which it is fed into the optical amplifier. An optical band-pass filter (OBPF) of optical bandwidth B_{opt} is placed between the optical amplifier and the

photodiode. The OBPf limits the ASE noise components reaching the photodiode and thus reduces spontaneous-spontaneous beat noise. An OBPf can also be placed before the optical amplifier to limit background noise but this is neglected in this thesis because the amplified background noise will be much smaller than the ASE noise, and it can still be removed by the OBPf after the optical amplifier. Coupling losses are also neglected. In order to incorporate these losses into the analysis, if desired, the BER curves shown later can be easily shifted by the appropriate value in dB. The P-I-N photodiode with quantum efficiency η converts the amplified optical power into current which would be electrically preamplified before being passed to the integrate-and-compare circuitry where the transmitted information is recovered.

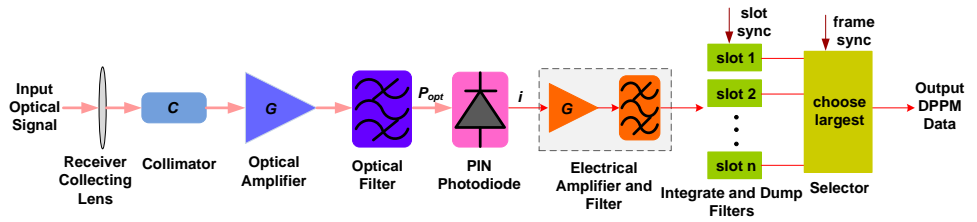


Figure 6.2: Optically preamplified FSO receiver

6.4 Atmospheric turbulence models

FSO links are commonly classified into various level of turbulence using the Rytov variance σ_R^2 which is given by [2, 12-14, 23]

$$\sigma_R^2 = 1.23C_n^2 k^{7/6} l^{11/6} \quad (6.1)$$

where C_n^2 (the refractive index structure constant) takes values typically within range $10^{-17} \text{ m}^{-2/3} \leq C_n^2 \leq 10^{-13} \text{ m}^{-2/3}$ [2, 23] and is taken to be constant for horizontal communication and modelled as a function of altitude for uplinks and downlinks, l is the optical link length, $k = 2\pi/\lambda$ is the optical wave number and λ is the optical wavelength. WT, MT and ST links are associated with $\sigma_R^2 < 1$, $\sigma_R^2 \approx 1$, and $\sigma_R^2 > 1$ respectively.

Several models for the probability density function (pdf) of irradiance fluctuation due to atmospheric turbulence have been proposed. The WT regime has commonly been modelled using the lognormal distribution; however it has been observed that the lognormal pdf peak and tail do not match with measured data [13]. Other existing models for characterising the WT regime include the *I-K* and GG distributions [2, 12, 13]. To address the strong regime, several models have also been proposed. The commonly used models in the literature include the *K* [2, 12, 13], lognormally modulated exponential [12, 13], and GG distributions [2, 12-14, 23, 24], whilst the negative exponential is well suited for the saturated turbulence regime [13, 23]. The GG distribution is a well-regarded distribution for characterising irradiance fluctuations under all turbulence conditions [2, 12-14, 23, 24]. Moreover, the GG distribution has been adopted for characterising the WT, MT and ST regimes mainly because of the closeness of results obtained to experimental data [13], the direct relationship with atmospheric turbulence parameters and its ability to cover the whole turbulence range [2, 12-14, 23, 24].

The GG pdf, initially proposed for FSO turbulence modelling by Andrews and Phillips [13], has been used extensively [2, 12, 14, 23, 24] to characterise the weak, moderate and strong turbulence regimes. The GG pdf, designated $p_{GG}(h_{turb})$, is given by [2, 12, 14, 23, 24]

$$p_{GG}(h_{turb}) = \frac{2(\alpha\beta)^{(\alpha+\beta)/2}}{\Gamma(\alpha)\Gamma(\beta)} h_{turb}^{\left(\frac{\alpha+\beta}{2}\right)-1} K_{\alpha-\beta}\left(2\sqrt{\alpha\beta h_{turb}}\right); \quad h_{turb} > 0 \quad (6.2)$$

where h_{turb} is the attenuation due to atmospheric turbulence, α is the effective number of large-scale eddies of the scattering process, β is the effective number of small-scale eddies of the scattering process, $K_n(\cdot)$ is the modified Bessel function of the 2nd kind of order n , and $\Gamma(\cdot)$ represents the gamma function.

Aperture-averaging is a commonly used method for mitigating turbulence-induced scintillation [2, 13-15, 18]. This method essentially entails increasing the RCL area such that it is larger than the fluctuating

irradiance correlation width $\rho_0 = (1.46C_n^2 k^2 l)^{-3/5}$ [13], resulting in averaging of the irradiance fluctuations over the RCL area such that a significant reduction in scintillation is achieved compared to that observed for a point receiver [2, 13-15, 18]. The decrease in irradiance fluctuation is typically measured using the aperture averaging factor $A = \sigma_I^2(D_{RX})/\sigma_I^2(0)$ [2, 13, 14], where $\sigma_I^2(D_{RX})$ is the scintillation index for RCL diameter D_{RX} ($D_{RX} = 0$ for a point receiver) and is given as [2, 13, 14]:

$$\sigma_I^2(D_{RX}) = \exp \left[\frac{0.49\sigma_R^2}{(1 + 0.653d^2 + 1.11\sigma_R^{12/5})^{7/6}} + \frac{0.51\sigma_R^2(1 + 0.69\sigma_R^{12/5})^{-5/6}}{1 + 0.9d^2 + 0.621d^2\sigma_R^{12/5}} \right] - 1 \quad (6.3)$$

where $d = \sqrt{kD_{RX}^2/4l}$ is the normalised RCL radius [2, 13, 14].

The α and β parameters for plane-wave propagation (including AA) are given as [2, 13, 14]:

$$\alpha = \left\{ \exp \left[\frac{0.49\sigma_R^2}{(1 + 0.653d^2 + 1.11\sigma_R^{12/5})^{7/6}} \right] - 1 \right\}^{-1} \quad (6.4)$$

$$\beta = \left\{ \exp \left[\frac{0.51\sigma_R^2(1 + 0.69\sigma_R^{12/5})^{-5/6}}{1 + 0.9d^2 + 0.621d^2\sigma_R^{12/5}} \right] - 1 \right\}^{-1} \quad (6.5)$$

6.5 Theoretical analysis

Due to the simplicity of the GA, it has been widely used for the design of optically amplified communication links [9, 17, 25]. However, the GA does not always give a close estimation of the real BER curve as it uses only two moments to describe the signal plus noise, namely the mean and variance. More sophisticated MGF-based techniques have been proposed in [10, 11, 26] for better statistical analysis of the optical preamplification process. Alongside the GA, the MGF-based approach forms the basis of this thesis, using techniques such as the CB and MCB, the latter having been

specifically mathematically developed in [26] to improve on the CB for the situation where there is both Gaussian receiver thermal noise and signal dependent noise present.

The MGF (conditional on h_{turb}) was derived from e.g. [11] for the integrating receiver (over each slot time t_s) assumed in this thesis. This is meaningful as the irradiance fluctuations are much slower than the data rate. It is given as:

$$M_Y(s|h_{turb}, P) = \left[1 - \frac{R'N_0sq}{t_s} \right]^{-L} \exp \left(\frac{R'Gs q P_{pulse}(P) h_{turb}}{1 - \frac{R'N_0sq}{t_s}} \right) \quad (6.6)$$

where $P_{pulse}(P)$ is the power of the rectangular pulse and P is the average DPPM power, both at the optical amplifier input. Also s is the standard parameter in the transform domain for the MGF, q is the electron charge, $L = B_0 m_t t_s$ is the product of spatial and temporal modes, B_0 is the OBPB bandwidth, m_t is the number of polarisation modes, $N_0 = 0.5(NFG - 1)hf_c$ is the ASE power spectral density (PSD) in single polarisation, $R' = \eta/hf_c$, G is the optical amplifier gain, h is Planck's constant and f_c is the optical carrier frequency.

The Gaussian receiver thermal noise (of variance σ_{th}^2) is then straightforwardly included in the overall conditional MGF (for a random variable designated X) [11, 27, 28]

$$M_X(s|h_{turb}, P) = \exp \left(\frac{\sigma_{th}^2 s^2}{2} \right) M_Y(s|h_{turb}, P) \quad (6.7)$$

where shot noise has been neglected.

In this analysis, X_{tr} is taken to be the random variable representing the integration for the slot which contains the transmitted pulse and X_f is the random variable representing the integration for slots in which there was no

pulse transmitted. The means and variances of the transmitted pulse $\mu_{X_r}(h_{turb}, P)$ and $\sigma_{X_r}^2(h_{turb}, P)$, and empty slot μ_{X_f} and $\sigma_{X_f}^2$ (assuming no leakage signal light in wrong slots) are derived from their respective MGFs and are given as

$$\mu_{X_r}(h_{turb}, P) = GP_{pulse}(P)h_{turb}R'q + (LN_0R'q/t_s) \quad (6.8)$$

$$\mu_{X_f} = LN_0R'q/t_s \quad (6.9)$$

$$\sigma_{X_r}^2(h_{turb}, P) = \sigma_{th}^2 + (2N_0GP_{pulse}(P)h_{turb}R'^2q^2/t_s) + (LN_0^2R'^2q^2/t_s^2) \quad (6.10)$$

$$\sigma_{X_f}^2 = \sigma_{th}^2 + (LN_0^2R'^2q^2/t_s^2) \quad (6.11)$$

The DPPM BER is given by [2, 4, 29], here noting the dependence on h_{turb} relevant to the current discussion

$$BER(h_{turb}, P) = \frac{nP_{we}(h_{turb}, P)}{2(n-1)} \quad (6.12)$$

where $P_{we}(h_{turb}, P)$ is the symbol error probability. Following the treatment of [4], given that each transmitted word has equal probability, the probability of successful reception of a word $P_{ws}(h_{turb}, P) = 1 - P_{we}(h_{turb}, P)$ is bounded by exploiting the fact that for a particular frame, the events $\{X_{tr} > X_1\}, \dots, \{X_{tr} > X_j\}, \dots, \{X_{tr} > X_n\}$ (excluding, the case of $j = tr$) are each no less likely to occur given that any combination of the others have also occurred and write that

$$P_{ws}(h_{turb}, P) \geq \prod_{j=1, j \neq tr}^n P(X_{tr} > X_j | h_{turb}, P) = (P(X_{tr} > X_f | h_{turb}, P))^{n-1}, \quad (6.13)$$

Then $P_{we}(h_{turb}, P)$ can be expressed as [4]

$$P_{we}(h_{turb}, P) \leq 1 - (1 - P(X_f > X_{tr} | h_{turb}, P))^{n-1} \quad (6.14)$$

Under the assumption that the random variables X_{tr} and X_f are Gaussian, the GA expression for $P_{we,GA}(h_{turb}, P)$ is given by using (6.14) [4]

$$P_{we,GA}(h_{turb}, P) \leq 1 - \left(1 - 0.5 \operatorname{erfc} \left(\frac{\mu_{X_r}(h_{turb}, P) - \mu_{X_f}}{\sqrt{2(\sigma_{X_r}^2(h_{turb}, P) + \sigma_{X_f}^2)}} \right) \right)^{n-1} \quad (6.15)$$

The application of an upper bound upon $P_{we}(h_{turb}, P)$ using CB technique will also yield upper bound upon $P(X_f > X_{tr})$, hence for $s > 0$, the CB is given as [4]

$$P(X_f > X_{tr} | h_{turb}, P) \leq M_{X_f}(s | h_{turb}, P) M_{X_r}(-s | h_{turb}, P), \quad (6.16)$$

The tightest CB can be obtained by finding the optimum value of s (i.e. s_{opt}).

$$P_{we,CB}(h_{turb}, P) \leq 1 - \left(1 - M_{X_r}(-s_{opt} | h_{turb}, P) M_{X_f}(s_{opt} | h_{turb}, P) \right)^{n-1} \quad (6.17)$$

The general case for the MCB is $P(X > \varphi) \leq \exp(-s\varphi) M_X(s) / s\sigma_{th} \sqrt{2\pi}$, where φ is fixed and X includes a Gaussian component of variance σ_{th}^2 . In comparing X_f and X_{tr} whose Gaussian components each have variance σ_{th}^2 , the effective variance of the Gaussian contribution becomes $\sigma_{th}'^2 = 2\sigma_{th}^2$ so yielding

$$P(X_f > X_{tr} | h_{turb}, P) \leq \frac{M_{X_f}(s | h_{turb}, P) M_{X_r}(-s | h_{turb}, P)}{s\sigma_{th}' \sqrt{2\pi}} \quad (6.18)$$

This MCB expression (6.18) is then used, with (6.14), to obtain $P_{we,MCB}(h_{turb}, P)$:

$$P_{we,MCB}(h_{turb}, P) \leq 1 - \left(1 - \left(\frac{M_{X_r}(-s_{opt} | h_{turb}, P) M_{X_f}(s_{opt} | h_{turb}, P)}{2s_{opt}\sigma_{th} \sqrt{\pi}} \right) \right)^{n-1} \quad (6.19)$$

The overall DPPM BER is given as:

$$BER_{Z,GG}(P) = \int_0^{\infty} BER_Z(h_{turb}, P) P_{GG}(h_{turb}) dh_{turb} \quad (6.20)$$

where $BER_Z(h_{turb}, P)$ represents the BERs obtainable from (6.12) using the $P_{we}(h_{turb}, P)$ bounds of (6.15), (6.17) and (6.19) ($Z = GA, CB$ and MCB) while $p_{GG}(h_{turb})$ represents the GG atmospheric turbulence model given in (6.2). Note that for CB and MCB each $BER_Z(h_{turb}, P)$ will need a different s_{opt} for each h_{turb} and P combination. This is well known from non-turbulent (fibre) communications (e.g. [11]) where the averaging in (6.20) is not required. Hence to perform the integration in (6.20) numerically, the appropriate s_{opt} must be found for each step in the integration.

6.6 Results and discussion

Table 6.1: Parameters used in calculations

Parameter	Description	Value
R_b	Binary data rate	2.5 Gb/s [17]
λ	Optical wavelength	1.55 μm [17]
B_{opt}	Optical-filter bandwidth	80 GHz
G	Optical amplifier gain	30.6 dB (or 8.8 dB) [11]
NF	Amplifier noise figure	4.77 dB (e.g. for an EDFA)
η	Receiver quantum efficiency	0.75
D_{RX}	Receiver collecting lens diameter	1mm, 20 mm and 50 mm [13, 14]
l	Optical link length	1000 m and 1500 m [14]
m_t	Polarisation states of ASE noise	2 (no polarisation filtering)

The parameters used in this model are presented in Table 6.1. Three different atmospheric conditions characterised by the refractive-index structure parameter C_n^2 were taken into consideration. The WT, MT, and ST regimes are considered, for which we set $C_n^2 = 4.74 \times 10^{-15} \text{ m}^{-2/3}$, $C_n^2 = 3.8 \times 10^{-14} \text{ m}^{-2/3}$ and $C_n^2 = 8.3 \times 10^{-14} \text{ m}^{-2/3}$, respectively and $l=1500$

m and 2000 m. Using (6.1), the calculated Rytov variances are $\sigma_R^2 = 0.2$ (WT), $\sigma_R^2 = 1.6$ (MT), and $\sigma_R^2 = 3.5$ (ST), and $\sigma_R^2 = 0.3$ (WT), $\sigma_R^2 = 2.7$ (MT), and $\sigma_R^2 = 5.9$ (ST) for $l=1500$ m and 2000 m, respectively. It should be noted that the impact of link length is here only considered on the turbulence (via Rytov variance). Clearly in a full link budget beam spreading and other losses would need to be calculated. The coupling loss which usually arises from turbulence-deformed phase of the received optical signal has been neglected for simplicity [14]. The DPPM receiver thermal noise variance $\sigma_{th,DPPM}^2$ is given as the product of the $\sigma_{th,OOK}^2$ and the DPPM bandwidth expansion factor ($2^M/M$) [30], where $\sigma_{th,OOK} = 7 \times 10^{-7}$ A (chosen to be consistent with the back-to-back sensitivity of -23 dBm at a BER of 10^{-12} of a typical 2.5 Gbit/s receiver for no turbulence and non-amplified systems) is assumed for later comparison. The choice of OBPF of 80 GHz is to be able to comfortably accommodate the largest DPPM coding level ($M = 7$) which has a slot rate of $2^7/7 \times 2.5 \times 10^9 = 45.7$ GHz. The optically preamplified receiver sensitivity used in this thesis thus is the average power (in dBm) at the RCL required to obtain the target BER. However, it is straightforward to interpret the figures with any particular coupling loss by shifting the appropriate BER curves by the equivalent loss value in dB. Additionally, in practical FSO systems, the typical target BER under the influence of turbulence, and in the absence of error-correcting code is usually 10^{-9} [2, 14].

Figure 6.3 shows the aperture averaging factor (for a plane-wave propagation) as a function of the RCL diameter using $l=1500$ m. This plot will facilitate the understanding of some of our results. The behaviour of the strong turbulence (in particular that ST almost coincides with the MT for the $D_{RX} = 20$ mm and 50 mm cases) can be linked to the levelling effect which occurs when D_{RX} falls within the spatial coherence radius ρ_0 and scattering disk $l/k\rho_0$ range (i.e. $\rho_0 < D_{RX} < l/k\rho_0$ [14]). In this paper, the levelling effect can be attributed to range $8.2 \text{ mm} < D_{RX} < 45 \text{ mm}$ and so the choice of $D_{RX} = 20$ mm (and to an extent at $D_{RX} = 50$ mm) will exhibit

this for strong enough turbulence. Also, it can be seen that a continual decrease in AA factor occurs when $D_{RX} > l/k\rho_0$.

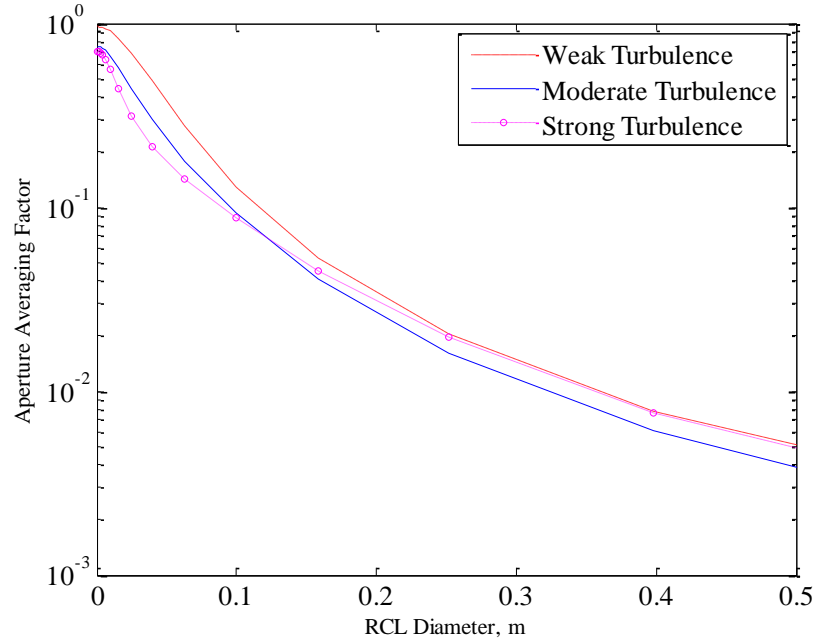
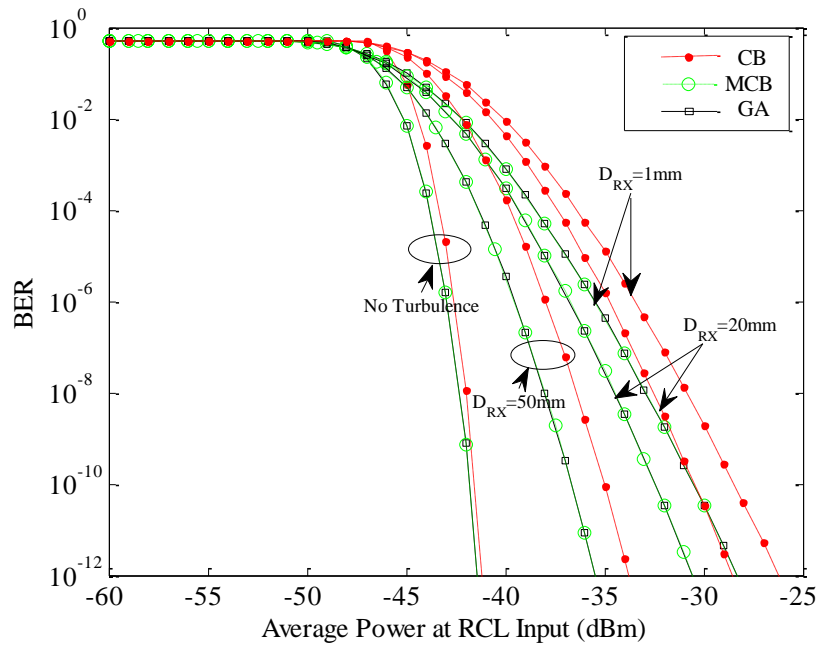


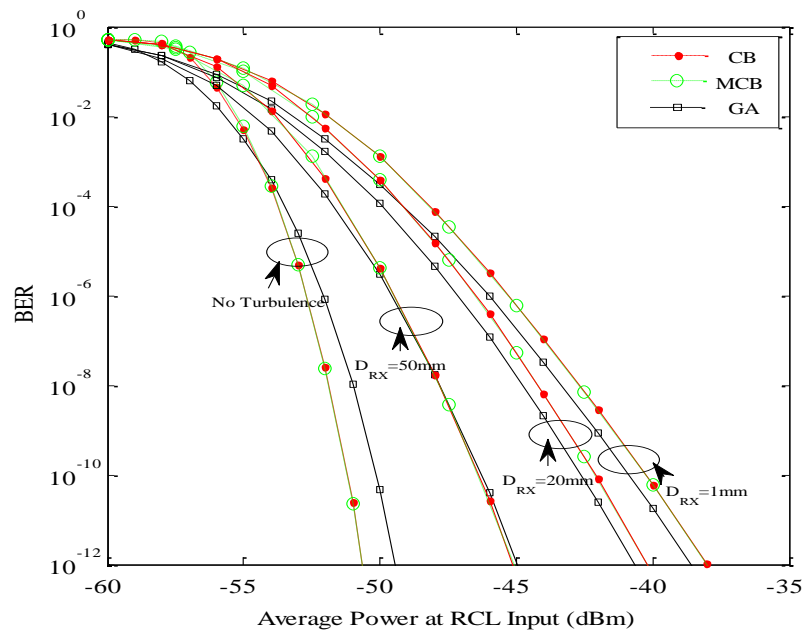
Figure 6.3: AA factor vs. RCL diameter for $l=1500$ m

In Figures 6.4-6.6, the BER curves for plane wave propagation using GA, CB and MCB are presented for no turbulence (NT), WT, MT, and ST using $M = 5$, $l=1500$ m, $G = 8.8$ dB and 30.6 dB, $D_{RX} = 1$ mm, 20 mm, and 50 mm, whilst other parameters are stated in Table 6.1. For the $G = 8.8$ dB case, the CB is clearly seen to exceed both the MCB and GA BERs (which are almost matching) for all employed atmospheric turbulence models. The discrepancy between CB and MCB vanishes when $G = 30.6$ dB, i.e. when due to the ASE increase the receiver thermal noise becomes less significant and, instead, the GA deviates. The GA exceeds the CB and MCB for NT (a similar GA positioning obtained in [11] for non-turbulent case) and WT ($D_{RX} = 50$ mm), whilst in other turbulence regimes, it is exceeded by the CB and MCB (which give similar BER values). It can be seen from the BER curves in general that the GA results are inconsistent, in that it is not possible to be certain whether the GA will overestimate or underestimate the BER, whilst the MCB provides the tightest bound upon the BER, hence

it will be a trustworthy method to use. In the case of WT (Figure 6.4), on increasing the RCL diameter from 20 mm to 50 mm the receiver sensitivity improves by about 4 dB for GA, CB and MCB at target BER of 10^{-9} . In comparison to $D_{RX} = 1$ mm, at target BER, improvements of about 2 dB and 6 dB in receiver sensitivity were observed for WT, for $D_{RX} = 20$ mm and 50 mm, respectively. However, it is noteworthy that the improvement achieved due to AA for WT regimes is less impressive compared to that for MT and ST regimes (which are discussed later).



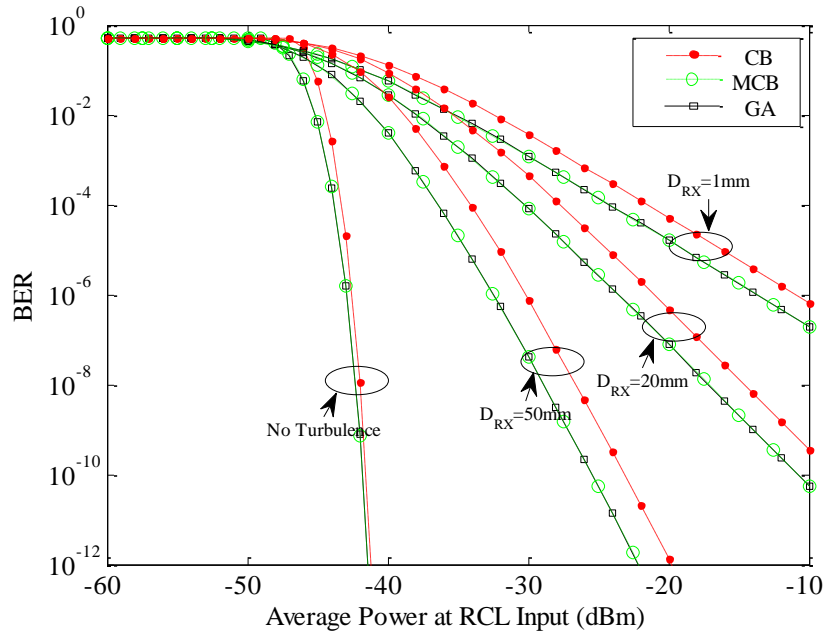
(a)



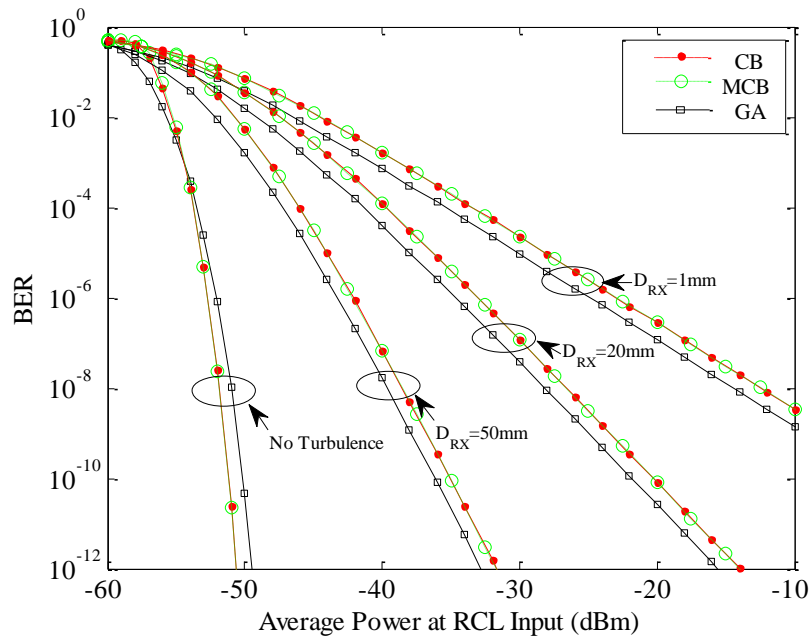
(b)

Figure 6.4: BER vs. average power at receiver collecting lens (RCL) input (dBm) using $M = 5$, $l = 1500$ m, $D_{RX} = 1$ mm, 20 mm and 50 mm for NT and WT with AA (a) $G = 8.8$ dB and (b) $G = 30.6$ dB

In the MT case (Figure 6.5), at target BER, an improvement was attained, about 16 dB and 28 dB, for $D_{RX} = 20$ mm and 50 mm respectively, when compared to $D_{RX} = 1$ mm. The effect of AA observed in the WT and MT cases can be linked to the D_{RX} used being greater than the Fresnel zone $\sqrt{l/k}$ (i.e. $D_{RX} > 19.2$ mm) (see [14] for more details). Finally, in the case of ST regime (Figure 6.6), a very significant performance improvement is clearly achieved by applying AA (moving from 1 mm to 20 mm or 50 mm). The similarity between the MT and ST BERs can be traced to the levelling effect which was explained earlier. As the maximum received average power is limited (as high powers will ultimately exceed the receiver specification (in practical FSO applications)) the use of AA is clearly seen to make FSO systems at BER of 10^{-9} or better feasible whereas, at very small RCL diameter, they are not. It should be noted that all calculated BERs will improve with increasing average power although this has not been shown because the omitted high powers will not be practicable with photodiode power specifications.

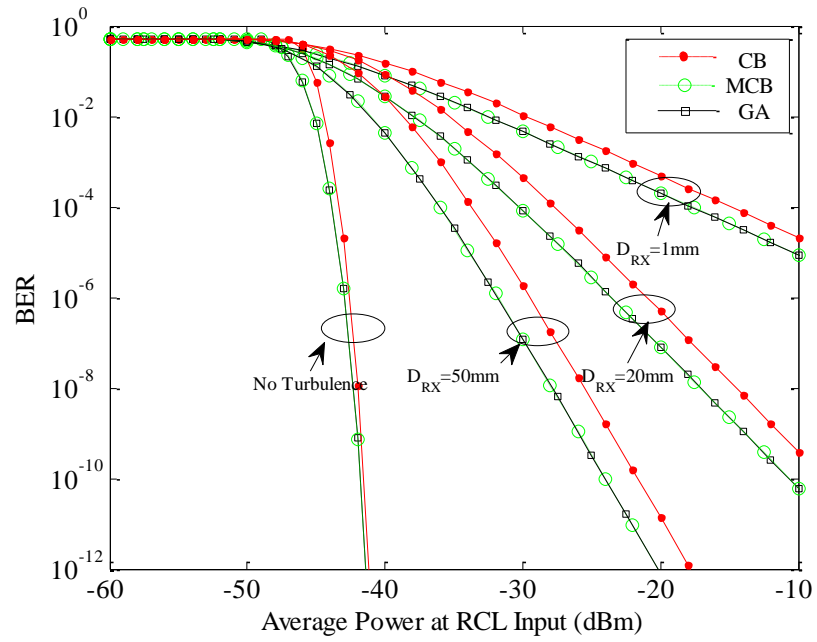


(a)

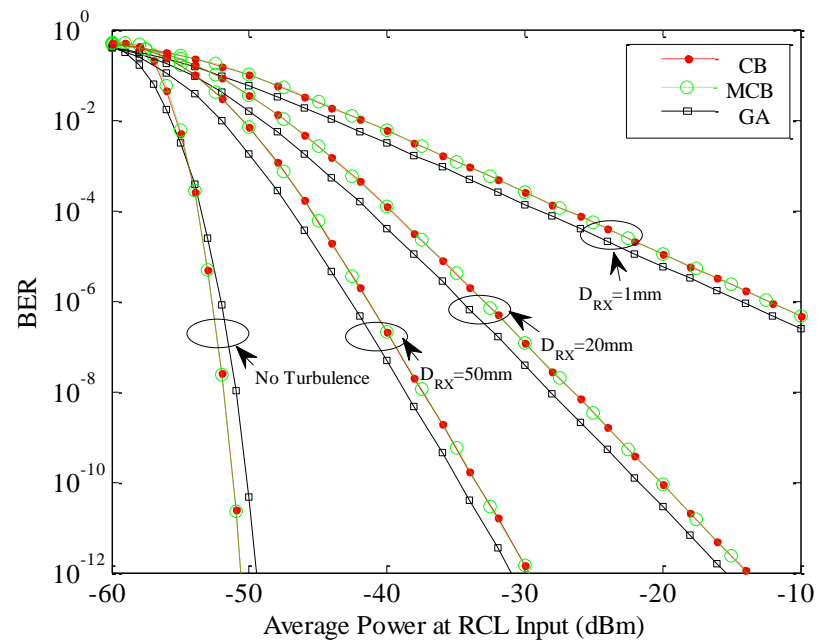


(b)

Figure 6.5: BER vs. average power at receiver collecting lens (RCL) input (dBm) using $M = 5$, $l = 1500$ m, $D_{RX} = 1$ mm, 20 mm and 50 mm for NT and MT with AA (a) $G = 8.8$ dB and (b) $G = 30.6$ dB



(a)



(b)

Figure 6.6: BER vs. average power at receiver collecting lens (RCL) input (dBm) using $M = 5$, $l = 1500$ m, $D_{RX} = 1$ mm, 20 mm and 50 mm for NT and ST with AA (a) $G = 8.8$ dB and (b) $G = 30.6$ dB

In Figure 6.7, the BER curves are presented for two typical FSO optical link lengths i.e. $l=1500$ m and $l=2000$ m, using $G = 30.6$ dB, $D_{RX} = 1$ mm and $M = 5$ for NT with WT, MT, and ST regimes, respectively. Here it can be seen that the effect of turbulence becomes more severe for the longer optical link (recall that C_n^2 is fixed, so the Rytov variance is where the length change impacts), for example, at target BER, the receiver sensitivity degrades by about 5 dB (WT), 12 dB (MT) and 8 dB (ST) as optical link length increase from 1500 m to 2000 m. Specifically, the effect of the optical link length gradually becomes less significant as the turbulence strength approaches very strong regimes, as shown in Figure 6.7.

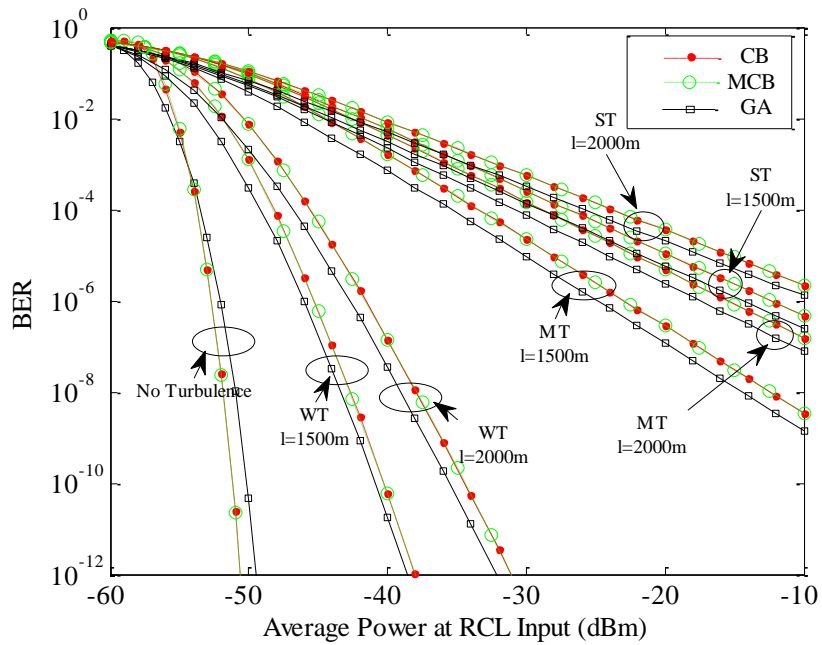


Figure 6.7: BER vs. average power at receiver collecting lens (RCL) input (dBm) using $M = 5$, $l=1500$ m and 2000 m, $G = 30.6$ dB, $D_{RX} = 1$ mm for NT and WT, MT and ST, all with AA

In Figure 6.8 (overleaf and page 117), the receiver sensitivity for each DPPM coding level ($M = 1-7$) is presented for NT with WT, MT, and ST, respectively, using GA, CB and MCB, $G = 30.6$ dB, $l=1500$ m, $D_{RX} = 1$ mm, 20 mm, and 50 mm, at target BER of 10^{-9} . It can be seen clearly that the receiver sensitivity improves with increase in coding level (and thus

increase in DPPM complexity) for all turbulence cases (and would continue to improve for $M > 7$), although in the absence of AA (e.g. at $D_{RX} = 1$ mm) the overall FSO receiver system performance is hugely affected as turbulence strength increases. At $M = 5$, $G = 30.6$ dB and $R_b = 2.5$ Gb/s, for NT condition, receiver sensitivities of about -50.53 dBm (~27.4 photons/bit) (GA), -51.49 dBm (~22 photons/bit) (CB), and -51.59 dBm (~21.5 photons/bit) (MCB) can be achieved, which implies an improvement when compared to the fundamental limit (38 photons/bit) of non-turbulent optically preamplified OOK-NRZ as stated in [31]. It can be deduced from the sensitivity curve that $M < 7$ may be a more sensible coding level to use, as sensitivity levels off to some extent as $M = 7$ is approached. For example, considering the MCB case, the sensitivities at $M = 5$ and $M = 6$ are no more than 1 dB less than that at $M = 7$ (for all turbulence regimes) but are less complex and thus more readily realized. Next it is seen that the advantage over OOK-NRZ is so great that such a reduction in M value is possible while still leaving DPPM advantageous.

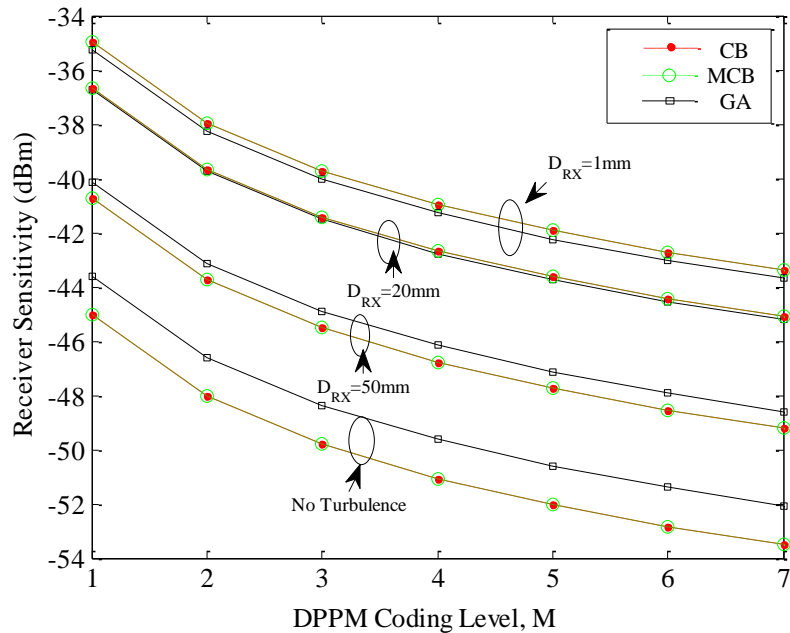


Figure 6.8 (a) for no turbulence and weak turbulence,

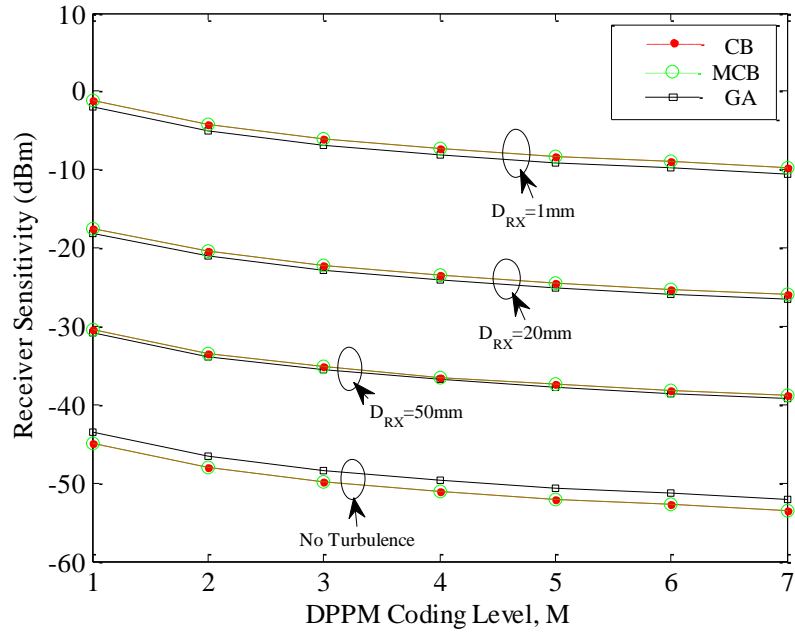


Figure 6.8 (b) for no turbulence and moderate turbulence,

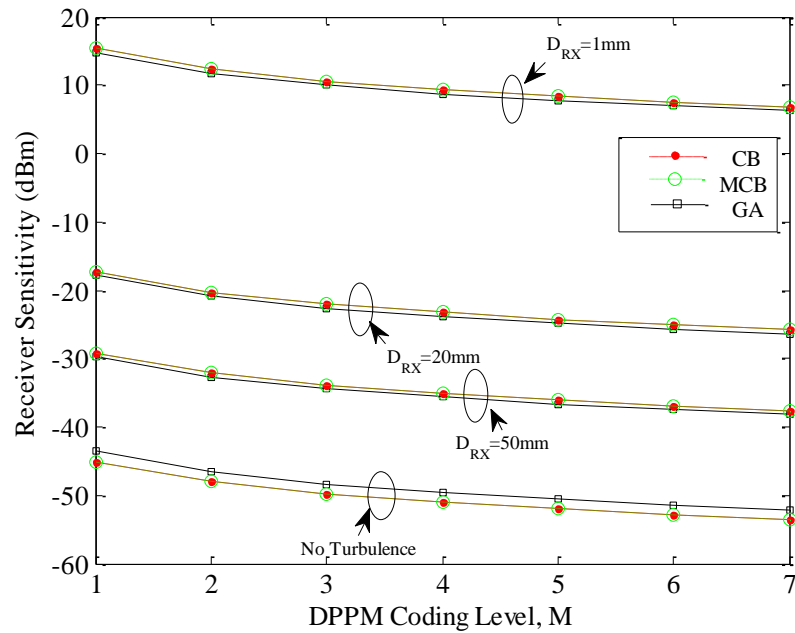


Figure 6.8 (c) for no turbulence and strong turbulence

Figure 6.8: Receiver sensitivity (dBm) vs. DPPM coding level M at BER of 10^{-9} using $G = 30.6$ dB, $l = 1500$ m, $D_{RX} = 1$ mm, 20 mm and 50 mm, all with AA

In Figure 6.9 (overleaf and page 119), a comparison is made between DPPM at $M = 5$ and an equivalent optically preamplified OOK-NRZ FSO

system using $l = 1500$ m, $D_{RX} = 20$ mm and MCB method for both systems. Other parameters used are as stated in Table 6.1. At target BER (using MCB), DPPM offers about 9 dB sensitivity improvements over the OOK-NRZ-FSO system in the absence of turbulence. When impaired by turbulence, the sensitivity improvement of DPPM over OOK-NRZ is reduced, respectively, to about 7 dB (WT), 8 dB (MT) and 8 dB, (ST).

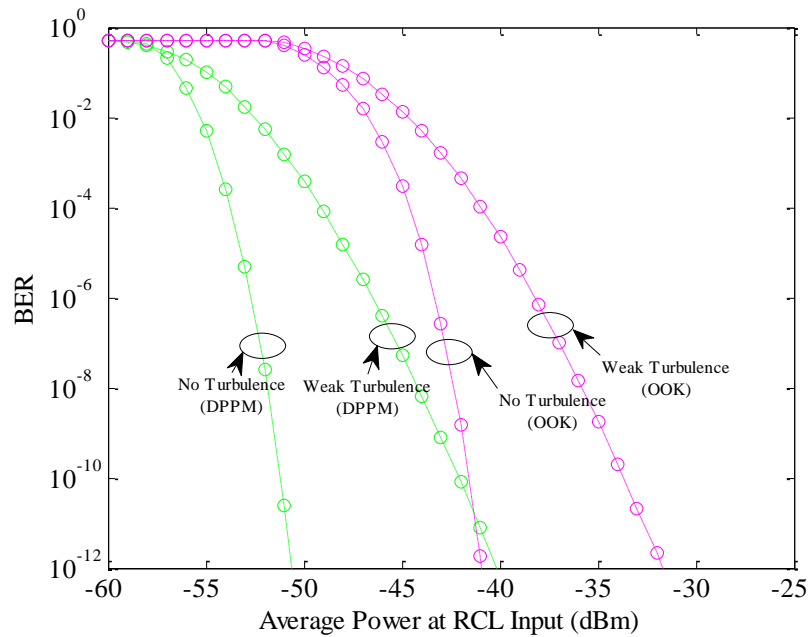


Figure 6.9 (a) for no turbulence and weak turbulence,

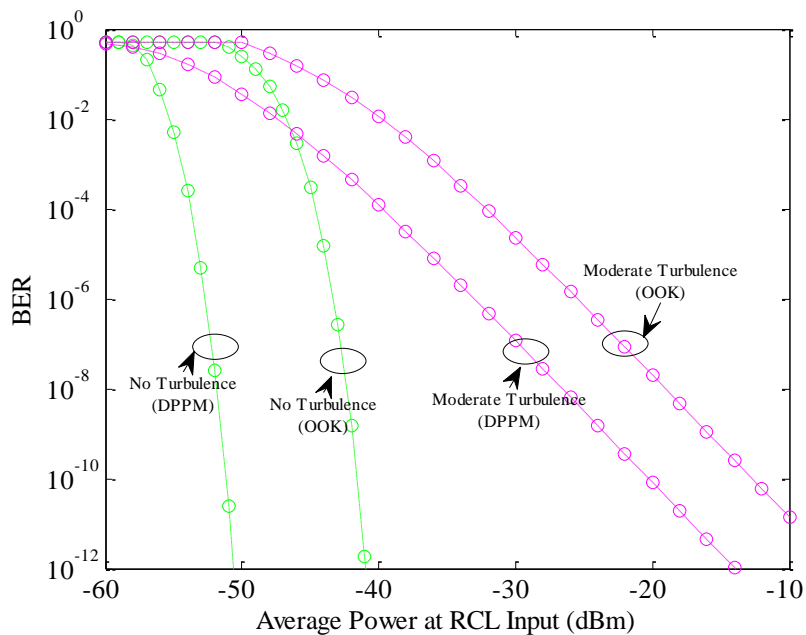


Figure 6.9 (b) for no turbulence and moderate turbulence,

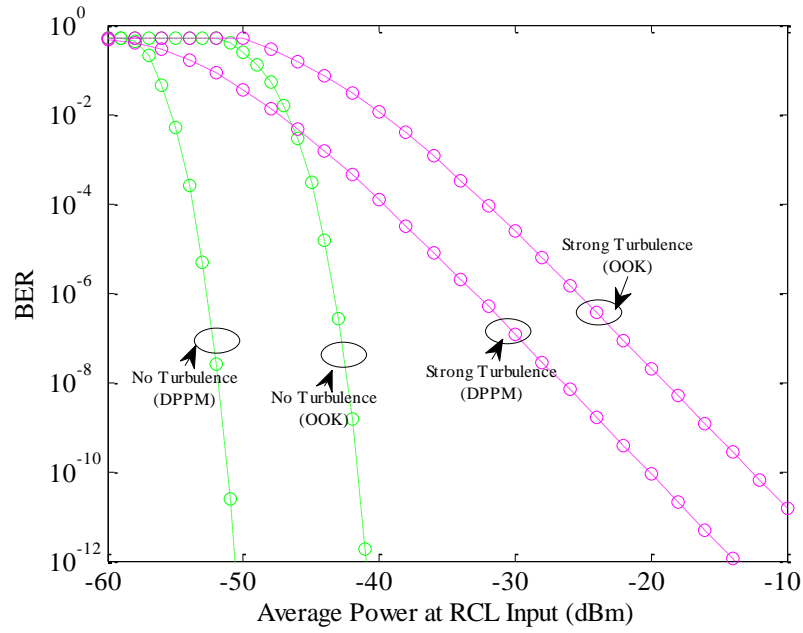


Figure 6.9 (c) for no turbulence and strong turbulence

Figure 6.9: BER vs. average power at receiver collecting lens (RCL) input (dBm) for DPPM and OOK using MCB, while $M = 5$, $l=1500$ m, $G = 30.6$ dB, and $D_{RX} = 20$ mm, all with AA

6.7 Summary

BER analyses for optically preamplified DPPM FSO systems are presented using GA, CB and MCB for WT, MT and ST regimes whilst adopting the GG distribution as the atmospheric turbulence model. A comparison is made between the MGF-based techniques (CB and MCB) and the commonly used Gaussian approximation, with the MCB seen to be a safer method. A comparison is also made between the optically preamplified DPPM and the OOK-NRZ-FSO systems. The results show a considerable improvement in receiver sensitivity over OOK-NRZ using the DPPM technique. The use of AA as a turbulence mitigating approach is investigated with the results showing significant improvements, especially in the MT and ST regimes. However, an effective AA is only achievable by using a sufficiently large RCL diameter.

6.8 References

- [1] I. Garrett, "Pulse-position modulation for transmission over optical fibres with direct or heterodyne detection," *IEEE Transaction on Communications*, vol. 31, no. 4, pp. 518-527, Apr. 1983.
- [2] A. K. Majumdar, "Free-space laser communication performance in the atmospheric channel," *Journal of Optical and Fiber Communications Research*, vol. 2, no. 4, pp. 345-396, 2005.
- [3] S. S. Muhammad, W. Gappmair, and E. Leitgeb, "PPM channel capacity evaluation for terrestrial FSO links," *Proceedings of the 2006 International Workshop on Satellite and Space Communications*, pp. 222-226, Sep. 2006.
- [4] A. J. Phillips, R. A. Cryan, and J. M. Senior, "An optically preamplified intersatellite PPM receiver employing maximum likelihood detection," *IEEE Photonic Technology Letter*, vol. 8, no. 5, pp. 691-693, May 1996.
- [5] A. Biswas, V. Vilnrotter, W. Farr, D. Fort, and E. Sigman, "Pulse position modulated ground receiver design for optical communications from deep space," *Proc. SPIE*, San Jose, CA, vol. 4635, pp. 224-235, Jan. 2002.
- [6] J. R. Lesh, J. Katz, H. H. Tan, and D. Zwillinger, "2.5 bit/detected photon demonstration program, analysis and phase I results," *TDA Progress Rep., Jet propulsion Laboratory*, Pasadena, CA, pp. 115-132, Oct. 1981.
- [7] A. J. Phillips, R. A. Cryan, and J. M. Senior, "Optically preamplified pulse-position modulation for fibre-optic communication systems," *IEE Proceedings - Optoelectronics*, vol. 143, no. 2, pp. 153-159, Apr. 1996.
- [8] K. Kiasaleh, "Performance of APD-based, PPM free-space optical communication systems in atmospheric turbulence," *IEEE Transactions on Communications*, vol. 53, no. 9, pp. 1455-1461, Sep. 2005.
- [9] Y. Yamamoto, "Noise and error rate performance of semiconductor laser amplifiers in PCM-IM optical transmission systems," *IEEE Journal of Quantum Electronics*, vol. 16, no. 10, pp. 1073-1081, Oct. 1980.
- [10] S. D. Personick, "Applications for quantum amplifiers in simple digital optical communication systems," *Bell System Technical Journal*, vol. 52, no. 1, pp. 117-133, Jan. 1973.
- [11] L. F. B. Ribeiro, J. R. F. Da Rocha, and J. L. Pinto, "Performance evaluation of EDFA preamplified receivers taking into account intersymbol interference," *Journal of Lightwave Technology*, vol. 13, no. 2, pp. 225-232, Feb. 1995
- [12] M. A. Al-Habash, L. C. Andrews, and R. L. Phillips, "Mathematical model for the irradiance probability density function of a laser beam propagating through turbulent media," *Opt. Eng.*, vol. 40, no. 8, pp. 1554-1562, Aug. 2001.
- [13] L. C. Andrews and R. L. Phillips, *Laser beam propagation through random media*, Second Edition, SPIE Press, Bellingham, Washington, 2005.

- [14] M. A. Khalighi, N. Schwartz, N. Aitamer, and S. Bourennane, "Fading reduction by aperture averaging and spatial diversity in optical wireless systems," *IEEE/OSA Journal of Optical Communications and Networking*, vol. 1, no. 6, pp. 580-593, Nov. 2009.
- [15] F. S. Vetelino, C. Young, and L. C. Andrews, "Fade statistics and aperture averaging for Gaussian beam waves in moderate-to-strong turbulence," *Applied Optics*, vol. 46, no. 18, pp. 3780-3789, June 2007.
- [16] X. Zhu and J. M. Kahn, "Free-space optical communication through atmospheric turbulence channels," *IEEE Transactions on Communications*, vol. 50, no. 8, pp. 1293-1300, Aug. 2002.
- [17] M. Razavi and J. H. Shapiro, "Wireless optical communications via diversity reception and optical preamplification," *IEEE Transactions on Wireless Communications*, vol. 4, no. 3, pp. 975-983, May 2005.
- [18] H. Yuksel and C. Davis, "Aperture averaging experiment for optimizing receiver design and analyzing turbulence on free space optical communication links," *Conference on Lasers & Electro-Optics*, Baltimore, Maryland, pp. 743-745, May 2005.
- [19] A. O. Aladeloba, A. J. Phillips, and M. S. Woolfson, "Performance evaluation of optically preamplified digital pulse position modulation turbulent free-space optical communication systems," *IET Optoelectronics*, vol. 6, no. 1, pp. 66-74, Feb. 2012.
- [20] M. S. Lesson, "Pulse position modulation for spectrum-sliced transmission," *IEEE Photonic Technology Letter*, vol. 4, no. 3, pp. 1191-1193, Apr. 2004.
- [21] F. M. Davidson and X. M. Sun, "Slot clock recovery in optical PPM communication systems with Avalanche photodiode photodetectors," *IEEE Trans. Commun.*, vol. 37, no. 11, pp. 1164-1172, Nov. 1989.
- [22] X. M. Sun and F. M. Davidson, "Word timing recovery in direct detection optical PPM communication systems with Avalanche photodiodes using a phase lock loop," *IEEE Trans. Commun.*, vol. 38, no. 5, pp. 666-673, May 1990.
- [23] S. Karp, R. M. Gagliardi, S. E. Moran, and L. B. Stotts, *Optical channels: fibers, clouds, water and the atmosphere*, New York: Plenum Press, 1988.
- [24] H. E. Nistazakis, T. A. Tsiftsis, and G. S. Tombras, "Performance analysis of free-space optical communication systems over atmospheric turbulence channels," *IET Communications*, vol. 3, no. 8, pp. 1402-1409, 2009.
- [25] A. J. Phillips, R. A. Cryan, and J. M. Senior, "Performance evaluation of optically pre-amplified PPM systems," *IEEE Photonics Technology Letters*, vol. 6, no. 5, pp. 651-653, May 1994.
- [26] J. O'Reilly and J. R. F. Da Rocha, "Improved error probability evaluation methods for direct detection optical communication systems," *IEEE Transactions on Information Theory*, vol. 33, no. 6, pp. 839-848, Nov. 1987.
- [27] K. W. Cattermole and J. J. O'Reilly, *Mathematical topics in telecommunications volume 2: problems of randomness in*

- communication engineering*, Pentech Press Limited, Plymouth, 1984.
- [28] I. T. Monroy and E. Tangdionga, *Crosstalk in WDM communication networks*, Kluwer Academic Publishers, Norwell, Massachusetts, USA, 2002.
- [29] X. M. Zhu and J. M. Kahn, "Performance bounds for coded free-space optical communications through atmospheric turbulence channels," *IEEE Transactions on Communications*, vol. 51, no. 8, pp. 1233-1239, Aug. 2003.
- [30] M. J. Sibley, *Optical communications*, Second Edition, Macmillian Press Limited, London, 1995.
- [31] P. S. Henry, *Error-rate performance of optical amplifiers*, Optical Fiber Communication Conference, Houston, Texas, vol. 5, Feb. 1989.

CHAPTER 7 Inclusion of pointing error and geometric spreading in the optically preamplified receiver model for turbulent FSO communication systems

7.1 Introduction

In addition to atmospheric obstacles, FSO systems are also affected by pointing error (PE) which arise due to inaccurate tracking systems or mechanical vibrations caused by natural phenomena (e.g. strong winds, thermal expansion and weak earthquakes [1-5]). Thus the existence of PE will further limit the optimal performance of the FSO system. Statistical analysis of the PE has been earlier studied for FSO systems over space channels [6]. The combined effect of PE and atmospheric turbulence on terrestrial FSO system performance has also been studied, for example theoretical calculations of the bit error rate (BER) by Arnon [1] (specifically for PE due to building sway), and Borah and Voelz [2]. In [3], the channel capacity and outage probability with main focus on beam optimization was investigated for FSO links experiencing both PE and turbulence. Furthermore, a BER analysis for a K distribution-based strong turbulence channel was studied in [5], also taking into account the PE effect. In all the above works on PE and turbulence combined, the emphasis was on OOK signaling. In this chapter such considerations are extended to the digital pulse position modulation (DPPM) format, which is well known for its power efficiency advantage, and compared with equivalent OOK-NRZ-FSO systems.

Furthermore, since the FSO system experiences significant performance impairment due to PE and turbulence, it is advantageous to compensate for this (and, of course, for coupling and atmospheric losses) by the inclusion of optical amplification. Thus the combined effects of atmospherically-induced scintillation and PE due to building sway on an optically preamplified FSO

system are the main focus of this chapter. Unfortunately optical amplifiers also introduce optical noise known as amplified spontaneous emission (ASE). At the receiver, the ASE noise beats with itself to form spontaneous-spontaneous beat noise and with the incoming signal to form the signal-spontaneous beat noise, in the electrical domain. The inclusion of ASE significantly complicates optical performance analysis in fibre/non-turbulent communications and when considered in conjunction with turbulence and PE the situation becomes more complex still.

Relative to the commonly used Gaussian approximation (GA) [4, 5, 7-9] the use of moment generating function (MGF) based techniques, specifically the modified Chernoff bound (MCB) (an upper bound upon the BER clearly frequently more accurate than the GA which sometimes exceeds it in non-turbulent systems [10]), and the saddlepoint approximation (SPA) (not previously applied to optically preamplified DPPM of any sort), represent a robust way of describing the signal and noise performance for an optically preamplified direct detection receiver [10-13], and, therefore, these are used in the analysis, suitably adapted to accommodate turbulence and PE. The works in chapters 5 and 6 [14, 15], detail why the GA is inferior to the MCB (in systems without PE and geometric spread (GS)). The present analysis led to publication [16].

7.2 Theoretical model

The emphasis of this analysis will be on two of the main modulation formats proposed for the free-space channel, namely the DPPM and OOK-NRZ formats, and in particular the performance advantages obtainable with the former. The OOK format is the current modulation format for commercial FSO communication systems because of the simplicity of the transceiver hardware. The DPPM format helps achieve a significant improvement in power efficiency, and is particularly applicable to the FSO channel due to the non-dispersive channel nature [17-19]. These advantages of the DPPM format however come at the expense of greater channel bandwidth requirements. DPPM involves dividing the time allocated for an M bit binary word (at data rate R_b) into $n = 2^M$ equal size time slots whose

length is given as $t_s = MT_b/n$, where $T_b = 1/R_b$. Each frame consists of one pulse whose position corresponds to the value of the M bit word.

7.2.1 Receiver model

Figure 7.1 shows the schematic diagram of a direct detection optically preamplified FSO receiver. The optical signal is collected by the receiver collecting lens (RCL) and then coupled using a collimator (e.g. as in [20]) into the optical amplifier of gain G and spontaneous emission parameter n_{sp} . Coupling loss is neglected in this analysis, but can be introduced by subtracting the coupling loss dB value from the required optical power (in dBm). The optical bandpass filter (OBPF) (with bandwidth B_0 and centered at carrier frequency f_c) at the output of the amplifier helps in reducing the optical background noise and ASE noise accompanying the optical signal. Moreover, it should be noted that any optical background noise that accompanies the signal will typically be negligible compared to the ASE noise, even when it has been amplified, and hence is neglected. The pin photodiode with quantum efficiency, η , converts the information-bearing optical signal into electrical current. An integrate-and-dump receiver is assumed for both OOK-NRZ and DPPM (over T_b for OOK-NRZ and over t_s for DPPM). In the DPPM case, at the decision circuit, each DPPM slot is integrated, and the results obtained per frame are compared in order to obtain the slot (and hence word) with the highest value. In the OOK-NRZ case, at the decision circuit, the bit is sampled and then compared with threshold. In contrast to the OOK-NRZ based FSO communication system, DPPM based systems can thus be threshold independent.

Unlike in OOK-NRZ-based optical fibre systems, where the decision threshold is steady, the OOK-NRZ-based FSO systems experience fluctuating instantaneous irradiance. The decision circuit at the receiver thus uses an adaptive threshold because of the near optimal performance that is achievable. The Kalman filtering method used in e.g. [21] represents a realistic adaptive approach of achieving optimal threshold for each instantaneous irradiance level, and such a threshold (however obtained) is

assumed for OOK-NRZ here. Furthermore, $B_e = 1/2T$ is the noise equivalent bandwidth, assuming a receiver with integrate-and-dump response over time T (where T is T_b or t_s), m_t is number of polarization modes for ASE noise, $R' = \eta/E$, $N_0 = n_{sp}(G-1)E$ is the ASE noise power spectral density (PSD) in W/Hz (in single polarization), and E is the photon energy.

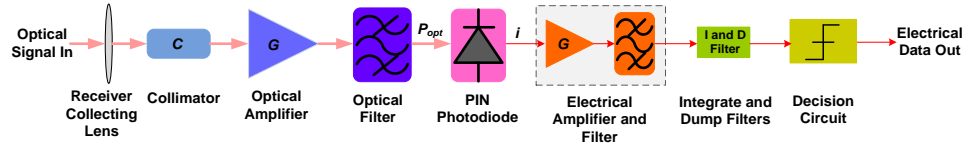


Figure 7.1 The direct detection optically preamplified FSO receiver.

Decision circuit is thresholded for OOK-NRZ and a comparison over slots in frame for DPPM

7.2.2 Atmospheric channel model with pointing error

The refractive index structure parameter C_n^2 is commonly used for estimating the turbulence strength of the atmosphere [22]. C_n^2 (which typically takes value within range $10^{-17} \text{ m}^{-2/3} \leq C_n^2 \leq 10^{-13} \text{ m}^{-2/3}$ [2, 3, 8, 18, 22, 23]) is used to calculate the Rytov variance $\sigma_R^2 = 1.23C_n^2 k^{7/6} l^{11/6}$ with optical wave number $k = 2\pi/\lambda$, and optical link length l . Weak turbulence (WT), moderate turbulence (MT) and strong turbulence (ST) links are associated with $\sigma_R^2 < 1$, $\sigma_R^2 \approx 1$, and $\sigma_R^2 > 1$ [22], respectively. The homogenous turbulence condition, which is typically considered for terrestrial FSO systems [22, 24, 25], is assumed.

The gamma-gamma (GG) distribution model is adopted for characterizing the WT, MT and ST regimes because the model produces results that are close to experimentally-measured data [22]. The GG distribution model is valid for a wide range of turbulence regimes, as it takes into consideration both the large-scale and small-scale effects on an optical signal traversing a turbulent atmospheric channel. In addition, the direct relationship with atmospheric turbulence parameters, and the

existence of simple closed-form expressions, are other factors motivating the use of the GG model in the analysis [18, 22, 24]. The GG probability density function (pdf) for attenuation due to turbulence is given by [18, 22, 24]

$$p_{GG}(h_a) = \frac{2(\alpha\beta)^{(\alpha+\beta)/2}}{\Gamma(\alpha)\Gamma(\beta)} h_a^{\left(\frac{\alpha+\beta}{2}\right)-1} K_{\alpha-\beta}\left(2\sqrt{\alpha\beta h_a}\right); \quad h_a > 0 \quad (7.1)$$

where h_a is attenuation due to atmospheric turbulence, $1/\alpha$ is the aperture-averaged variance of large-scale eddies of the scattering process and $1/\beta$ is the aperture-averaged variance of small-scale eddies of the scattering process [18, 22], $K_n(\cdot)$ is modified Bessel function of the second kind of order n , and $\Gamma(\cdot)$ represents the gamma function.

$$\alpha = \left\{ \exp \left[\frac{0.49\sigma_R^2}{\left(1 + 0.653d^2 + 1.11\sigma_R^{12/5}\right)^{7/6}} \right] - 1 \right\}^{-1} \quad (7.2)$$

$$\beta = \left\{ \exp \left[\frac{0.51\sigma_R^2 \left(1 + 0.69\sigma_R^{12/5}\right)^{-5/6}}{1 + 0.9d^2 + 0.621d^2 \sigma_R^{12/5}} \right] - 1 \right\}^{-1} \quad (7.3)$$

where $d = \sqrt{kr_{RX}^2/l}$ is the normalized RCL radius and r_{RX} is the RCL radius. Aperture averaging (AA) has been incorporated, as it helps to reduce the effect of atmospheric turbulence-induced irradiance fluctuations by using a receiver aperture of sufficient size (larger than the irradiance correlation width [2, 22, 26-29]).

The beam width of a Gaussian laser beam w_z due to diffraction and turbulence effects grows with the optical link length, and it is given as [22, 30]

$$w_z = w_d \left[1 + 1.33\sigma_R^2 \left(\frac{2l}{kw_d^2} \right)^{5/6} \right]^{\frac{1}{2}} \quad (7.4)$$

$$w_d = w_0 \left[1 + \left(\frac{l}{l_R} \right)^2 \right]^{\frac{1}{2}}$$

where w_0 is the minimum value of w_z at a point ($l = 0$) along the beam axis, w_d is the beam width due to diffraction effects only, and $l_R = \pi w_0^2/\lambda$

is called the Rayleigh range (the distance at which the diffraction-limited beam width spreads by a factor of $\sqrt{2}$).

The Gaussian beam at the receiver is approximated as a plane wave for aspects such as the turbulence modelling and the beam characterisation of this analysis (and was in related works, for example [3-5]), though the pointing error analysis relies on its Gaussian nature. When the plane wave assumption is made, the beam width at the receiver must be much greater than the diameter of the receiver [31] and this will be true in this analysis. For example, using $l = 1500$ m and $w_0 = 0.002$ m the calculated beam widths are $w_z = 0.3756$ m ($C_n^2 = 4.74 \times 10^{-15} \text{ m}^{-2/3}$), 0.380 m ($C_n^2 = 3.8 \times 10^{-14} \text{ m}^{-2/3}$) and 0.3859 m ($C_n^2 = 8.3 \times 10^{-14} \text{ m}^{-2/3}$). These values comfortably exceed the RCL diameters of 0.025 m and 0.05 m assumed in the analysis later.

The pdf for attenuation, due to PE and GS, (based on Rayleigh distribution [3]) is given as [3]

$$p_{PE}(h_p) = \frac{\gamma^2}{A_0^{\gamma^2}} h_p^{\gamma^2-1}; \quad 0 \leq h_p \leq A_0 \quad (7.5)$$

where $h_p \approx A_0 \exp(-2r_d^2/w_{z_{eq}}^2)$ is the attenuation due to GS and PE, r_d is the radial distance from the centre axis of the beam, $\gamma = w_{z_{eq}}/2\sigma_{PE}$, jitter-induced PE standard deviation at the receiver is σ_{PE} , $w_{z_{eq}}^2 = w_z^2 \sqrt{\pi} \text{erf}(\nu)/2\nu \exp(-\nu^2)$ is the (square of the) equivalent beam width, $A_0 = [\text{erf}(\nu)]^2$ is the fraction of the collected power at receiver radial displacement of zero, and $\nu = (\sqrt{\pi} r_{RX})/(\sqrt{2} w_z)$ [3]

The combined pdf for attenuation due to turbulence, PE and GS can then be expressed as [3]

$$p(h_{tot}) = \int p_{PE}(h_{tot}|h_a) p_{GG}(h_a) dh_a \quad (7.6)$$

where $h_{tot} = h_a h_p$ and $p_{PE}(h_{tot}|h_a)$ is the probability distribution for PE conditioned on h_a , such that

$$p_{PE}(h_{tot}|h_a) = \frac{1}{h_a} p_{PE}\left(\frac{h_{tot}}{h_a}\right) = \frac{\gamma^2}{A_0^{\gamma^2}} \left(\frac{h_{tot}}{h_a}\right)^{\gamma^2-1}; \quad 0 \leq h_{tot} \leq A_0 h_a \quad (7.7)$$

On substituting (7.1) and (7.7) into (7.6), the combined pdf can be rewritten as

$$p(h_{tot}) = \frac{2\gamma^2(\alpha\beta)^{(\alpha+\beta)/2}}{A_0^{\gamma^2}\Gamma(\alpha)\Gamma(\beta)} h_{tot}^{\gamma^2-1} \int_{h_{tot}/A_0}^{\infty} h_a^{\frac{(\alpha+\beta)}{2}-1-\gamma^2} K_{\alpha-\beta}(2\sqrt{\alpha\beta h_a}) dh_a \quad (7.8)$$

Analytical expressions for $p(h_{tot})$ can be found in [4].

7.2.3 Optically preamplified receiver model

For receivers with an integrate-and-dump response, as assumed here, the moment generating function can be derived from e.g. [10-12] as

$$M_{Y_j}(s|h_{tot}, P) = \frac{\exp\left(\frac{R'G(e^{sq}-1)P_j(P)h_{tot}}{1-\frac{R'N_0(e^{sq}-1)}{T}}\right)}{\left[1-\frac{R'N_0(e^{sq}-1)}{T}\right]^{B_0 m_r T}} \quad (7.9)$$

where $P_j(P) = a_j P$, $j = \{0,1\}$, $a_0 = 2/(r+1)$, $a_1 = 2r/(r+1)$, r is the extinction ratio (for OOK-NRZ), and $j = \{pulse, empty\}$, $a_{pulse} = 2^M$ and $a_{empty} = 0$ (for DPPM). Given the assumption of a clean atmosphere, P corresponds to the transmitted average power, and h_{tot} embodies the instantaneous attenuation due to turbulence, PE and GS, q is the electron charge, s is a strictly positive real number, and any such s provides a bound. The Gaussian receiver thermal noise is then straightforwardly included in the overall conditional MGF (for a random variable designated X) [10-12]

$$M_{X_j}(s|h_{tot}, P) = M_{th}(s)M_{Y_j}(s|h_{tot}, P) \quad (7.10)$$

where $M_{th}(s) = \exp\left(\frac{\sigma_{th}^2 s^2}{2}\right)$.

7.2.4 BER for OOK-NRZ

The BER (conditioned on h_{tot}) using the MGF-based MCB and SPA, for OOK-NRZ-FSO systems with optimal threshold, can be written as [10-12]

$$BER_{OOK,MCB}(h_{tot}, P) = \frac{M_{th}(s)}{s\sigma_{th,OOK}\sqrt{2\pi}} \sqrt{M_{Y_1}(-s|h_{tot}, P)M_{Y_0}(s|h_{tot}, P)} \quad s > 0 \quad (7.11)$$

$$BER_{OOK,SPA}(h_{tot}, P) = \frac{M_{th}(s)}{2s\sqrt{2\pi}} \sqrt{M_{Y_1}(-s|h_{tot}, P)M_{Y_0}(s|h_{tot}, P)} \times \left[\frac{1}{\sqrt{\Psi_0''(s)}} + \frac{1}{\sqrt{\Psi_1''(s)}} \right] \quad s > 0 \quad (7.12)$$

$$\Psi_0(s) = \ln\left(\frac{M_{X_0}(s) \cdot \exp(-sD)}{s}\right) \quad (7.13)$$

$$\Psi_1(s) = \ln\left(\frac{M_{X_1}(-s) \cdot \exp(sD)}{s}\right)$$

where D is the optimum value for the decision threshold as given in [10-12]. Note that the SPA and MCB are strictly firstly applied to 1 and 0 separately with distinct s parameters, s_1 and s_0 [10-12]. Thus these expressions (7.11)-(7.12) are simplified versions used with only a little loss of accuracy by performing a one-dimensional optimisation on the variable $s = s_1 = -s_0$ [10-12]. Equations (7.11)-(7.12) hold for a specific received optical power at the RCL input, namely the product of the combined turbulence, PE and GS attenuation h_{tot} and the average transmitted optical power P .

7.2.5 BER for DPPM

In the case of the DPPM based FSO system, the BER (conditioned on h_{tot}) is given as [15, 19, 32]

$$BER_{DPPM}(h_{tot}, P) = \frac{nP_{we}(h_{tot}, P)}{2(n-1)} \quad (7.14)$$

where $P_{we}(h_{tot}, P)$ (shown in (18) and (20) following, for SPA and MCB respectively) is the word error probability. Following the treatment of [19], given that each transmitted word has equal probability, the probability of

successful reception of a word $P_{ws}(h_{tot}, P) = 1 - P_{we}(h_{tot}, P)$ can be lower bounded as:

$$P_{ws}(h_{tot}, P) \geq \prod_{m=1, m \neq \text{pulseslot}}^n P(X_{pulse} > X_{empty_m} | h_{tot}, P) \quad (7.15)$$

$$= (P(X_{pulse} > X_{empty} | h_{tot}, P))^{n-1}$$

where X_{pulse} is the random variable for the integration for the slot containing the transmitted pulse and X_{empty} is similar for slots in which there was no pulse transmitted. Then $P_{we}(h_{tot}, P)$ can be expressed as [19]

$$P_{we}(h_{tot}, P) \leq 1 - (1 - P(X_{empty} > X_{pulse} | h_{tot}, P))^{n-1} \quad (7.16)$$

The general case for a threshold independent DPPM-based SPA can be written as $P(X < 0) \leq M_X(-s) / s\sqrt{2\pi\Psi''(s)}$, where $s > 0$. Assuming random variable $X = X_{pulse} - X_{empty}$, this implies that $M_X(s) = M_{X_{pulse}}(s)M_{X_{empty}}(-s)$, and

$$P(X_{empty} > X_{pulse} | h_{tot}, P) = P(X_{pulse} - X_{empty} < 0 | h_{tot}, P)$$

$$\leq \frac{M_{X_{pulse}}(-s | h_{tot}, P) M_{X_{empty}}(s | h_{tot}, P)}{s\sqrt{2\pi\Psi''(s)}} \quad (7.17)$$

This SPA expression (7.17) is then used, with (7.16), to obtain $P_{we,SPA}(h_{tot}, P)$:

$$P_{we,SPA}(h_{tot}, P) \leq 1 - \left(1 - \left(\frac{M_{X_{pulse}}(-s | h_{tot}, P) M_{X_{empty}}(s | h_{tot}, P)}{s\sqrt{2\pi\Psi''(s)}} \right) \right)^{n-1} \quad (7.18)$$

$$\Psi(s) = \ln \left(\frac{M_{X_{pulse}}(-s | h_{tot}, P) M_{X_{empty}}(s | h_{tot}, P)}{s} \right) \quad (7.19)$$

The MCB expression for (7.16) is [15]

$$P_{we,MCB}(h_{tot}, P) \leq 1 - \left(1 - \left(\frac{M_{X_{pulse}}(-s | h_{tot}, P) M_{X_{empty}}(s | h_{tot}, P)}{2s\sigma_{th,DPPM}\sqrt{\pi}} \right) \right)^{n-1} \quad (7.20)$$

The BER_{DPPM} for SPA and MCB, can be calculated by substituting (18) and (20), respectively, into (7.14).

7.2.6 Average BER

The average BER is given as

$$\overline{BER}_{Y,Z}(P) = \int_0^{\infty} BER_{Y,Z}(h_{tot}, P) p(h_{tot}) dh_{tot} \quad (7.21)$$

where $BER_{Y,Z}(h_{tot}, P)$ represents the BERs shown in equations (7.11) and (7.12) for OOK-NRZ and shown in (7.14), obtainable from (7.18) and (7.20), for DPPM. $Y=OOK$ or DPPM and $Z = SPA$ or MCB.

In order to obtain the tightest form of the MCB and SPA BERs, an optimized s (s_{opt}) that gives the minimum BER at each h_{tot} calculation in the numerical evaluation of (7.21) should be used. The s_{opt} can be obtained by differentiating $BER_{Y,Z}(h_{tot}, P)$ with respect to s , and setting the result to zero to find a stationary point.

7.3 Results and discussion

In this section, the numerical results in terms of BER, required optical power, and power penalty calculations on the performance for an optically preamplified terrestrial FSO communication system affected by turbulence and PEs are presented. The parameters for the system are presented in Table 7.1. The WT, MT and ST conditions are defined here by $C_n^2 = 4.74 \times 10^{-15} \text{ m}^{-2/3}$, $C_n^2 = 3.8 \times 10^{-14} \text{ m}^{-2/3}$ and $C_n^2 = 8.3 \times 10^{-14} \text{ m}^{-2/3}$, respectively. The corresponding values of the Rytov variance σ_R^2 at optical link length of 1500 m are 0.2 (WT), 1.6 (MT), and 3.5 (ST).

Table 7.1: Parameter values for calculation

Symbol	Quantity	Value
R_b	Bit rate	2.5 Gb/s
λ	Optical wavelength	1.55 μm
B_0	Optical-filter bandwidth	70 GHz
G	Optical amplifier gain	30 dB
n_{sp}	Spontaneous emission factor	1.5 (noise figure 4.77 dB)
η	Quantum efficiency	0.8
r	OOK-NRZ Extinction ratio	10 dB
D_{RX}	RCL diameter	25, 50 mm
m_t	Polarization states of ASE noise	2
l	Optical link length	1500 m
σ_{PE}/r_{RX}	Normalized PE standard deviation	0.1, 3, 5 [3-5]

Normalized beamwidths $w_z/r_{RX} = 15$ and 30 can be determined by varying the RCL diameter, that is, $w_z/r_{RX} = 15$ (for $D_{RX} = 50$ mm), $w_z/r_{RX} = 30$ (for $D_{RX} = 25$ mm), assuming a transmitting beam divergence angle of 2.5×10^{-4} rad and $l = 1500$ m. These values are approximately the same for all turbulence parameters stated above (from (7.4) the only parameter that is changing is σ_R^2 and this is not making a significant difference i.e. turbulence is not significantly increasing beamwidth beyond the diffraction-limited value), while other parameters are as stated on Table 7.1. The choice of OBPF of 70 GHz is to be able to comfortably accommodate the largest DPPM coding level considered ($M = 5$) which has a slot rate of $2^5/5 \times 2.5 \times 10^9 = 16$ GHz. The standard target BER of 10^{-9} for FSO systems [8, 9, 17, 18] is used throughout this paper. Coupling losses have been neglected in analysis, but can easily be included by subtracting the coupling loss dB value from the required optical power P (in dBm) which is plotted. The required optical power used in this work is the

transmitter average power (in dBm) required to obtain the target BER in the presence of the actual turbulence, PE and GS. For the OOK-NRZ-based FSO system, $\sigma_{th,OOK} = 7 \times 10^{-7}$ A was used in this paper. This value is chosen to be consistent with the back-to-back sensitivity of -23 dBm at a BER of 10^{-12} for a typical unamplified 2.5 Gb/s receiver for no turbulence [33]. Also, the DPPM based FSO thermal noise $\sigma_{th,DPPM}^2$ is given as the product of the NRZ OOK thermal noise $\sigma_{th,OOK}^2$ and the DPPM bandwidth expansion factor ($2^M/M$ [34]).

Figures 7.2-7.4 shows the MCB-based BER as a function of average transmitted optical power (dBm) using $\sigma_{PE}/r_{RX} = 0.1, 3$ and 5 , DPPM coding level $M = 5$, $G = 30$ dB, for no turbulence (NT) (with GS), turbulence only (with GS but no PE) (i.e. WT (Figure 7.2), MT (Figure 7.3), and ST (Figure 7.4)), and combined turbulence PE and GS using (a) $D_{RX} = 25$ mm (which translates to about $w_z/r_{RX} = 30$), and (b) $D_{RX} = 50$ mm (which translates to about $w_z/r_{RX} = 15$). It can be seen clearly from the BER results that the turbulence and PE combined introduces additional power penalty compared to the turbulence only situation. Note that the BER curve can be obtained for higher average powers than shown, however these powers may exceed typical FSO specifications [18]. It can be seen in Figure 7.2 (WT) that for normalized beam widths $w_z/r_{RX} = 30$, the BERs due to the combined turbulence and PE effect (for $\sigma_{PE}/r_{RX} = 5$) are less than when $w_z/r_{RX} = 15$. This implies that reducing r_{RX} can help ease the combined effect of PE and turbulence when the PE is particularly significant. When the PE is less significant then the impact of more GS loss makes this undesirable and the larger r_{RX} is better. In Figures 7.3 (MT) and 7.4 (ST), the smaller radius does not have an advantage, even at the large PE. Beam width optimization which involves choosing a suitable beam width that minimizes the required transmitted power, represent a way of balancing-out the effects of PE and turbulence on the BER [3, 5]. The combined effects would become more severe as optical link length increases because the impact of turbulence becomes stronger and the beam width increases also as

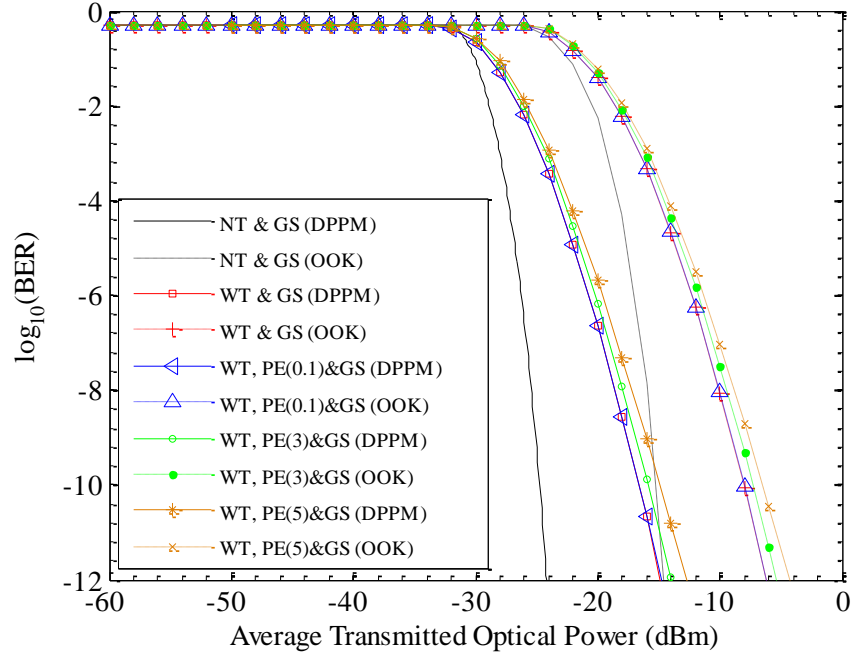
a function of the optical link length (as shown in (7.4)). It is however important that in designing these types of FSO system there needs to be a precise control over the w_z/r_{RX} which can be achieved at the transmitter. In the case of the NT with GS case (can be seen in Figures 7.2, 7.3 and 7.4), on increasing the RCL diameter from 25 mm to 50 mm, the required optical power transmitted improves by approximately 6 dB for both modulation formats which corresponds to the dB value of their area ratio.

In the WT case (Figure 7.2), on increasing the RCL diameter from 25 mm to 50 mm, an improvement of approximately 9 dB (WT with GS case) and approximately 9 dB and 5 dB (WT, PE and GS case for $\sigma_{PE}/r_{RX} = 0.1$ and 3, respectively) were observed for both modulation formats, at a target BER of 10^{-9} . The high BERs observed in the WT, PE and GS case of $\sigma_{PE}/r_{RX} = 5$, can be linked to the fact that the GG pdf is less widely spread in that case and thus interacts differently with the PE plus GG pdf (7.5) to create the overall pdf (7.8) as σ_{PE} worsens ($\gamma \rightarrow 0$) such that the PE plus GS pdf becomes concentrated nearer to $h_p = 0$.

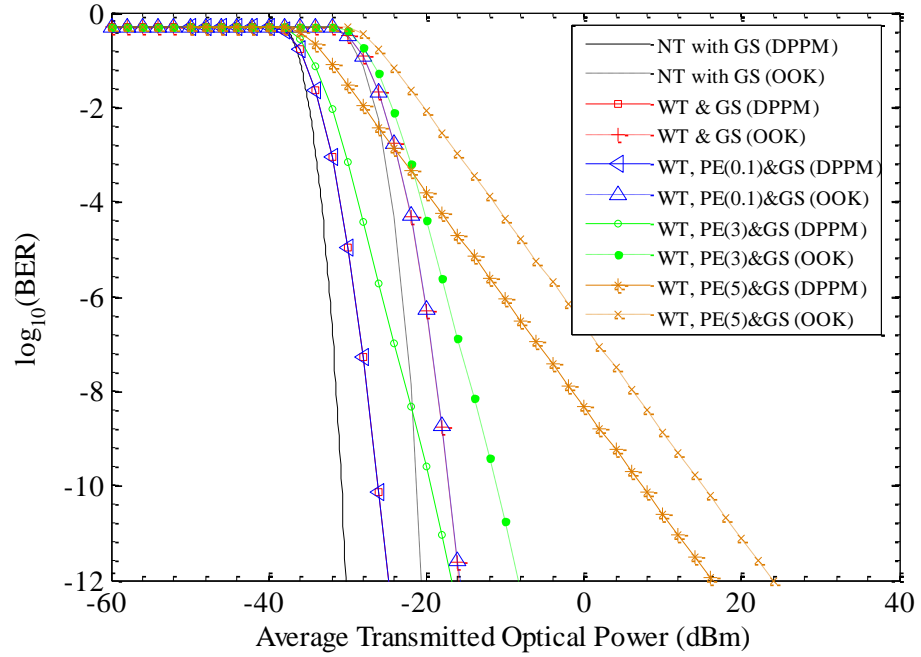
In the MT case (Figure 7.3), an improvement in required optical power of approximately 14 dB (MT with GS case) and 22 dB ($\sigma_{PE}/r_{RX} = 3$) and 2 dB ($\sigma_{PE}/r_{RX} = 5$) for both modulation formats, at target BER of 10^{-9} was seen for increasing D_{RX} from 25 to 50 mm. Finally in the ST case (Figure 7.4), an improvement in required optical power of approximately 14 dB (ST with GS case) and 22 dB (for $\sigma_{PE}/r_{RX} = 3$) and 2 dB (for $\sigma_{PE}/r_{RX} = 5$) (ST, PE and GS case) for both modulation formats, at target BER of 10^{-9} was seen for increasing D_{RX} from 25 to 50 mm. In Figures 7.2, 7.3 & 7.4, the BER for both modulation formats (WT, MT and ST with GS cases) at $\sigma_{PE}/r_{RX} = 0.1$ are all seen to be similar to the turbulence plus GS only cases. This happens since the PE contribution would be relatively small at this value and the use of AA helps to reduce the PE and turbulence effect. Thus the $\sigma_{PE}/r_{RX} = 0.1$ can be approximated as a turbulence only case. Further, note that the effects of $\sigma_{PE}/r_{RX} = 0.1$ can be more significant for the point receiver case shown (without optical amplification) in [5].

The similarity between the MT and ST BERs (seen in Figures 7.3 & 7.4) can be traced to the leveling effect [22, 27] which happens when the receiver diameter (e.g. 25 mm) used falls between the values for the plane-wave spatial coherence radius ρ_0 (which is calculated as 8.2 mm for $l=1500\text{m}$ and $C_n^2 = 8.3 \times 10^{-14} \text{ m}^{-2/3}$) and the scattering disk $z/k\rho_0$ (which is calculated as 45 mm for $l=1500\text{m}$ and $C_n^2 = 8.3 \times 10^{-14} \text{ m}^{-2/3}$). When the diameter lies outside this range, but close to it, (e.g. 50 mm) the effect is still present to some extent.

It can be deduced from the plots (Figures 7.2-7.4) that the DPPM technique is capable of providing better performance when compared to the OOK-NRZ technique. From the results shown, at $M = 5$, $\sigma_{PE}/r_{RX} = 3$ and $D_{RX} = 50 \text{ mm}$ ($w_z/r_{RX} = 15$), a required optical power advantage of about 9 dB (NT with GS), 8 dB (WT, PE and GS), 7 dB (MT, PE and GS), and 7 dB (WT, PE and GS), respectively, were achieved over a comparable OOK-NRZ system. On increasing the normalized beam width value to 30 (reducing D_{RX} to 25mm), similar required optical power advantage were observed for the whole range of turbulence, PE and GS cases considered. Finally, it can be seen from Figures 7.2-7.4, that on increasing the normalized PE standard deviation from 3 to 5, an additional power penalty of less than 2 dB (for $D_{RX} = 25 \text{ mm}$ ($w_z/r_{RX} = 30$)), respectively, were observed for WT, MT and ST, all including PE and GS, whilst about 20 dB (WT), 18 dB (MT) and 14 dB (ST), all including PE and GS, were observed for $D_{RX} = 50 \text{ mm}$ ($w_z/r_{RX} = 15$), in both modulation formats.



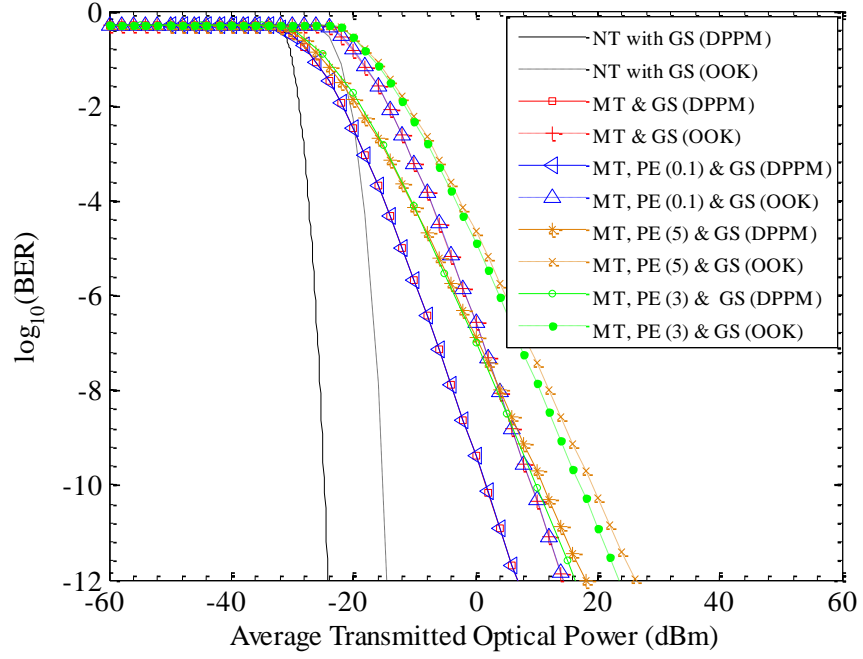
(a)



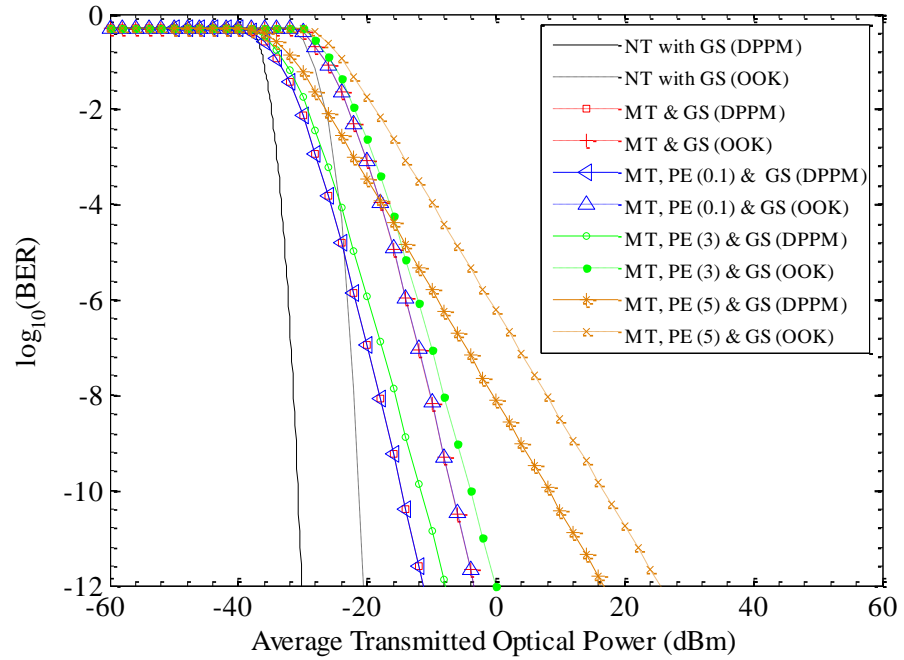
(b)

Figure 7.2 MCB BER as a function of average transmitted optical power (dBm) for normalized PE standard deviation $\sigma_{PE}/r_{RX} = 0.1, 3$ & 5 , $M = 5$, $G = 30$ dB for NT with GS, WT only (with GS, no PE) and combined WT, PE and GS (a) $D_{RX} = 25$ mm ($w_z/r_{RX} = 30$) (b) $D_{RX} = 50$ mm ($w_z/r_{RX} =$

15)



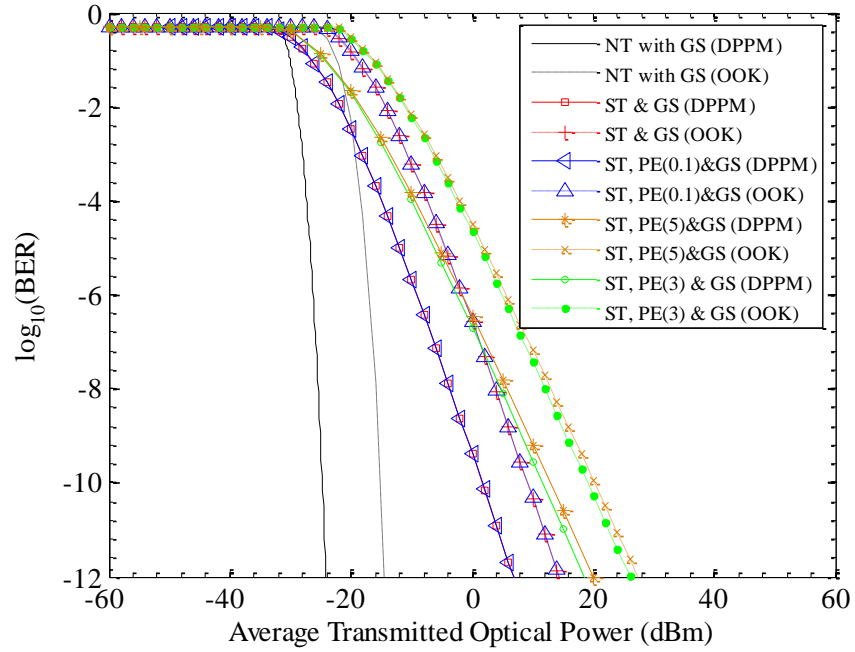
(a)



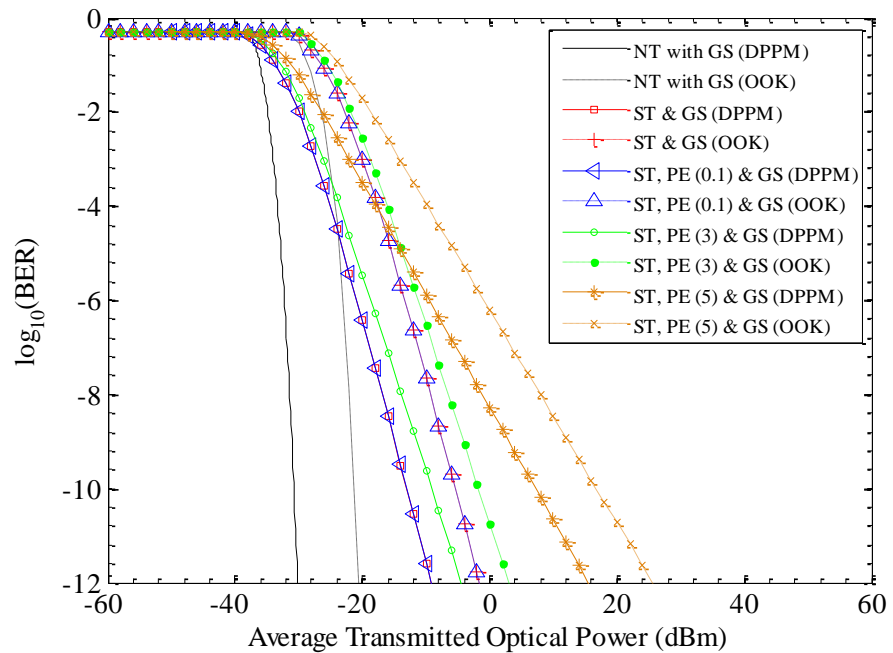
(b)

Figure 7.3 MCB BER as a function of average transmitted optical power (dBm) for normalized PE standard deviation $\sigma_{PE}/r_{RX} = 0.1, 3 \text{ \& } 5$, $M = 5$, $G = 30\text{dB}$ for NT with GS, MT only (with GS, no PE) and combined MT, PE and GS (a) $D_{RX} = 25 \text{ mm}$ ($w_z/r_{RX} = 30$) (b) $D_{RX} = 50 \text{ mm}$ ($w_z/r_{RX} =$

15)



(a)



(b)

Figure 7.4 MCB BER as a function of average transmitted optical power (dBm) for normalized PE standard deviation $\sigma_{PE}/r_{RX} = 0.1, 3$ & $5, M = 5, G = 30$ dB for NT with GS, ST only (with GS, no PE) and combined ST, PE and GS (a) $D_{RX} = 25$ mm ($w_z/r_{RX} = 30$) (b) $D_{RX} = 50$ mm ($w_z/r_{RX} = 15$)

Figures 7.5-7.7 shows the required optical power (dBm) at BER of 10^{-9} as a function of the DPPM coding level ($M = 1-5$) for NT with GS, WT

(only) with GS, and WT, PE and GS (Figure 7.5); NT with GS, MT (only) with GS, and MT, PE and GS (Figure 7.6); and NT with GS, ST (only) with GS, and ST, PE and GS (Figure 7.7); for optical gain $G = 30$ dB, normalized PE variance $\sigma_{PE}/r_{RX} = 3$ & 5 and $D_{RX} = 50$ mm ($w_z/r_{RX} = 15$), with the OOK-NRZ required optical powers for comparison. It can be seen that as the DPPM coding level increases, the required optical power decreases. However, a DPPM FSO system with coding level of 5 seems to be a sensible approach practically as coding levels greater than 5 do not improve the required transmitting power very significantly, but they do rather imply greater complexity in receiver design [18]. Furthermore, the coding level is restricted by the limitation on the slot rate placed by the optical filter bandwidth.

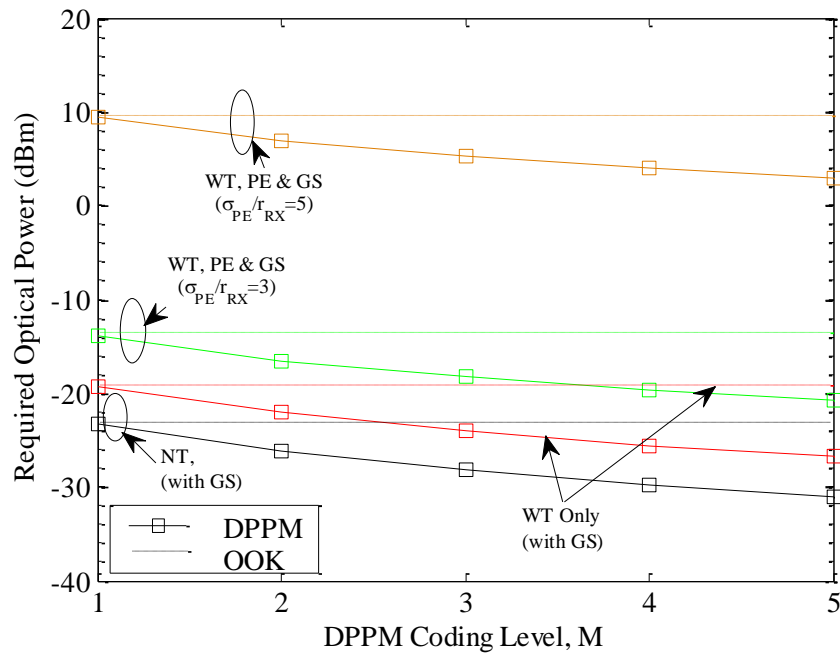


Figure 7.5 Required optical power (dBm) at MCB BER of 10^{-9} as a function of the DPPM coding level ($M = 1-5$) for NT with GS, WT only with GS, and combined WT, PE and GS using $\sigma_{PE}/r_{RX} = 3$ & 5, and $D_{RX} = 50$ mm ($w_z/r_{RX} = 15$). Also shown are the corresponding powers for OOK-NRZ

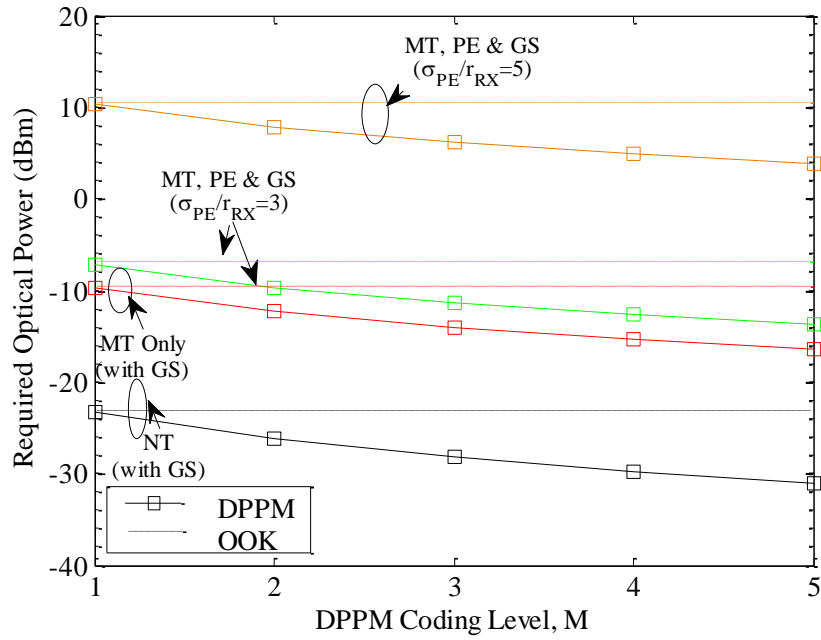


Figure 7.6 Required optical power (dBm) at MCB BER of 10^{-9} as a function of the DPPM coding level ($M = 1-5$) for NT with GS, MT only with GS, and combined MT, PE and GS using $\sigma_{PE}/r_{RX} = 3$ & 5, and $D_{RX} = 50$ mm ($w_z/r_{RX} = 15$). Also shown are the corresponding powers for OOK-NRZ

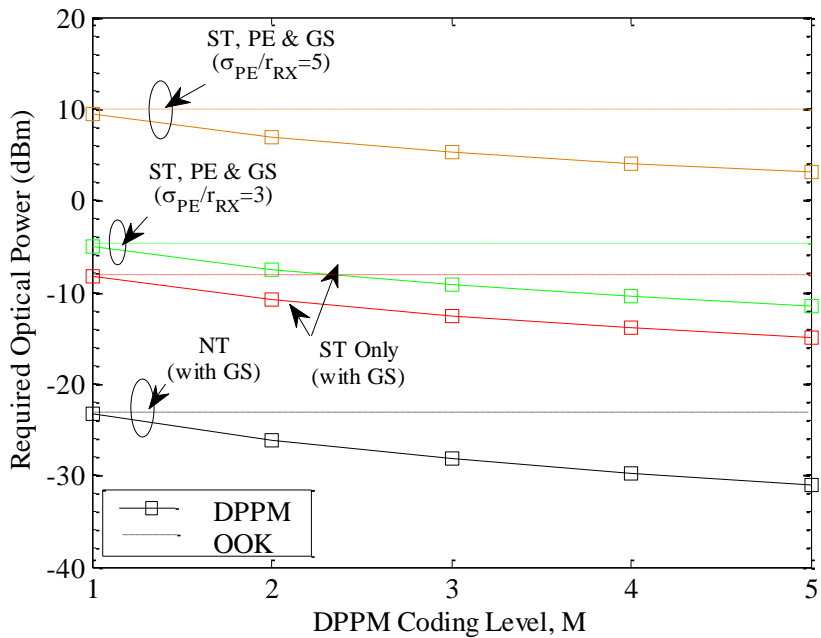


Figure 7.7 Required optical power (dBm) at MCB BER of 10^{-9} as a function of the DPPM coding level ($M = 1-5$) for NT with GS, ST only with GS, and combined ST, PE and GS using $\sigma_{PE}/r_{RX} = 3$ & 5, and $D_{RX} = 50$ mm ($w_z/r_{RX} = 15$). Also shown are the corresponding powers for OOK-NRZ

Figures 7.8-7.10 shows the DPPM and OOK BER as a function of average transmitted optical power (dBm) for SPA and MCB using $\sigma_{PE}/r_{RX} = 3$, DPPM coding level $M = 5$, $G = 30$ dB, $D_{RX} = 25$ mm ($w_z/r_{RX} = 30$), for NT with GS, turbulence only with GS (no PE) i.e. WT (Figure 7.8), MT (Figure 7.9), and ST (Figure 7.10), and combined turbulence, PE and GS. In the NT case (shown in Figures 7.8, 7.9, & 7.10), the SPA BER is seen to be slightly lower than the MCB BER, about 1 dB less than the MCB at target BER. In the WT and PE (Figure 7.8), MT and PE (Figure 7.9), and ST and PE (Figure 7.10) cases, the MCB-SPA BER curve separation increases (at target BER, about 1 dB more than what was seen in the NT case) as the turbulence strength increases. Nonetheless, from the MCB-SPA comparison performed in the analysis, it cannot be said necessarily that the SPA is more accurate than the MCB (which has the advantage of being an upper bound and computationally quicker (as in NT [10, 12])) but overall both methods are seen to give BERs in reasonable agreement for the range of turbulence and PE conditions considered.

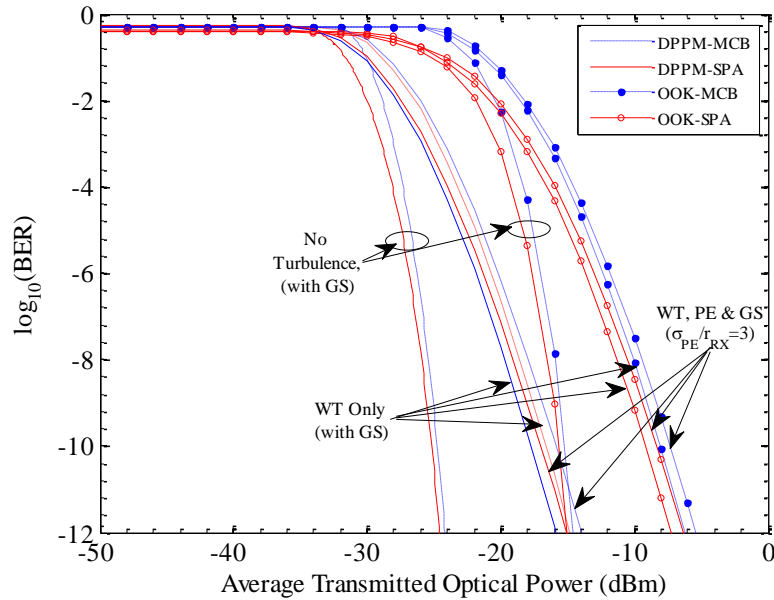


Figure 7.8 DPPM and OOK BER as a function of average transmitted optical power (dBm) for normalized PE standard deviation $\sigma_{PE}/r_{RX} = 3$, $M = 5$, $G = 30$ dB, $D_{RX} = 25$ mm ($w_z/r_{RX} = 30$) for NT with GS, WT only (with GS, no PE) and combined WT, PE and GS, using SPA and MCB

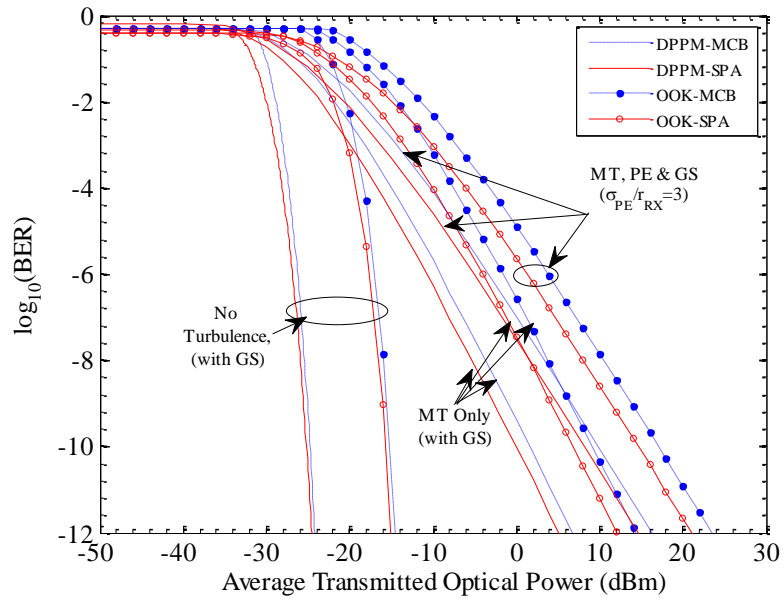


Figure 7.9 DPPM and OOK BER as a function of average transmitted optical power (dBm) for normalized PE standard deviation $\sigma_{PE}/r_{RX} = 3$, $M = 5$, $G = 30$ dB, $D_{RX} = 25$ mm ($w_z/r_{RX} = 30$) for NT with GS, MT only (with GS, no PE) and combined MT, PE and GS, using SPA and MCB

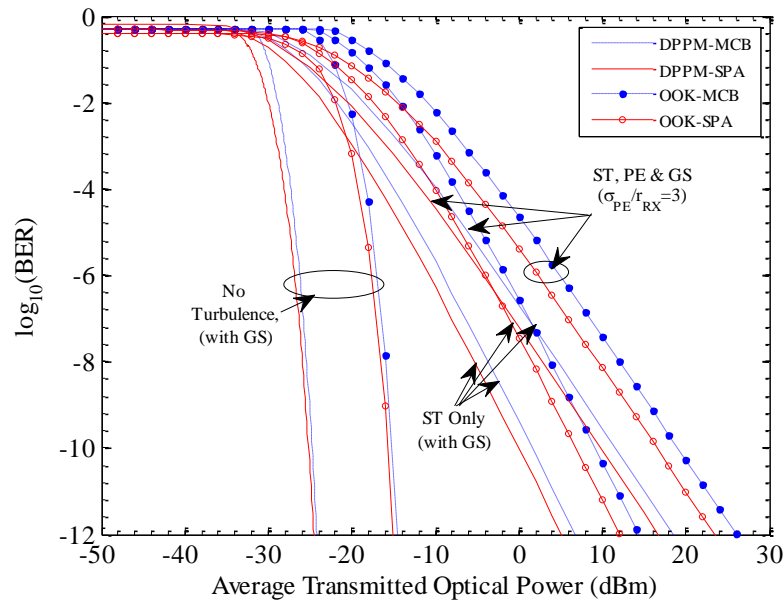
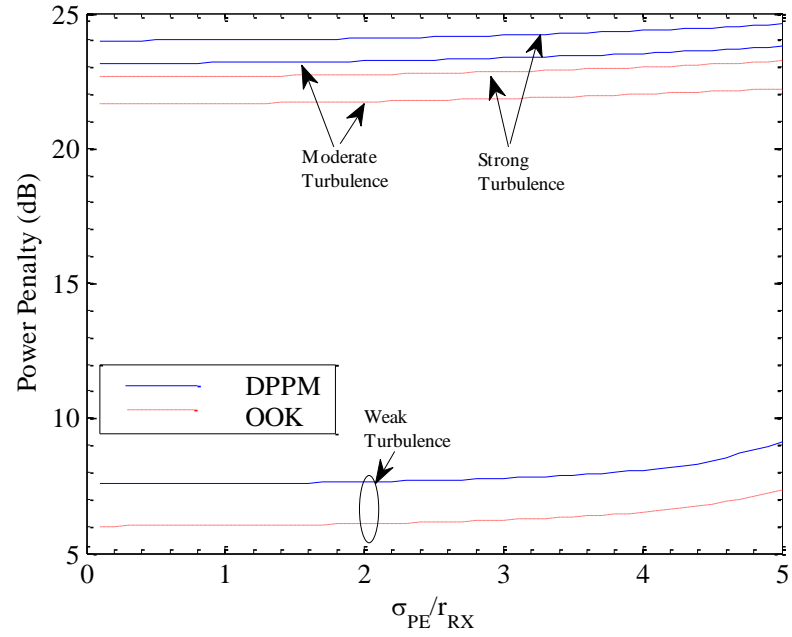
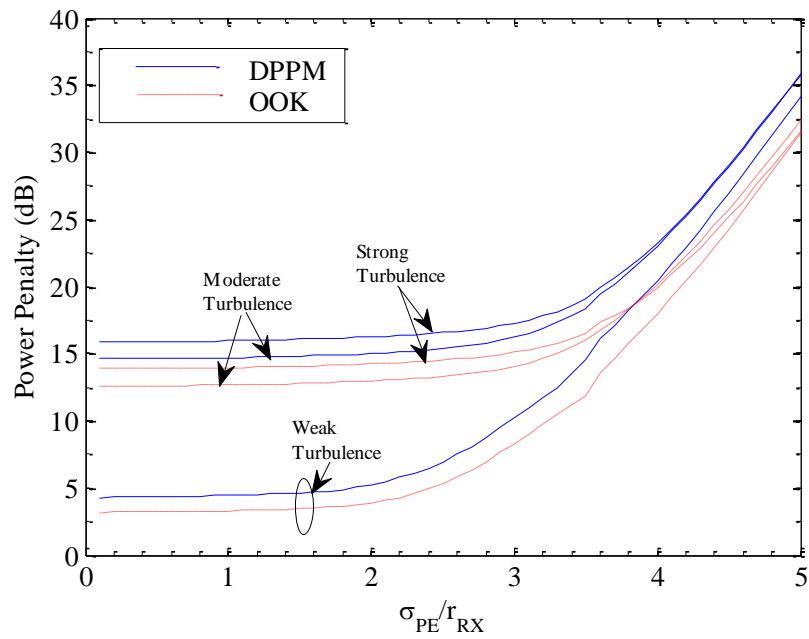


Figure 7.10 DPPM and OOK BER as a function of average transmitted optical power (dBm) for normalized PE standard deviation $\sigma_{PE}/r_{RX} = 3$, $M = 5$, $G = 30$ dB, $D_{RX} = 25$ mm ($w_z/r_{RX} = 30$) for NT with GS, ST only (with GS, no PE) and combined ST, PE and GS, using SPA and MCB

Figure 7.11 shows the power penalty (dB) (relative to NT with GS) as a function of the normalised PE standard deviation σ_{PE}/r_{RX} using $M = 5$, $G = 30$ dB for WT, MT and ST (all with GS) for $D_{RX} = 25$ mm (which translates to about $w_z/r_{RX} = 30$) (Figure 7.11a) and $D_{RX} = 50$ mm (which translates to about $w_z/r_{RX} = 15$) (Figure 7.11b). In the case of $D_{RX} = 25$ mm ($w_z/r_{RX} = 30$) (Figure 7.11a), on increasing σ_{PE}/r_{RX} , very small changes in power penalty are observed for $\sigma_{PE}/r_{RX} < 3$, while the MT and ST have almost the same values for both the DPPM and OOK cases. The similarity in the MT and ST cases can be linked to the levelling effect which has been explained earlier. In the case of $D_{RX} = 50$ mm ($w_z/r_{RX} = 15$) (Figure 7.11b), an increase in the power penalty becomes obvious as σ_{PE}/r_{RX} becomes greater than 2.5. Moreover, the power penalties give similar values as σ_{PE}/r_{RX} approaches 5. The closeness of the MT and ST power penalties can also be linked to the levelling effect. Overall, it can be seen that the PE effects are more severe in the WT cases for reasons discussed earlier regarding Figure 7.2.



(a)



(b)

Figure 7.11 Power penalty (dB) (relative to NT with GS) as a function of normalized PE standard deviation σ_{PE}/r_{RX} using $M = 5$ (DPPM only), $G = 30\text{dB}$ for WT, MT and ST (all with GS) (a) $D_{RX} = 25\text{ mm}$ ($w_z/r_{RX} = 30$) (b) $D_{RX} = 50\text{ mm}$ ($w_z/r_{RX} = 15$)

7.4 Summary

An optically preamplified FSO communication system employing DPPM and OOK-NRZ schemes have been analysed using the MCB and SPA method for combined turbulence and PE. It can be seen that the combined impairments introduce severe effects on the performance of the FSO system. These results will be helpful for designing FSO communication systems that experience the above mentioned conditions. The DPPM scheme represent a promising means of further enhancing the FSO power efficiency with an improvement over OOK-NRZ as high as 8 dB achievable in weak turbulence plus the PE and GS conditions. The SPA method is seen to give slightly more optimistic BERs than the MCB, though still with a good level of agreement, but if speed is the main issue, then MCB would be a better option. Finally, it can be confirmed that the system BER and penalty depends, amongst other factors, on the size of the receiver optics and the beams jitter standard deviation.

7.5 References

- [1] S. Arnon, "Optimization of urban optical wireless communication systems," *IEEE Transactions on Wireless Communications*, vol. 2, no. 4, pp. 626-629, July 2003.
- [2] D. K. Borah and D. G. Voelz, "Pointing error effects on free-space optical communication links in the presence of atmospheric turbulence," *Journal of Lightwave Technology*, vol. 27, no. 18, pp. 3965-3973, Sept. 2009.
- [3] A. A. Farid and S. Hranilovic, "Outage capacity optimization for free-space optical links with pointing errors," *Journal of Lightwave Technology*, vol. 25, no. 7, pp. 1702-1710, July 2007.
- [4] W. Gappmair, S. Hranilovic, and E. Leitgeb, "Performance of PPM on terrestrial FSO links with turbulence and pointing errors," *IEEE Communications Letters*, vol. 14, no. 5, pp. 468-470, May 2010.
- [5] H. G. Sandalidis, T. A. Tsiftsis, G. K. Karagiannidis, and M. Uysal, "BER performance of FSO links over strong atmospheric turbulence channels with pointing errors," *IEEE Communications Letters*, vol. 12, no. 1, pp. 44-46, Jan. 2008.
- [6] L. C. Andrews and R. L. Phillips, "Pointing errors and fade statistics associated with a laser satellite-communication system," *Proc. of SPIE, Optics in Atmospheric Propagation, Adaptive Systems, and Lidar Techniques for Remote Sensing, Taormina, Italy*, vol. 2956, pp. 166-177, Jan. 1997.

- [7] Q. L. Cao, M. Brandt-Pearce, and S. G. Wilson, "Free space optical MIMO system using PPM modulation and a single optical amplifier," *Second International Conference in Communications and Networking in China*, vol. 1, pp. 1113-1117, Aug. 2007.
- [8] M. Razavi and J. H. Shapiro, "Wireless optical communications via diversity reception and optical preamplification," *IEEE Transactions on Wireless Communications*, vol. 4, no. 3, pp. 975-983, May 2005.
- [9] X. Zhu and J. M. Kahn, "Free-space optical communication through atmospheric turbulence channels," *IEEE Transactions on Communications*, vol. 50, no. 8, pp. 1293-1300, Aug. 2002.
- [10] L. F. B. Ribeiro, J. R. F. Da Rocha, and J. L. Pinto, "Performance evaluation of EDFA preamplified receivers taking into account intersymbol interference," *Journal of Lightwave Technology*, vol. 13, no. 2, pp. 225-232, Feb. 1995
- [11] K. W. Cattermole and J. J. O'Reilly, *Mathematical topics in telecommunications volume 2: problems of randomness in communication engineering*, Pentech Press Limited, Plymouth, 1984.
- [12] I. T. Monroy and E. Tangdiongga, *Crosstalk in WDM communication networks*, Kluwer Academic Publishers, Norwell, Massachusetts, USA, 2002.
- [13] J. O'Reilly and J. R. F. Da Rocha, "Improved error probability evaluation methods for direct detection optical communication systems," *IEEE Transactions on Information Theory*, vol. 33, no. 6, pp. 839-848, Nov. 1987
- [14] A. O. Aladeloba, A. J. Phillips, and M. S. Woolfson, "Improved bit error rate evaluation for optically pre-amplified free-space optical communication systems in turbulent atmosphere," *IET Optoelectronics*, vol. 6, no. 1, pp. 26-33, Feb. 2012.
- [15] A. O. Aladeloba, A. J. Phillips, and M. S. Woolfson, "Performance evaluation of optically preamplified digital pulse position modulation turbulent free-space optical communication systems," *IET Optoelectronics*, vol. 6, pp. 66-74, no. 1, Feb. 2012.
- [16] A. O. Aladeloba, A. J. Phillips, and M. S. Woolfson, "DPPM FSO communication systems impaired by turbulence, pointing error and ASE noise," *International Conference on Transparent Optical Networks*, July 2012.
- [17] D. O. Caplan, "Laser communication transmitter and receiver design," *Journal of Optical Fibre Communication Report*, vol. 4, no. 4, pp. 225-362, 2007.
- [18] A. K. Majumdar, "Free-space laser communication performance in the atmospheric channel," *Journal of Optical and Fiber Communications Research*, vol. 2, no. 4, pp. 345-396, 2005.
- [19] A. J. Phillips, R. A. Cryan, and J. M. Senior, "An optically preamplified intersatellite PPM receiver employing maximum likelihood detection," *IEEE Photonic Technology Letter*, vol. 8, no. 5, pp. 691-693, May 1996.
- [20] M. Abtahi, P. Lemieux, W. Mathlouthi, and L. A. Rusch, "Suppression of turbulence-induced scintillation in free-space optical communication systems using saturated optical amplifiers,"

- Journal of Lightwave Technology*, vol. 24, no. 12, pp. 4966-4973, Dec. 2006.
- [21] C. Chen, H. Yang, H. Jiang, J. Fan, C. Han, and Y. Ding, "Mitigation of Turbulence-Induced Scintillation Noise in Free-Space Optical Communication Links Using Kalman Filter," *IEEE Congress on Image and Signal Processing, Hainan, China*, vol. 5, pp. 470-473, May 2008.
- [22] L. C. Andrews and R. L. Phillips, *Laser beam propagation through random media*, Second Edition, SPIE Press, Bellingham, Washington, 2005.
- [23] S. Karp, R. M. Gagliardi, S. E. Moran, and L. B. Stotts, *Optical channels: fibers, clouds, water and the atmosphere*, New York: Plenum Press, 1988.
- [24] M. A. Al-Habash, L. C. Andrews, and R. L. Phillips, "Mathematical model for the irradiance probability density function of a laser beam propagating through turbulent media," *Opt. Eng.*, vol. 40, no. 8, pp. 1554-1562, Aug. 2001.
- [25] W. O. Popoola and Z. Ghassemlooy, "BPSK subcarrier intensity modulated free-space optical communications in atmospheric turbulence," *Journal of Lightwave Technology*, vol. 27, no. 8, pp. 967-973, Apr. 2009.
- [26] L. C. Andrews, R. L. Phillips, C. Y. Hopen, and M. A. Al-Habash, "Theory of optical scintillation," *J. Opt. Soc. Am. A*, vol. 16, no. 6, pp. 1417-1429, June 1999.
- [27] M. A. Khalighi, N. Schwartz, N. Aitamer, and S. Bourennane, "Fading reduction by aperture averaging and spatial diversity in optical wireless systems," *Journal of Optical Communications and Networking, IEEE/OSA* vol. 1, no. 6, pp. 580-593, Nov. 2009.
- [28] F. S. Vetelino, C. Young, L. Andrews, and J. Rekolons, "Aperture averaging effects on the probability density of irradiance fluctuations in moderate-to-strong turbulence," *Applied Optics*, vol. 46, no. 11, pp. 2099-2108, Apr. 2009.
- [29] X. M. Zhu and J. M. Kahn, "Communication techniques and coding for atmospheric turbulence channels," *Journal of Optical and Fiber Communications Reports*, vol. 4, no. 6, pp. 363-405, 2007.
- [30] N. S. Kopeika and A. Zilberman, "Vertical profiles of aerosol and optical turbulence strength and their effects on atmospheric propagation," *Proc. of SPIE*, San Jose, CA, USA, vol. 3927, pp. 460-467, Jan. 2000.
- [31] H. J. Eom, G. Y. Hur, T. J. Park, and S. Kozaki, "Gaussian beam scattering from a semicircular boss above a conducting plane," *IEEE Transaction on Antennas and Propagation*, vol. 41, no. 1, pp. 106-108, Jan. 1993.
- [32] W. Gappmair and S. S. Muhammad, "Error performance of terrestrial FSO links modelled as PPM/Poisson channels in turbulent atmosphere," *Electronics Letters*, vol. 43, no. 5, pp. 302-304, Mar. 2007.
- [33] R. Ma, T. J. Zuo, S. Sujecki, and A. J. Phillips, "Improved performance evaluation for DC-coupled burst mode reception in the

- presence of amplified spontaneous emission noise and interchannel crosstalk," *Optoelectronics, IET*, vol. 4, no. 3, pp. 121-132, 2010.
- [34] M. J. Sibley, *Optical communications*, Second Edition, Macmillian Press Limited, London, 1995.

CHAPTER 8 WDM FSO network impaired by ASE noise and turbulence-accentuated interchannel crosstalk

8.1 Introduction

Over the years, there has been an exponential rise in the demand for broadband applications and services [1, 2]. Optical carrier technologies can be a good solution for the access networks since they potentially offer huge bandwidth [2-6]. Passive optical networks (PONs) are the main contenders for optical access networks (i.e. the last mile connection between individual homes and businesses and the public network) and have gradually replaced the copper-based access network technologies. Optical fibre has many advantages (low cost, no electromagnetic interference problems, and less power loss) over the incumbent copper systems [7, 8]. The roll-out of fibre in the access network has been reported in Japan and South East Asia. European telecom operators however are gradually shifting focus from the use of the installed copper twisted pair (using ADSL/VDSL) to gigabit-capable G-PON systems [9].

At the moment, time division multiplexing (TDM/TDMA) systems are the most popular architecture for PONs although they are only suitable for a limited number of optical network units (ONUs) (unless augmented by optical amplification [9]) and they typically use power splitters. Wavelength division multiplexing (WDM) systems, on the other hand, allow more ONUs to be connected at high data rates and assign a distinct pair of dedicated wavelengths to each ONU such that a point-to-point connection is established between the ONU and the optical line terminator (OLT) [1]. Major drivers for the WDM PON are the potential increase in the bandwidth and the greater data security that can be offered to the ONUs compared to the TDM/TDMA system [1, 2, 10-12]. While the WDM system is technically interesting, the major challenge for its commercialisation is the higher cost of the equipment (for example arrayed waveguide grating (AWG)-based multiplexer (mux)/de-multiplexer

(demux) and wavelength specific sources) compared to the TDM/TDMA system which uses power splitters and low-cost sources [1, 10, 11].

Free-space optical (FSO) communications simply entails transmission of the optical signal through the earth's atmosphere and its subsequent reception. FSO communications has been successfully applied for short distance links (up to 4 km [5]). Relative to fibre systems, FSO communications has the advantage of ease of set-up and teardown, provision of access in difficult locations, and relatively lower cost (i.e. no purchasing and installing of fibre, especially if it otherwise had to go underground) [13-16]. FSO communication-based access networks have competitive advantages over RF (or millimetre-wave) systems such as improved security, no spectrum licensing and the faster speed over the short-haul access [4, 5]. Despite the advantages of FSO communications, it is faced by considerable challenges such as the effects of atmospheric attenuation and turbulence-induced scintillation, which have severe effects on the propagating field [4, 5, 7, 14, 17, 18]. A WDM access network using FSO communications in the distribution link is a realistic proposition since both optical fibre and FSO systems operate using similar optical transmission wavelengths and system components [7, 10, 17, 19]. Therefore, the integration of both technologies may yield a cost effective and reliable hybrid optical access network solution.

For long propagation distances, the use of optical amplifiers becomes necessary. However, the optically amplified signal is accompanied by ASE noise which somewhat offsets the performance benefits of the amplifier and complicates performance calculations [20-22]. The use of optical amplifiers for extending the maximum reach and/or split in optical access networks (SuperPONs) was investigated in the 1990s [23] whilst long-range PONs, which incorporate WDM, are under investigation [9].

The presence of interchannel crosstalk in WDM systems is well reported [8, 24], however, it will be seen that the turbulent nature of the atmospheric channel in the distribution link of the hybrid optical access network causes a fluctuating interchannel crosstalk effect that significantly exacerbates its negative impact on performance. Experimental work has been reported in [10, 25, 26] that demonstrates the performance of WDM-FSO networks

such as FSO communications between two tall building rooftops separated by link length of up to 210 m [10], in-building test bed FSO communications using a climatic chamber to simulate a whole range of turbulence conditions [25], and indoor-based WDM FSO communication with link length of 2.43 m [26], with their results revealing the feasibility of hybrid optical network. The effect of interchannel crosstalk has been investigated in [27] for an all-fibre hybrid TDM/WDM-PON with burst-mode reception at the OLT. The influence of turbulence-accentuated interchannel crosstalk on system performance has not been addressed previously and is thus here the main focus. The work in this chapter has been published in the Journal of Optical Communications and Networking.

8.2 System design and description

Typically, a WDM PON connects a multi-wavelength OLT to ONUs, which might be located in homes, in buildings, or at the kerb, over an interconnecting fibre system. Figure 8.1 shows the proposed WDM PON using FSO communications instead of the conventional optical fibre as distribution link. In WDM networks, the suboptimal performance of the remote node (which comprises of the mux/demux and transmitting lenses) in the downstream transmission and the imperfection of the OLT demux in the upstream transmission leads to the reception of optical signals of undesired wavelengths. This type of crosstalk is called interchannel crosstalk and it acts as a noise field at the receiver photodetector. The interchannel crosstalk effect is potentially more severe in the upstream transmission as it may be exacerbated by turbulence while in the downstream transmission the ONUs can typically be arranged so as to prevent the introduction of further crosstalk at the ONU photodiode (or an optical bandpass filter could optionally be placed before the ONU photodiode to further limit the crosstalk effect). It should also be mentioned that intrachannel crosstalk can exist in principle (in the upstream) if the diffraction and turbulence-induced spreading of the laser beam along the propagation path leads to a fraction of the transmit power falling within the field of view of an unintended collecting lens. However this is neglected

here as it can generally be avoided by ensuring that ONUs are not lined up to have near identical transmission paths.

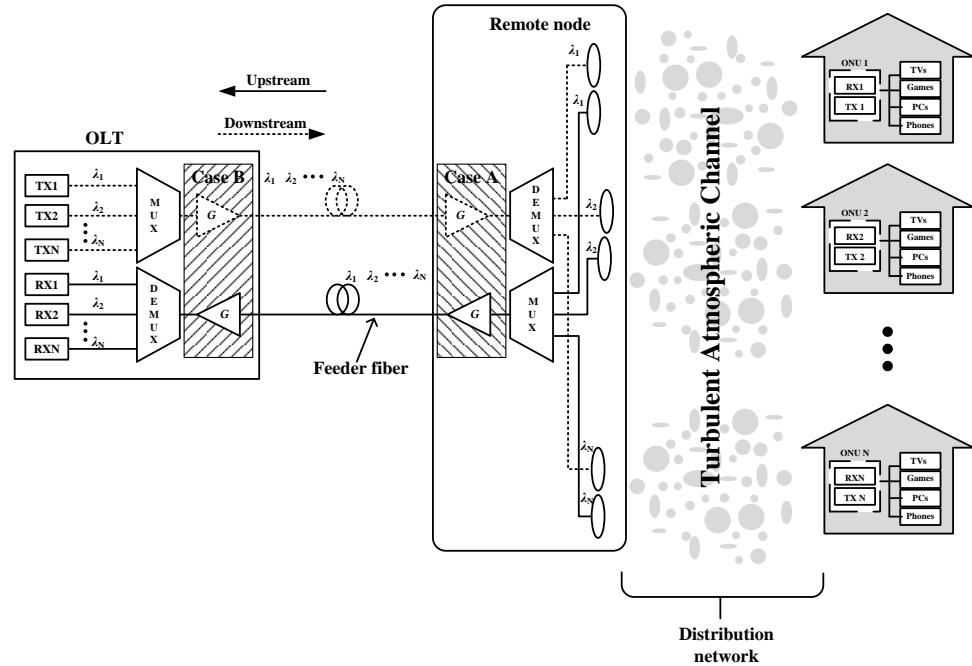


Figure 8.1: Schematic representation of a WDM network using FSO link for the final distribution stage, with optical amplifier located at remote node (case A) or at OLT demux input (case B). ONUs will be distributed at different angles around the remote node.

8.2.1 Upstream transmission

In the upstream, each ONU gets a dedicated and independent point-to-point optical link to the OLT. A laser, which is set at a predetermined wavelength, is used as optical source for each transmitter. The distribution network (atmospheric channel) conveys the upstream optical signals from the ONUs to a mux which combines the input signals and transmits them through a single optical feeder fibre to the OLT. At the destination, the demux separates the multi-wavelength optical signals into constituent wavelengths. Several WDM mux/demux technologies exist in the market although each technology has its own advantages in terms of cost, performance, technical complexity and reliability. The AWG-based mux/demux devices are very popular mainly because of their low chromatic

dispersion loss, however, the complexity and cost of production as well as the temperature-dependent loss variations are the main drawbacks for the device [1, 8]. The free-space diffraction grating has been proven to be a more promising technology for overcoming the drawbacks encountered in AWG-based and other older mux/demux devices [28]. For performance calculations it is assumed to have signal mux/demux loss L_{mux} and L_{demux} (≤ 3.5 dB), adjacent channel additional loss $L_{demux,adj}$ (typically > 30 dB) and non-adjacent channel additional loss $L_{demux,nonadj}$ (typically > 35 dB) [1, 2, 28]. The optical wavelengths are assumed to be in the C band (i.e. around 1550 nm) with channel spacing of 100 GHz [2] on the ITU-T grid. This wavelength choice exploits low atmospheric (and fibre) attenuation due to absorption within the wavelength band, and the suitability for EDFAs and high quality transmitters and receivers [3, 8, 22]. The ONU transmitters each transmit optical signals (on wavelengths $\lambda_1, \lambda_2, \dots, \lambda_N$, N is number of ONUs connected to the network) towards corresponding receiver collecting lens (RCL) of diameter D_{RX} at the remote node. For the sake of definiteness, the ONU transmit power is treated as not exceeding 20 dBm, which falls within the maximum possible value according to laser skin and eye safety regulations [29-31]. The FSO system transmitted power values typically exceed conventional ONU transmit powers both since the atmospheric channel is highly attenuating and as it does not suffer from the non-linear effects that occur in optical fibre. The optical beam spreads out due to diffraction effects and wave front distortion in the optical wave induced by atmospheric turbulence [32], as it approaches the RCL with beam pattern characterized by its transmit divergence angle θ .

Each RCL, located at the remote node, collects the corresponding incident optical signal and then couples it through a short length of fibre (using a fibre collimator as per [20]) to the mux. An optical preamplifier of gain G and noise figure NF can be placed either at the remote node output to effectively increase the transmitted power through the feeder fibre or at the demux input to help increase the effective OLT receiver sensitivity. A PIN photodiode with quantum efficiency η is placed after the

demux to convert the information-bearing light into an electrical signal. This electrical signal is then electrically preamplified and filtered before being passed to the decision device where the threshold is applied. The process of photodetection can be described as a square law detection in which the signal beats with ASE noise, causing signal-ASE beat noise, and also the ASE beats with itself causing ASE-ASE beat noise. An integrate-and-dump receiver is assumed at the decision circuit with electrical bandwidth $B_e = 1/2T_b$, where $T_b = 1/R_b$ and R_b is the data rate. The bit is sampled and then compared with threshold. For the OOK-NRZ assumed here, the Kalman filtering method [33] represents a realistic adaptive approach of achieving near optimal threshold for each instantaneous level, and such an optimal threshold (however obtained) is assumed here.

8.2.2 Downstream transmission

In the downstream transmission, there exists N separate laser transmitters at the OLT and they transmit signals belonging to each ONU on a particular wavelength in a point-to-point fashion. In the downstream performance calculation, the same assumptions as in the upstream transmission are made, for the optical wavelengths, channel spacing and the use of an appropriate method to achieve optimal threshold in the OOK scheme, whilst maximum OLT transmit powers are lower (typically 10 dBm [2]) because an optical amplifier (such as an EDFA) is placed at the remote node to minimize damaging fibre non-linearity (versus placing at the OLT). The fibre-to-air loss at the remote node is neglected in the analysis. The difference between the upstream and downstream losses is the air-to-fibre coupling loss which is present in the upstream while in the downstream there is an assumption of no fibre at ONU. There will be downstream interchannel crosstalk due to the imperfection of the remote node demux. This crosstalk is however not accentuated by the atmospheric turbulence, since the crosstalk occurs before reaching the distribution link and thus experiences essentially the same atmospheric link turbulence behaviour as the signal.

8.2.3 Optical amplifier placement

In both the upstream and downstream transmissions, the impact of the optical amplifier location is been considered for two cases. Case A is when the optical amplifier is placed at the remote node and Case B is when the optical amplifier is placed at the OLT.

In the upstream Case A, the ASE noise experiences loss due to feeder fibre attenuation and OLT demux loss, while in the upstream Case B, the ASE noise suffers from OLT demux loss only. In some cases the location of the upstream optical amplifier may not make much difference to the performance considering that the OSNR differs by only about 4 dB between Case A and Case B (for 20 km fibre), which is not particularly significant when OSNR is good. Therefore, the upstream amplifier location choice may mainly depend on practical issues such as the availability of powering, at the remote node, which in turn depends on the powering of the pointing and tracking system, if needed.

In the downstream Case A, the ASE noise suffers remote node demux loss, atmospheric attenuation, and beam spreading loss, while in the downstream Case B, the ASE noise additionally experiences feeder fibre attenuation. Similar issues to the upstream exist regarding amplifier placement but with the additional need not to launch too much power into the fibre in the downstream Case B due to non-linearity issues.

8.3 Turbulence modelling

Atmospheric scintillation happens as a result of thermally-induced changes in the refractive index of the air along the optical link, which in turn causes rapid fluctuation of the optical signal at the receiver, reduction in the degree of coherence of the optical signal [34], and potentially poor bit error rate (BER) FSO performance. The Gamma-Gamma (GG) distribution model is widely used for characterising the whole range of turbulence effects, i.e. weak, moderate and strong, not only because closed form expressions exist but also because of their direct dependence on turbulence parameters and the closeness of results obtained with experimental data [14,

17, 35, 36]. The GG probability density function (pdf) is given as [14, 17, 35, 36]

$$p_{GG}(h_{turb}) = \frac{2(\alpha\beta)^{(\alpha+\beta)/2}}{\Gamma(\alpha)\Gamma(\beta)} h_{turb}^{(\alpha+\beta)/2-1} K_{\alpha-\beta}(2\sqrt{\alpha\beta h_{turb}}); \quad h_{turb} > 0 \quad (8.1)$$

where h_{turb} is the attenuation due to atmospheric turbulence, α is the effective number of large-scale eddies of the scattering process, β is the effective number of small-scale eddies of the scattering process, $K_n(\cdot)$ is the modified Bessel function of the 2nd kind of order n , and $\Gamma(\cdot)$ represents the gamma function. It is noteworthy that the turbulence modelling of the optical signal and the interferer (which travel over physically distinct paths, and where the term interferer is used in the loose sense to refer to a crosstalk signal – there is no actual beating in the performance analysis) are assumed to be uncorrelated in the upstream analysis, hence the signal and interferer GG pdfs are treated independently.

The α and β parameters for plane-wave propagation (for arbitrary aperture size) are given as [14, 17, 35, 36]

$$\alpha = \left\{ \exp \left[\frac{0.49\sigma_R^2}{(1 + 0.65d^2 + 1.11\sigma_R^{12/5})^{7/6}} \right] - 1 \right\}^{-1} \quad (8.2)$$

$$\beta = \left\{ \exp \left[\frac{0.51\sigma_R^2(1 + 0.69\sigma_R^{12/5})^{-5/6}}{1 + 0.9d^2 + 0.62d^2\sigma_R^{12/5}} \right] - 1 \right\}^{-1} \quad (8.3)$$

where $d = \sqrt{kD_{RX}^2/4l_{fso}}$ is the normalized RCL radius, $\sigma_R^2 = 1.23C_n^2 k^{7/6} l_{fso}^{11/6}$ is the Rytov variance is the measure of optical turbulence strength whose value changes by increasing the refractive index structure constant C_n^2 or FSO optical link length l_{fso} , or both, C_n^2 have typical range from around $10^{-17} \text{ m}^{-2/3}$ for conditions when the turbulence is weak and up to around $10^{-13} \text{ m}^{-2/3}$ when the turbulence is strong, $k = 2\pi/\lambda$ is the optical wave number and λ is the optical wavelength [14, 17, 35, 36].

8.4 General BER analysis

In its most general form, under the assumption of independent signal and crosstalk channels (e.g. as in the upstream), the average upstream (turbulence accentuated) BER can be obtained as

$$\overline{BER} = \int_0^\infty \int_0^\infty BER(h_{turb,sig}, h_{turb,int}) p_{GG,sig}(h_{turb,sig}) p_{GG,int}(h_{turb,int}) dh_{turb,sig} dh_{turb,int} \tag{8.4}$$

where $p_{GG,sig}(h_{turb,sig})$ and $p_{GG,int}(h_{turb,int})$ are the GG distributions for signal and interferer, respectively each defined by different α , β and σ_R^2 respectively. Thus the signal and interferer experience turbulent links that are treated as independent. This is meaningful in the upstream where the paths are completely separate but not in the downstream.

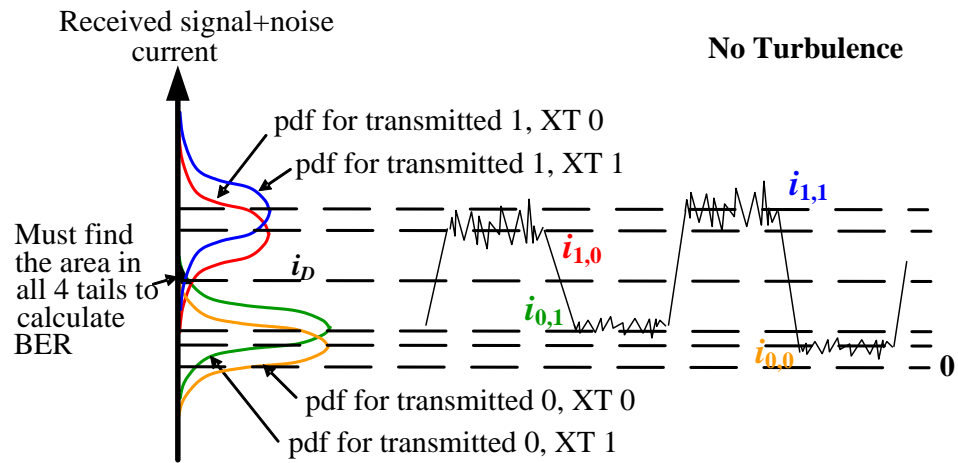


Figure 8.2 Probability density functions in the presence of one interchannel crosstalk of similar type to the signal. Data pattern here is 1010, crosstalk pattern is 0110

Using a Gaussian approximation, in a simple case of one source of interchannel crosstalk whose data take two different values of (0, 1), there would be a total of 4 different terms (shown in Fig. 8.2) in the overall BER which is given by:

$$\begin{aligned}
 BER &= P(1|0,0)P(0,0) + P(1|0,1)P(0,1) + P(0|1,0)P(1,0) + P(0|1,1)P(1,1) \\
 &= \frac{1}{4} [P(1|0,0) + P(1|0,1) + P(0|1,0) + P(0|1,1)]
 \end{aligned} \tag{8.5}$$

where the crosstalk and signal are both assumed to carry equiprobable (and independent) data, so $P(0,0) = P(0,1) = P(1,0) = P(1,1) = 1/4$. The probability of a '0' being received given a '1' is transmitted and given arbitrary crosstalk data d_{int} (representing crosstalk data 0 or 1), is

$$P(0|1, d_{int}) = \frac{1}{2} \operatorname{erfc} \left(\frac{i_{d_{sig}(1), d_{int}} - i_D}{\sqrt{2} \sqrt{(\sigma_{sig(1), d_{int}}^2)_{-ASE} + \sigma_{ASE-ASE}^2 + \sigma_{shot, ASE}^2 + \sigma_{shot(1, d_{int})}^2 + \sigma_{th}^2}} \right) \tag{8.6}$$

Similarly for '1' received given a '0' transmitted and given arbitrary crosstalk data d_{int} :

$$P(1|0, d_{int}) = \frac{1}{2} \operatorname{erfc} \left(\frac{i_D - i_{d_{sig}(0), d_{int}}}{\sqrt{2} \sqrt{(\sigma_{sig(0), d_{int}}^2)_{-ASE} + \sigma_{ASE-ASE}^2 + \sigma_{shot, ASE}^2 + \sigma_{shot(0, d_{int})}^2 + \sigma_{th}^2}} \right) \tag{8.7}$$

where i_D is the threshold.

However, based on the assumption that the combination of data 1 and crosstalk 0 is more likely to yield an error (0) than data 1 and crosstalk 1, and equally the combination of data 0 and crosstalk 1 is more likely to yield an error (1) than data 0 and crosstalk 0, a BER (conditioned on $h_{turb, sig}$ and $h_{turb, int}$, where $h_{turb, sig}$ and $h_{turb, int}$ are the attenuation due to turbulence for signal and interferer, respectively) for upstream transmission, can be written as

$$BER(h_{turb, sig}, h_{turb, int}) = \frac{1}{4} \operatorname{erfc} \left(\frac{Q(h_{turb, sig}, h_{turb, int})}{\sqrt{2}} \right) \tag{8.8}$$

$$Q(h_{turb, sig}, h_{turb, int}) = \frac{i_{1,0}(h_{turb, sig}, h_{turb, int}) - i_{0,1}(h_{turb, sig}, h_{turb, int})}{\sigma_{1,0}(h_{turb, sig}, h_{turb, int}) + \sigma_{0,1}(h_{turb, sig}, h_{turb, int})} \tag{8.9}$$

where $i_{d_{sig}, d_{int}} = i_{d_{sig}} + i_{d_{int}}$ is the resulting signal ($d_{sig} = 0$ or 1) and interferer ($d_{int} = 0$ or 1) current at the OLT decision circuit, $i_{d_{sig}}(h_{turb, sig}) = a_{d_{sig}} RP_{R, sig}(h_{turb, sig})$ is the upstream signal current for data 1 and 0, $i_{d_{int}}(h_{turb, int}) = a_{d_{int}} RP_{R, int}(h_{turb, int})$ is the upstream interferer current for data 1 and 0. $P_{R, sig}$ and $P_{R, int}$ are respectively the instantaneous received signal and interferer average powers. Also $a_0 = 2/(r+1)$, $a_1 = 2r/(r+1)$, r is the signal and interferer extinction ratio (i.e. assumed to be the same), $R = \eta q/E$ is the responsivity (in A/W), q is the electron charge, $E = hf_c$ is the photon energy (corresponding signal and interferer values differs slightly) and h is Planck's constant.

The total OLT receiver noise variance $\sigma_{d_{sig}, d_{int}}^2$ is the summation of the shot noise variance $\sigma_{shot(d_{sig}, d_{int})}^2$, thermal noise variance σ_{th}^2 , shot-ASE beat noise variance $\sigma_{shot, ASE}^2$, signal-ASE beat noise variance $\sigma_{sig(d_{sig}, d_{int})-ASE}^2$, and ASE-ASE beat noise variance $\sigma_{ASE-ASE}^2$.

$$\sigma_{shot(d_{sig}, d_{int})}^2(h_{turb, sig}, h_{turb, int}) = 2qi_{d_{sig}, d_{int}}(h_{turb, sig}, h_{turb, int})B_e \quad (8.10)$$

$$\sigma_{shot, ASE}^2 = 2m_t B_0 N_0 q R B_e \quad (8.11)$$

$$\sigma_{sig(d_{sig}, d_{int})-ASE}^2(h_{turb, sig}, h_{turb, int}) = 4RN_0 i_{d_{sig}, d_{int}}(h_{turb, sig}, h_{turb, int})B_e \quad (8.12)$$

$$\sigma_{ASE-ASE}^2 = 2m_t R^2 N_0^2 B_0 B_e \quad (8.13)$$

where m_t is the number of polarisation states of ASE noise (normally $m_t = 2$), B_0 is the optical bandpass filter bandwidth (in Hz) and the ASE noise power spectral density (PSD) in a single polarisation state at the photodiode is N_0 .

8.5 Turbulence accentuated crosstalk

To develop insight into the behaviour of the system it is useful to consider firstly the case where the signal experiences turbulence and the interferer does not. To do so equations (8.4)-(8.13) are employed in an optically preamplified case (gain G , and the ASE PSD at amplifier output is $N_0 = 0.5(NFG - 1)E$) and a non-amplified receiver case ($G = 1$). Then $P_{R,sig}(h_{turb,sig}) = GP_{inst,sig}(h_{turb,sig})$, where $P_{inst,sig}(h_{turb,sig})$ is the instantaneous received signal power as a function of the instantaneous channel turbulence and thus $P_{inst,sig}(1)$ is also the turbulence free average received power of the signal at the preamplifier input. $P_{R,int} = GP_{int}$ is fixed by setting a signal to crosstalk ratio $C_{XT} = P_{R,sig}(1)/P_{int}$ where P_{int} is the crosstalk power (that, in this case, is not turbulent affected).

Also of interest is the case where the interferer experiences turbulence and the signal does not. Then $P_{R,int}(h_{turb,int}) = GP_{inst,int}(h_{turb,int})$ where $P_{inst,int}(h_{turb,int})$ is the instantaneous received interferer power as a function of the instantaneous channel turbulence, $P_{R,sig} = GP_{sig}$ is fixed by setting a signal to crosstalk ratio $C_{XT} = P_{sig}/P_{R,int}(1)$ where $P_{R,int}(1)$ is also the turbulence free average received power of the interferer at the preamplifier input and P_{sig} is the signal power which is not affected by turbulence.

8.5.1 Example results

BER versus average received signal power results, for FSO communication system operating under various atmospheric turbulence conditions, with the main focus on the turbulence-accentuation of the interchannel crosstalk, are presented in this section. The parameters used are: laser wavelength, $\lambda = 1.55 \mu m$, data rate $R_b = 2.5 \text{ Gbps}$, extinction ratio, $r = 10 \text{ dB}$ (for signal and interferer), optical bandpass filter, $B_0 = 60 \text{ GHz}$, quantum efficiency $\eta = 0.8$, amplifier noise figure, $NF = 4.77 \text{ dB}$ and optical gain, $G = 30.6 \text{ dB}$. The thermal noise current is assumed to be $7 \times 10^{-7} \text{ A}$. This value is obtained from an unamplified

receiver with back-to-back sensitivity of -23 dBm at BER of 10^{-12} [8]. The weak (WT) and strong (ST) turbulence conditions over an optical link length $l = 1000$ m are characterised by $C_n^2 = 8.4 \times 10^{-15} \text{ m}^{-2/3}$ and $C_n^2 = 1 \times 10^{-13} \text{ m}^{-2/3}$, respectively. Results are presented for (i) no interferer, no turbulence (S) (ii) signal with interferer, no turbulence (S,XT) (iii) signal with turbulence, no interferer (turbS) (iv) signal with turbulence, interferer with no turbulence (turbS,XT), and (v) signal with no turbulence, interferer with turbulence (S,turbXT) cases.

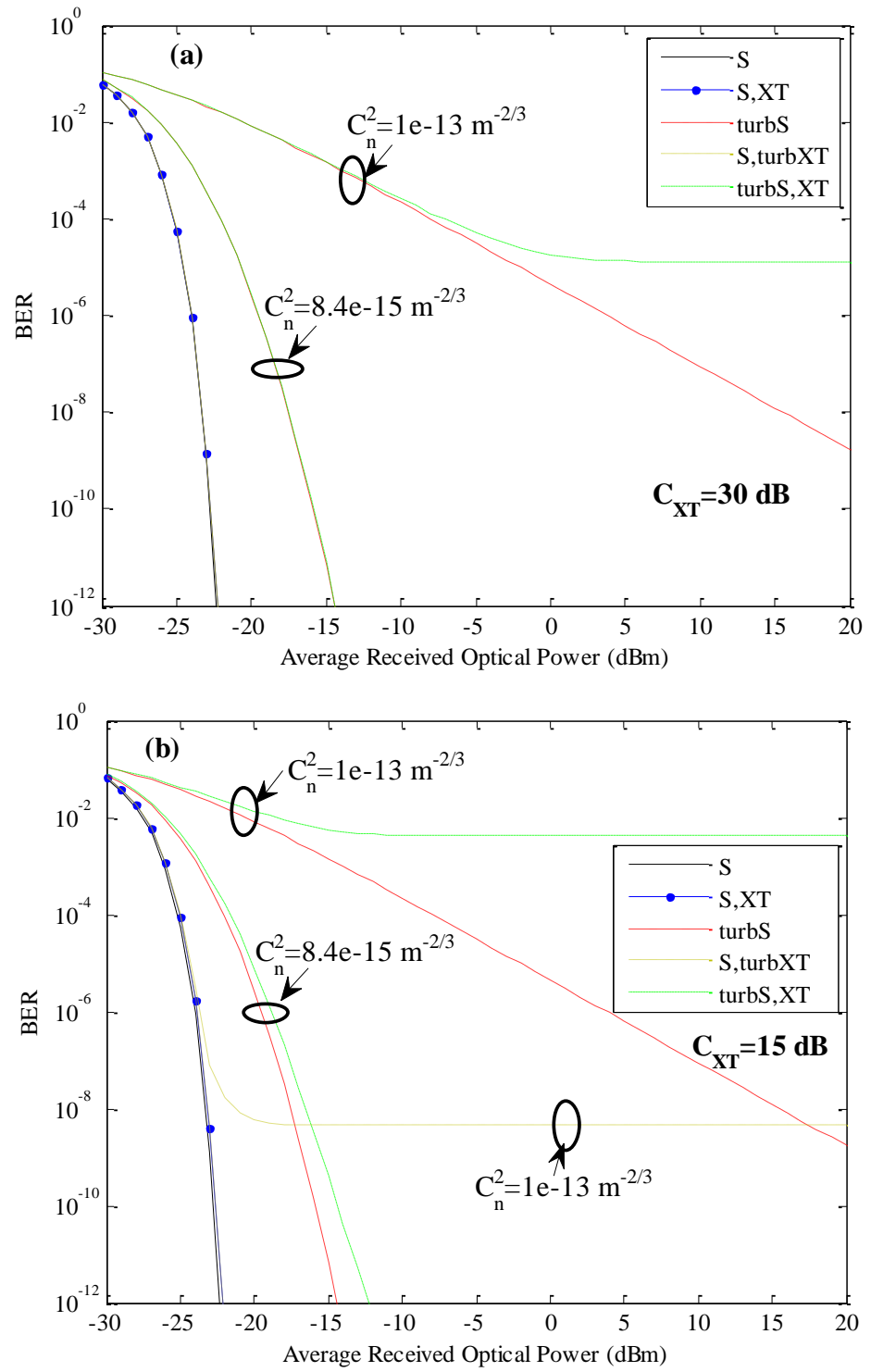


Figure 8.3 BER versus average received signal optical power (dBm) for WT and ST (no amplifier) (a) $C_{XT} = 30$ dB (b) $C_{XT} = 15$ dB

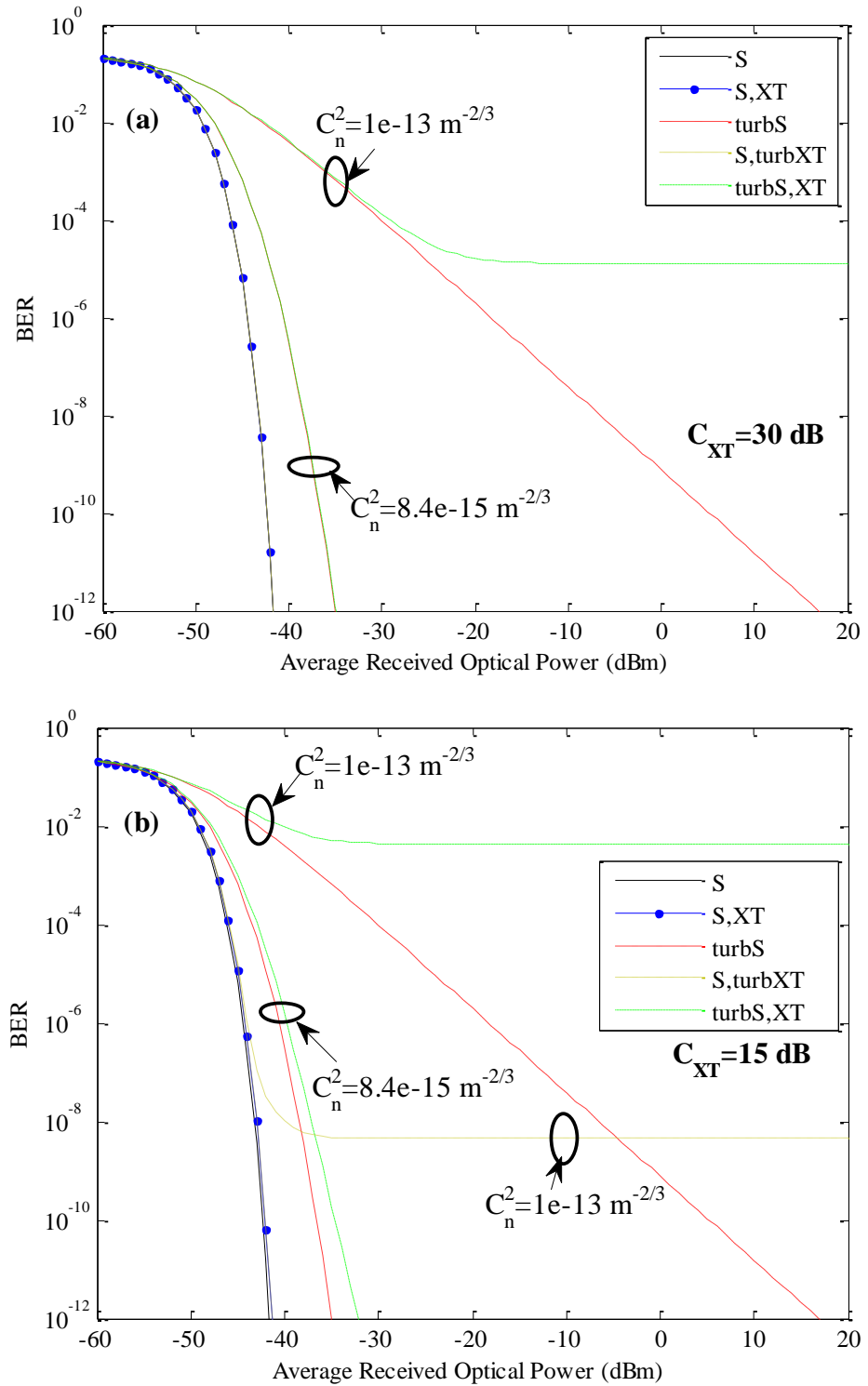


Figure 8.4 BER versus average received signal optical power (dBm) for WT and ST ($G=30$ dB) (a) $C_{XT} = 30$ dB (b) $C_{XT} = 15$ dB

It can be seen from the results (Figs. 8.3 (non-amplified case) and 8.4 (optically preamplified case)) that the turbulence accentuation of the crosstalk introduces BER floors which rise with the turbulence strength. In the weak turbulence cases, error floors occur at much lower BERs than the range shown, using a signal-to-crosstalk ratio of 30 dB and 15 dB. In the strong turbulence case, the turbS,XT BER floors (when $C_{XT} = 30$ dB), while the turbS,XT and S,turbXT both floor (when $C_{XT} = 15$ dB).

To understand turbulence accentuation of crosstalk, consider firstly the S,turbXT case and note that turbulent crosstalk can sometimes increase its 1 value so that {data 0, crosstalk 1} is greater than {data 1, crosstalk 0} (neglecting receiver noises). This applies when $h_{turb,int}$ is high enough, and, when it is (as data rate much faster than the turbulence), it effectively holds this value long enough for the threshold to adapt and be set above the {data 1, crosstalk 0} value but below {data 0, crosstalk 1} value, inevitably leading to errors (except when receiver noises operate to correct them). This occurs when $h_{turb,int} > C_{XT}$, so integrating this tail of the crosstalk's turbulence pdf sets the error floor. The floor starts once the signal power and crosstalk are sufficiently large that the noises are very unlikely to cause a reverse threshold crossing.

Similar arguments apply for the turbS,XT case, except this time there comes a point, by attenuating the signal, where {data 1, crosstalk 0} is brought lower than {data 0, crosstalk 1}, again neglecting receiver noises and leading to a threshold set below {data 0, crosstalk 1} and above {data 1, crosstalk 0}. This occurs when $h_{turb,sig} < 1/C_{XT}$, setting the error floor value via integration of the signal's turbulence pdf.

In the non-amplifier case (Fig. 8.3), the S,turbXT case and the turbS,XT case superficially seem the same, as the instantaneous crosstalk ratio (not the same as C_{XT} which used the average or turbulence free values in its definition) will have the same statistics in both cases. However, the difference is that in one (S,turbXT) the ratio between the signal power and the noise does not change, whilst in the other (turbS,XT), the ratio between the signal power and noise varies greatly, and the additional variation in the

second case is what makes it perform worse. The same effect is observed when an optical amplifier is placed in the signal path (on the assumption that the optical filtering (e.g. provided by a wavelength demultiplexer or an optical bandpass filter) does not reduce the crosstalk power or equivalently that the crosstalk, whilst still being interchannel in the sense of not causing beat noise, actually lies within the pass band). The optical amplifier case is presented in Fig. 8.4 for a signal to crosstalk ratio of 30 dB and 15 dB, respectively. It is straightforward to adjust this to take into account a specific crosstalk rejection by the optical filtering instead.

8.6 BER Evaluation for Hybrid WDM-PON-FSO System

8.6.1 Upstream transmission:

The same basic equations (8.4)-(8.13) can be used in the specific system calculations described here. The single crosstalk can be used in situations where a dominant interferer exists (e.g. in some sparsely populated DWDM grids or where particular interferer transmitters are higher powered). Now the average received optical power at the OLT photodiode for the desired signal and an interferer are given, respectively, as:

$$P_{R,sig}(h_{turb,sig}) = GP_{u_{T,sig}} h_{turb,sig} L_{fso,sig} L_{bs,sig} L_{c,sig} L_{mux} L_{fibre} L_{demux} \quad (8.14)$$

$$P_{R,int}(h_{turb,int}) = GP_{u_{T,int}} h_{turb,int} L_{fso,int} L_{bs,int} L_{c,int} L_{mux} L_{fibre} L_{demux} L_{demux,XT} \quad (8.15)$$

where $L_{demux,XT}$ is the crosstalk i.e. additional loss (above L_{demux}) the interferer has when coupled onto the signal photodiode by the demux. Also $P_{u_{T,sig}}$ and $P_{u_{T,int}}$ are the ONU transmit power of the signal and interferer, respectively. In principle, these could be allowed to differ in a power control algorithm. $L_{fso} = 10^{(-\alpha_{fso} l_{fso}/10)}$ is the loss due to atmospheric attenuation, α_{fso} is the atmospheric attenuation factor in dB/km, $L_{fibre} = 10^{(-\alpha_{fibre} l_{fibre}/10)}$ is the loss due to fibre attenuation and α_{fibre} is the fibre attenuation factor in dB/km. The loss due to beam spreading L_{bs} in the FSO link for signal and interferer can be calculated from [3, 14].

$$L_{bs} = \left(\frac{D_{RX}}{\theta l_{fso}} \right)^2 \quad (8.16)$$

and can of course be stated separately for the signal and the interferer.

Under the assumption that the end facet of the short single mode fibre leading to the mux is positioned in the focal plane of the RCL, the coupling loss L_c for the signal and interferer can be calculated from [37]

$$L_c = 1 - \left\{ 8a^2 \int_0^1 \int_0^1 \exp \left[- \left(a^2 + \frac{A_{RX}}{A_C} \right) (x_1^2 + x_2^2) \right] \times I_0 \left(2 \frac{A_{RX}}{A_C} x_1 x_2 \right) x_1 x_2 dx_1 dx_2 \right\} \quad (8.17)$$

where a is the ratio of the RCL radius to the radius of the backpropagated fibre mode, $A_{RX} = \pi D_{RX}^2 / 4$ is the area of the RCL, $A_C = \pi \rho_C^2$ is the spatial coherence area of the incident plane wave, $\rho_C = (1.46 C_n^2 k^2 l_{fso})^{-3/5}$ is the spatial coherence radius, and $I_0(\cdot)$ is the modified Bessel function of the first kind and zero order.

At the amplifier output the ASE PSD is $N_{0OA} = 0.5(NFG - 1)E$. Different values of N_0 would be experienced, depending on the position of the optical amplifier. In the upstream Case A, the received ASE noise PSD can be written as $N_0 = N_{0OA} L_{fibre} L_{demux}$, while in the Case B, the received ASE noise PSD can be written as $N_0 = N_{0OA} L_{demux}$.

8.6.2 Downstream transmission:

The interchannel crosstalk present here is treated as non-turbulence-accentuated as (setting aside wavelength difference impact on σ_R^2) it travels over the same atmospheric path as the signal. The downstream BER (conditioned on h_{turb}) is given by

$$BER_d(h_{turb}) = \frac{1}{4} \operatorname{erfc} \left(\frac{Q_d(h_{turb})}{\sqrt{2}} \right) \quad (8.18)$$

$$Q_d(h_{turb}) = \frac{i_{d_{1,0}}(h_{turb}) - i_{d_{0,1}}(h_{turb})}{\sigma_{d_{1,0}}(h_{turb}) + \sigma_{d_{0,1}}(h_{turb})} \quad (8.19)$$

where $i_{d_{d_{sig}, d_{int}}} = i_{d_{d_{sig}}} + i_{d_{d_{int}}}$ is the resulting signal ($d_{sig} = 0$ or 1) and interferer ($d_{int} = 0$ or 1) current at the ONU decision circuit, $i_{d_{d_{sig}}}(h_{turb}) = a_{d_{d_{sig}}} RP_{d_{R_{sig}}}(h_{turb})$ and $i_{d_{d_{int}}}(h_{turb}) = a_{d_{d_{int}}} RP_{d_{R_{int}}}(h_{turb})$ are the downstream signal and interferer currents, respectively for data 1 and 0.

The average received optical power at the ONU photodiodes for desired signal and interferer are given, respectively, as:

$$P_{d_{R, sig}}(h_{turb}) = GP_{d_{T, sig}} h_{turb} L_{mux} L_{fibre} L_{demux} L_{fso} L_{bs} \quad (8.20)$$

$$P_{d_{R, int}}(h_{turb}) = GP_{d_{T, int}} h_{turb} L_{mux} L_{fibre} L_{demux} L_{demux, XT} L_{fso} L_{bs} \quad (8.21)$$

where $P_{d_{T, sig}}$ and $P_{d_{T, int}}$ are the OLT transmit power of the signal and interferer, respectively.

The equations (8.10)-(8.13) may again be used for the electrical domain noises, though the $h_{turb, int}$ dependency disappears.

In downstream Case A, the effective ASE noise PSD in a single polarisation state at the photodiode is given as $N_0 = N_{0OA} L_{demux, sig} L_{fso, sig} L_{bs, sig}$, whereas in Case B, it is given as $N_0 = N_{0OA} L_{fibre} L_{demux, sig} L_{fso, sig} L_{bs, sig}$.

The average downstream BER is given as

$$\overline{BER}_{d, av}(P_{d_{T, sig}}, P_{d_{T, int}}) = \int_0^{\infty} BER_d(h_{turb}) p_{GG, sig}(h_{turb}) dh_{turb} \quad (8.22)$$

8.7 Results and Discussion

Table 8.1 List of key parameters used in the calculation for both transmissions

Parameter	Description	Value
λ_{sig}	Desired signal wavelength	1550 nm
R_b	Data rate	2.5 Gbps
D_{RX}	RCL diameter	13 mm [30, 38]
G	Optical amplifier gain	30 dB
NF	Noise figure	4.77 dB
B_0	Demux channel bandwidth	60 GHz
r	Extinction ratio	10 dB (signal and interferer)
l_{fibre}	Feeder fibre length	20 km [1]
l_{fso}	Maximum FSO length	2 km
α_{fibre}	Feeder fibre attenuation	0.2 dB/km [1, 2]
α_{fso}	Atmospheric channel attenuation	0.2 dB/km (very clear air) [1, 12, 13]
θ	Transmission divergence angle	0.2 mrad
L_{demux}	Signal mux/demux loss	3.5 dB [1, 2, 24]
η	Quantum efficiency	0.8

Results in terms of required optical power at several BER values are presented to predict the performance for various scenarios of the optical fibre and FSO-based WDM network. The BER calculations are based on the GG pdf, whilst the turbulent strength is characterised by $C_n^2 = 10^{-17} \text{ m}^{-2/3}$, $C_n^2 = 10^{-15} \text{ m}^{-2/3}$ and $C_n^2 = 10^{-13} \text{ m}^{-2/3}$. If the equivalent $\sigma_R^2 < 1$ there is the weak turbulence (WT) condition, if $\sigma_R^2 \approx 1$ there is the moderate turbulence (MT) condition, and if $\sigma_R^2 > 1$ there is the strong turbulence (ST) condition. The required optical power used in this work is the transmitter power, stated in dBm, to obtain a target BER. The choice of target BERs of 10^{-12} is follows a typical PON target, whilst the choice of 10^{-6} is to show the impact of change in the target BER. The main parameters used for the calculations are presented in Table 8.1. The parameter $a = 1.12$ corresponds to the optimum value of a for a fully coherent incident plane wave [37]. Other parameters used will be stated

accordingly. No dispersion or nonlinear effects in the optical fibre are calculated. For the 20 km feeder, small penalties maybe expected but are not significant. The RCL diameter is considered to be 13 mm which is consistent with the experimental works of [30, 38]. The choice of small size lenses, each coupled to single core fibre, help to limit the possibility of angular misalignment, and allows for the practical use of a small-size core fibre [38]. The advantage of using a small-size core fibre is its potential compatibility with existing devices and systems, which would increase the practicality of the design.

8.7.1 Downstream transmission:

Figure 8.5 shows the downstream required transmitted optical power (dBm) at target BERs of 10^{-12} and 10^{-6} as a function of the FSO link length (m) for no interferer and single interferer cases (a) $L_{demux,XT} = 30$ dB and (b) $L_{demux,XT} = 15$ dB for Case A with signal and crosstalk transmit powers the same. Clearly, as the atmospheric channel becomes more turbulent, the required optical power increases. Similarly, the presence of an adjacent channel interferer necessitates an additional power requirement for the system. In Fig. 8.5a, both the no-interferer and single-interferer cases have very similar required transmit powers, due to the high signal to crosstalk ratio (and absence of any turbulence-accentuating of the crosstalk effect). However, with a poor demux device (in this case having a interferer loss of 15 dB), as shown in Fig. 8.5b, it can be seen that the crosstalk effect becomes more noticeable though, as expected, not dramatically so. In the strong turbulence regions (where $C_n^2 = 10^{-13} \text{ m}^{-2/3}$), it can be seen that the required optical power tends towards a steady value as the turbulence strength increases. This can be attributed to the levelling effect which occurs when the RCL diameter used falls between the spatial coherence radius and the scattering disk [39] as it does in this case. It can be seen that as FSO link length increases, the required optical power increases as well. This is because the beam spreading loss and the scintillation noise induced by atmospheric turbulence increases with FSO link length. Additionally, it

can be deduced from Fig. 8.5 that, if the transmitted power can be increased as high as 10 dBm, it can compensate for the turbulence effects for all C_n^2 values considered except for $C_n^2 = 10^{-13} \text{ m}^{-2/3}$ and $l_{fso} > 1200 \text{ m}$ in the single interferer case (Fig. 8.5a (ii)). This is based on the fact that, as the Rytov variance increases beyond unity, the required transmitted power tends to values that are too high to guarantee compliance with eye safety and device power limitations. From Fig. 8.5, if the OLT transmitter power is fixed at say 10 dBm (to limit fibre non-linearity), it can be deduced that FSO link lengths close to 2000 m can be used to achieve BERs of 10^{-12} and 10^{-6} for most turbulence conditions considered in the analysis, in the presence of a single interferer case. In case B, where the amplifier is placed at the OLT transmitter, quite similar results would be obtained as in case A which was discussed earlier (due to the low loss in the optical fibre). However, the main issue is the low permitted transmitter power (about -10 dBm [8]) for transmission through an optical fibre, due to non-linearity issues. Using -10 dBm as the maximum transmitted power, the low power in the optical fibre limits the FSO link length (to achieve a BER of 10^{-12} with a single interferer) to about 500 m (for $C_n^2 = 10^{-13} \text{ m}^{-2/3}$), 1000 m (for $C_n^2 = 10^{-15} \text{ m}^{-2/3}$) and 2000 m (for $C_n^2 = 10^{-17} \text{ m}^{-2/3}$). For a BER of 10^{-6} (Fig. 8.5b (ii)), FSO link length is limited to about 800 m (for $C_n^2 = 10^{-13} \text{ m}^{-2/3}$), and up to 2000 m (for $C_n^2 = 10^{-15} \text{ m}^{-2/3}$ and $C_n^2 = 10^{-17} \text{ m}^{-2/3}$).

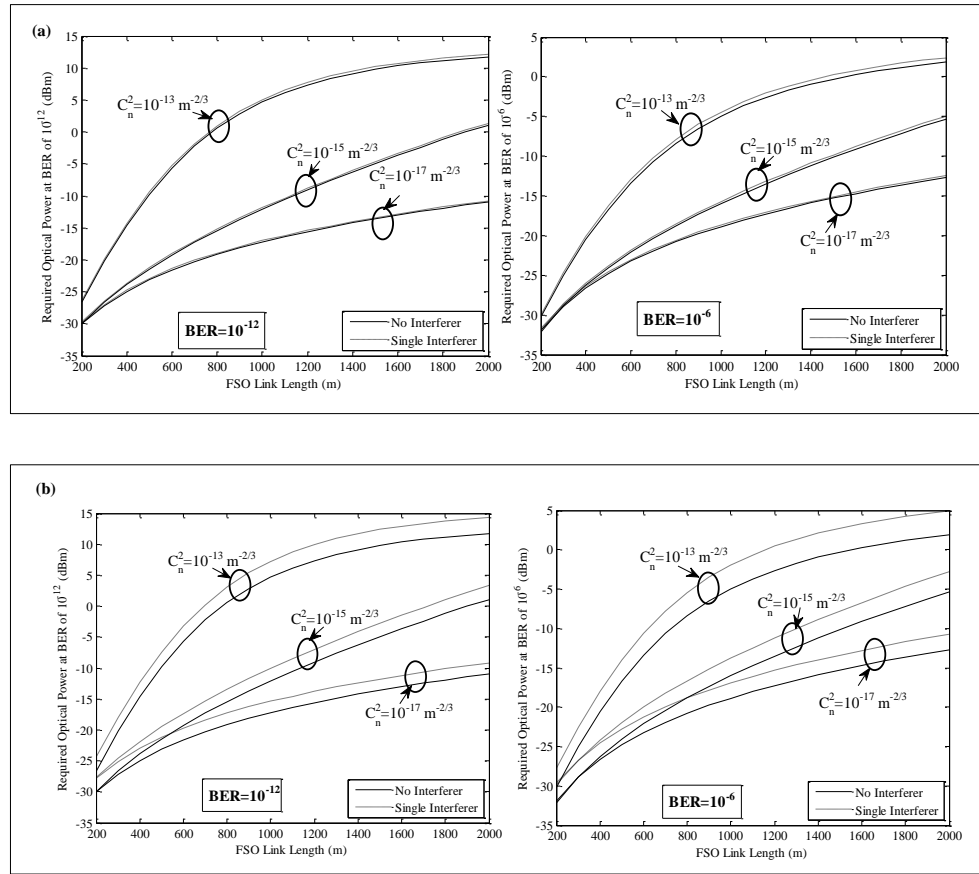


Figure 8.5 Downstream required transmitted optical power (dBm) at target BERs of 10^{-12} and 10^{-6} as a function of the FSO link length (m) for no interferer and single interferer cases (a) $L_{demux,XT} = 30$ dB and (b) $L_{demux,XT} = 15$ dB. OA was at the remote node (Case A)

Figure 8.6 shows the downstream required transmitted optical power (dBm) at target BERs of 10^{-12} and 10^{-6} , as a function of the transmitter divergence angle (rad) with $l_{fso} = 1000$ m, for no interferer and single interferer cases (a) $L_{demux,XT} = 30$ dB and (b) $L_{demux,XT} = 15$ dB. It can be seen that the required optical power increases with the OLT transmit divergence and turbulence strength. On comparing Fig. 8.6a and 8.6b, it can be seen that the effect of the crosstalk becomes more prominent when a poor demux device is used. In the case of the non-tracking system with relatively large transmit divergence greater than 1 mrad, it can be seen that more power than in tracking systems will be required to attain the target BER. This

system type would be required to have beam widths greater than both the receiving and transmitting diameters, in order to compensate for any motions due to building sway. In the case of a system with automatic pointing and tracking, the transmit divergence angle can be narrowed sufficiently (typically with divergence $\ll 1$ mrad), which allows for a secure transmission with a large proportion of the transmitted power being collected at the RCL. Thus, as shown in Fig. 8.6 (and neglecting pointing error [40]), the required power for tracking systems is lower which provides the system with enough power to overcome potential adverse weather conditions. From Fig. 8.6, assuming the transmitter power of, say, 10 dBm (possible in case A), in order to achieve a BER of 10^{-12} and l_{fso} of 1000 m, a small transmit divergence angle (say about 0.05 mrad) has to be used, and this can be achieved by using a tracking system. Although the inclusion of a tracking system helps improve the system performance, it also adds considerable cost and complexity to the FSO-based distribution link particularly if required for each ONU. Tracking systems will also have pointing jitter errors not included in the current analysis [40]. In a non-tracking system with single crosstalk (with transmit divergence of 2 mrad), the maximum FSO link length in case A (max. transmit power of 10 dBm) is less than 700 m, while in case B (with max. transmit power of -10 dBm) the FSO link length is about 400 m.

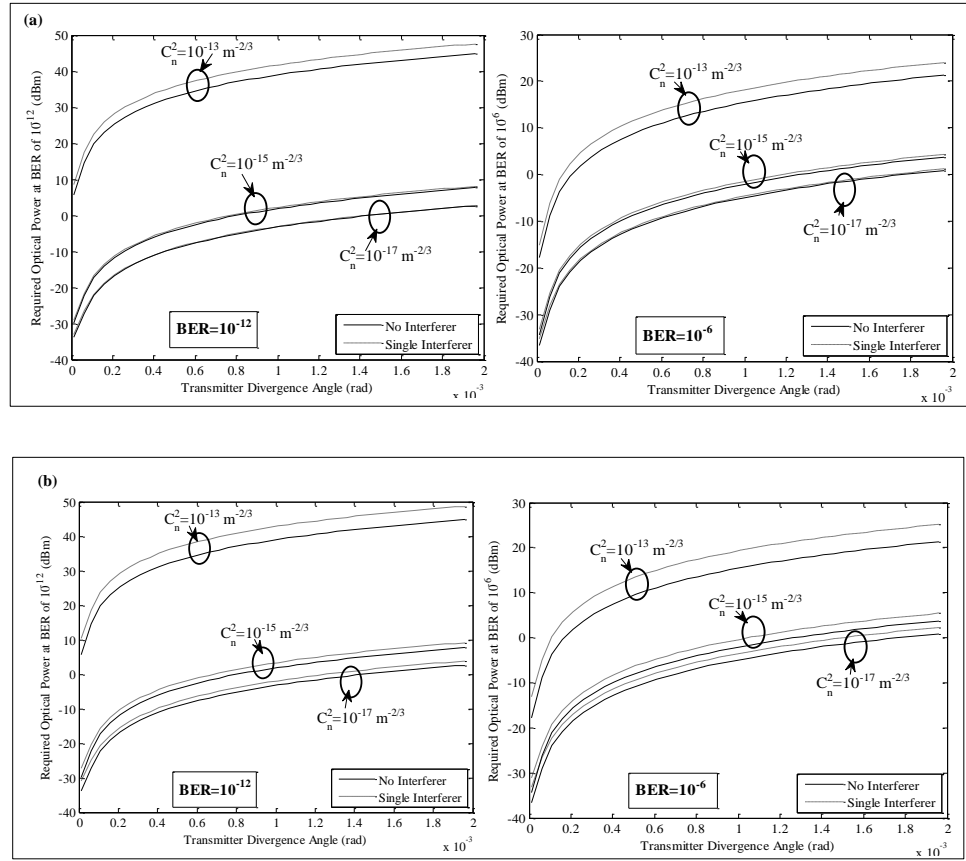


Figure 8.6 Downstream required transmitted optical power (dBm) at target BERs of 10^{-12} and 10^{-6} as a function of the transmitter divergence angle (rad) with $l_{fso} = 1000$ m for no interferer and single interferer cases (a)

$L_{demux,XT} = 30$ dB and (b) $L_{demux,XT} = 15$ dB. OA was at the remote node (Case

A)

8.7.2 Upstream transmission:

Figure 8.7 shows the upstream required transmitted optical power (dBm) at target BERs of 10^{-12} and 10^{-6} as a function of the FSO link length (m) with equal signal and interferer FSO link lengths (and transmit powers), $L_{demux,XT} = 30$ dB for no interferer and single interferer Case A. It can be seen in both cases that, as the FSO link lengths and turbulence strength increases, the ONU transmit power required to attain the target BER increases as well. On comparing the upstream and downstream results i.e. Figs. 8.7 and 8.5a, it can be seen that the required transmit power is higher

in the upstream case (Fig. 8.7) (e.g. by about 5 dB when $C_n^2 = 10^{-13} \text{ m}^{-2/3}$ and $l_{fso} = 2000 \text{ m}$). While turbulence accentuation of crosstalk will occur, it is not the dominant issue here due to the assumption of similar crosstalk and signal powers and lengths. The main factors leading to higher upstream required power are the additional coupling loss via the RCL into fibre that occurs in the upstream (in the downstream one can couple directly onto the photodiode) and as the upstream received OSNR is typically worse. Further, in the upstream, the ONU transmit power can be up to 20 dBm, which fulfils eye-safety conditions for a C-band wavelength range [40]. Therefore, using a reference power of 20 dBm in Fig. 8.7, it can be seen that a FSO link length of about 2000 m can be used to achieve both target BER values for all atmospheric turbulence conditions with a single interferer.

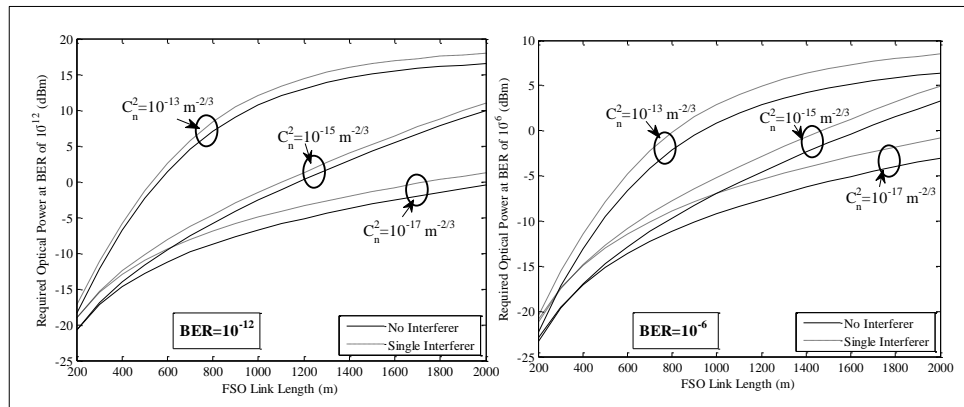


Figure 8.7 Upstream required transmitted optical power (dBm) at target BERs of 10^{-12} and 10^{-6} as a function of the FSO link length (m) with equal signal and interferer FSO link lengths, $L_{demux,XT} = 30 \text{ dB}$ for no interferer and single cases

Figure 8.8 shows the upstream required transmitted optical power (dBm) at target BERs of 10^{-12} and 10^{-6} as a function of the transmitter divergence angle (rad) for no-interferer and single-interferer cases with $l_{fso} = 1000$ m and $L_{demux,XT} = 30$ dB. As in the downstream (Fig. 8.6a), the required transmitter power increases with transmitter divergence and in the presence of crosstalk, although the required powers are greater in upstream than the downstream case for similar reasons mentioned earlier (the ASE loss). Using a transmit power of 20 dBm, a tracking system would be required to achieve small transmit divergence, FSO link length of 1000 m and BER of 10^{-12} for the whole range of atmospheric turbulence conditions, while in a non-tracking system with divergence of 2 mrad, the maximum FSO link length is about 600 m at BER of 10^{-12} for the strong turbulence condition.

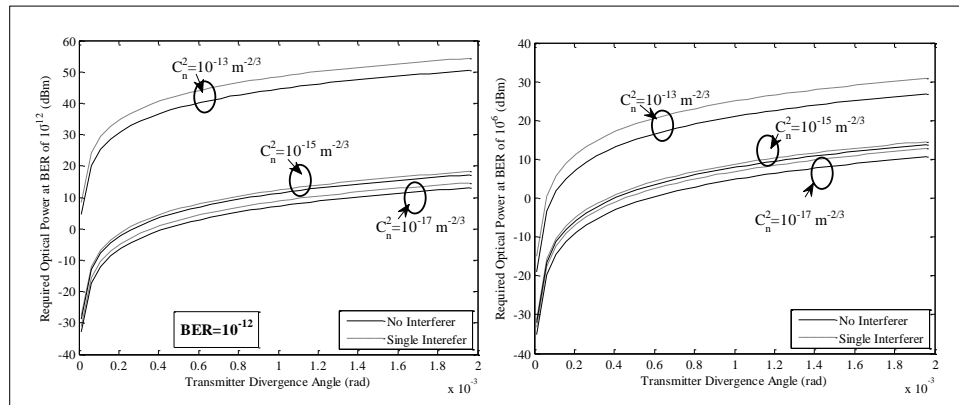


Figure 8.8 Upstream required transmitted optical power (dBm) at target BERs of 10^{-12} and 10^{-6} as a function of the transmitter divergence angle (rad) for no interferer and single interferer cases with $l_{fso} = 1000$ m and

$$L_{demux,XT} = 30 \text{ dB}$$

So far it has been assumed that the signal and interferer have identical launch power and distance. The distance requirement is now set aside (but that on launch power retained). Figure 8.9 shows the upstream required transmitted optical power (dBm) at target BERs of 10^{-12} and 10^{-6} as a function of the FSO link lengths for signal and interferer (m) for the single interferer case with $L_{demux,XT}=15$ dB. It can be seen from Fig. 8.9, that when the interferer is closer to the remote node than the desired signal, the crosstalk effect becomes more significant and the required transmit power increases. Furthermore, the sudden increase in required power seen on the left of Fig. 8.9 (for both turbulence strengths considered) i.e. when the FSO link length of the interferer is much closer (less than 200 m) to the remote node and the signal FSO link length is further away (say about 1500 m), can be related to the same turbulence accentuation effect which led to error floors in the turbS,XT case discussed earlier (see Fig. 8.3b). In fact for some FSO link length combinations, it is not possible to attain the target BER requirement.

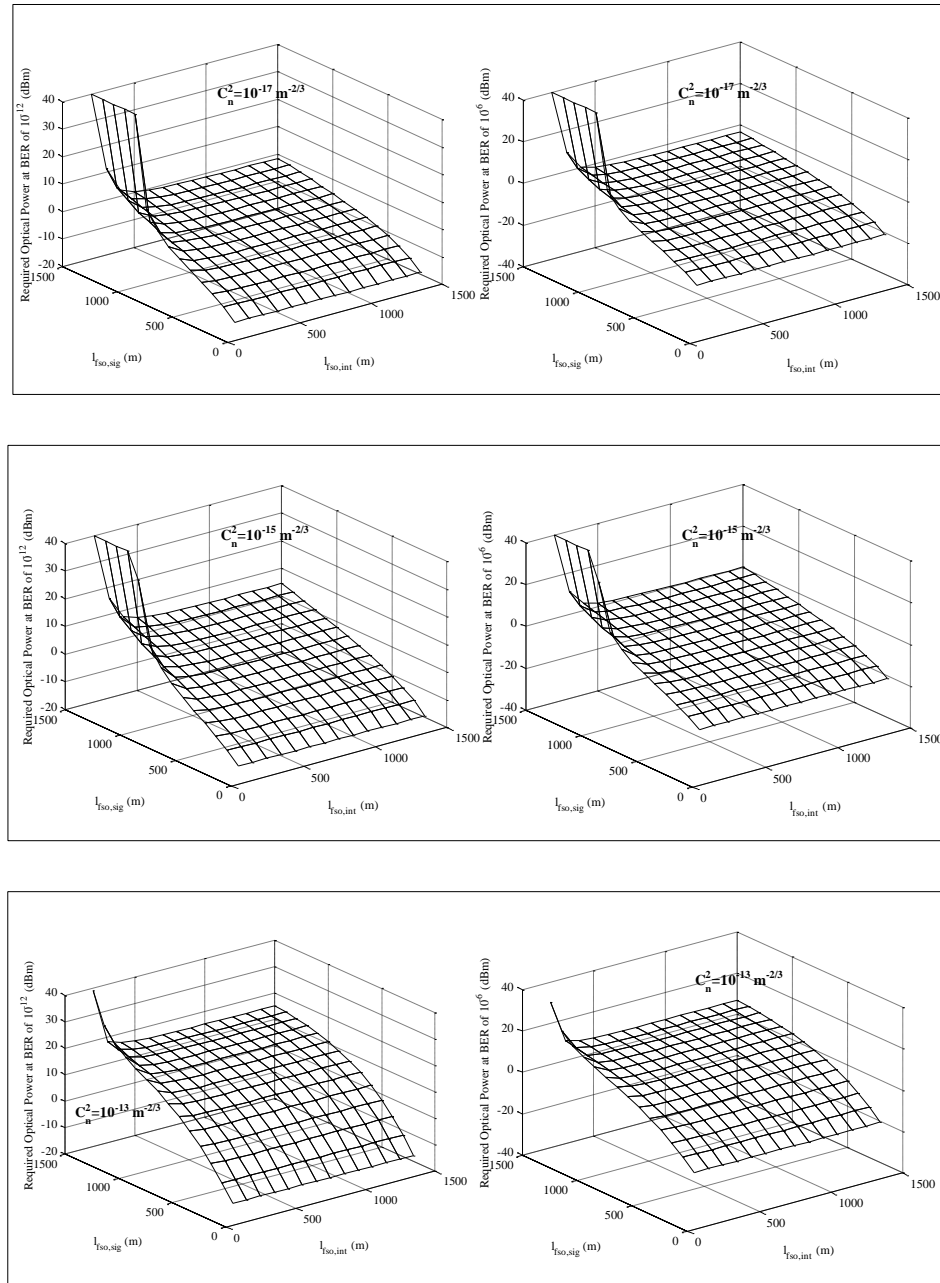


Figure 8.9 Upstream required transmitted optical power (dBm) at target BERs of 10^{-12} and 10^{-6} as a function of the FSO link lengths for signal and interferer (m) for the single interferer case with $L_{demux,XT} = 15$ dB

Figure 8.10 again shows the upstream required transmitted optical power (dBm) at target BERs of 10^{-12} and 10^{-6} as a function of the FSO link lengths for signal and interferer (m) for the single interferer case with $L_{demux,XT} = 15$ dB. However, different from Fig. 8.9, now there is assumed a power control algorithm that ensures the average power at the RCL or OLT for each signal is fixed. A similar argument as in Fig. 8.9 can be established here, but in this case it relates to the turbulence accentuating of the interferer, $S_{,turbXT}$ case (since the effect of turbulence would be greater on the interferer than the desired signal in the regions). Also, at some point when $l_{fso,sig} \ll l_{fso,int}$, there would be occurrence of error floor which restricts the attainment of the target BER. In regions without BER floor effects, this power control approach increases the required optical power to attain the target BERs compared to Fig. 8.9.

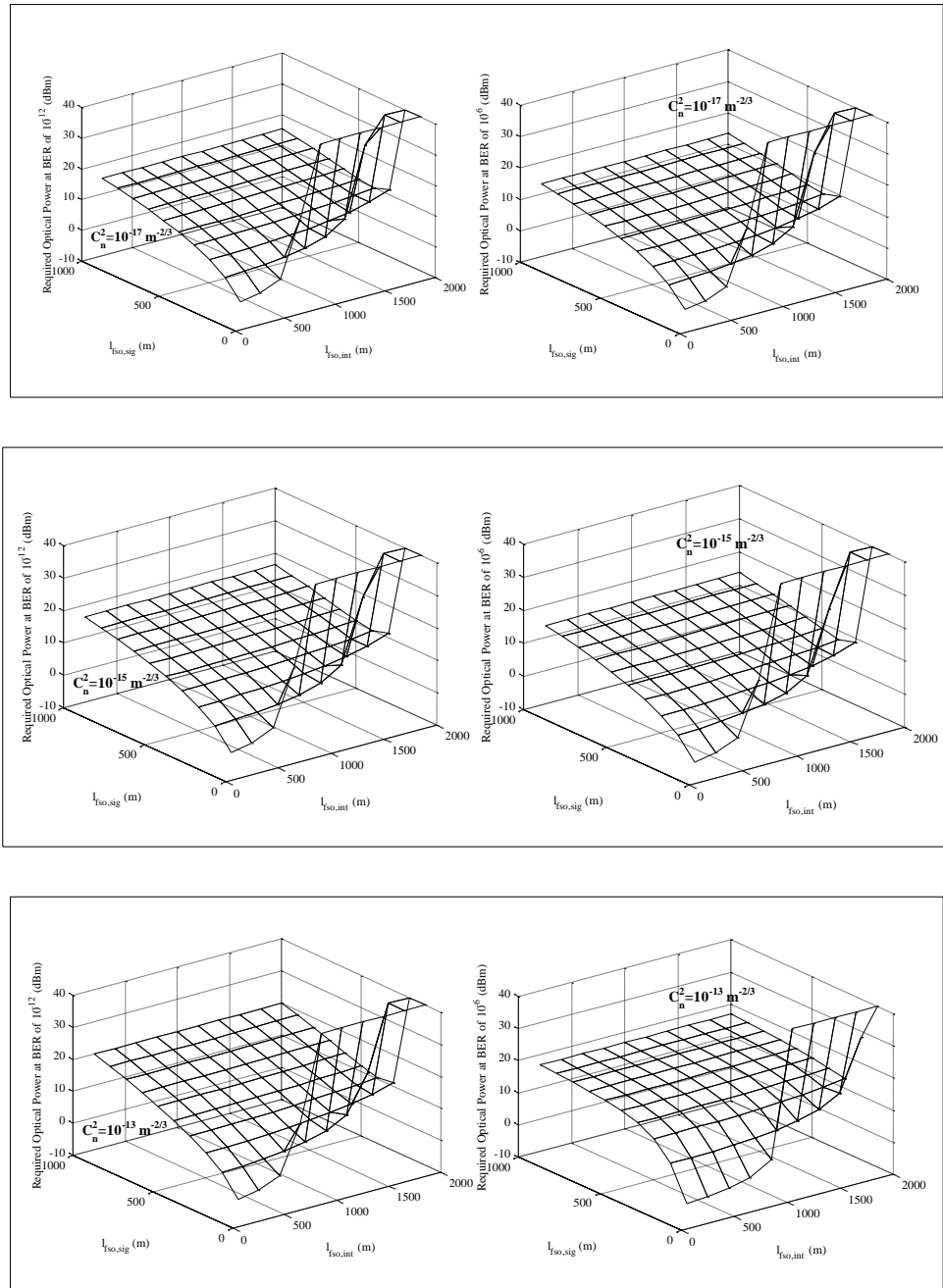


Figure 8.10 Upstream required transmitted optical power (dBm) (under the assumption of a power control algorithm that ensures the average power at the RCL or OLT for each signal is fixed) at target BERs of 10^{-12} and 10^{-6} as a function of the FSO link lengths for signal and interferer (m) for the single interferer case with $L_{demux,XT} = 15$ dB

8.8 Summary

In this chapter, a WDM network incorporating free-space optical communications for the distribution link has been studied. It can be deduced from this analysis that interchannel crosstalk, turbulence-induced scintillation, and ASE noises are dominant causes of system degradation, especially in the upstream transmission, causing error floors in the two extremes of signal turbulent but crosstalk not and crosstalk turbulent but signal not. The results obtained indicate that, in clear atmosphere, FSO distribution link lengths (up to 2000 m) and sufficiently higher signal-to-crosstalk ratio, the proposed system can achieve human-safe and high capacity access networks. The location of the optical amplifier will make little difference to the performance calculations in both directions, but the issue of capping of the fibre launch power is significant in the downstream. Finally, the optical amplifier positioning would also depend on other design considerations, such as fibre non-linearity and powering of a pointing and tracking system at the remote node.

8.9 References

- [1] C. H. Lee, W. V. Sorin, and B. Y. Kim, "Fiber to the home using a PON infrastructure," *Journal of Lightwave Technology*, vol. 24, pp. 4568-4583, 2006.
- [2] J. Prat, *Next-generation FTTH passive optical networks: research towards unlimited bandwidth access*, Springer Science, 2008.
- [3] S. Bloom, E. Korevaar, J. Schuster, and H. A. Willebrand, "Understanding the performance of free-space optics," *Journal of Optical Networking*, vol. 2, pp. 178-200, June 2003.
- [4] D. O. Caplan, "Laser communication transmitter and receiver design," *Journal of Optical Fibre Communication Report*, vol. 4, pp. 225-362, 2007.
- [5] T. H. Carbonneau and D. R. Wisely, "Opportunities and challenges for optical wireless; the competitive advantage of free space telecommunications links in today's crowded marketplace," *Proc. SPIE Wireless Technologies and Systems: Millimeter-Wave and Optical*, vol. 3232, pp. 119-128, January 1998.
- [6] D. Killinger, "Free space optics for laser communication through the air," *Optics and Photonics News*, vol. 13, pp. 36-42, October 2002.

- [7] S. Karp, R. M. Gagliardi, S. E. Moran, and L. B. Stotts, *Optical channels: fibers, clouds, water and the atmosphere*, New York: Plenum Press, 1988.
- [8] R. Ramaswami and K. N. Sivarajan, *Optical networks- a practical perspective*, Second Edition, Academic Press, London, 2002.
- [9] R. P. Davey, D. B. Grossman, M. Rasztoivits-Wiech, D. B. Payne, D. Nettet, A. E. Kelly, A. Rafel, S. Appathurai, and S. Yang, "Long-reach passive optical networks," *Journal of Lightwave Technology*, vol. 27, pp. 273-291, Feb. 2009.
- [10] E. Ciaramella, Y. Arimoto, G. Contestabile, M. Presi, A. D'Errico, V. Guarino, and M. Matsumoto, "1.28 terabit/s (32x40 Gbit/s) WDM transmission system for free space optical communications," *IEEE Journal on Selected Areas in Communications*, vol. 27, pp. 1639-1645, 2009.
- [11] L. Kazovsky, W. Shing-Wa, T. Ayhan, K. M. Albeyoglu, M. R. N. Ribeiro, and A. Shastri, "Hybrid optical wireless access networks," *Proceedings of the IEEE*, vol. 100, pp. 1197-1225, 2012.
- [12] E. S. Son, K. H. Han, J. H. Lee, and Y. C. Chung, "Survivable network architectures for WDM PON," *Optical Fiber Communication Conference (OFC), Anaheim, California, Mar., 2005*.
- [13] E. Leitgeb, M. Gedhart, and U. Birnbacher, "Optical networks, last mile access and applications," *J. Opt. Fiber Commun.*, pp. 56-85, 2005.
- [14] A. K. Majumdar, "Free-space laser communication performance in the atmospheric channel," *Journal of Optical and Fiber Communications Research*, vol. 2, pp. 345-396, 2005.
- [15] J. C. Ricklin, S. M. Hammel, F. D. Eaton, and S. L. Lachinova, "Atmospheric channel effects on free-space laser communication," *J. Opt. Fiber Commun.*, vol. 3, pp. 111-158, 2006.
- [16] H. A. Willebrand and B. S. Ghuman, *Free-space optics: enabling optical connectivity in today's networks*, Sams Publishing, Indianapolis, Indiana 46240 USA, 2002.
- [17] L. C. Andrews and R. L. Phillips, *Laser beam propagation through random media*, Second Edition, SPIE Press, Bellingham, Washington, 2005.
- [18] E. Korevaar, I. Kim, and B. McArthur, "Atmospheric propagation characteristics of highest importance to commercial free space optics," *Proc. of SPIE, San Diego, CA*, vol. 4976, pp. 1-12, 2003.
- [19] T. Kamalakis, I. Neokosmidis, A. Tsipouras, S. Pantazis, and I. Andrikopoulos, "Hybrid free space optical / millimeter wave outdoor links for broadband wireless access networks," *IEEE 18th*

- International Symposium on Personal, Indoor and Mobile Radio Communications*, 2007, pp. 1-5.
- [20] M. Abtahi, P. Lemieux, W. Mathlouthi, and L. A. Rusch, "Suppression of turbulence-induced scintillation in free-space optical communication systems using saturated optical amplifiers," *Journal of Lightwave Technology*, vol. 24, pp. 4966-4973, 2006.
- [21] A. O. Aladeloba, A. J. Phillips, and M. S. Woolfson, "Improved bit error rate evaluation for optically pre-amplified free-space optical communication systems in turbulent atmosphere," *IET Optoelectronics*, vol. 6, pp. 26-33, February 2012.
- [22] M. Razavi and J. H. Shapiro, "Wireless optical communications via diversity reception and optical preamplification," *IEEE Transactions on Wireless Communications*, vol. 4, pp. 975-983, 2005.
- [23] A. J. Phillips, J. M. Senior, R. Mercinelli, M. Valvo, P. J. Vetter, C. M. Martin, M. O. Van Deventer, P. Vaes, and X. Z. Qiu, "Redundancy strategies for a high splitting optically amplified passive optical network," *Journal of Lightwave Technology*, vol. 19, pp. 137-149, 2001.
- [24] I. T. Monroy and E. Tangdiongga, *Crosstalk in WDM communication networks*, Kluwer Academic Publishers, Norwell, Massachusetts, USA, 2002.
- [25] D. M. Forin, S. Di Bartolo, G. M. Toshi Beleffi, F. Curti, G. Cincotti, A. Vecchi, S. Ragana, and A. L. J. Teixeira, "Giga ethernet free-space passive optical networks," *Fibre and Integrated Optics*, vol. 27, pp. 229-236, April 2008.
- [26] K. Wang, A. Nirmalathas, C. Lim, and E. Skafidas, "4X12.5 Gb/s WDM Optical Wireless Communication System for Indoor Applications," *Journal of Lightwave Technology*, vol. 29, pp. 1988-1996, July 2011.
- [27] A. J. Phillips, "Power penalty for burst mode reception in the presence of interchannel crosstalk," *IET Optoelectronics*, vol. 1, pp. 127-134, 2007.
- [28] C. X. Yu and D. T. Neilson, "Diffraction-grating-based (de)multiplexer using image plane transformations," *IEEE Journal of Selected Topics in Quantum Electronics*, vol. 8, pp. 1194-1201, 2002.
- [29] S. B. Alexander, *Optical communication receiver design*, SPIE Optical Engineering Press, Bellingham, Washington, vol. TT22, 1997.
- [30] F. S. Vetelino, C. Young, L. Andrews, and J. Reolons, "Aperture averaging effects on the probability density of irradiance fluctuations in moderate-to-strong turbulence," *Applied Optics*, vol. 46, pp. 2099-2108, April 2007.

- [31] I. E. C. (IEC), "Safety of Laser Products—Part 1: Equipment Classification, Requirements, and User's Guide, IEC 60825-1 (IEC, 2001), <http://www.iec.ch>. New classification standard adopted as of 1 March 2001," Amendment 2 (2001).
- [32] N. S. Kopeika and A. Zilberman, "Vertical profiles of aerosol and optical turbulence strength and their effects on atmospheric propagation," *Proc. of SPIE*, vol. 3927, pp. 460-467, 2000.
- [33] C. Chen, H. Yang, H. Jiang, J. Fan, C. Han, and Y. Ding, "Mitigation of Turbulence-Induced Scintillation Noise in Free-Space Optical Communication Links Using Kalman Filter," *IEEE Congress on Image and Signal Processing, Hainan, China*, vol. 5, pp. 470-473, May 2008.
- [34] D. J. Wheeler and J. D. Schmidt, "Spatial coherence function of partially coherent Gaussian beams in atmospheric turbulence," *Applied Optics*, vol. 50, pp. 3907-3917, 2011.
- [35] M. A. Al-Habash, L. C. Andrews, and R. L. Phillips, "Mathematical model for the irradiance probability density function of a laser beam propagating through turbulent media," *Opt. Eng.*, vol. 40, pp. 1554-1562, August 2001.
- [36] M. A. Khalighi, N. Schwartz, N. Aitamer, and S. Bourennane, "Fading reduction by aperture averaging and spatial diversity in optical wireless systems," *Journal of Optical Communications and Networking, IEEE/OSA*, vol. 1, pp. 580-593, 2009.
- [37] Y. Dikmelik and F. M. Davidson, "Fiber-coupling efficiency for free-space optical communication through atmospheric turbulence," *Applied Optics*, vol. 44, 10 August 2005.
- [38] S. Spaunhorst, P. G. LoPresti, S. Pondelik, and H. Refai, "Evaluation of a novel FSO receiver for mitigating alignment errors," *Proc. of SPIE*, vol. 7324, pp. 1-8, 2009.
- [39] A. O. Aladeloba, A. J. Phillips, and M. S. Woolfson, "Performance evaluation of optically preamplified digital pulse position modulation turbulent free-space optical communication systems," *IET Optoelectronics*, vol. 6, pp. 66-74, February 2012.
- [40] A. O. Aladeloba, A. J. Phillips, and M. S. Woolfson, "DPPM FSO communication systems impaired by turbulence, pointing error and ASE noise," *14th International Conference on Transparent Optical Networks (ICTON)*, 2012, pp. 1-4.

CHAPTER 9 Conclusion and future works

9.1 Summary

This thesis has concentrated on the performance modelling of FSO communication systems experiencing atmospherically-induced scintillation noise, amplified spontaneous emission noise, optical crosstalk, beam spreading and pointing error due to building sway. The first chapter provides a brief historical perspective and introduction to the subject, and explained the need for optical amplification in FSO communication systems. In chapter 2, the existing FSO transmitter, optical amplifier and receiver properties, and the way in which the received optical field is converted from electrical to optical and then detected as electrical signals were presented. The various modulation formats that can be used for FSO communication systems are mentioned, with the main focus being on the OOK-NRZ and DPPM schemes.

It is well-known that FSO system performance is limited by atmospheric effects, with particular focus on turbulence-induced scintillation. Chapter 3 covers the atmospheric effects (attenuation due to scattering and absorption, and scintillation) and other mechanisms (beam spreading, pointing error) for optical signal loss and distortion in FSO communications. In particular, the useful models (lognormal pdf, K distribution, gamma-gamma pdf and negative exponential distribution) that can predict irradiance fluctuation over a wide range of atmospheric conditions are discussed in this chapter. The receiver noises and optical noises that are generated in an amplified FSO receiver set-up are highlighted in chapter 4. Various impaired BER evaluation methods, such as the MCB, CB and SPA (with the GA representing a simplified approach), are presented in this chapter.

The atmospheric turbulence pdfs mentioned in chapter 3, and the OOK-NRZ format, are used in the performance analysis of an optical preamplified FSO system. The inclusion of an optical amplifier, although increasing the received power, also generates ASE noise which is Gaussian. However, beating of the ASE noise with the signal and itself results in the formation of electrical domain beat noises, alongside the thermal and shot

noise. The beat noises cannot be considered to be Gaussian, and hence require a more comprehensive approach to describe the signal and noise behaviour [1-4] than the conventional GA-which is often used for simplicity. The MGF-based BER evaluation methods (i.e. CB, MCB and SPA), which have previously been applied for non-turbulent channels, were adapted for the turbulent atmospheric channel analysis and this original work forms the heart of chapter 5 of this thesis. The inclusion of turbulence presents an additional complexity into the treatment of the MGF formulation. The s parameter of the MGF was recalculated for each fluctuating irradiance values while the average BER was calculated by averaging the product of the BER and turbulence pdf over the fluctuating irradiance value. In chapter 5, the results obtained showed that the GA, MCB and SPA give sensible BER and power penalties while the CB deviates, in the low gain ($G=8.8$ dB) case. The GA gives good BERs for the low gain because the overall noise pdf can be approximated as Gaussian. In the high gain case ($G=30.6$ dB), the CB and MCB almost coincides while the SPA give slightly lower BERs and power penalties. The GA also gave good results in the high gain case for the main parameters used in the calculations, however, when the extinction ratio is change to infinity and the OBPF bandwidth is 76 GHz or lowered to 25 GHz, the GA is found to exceed the bounds. Based on the fact that it provides an upper bound upon the BER and the consistency of its results, the MCB can be conveniently recommended as the sensible approach to use for practical systems evaluation.

In chapter 6, an extension of the investigation in chapter 5 was performed for a DPPM-based FSO system incorporating aperture-averaging to lessen the atmospherically-induced signal fluctuations. A novel BER model for an optically preamplified DPPM-based MCB was presented in this chapter and then adapted for turbulent FSO performance calculation. The GG pdf was used to model the whole range of turbulence conditions because it is supported by simulation data. The BER and receiver sensitivity results were presented. The results showed that the DPPM (with a coding level of 5) provided better sensitivity (about 7-9 dB, for link length of 1500

m and depending on the turbulence strength) compared to a similar OOK-NRZ system. In addition, the aperture-averaging method was seen to give significant improvement in the BERs especially in the strong turbulence region. This improvement in the strong turbulence can be linked to the levelling effect which is treated in [5-7]. The MCB also gave the best results (compared to the GA and CB methods) using the DPPM format. This further confirms the superiority of the MCB technique. However the GA could still be a useful tool as it is far less computationally expensive compared to the MGF-based techniques.

In chapter 7, the performance evaluation of a preamplified DPPM and OOK-NRZ-based FSO system, experiencing pointing error due to building sway, and beam spreading, is presented. Building motion can occur due to several factors such as mechanical vibration, strong winds, thermal expansion and weak earthquakes [8-11]. Due to the narrowness of the laser beam width and receiver field-of-view, PE due to building sway can occur and this worsens the system performance. Also, optical turbulence (which arises due to small atmospheric temperature variations) gives rise to further BS beyond that due to diffraction alone. Typically, the beam spreads to a diameter larger than the receiver diameter, resulting in a loss of energy. The MCB-based BER and power penalty plots reveal the deleterious effect of combined turbulence, PE and BS. The additional transmit power required to attain unimpaired state at BER of 10^{-9} increases with turbulence strength and normalised PE variance, while as the normalised beam width becomes narrower the power penalty increases as well. The DPPM scheme is seen to give lower BERs than an equivalent OOK-NRZ system for non-turbulent system and for the whole range of turbulence strength considered.

In chapter 8, the system design and performance evaluation of a PON-like WDM access network using FSO communications as distribution link is presented. The performance calculations take into consideration several impairments, such as the interchannel crosstalk, air-coupling loss, BS loss, clear atmosphere loss, fibre attenuation, turbulence-induced scintillation noise and ASE noise. The combined turbulence and crosstalk analysis is

investigated for this kind of hybrid optical network for the first time to the best of the author's knowledge. Although the MCB is a better method, the choice of GA method is particularly necessary in this kind of situation to simplify the calculations doing which involves averaging over two turbulence variable (as per (8.4))-at least in the upstream transmission. The MCB could be used to tighten up the calculations once the general regions of interest have been identified. The turbulence accentuated crosstalk effect is considered for the two extremes of signal turbulent but crosstalk not and crosstalk turbulent but signal not, with error floors being observed in each cases. The results also show that upstream transmission gives a higher required transmit power at target BERs compared to the downstream transmission, in the presence of interchannel crosstalk. The maximum link length required to sustain the distribution link (in the both upstream and downstream transmissions) can be up to 2000 m for weak and moderate turbulence (with the downstream depending on the location of the optical amplifier). Also, as the turbulence strength increases, the crosstalk effect is seen to be more conspicuous. The location of the optical amplifier is dependent on practical considerations such as powering of a pointing and tracking system or avoidance of fibre non-linearity.

9.2 Conclusions

Through the analysis presented in chapters 5-8 by using theoretical model of the FSO systems in the presence of ASE noise, turbulence-induced scintillation noise and beam spreading, pointing error due to building sway and crosstalk, the following conclusions have risen as a result of the work summarised in 9.1:

- Optically preamplified FSO receivers are a very promising receiver configuration for use in a turbulent atmospheric channel.
- Facilitated by the use of MCB technique, a model for the utilisation of optically preamplified DPPM receivers, in both turbulent and non-turbulent systems, employing a receiver which integrates over the time

slot and compares the results to choose the largest has been developed for the first time in this work.

- Optically preamplified DPPM-based FSO systems can obtain receiver sensitivities of up to 9 dB (depending on the turbulence level) better than an equivalent OOK-NRZ FSO receiver. Furthermore the DPPM system sensitivity at the very low turbulence condition is shown to outperform the fundamental limits of an optically preamplified OOK-NRZ system.
- In low gain amplifier cases (for OOK-NRZ and DPPM schemes), the GA, SPA and MCB give approximately the same BERs, whereas the CB gives higher BERs. In the high gain amplifier case, the MCB and CB have almost the same BERs, and differs slightly from the SPA BERs. The GA exceeds the MCB, CB and SPA in the DPPM system whilst in the OOK-NRZ system; the GA exceeds the MCB, CB and SPA in the OOK-NRZ system at extinction ratio of infinity and lower OBPF bandwidths (e.g. 25 GHz).
- The application of MCB on BER, facilitated by a MGF formulation for the optically preamplification process represents a safe estimation method for FSO systems and should be used in practical system evaluation. Although the SPA is seen to give slightly lower BERs than the MCB, the MCB has the advantage of being an upper bound on the BER and is less complex than the SPA method. The GA may still have a role in initial quick calculations.
- The use of aperture-averaging technique can help reduce the effect of turbulence-induced scintillation particularly in the strong turbulence condition. The significant reduction observed in the strong turbulence case is attributed to the levelling effect which occurs when the receiver diameter falls between then spatial coherence radius and the scattering disk.

- The inclusion of pointing error and beam spreading into a turbulent FSO analysis result in additional power requirements. The power penalty increases as the normalised beam width at the receiver decreases. This is because when a narrow beam is transmitted (which translates to a narrow beam width at the receiver) and the receiver's field-of-view is narrow, pointing error due to building sway can affect the FSO transceiver's alignment and interrupt communication.
- The combination of FSO communications (assuming clear atmosphere) with optical fibre in a PON-like network results in the problematic collaboration of turbulence-induced scintillation and WDM interchannel crosstalk (for the two extremes of signal turbulent but crosstalk not and crosstalk turbulent but signal not) which causes error floors.
- In the hybrid WDN network, the main factors leading to higher upstream required power are the additional coupling loss via the RCL into fibre that occurs in the upstream (in the downstream we can couple directly onto the photodiode) and as the upstream received OSNR is typically worse.
- A maximum FSO link length of up to 2000 m can be reliably used to achieve human safe and high capacity access networks using high-speed FSO communication for distribution link (for fibre feeder length of 20 km and depending on turbulence level).
- The location of the optical amplifier in the hybrid WDM network will make little difference to the performance calculations in both directions but the issue of capping of the fibre launch power is significant in the downstream. The optical amplifier positioning would also depend on other design considerations such as fibre non-linearity and powering of a pointing and tracking system at the remote node.

9.3 Future work

The work carried-out in this thesis provides a model to study the impact of ASE noises, atmospheric turbulence, pointing error, beam spreading and optical crosstalk, using DPPM and OOK-NRZ formats. However there are some interesting research possibilities that can be pursued to further the work performed in this thesis.

- Since the work performed in this thesis has been entirely analytical/computational, experimental verification of the results should be attempted.
- The models developed in this thesis could be potentially extended to study the impact of the impairments for FSO systems using other modulation formats such as Differential phase shift keying (DPSK) and quadrature phase shift keying (QPSK).
- The crosstalk in the conventional WDM PONs is naturally interchannel. However, due to diffraction and turbulence-induced spreading of the laser beam along the propagation path, the beam width at the RCLs exceeds the radius of the receiver collecting lens (RCL), such that a fraction of the transmitted power falls on the RCL adjacent to the intended RCL, and (depending on FOV) some leakage signal might take an alternative path to the originally intended photodiode. Modelling such an intrachannel crosstalk effect in turbulent FSO communication-based WDM network could be a topic for future work.
- In WDM-TDM hybrid PONs, upstream packets are typically transmitted from the different ONUs to the OLT with the transmission process being governed by a time division multiple access (TDMA) protocol. The upstream (OLT) receiver is typically a DC-coupled burst mode receiver which must quickly obtain the decision threshold from a few bits in the preamble of each packet, necessary since average signal levels will vary from packet to packet [12]. The deployment of a FSO communications in distribution link is a cost effective and easier way of providing high-

speed connections in remote locations; however, one of the main challenges is the introduction of turbulence-induced scintillation noise during signal reception. The combined penalty for burst mode reception from the turbulence-accentuated optical crosstalk, the ASE noises (if optical preamplification is considered) and the threshold obtained from the preamble (which in itself subject to noise) is a topic to be investigated.

- The use of DPPM and OOK-NRZ code division multiple access (CDMA) multi-user network with turbulent FSO communications channels is another possible area of study. The inclusion of impairments, such as ASE noise and multi-user interference, must be investigated.
- Evaluation of BER for intersatellite links, taking into account imperfections in the channel such as satellite vibrations, background lights (reflected planetary light, integrated star light and zodiacal light) and cloud blockage, could be a topic for future work.
- The use of the saturation operation of optical amplifier gain to suppress the atmospherically-induced scintillation noise in a free-space optical communication system could be investigated theoretically.

9.4 References

- [1] K. W. Cattermole and J. J. O'Reilly, *Mathematical topics in telecommunications volume 2: problems of randomness in communication engineering*, Pentech Press Limited, Plymouth, 1984.
- [2] I. T. Monroy and E. Tangdionga, *Crosstalk in WDM communication networks*, Kluwer Academic Publishers, Norwell, Massachusetts, USA, 2002.
- [3] J. O'Reilly and J. R. F. Da Rocha, "Improved error probability evaluation methods for direct detection optical communication systems," *IEEE Transactions on Information Theory*, vol. 33, pp. 839-848, 1987.
- [4] L. F. B. Ribeiro, J. R. F. Da Rocha, and J. L. Pinto, "Performance evaluation of EDFA preamplified receivers taking into account intersymbol interference," *Journal of Lightwave Technology*, vol. 13, pp. 225-232, February 1995

- [5] M. A. Khalighi, N. Schwartz, N. Aitamer, and S. Bourennane, "Fading reduction by aperture averaging and spatial diversity in optical wireless systems," *Journal of Optical Communications and Networking, IEEE/OSA* vol. 1, pp. 580-593, 2009.
- [6] A. O. Aladeloba, A. J. Phillips, and M. S. Woolfson, "Performance evaluation of optically preamplified digital pulse position modulation turbulent free-space optical communication systems," *IET Optoelectronics*, vol. 6, pp. 66-74, February 2012.
- [7] L. C. Andrews, R. L. Phillips, and C. Y. Hopen, "Aperture averaging of optical scintillations: power fluctuations and the temporal spectrum," *Waves Random Media*, vol. 10, pp. 53-70, 2000.
- [8] S. Bloom, E. Korevaar, J. Schuster, and H. A. Willebrand, "Understanding the performance of free-space optics," *Journal of Optical Networking*, vol. 2, pp. 178-200, June 2003.
- [9] D. K. Borah and D. G. Voelz, "Pointing error effects on free-space optical communication links in the presence of atmospheric turbulence," *Journal of Lightwave Technology*, vol. 27, pp. 3965-3973, 2009.
- [10] A. A. Farid and S. Hranilovic, "Outage capacity optimization for free-space optical links with pointing errors," *Journal of Lightwave Technology*, vol. 25, pp. 1702-1710, 2007.
- [11] H. G. Sandalidis, T. A. Tsiftsis, G. K. Karagiannidis, and M. Uysal, "BER performance of FSO links over strong atmospheric turbulence channels with pointing errors," *IEEE Communications Letters*, vol. 12, pp. 44-46, 2008.
- [12] A. J. Phillips, "Power penalty for burst mode reception in the presence of interchannel crosstalk," *IET Optoelectronics*, vol. 1, pp. 127-134, 2007.